**DOKUZ EYLÜL UNIVERSITY**
**GRADUATE SCHOOL OF NATURAL AND APPLIED SCIENCES**

# TREATMENT OF FLUOROQUINOLONE ANTIBIOTICS USING NANO MAGNETITE-GRAPHENE OXIDE COMPOSITES

**by**
**Pelin ALİCANOĞLU**

**July, 2016**
**İZMİR**

# TREATMENT OF FLUOROQUINOLONE ANTIBIOTICS USING NANO MAGNETITE-GRAPHENE OXIDE COMPOSITES

**A Thesis Submitted to the**
**Graduate School of Natural and Applied Sciences of Dokuz Eylül University**
**In Partial Fulfillment of the Requirements for the Degree of Master of Science in Environmental Engineering Program**

**by**
**Pelin ALİCANOĞLU**

**July, 2016**
**İZMİR**

## M. Sc THESIS EXAMINATION RESULT FORM

We have read the thesis entitled **"TREATMENT OF FLUOROQUINOLONE ANTIBIOTICS USING NANO MAGNETITE- GRAPHENE OXIDE COMPOSITES"** completed by **PELİN ALİCANOĞLU** under supervision of **PROF. DR. DELIA TERESA SPONZA** and we certify that in our opinion it is fully adequate, in scope and in quality, as a thesis for the degree of Master of Science.

Prof.Dr. Delia T. SPONZA

Supervisor

Prof.Dr.Mustafa ODABAŞI

Jury Member

Doç.Dr.Metten Bilici BAŞKAN

Jury Member

Prof.Dr. Ayşe OKUR

Director

Graduate School of Natural and Applied Sciences

# ACKNOWLEDGMENTS

I would like to express my appreciation to my supervisor Prof. Dr. Delia Teresa SPONZA for her advice, useful comments, guidance and encouragement during my Master Degree studies.

I wish to thank Çağlar ULUSOY, Nefise ERDİNÇMER, Cansu DOĞAN, Gülce ÖZEL, Ezgi MERSİN and Gökçe GÜNEY for their contribution, guidance and support.

And also, I would like to express appreciation for the support of the sponsors; Dokuz Eylul University Scientific Research Project (KB.FEN.020) and TUBITAK 2210-C National Grant for Master Thesis Relevant to Priority Subjects.

Finally, my deepest gratitude to my lovely family, Orhan ALİCANOĞLU, Hilal ALİCANOĞLU and Çağlar ALİCANOĞLU.

Pelin ALİCANOĞLU

**TREATMENT OF FLUOROQUINOLONE ANTIBIOTICS USING NANO MAGNETITE - GRAPHENE OXIDE COMPOSITES**

# ABSTRACT

Excessive amount use of pharmaceuticals has resulted in their detection in effluents of wastewater treatment plants. In receiving environments, low concentrations of antibiotic traces can cause resistance to microorganisms. The combination of GO with magnetic nanoparticles to produce a magnetic graphene-based composite and it can be separated from the matrix rapidly and easily by an external magnetic field.

In this study the effects of concentration of Nano-GO/M composite, adsorption/irradiation time, pH of CIP and OFL, temperature affects and UV power affects were investigated and two energy sources (UV light and sunlight) were used to compare the photooxidation and adsorption process yields in a synthetic wastewater. Adsorption efficiencies of CIP and OFL were obtained as 30% and 35%, respectively (Nano-GO/M: 0.5 g/L, pH: 6.5, T: 21°C, time: 30 min). CIP and OFL adsorbed according to the Freundlich isotherm ($R^2$=0.98, $K_F$:1.31(unitlessss), n:1.38(unitlessss)), and Dubinin-Radushkevich ($R^2$=0.986, K′:8.84E-07($mol^2$ $kJ^{-2}$), $X'_m$: 0.7 mg/g) isotherm, respectively. The removal efficiencies of CIP (93%-80%) and OFL (96%-82%) for the photocatalytic studies under UV using Nano-GO/M are higher from the sunlight studies. (Nano-GO/M: 0.5 g/L, pH: 6.5, T: 21°C, time: 30 min for UV light) CIP was photodegraded according to first order reaction kinetic and OFL was photodegraded according to zero order reaction kinetic ($k_1$=0.8047 $min^{-1}$, $R^2$ =1 and $k_0$=.0.078 $min^{-1}$, $R^2$ =1). Also Nano-GO/M could be reused after six sequential treatment step with high removal efficiencies of both CIP (93%-75%) and OFL (96%-78%) via UV degradation.

**Keywords:** Ciprofloxacin, ofloxacin, graphene, magnetite, nano-composite, treatment, adsorption, photodegradation, sunlight

**FLUOROKUINOLAN GRUBU ANTiBiYOTiKLERiN NANO-MAGNETiT GRAFEN OKSiT BiLEŞiMLERi KULLANILARAK ARITILMASI**

## ÖZ


Farmasötiklerin aşırı kullanımı atıksu arıtma tesislerinin çıkış sularında saptanmasına sebep olmaktadır. Alıcı ortamlara verilen düşük konsantrasyonlardaki antibiyotik kalıntıları mikroorganizmalara direnç kazandırabilmektedir. Manyetik grafen tabanlı kompozit üretilerek, harici manyetik alan ile hızlı ve kolay bir şekilde matristen ayrılmaktadır.

Bu çalışmada, Nano-GO/M kompozit konsantrasyonu, adsorpsiyon/radyasyon süresi, pH, sıcaklık ve UV gücü etkileri araştırılmıştır ve fotooksidasyon prosesleri için iki farklı enerji kaynağı ( UV ışığı ve güneş ışığı) kullanılarak sentetik oluşturulan bir atıksuda giderim verimleri karşılaştırılmıştır. CIP ve OFL adsorpsiyon verimleri sırasıyla 30% ve 35% olarak saptanmıştır (Nano-GO/M: 0.5 g/L, pH: 6.5, T: 21°C, süre: 30 dk). CIP Freundlich izotermine ($R^2$=0.98, $K_F$:1.31 (birimsiz), n:1.38 (birimsiz)) göre ve OFL ise Dubinin-Radushkevich izotermine göre adsorbe olmuştur ($R^2$=0.986, K′:8.84E-07($mol^2$ $kJ^{-2}$), $X'_m$: 0.7 mg/g). UV ışığı kullanılarak yapılan calışmalarda CIP (93%-80%) ve OFL (96%-82%) giderim verimleri güneş ışığı verimlerine göre daha yüksektir (Nano-GO/M: 0.5 g/L, pH: 6.5, T: 21°C, süre: 30 dk, 300 W UV ışık altında). CIP fotodegredasyonu birinci derece reaksiyon kinetiğine göre, OFL fotodegredasyonu ise sıfırıncı derece reaksiyon kinetiğine göre gerçekleşmiştir ($k_1$=0.8047 $min^{-1}$, $R^2$ =1 and $k_0$=.0.078 $min^{-1}$, $R^2$ =1). Ayrıca Nano-GO/M kompozitini yeniden kullanarak, altı ardışık arıtma sonunda her iki antibiyotiğin (CIP: 93%-75%), OFL: 96%-78%) UV ışığı degredasyonunda yüksek verimler elde edilmiştir.



**Anahtar kelimeler:** Ciprofloxacin, ofloxacin, grafen, magnetit, nano-kompozit, arıtma, adsorpsiyon, fotodegredasyon, güneş ışığı

**CONTENTS**

**Page**

## LIST OF FIGURES

**Page**

## LIST OF TABLES

**Page**

# CHAPTER ONE
# INTRODUCTION

## 1.1 Introduction

Pharmaceuticals, newly recognized classes of environmental pollutants, are becoming increasingly problematic contaminants of either surface water or ground water around industrial and residential communities (Kyzas et al., 2015). Excessive amount use of pharmaceuticals has resulted in their detection in effluents of wastewater treatment plants. Many of these pharmaceuticals have low biodegradability in the environment and those taken by living beings are disposed of from living metabolism as unchanged or little transformed. Among widespread used antibiotics, fluoroquinolone antibiotics (FQ) are an important type with undetectable biodegradability (Kagle et al., 2009). FQs (ciprofloxacin, norfloxacin, levofloxacin, ofloxacin, clinafloxacin, etc.) constitute a class of potent oral antibiotics (Zhanel et al., 2002). Although absorptivity of orally administered FQs is high, a portion of the dose passes through the body into human and animal excrement (Goyne et al., 2005). Within the large class of FQs, CIP and OFL are used to treat urinary and respiratory tract infections in humans and animals (Goyne et al., 2005). In receiving environments, low concentrations of antibiotic traces can cause resistance to microorganisms (Bhandari et al., 2008). Concentrations of CIP and OFL in wastewaters have been obtained to range from ng to mg L−1, (i.e. 50 mg L−1 near drug manufacturing plants) (Larsson et al., 2007), therefore CIP and OFL removal from wastewater has become important. In the last literature surveys, a few studies have been reported for the removal of CIP from water which includes photooxidation (Belden et al., 2007), photo-Fenton oxidation (Sun et al., 2009), dissolved organic carbon (Carmosini & Lee, 2009), ozonation (De Witte et al., 2010), montmorillonite (Wang et al., 2011), surface modified carbon materials (Carabineiro et al., 2011), adsorption onto biocomposite fibers of graphene oxide/calcium alginate (Shaoling et al., 2013), adsorption on activated carbon (Yuanyuan et al., 2014). For OFL removal, only a few study reported, yet. OFL adsorption onto grape stalk (Nurchi et al., 2015), alumina and silica (Goyne et al., 2005), photooxidation with TiO2 (Hapeshi et al., 2010; Rodríguez et al., 2015).

Graphene has the perfect sp2 hybrid carbon nanostructure with two-dimensional carbon structure having excellent conductivity and the high specific surface area. Graphene oxide (GO) is a kind of novel two-dimensional graphene-based material, was developed for the removal of pollutants in the aquatic environment which have dispersibility and beneficial to remove pollutants in wastewater because of different functional groups, such as hydroxyl, carboxyl and epoxy groups (Zhen et al., 2013). These functional groups make GO suitable to remove the pharmaceuticals with low cost. Chen et al. (2015) studied CIP removal with GO. For initial 20 mg/L CIP concentration, 20 mg/L GO was used for sorption studies at pH=5 after 1 h contact time. Removal of CIP was reported as 74% and after 48 h sorption reached the equilibrium.

Magnetic Fe3O4 has the advantage for the usage as support material of composite adsorbent because it can be easily manipulated by an external magnetic field (Dong et al., 2010). In last literature surveys, there is only one study about CIP removal by magnetite. Rakshit et al. (2013), reported a study with nano sized magnetite to remove CIP. They studied on different solution properties such as pH (in the range of 3.4-8.4), ionic strengths (0.5, 0.1 and 0.01M), and initial CIP concentrations (in the range of 0.5–0.001 mM). For sorption studies, 10 g/L nano-Fe3O4(s) were used. Isotherm data were fitted with Freundlich isotherm with high R2 values (0.99, 0.97 and 0.98) for 0.5, 0.1 and 0.01M ionic strengths, respectively. Also they obtained that, the sorption of CIP on nano-$Fe_3O_4$(s) was strongly pH-dependent. Another study reported by Tang et al. (2013). A maximum CIP adsorption capacity of 10.91 mg/g investigated (for 5 mg/L initial CIP concentration using 0.2 g/L reduced-GO/M concentration within 24 hours retention time, at a pH of 6.2 and at a temperature of 25°C).

GO with large quantities of oxygen atoms on the surface are present in the forms of epoxy, hydroxyl, and carboxyl groups. These functional groups make GO hydrophilic and suitable to be an adsorbent (Gao et al., 2012). Especially, some iron oxide nanomaterials composited with GO as magnetic adsorbents were a better solution (Mostofizadeh et al., 2011). Thus, the combination of GO with magnetic nanoparticles

to produce a magnetic graphene-based composite and it will be separated from the matrix rapidly and easily by an external magnetic field.

## 1.2 The Aim of This Master Thesis

In this study, photocatalytic treatment and adsorption of CIP and OFL were studied with Nano-GO/M composite. The effects of increasing Nano-GO/M concentrations developed under laboratory conditions, on the yields of CIP and OFL, the effect of increasing of CIP and OFL concentrations on the CIP and OFL yields, effects of increasing contacting times or irradiation times on the CIP and OFL yields, the effects of acidic basic and neutral conditions on the yields of CIP and OFL adsorption yields and on the photocatalytic removal efficiencies of CIP and OFL were studied and compared.

The specific objectivities of the master thesis was;

- to evaluate the performance of the adsorption process on the yields of CIP/OFL using Nano-GO/M composite under laboratory conditions,
- to evaluate the performance of photocatalytic process using Nano-GO/M composite under laboratory conditions under UV and sunlight irradiations,
- to obtain the optimum treatment conditions for three different treatment processes on the removals of CIP and OFL (adsorption, UV and sunlight) using Nano-GO/M composite,
- to obtain the effects of increasing Nano-GO/M composite concentrations (0.5, 2 and 10 g/L) on the adsorption and photodegradation process,
- to obtain the optimum contacting time (15, 30, 60, 900 min) for maximum adsorption and photodegradation process,
- effects of pH (4, original pH of CIP and OFL solutions; 6.5 and 10) on the adsorption and photocatalytic removals of CIP and OFL,
- to compare the yields of adsorption, UV irradiation and sunlight irradiation according to the removal efficiencies,
- to choose the best treatment mechanism (adsorption, UV and sunlight process) for the maximum treatment of CIP and OFL,

- to explain the removal kinetic of CIP and OFL according to zero order kinetic, first order kinetic and second order kinetic for UV process,
- to make a cost analysis for UV removal process,
- to investigate the recovery of the Nano-GO/M.

## 1.3 Novelty of This Study

CIP and OFL treatment were investigated with classical and inadequate treatment methods. Batt, Kim & Aga (2007), studied the occurrence of ciprofloxacin, sulfamethoxazole, tetracycline, and trimethoprim antibiotics in four full-scale wastewater treatment plants (WWTPs) that differ in design and operating conditions. The detected concentrations (μg/L) ranged from 0.20 to 1.4 for ciprofloxacin, 0.21 to 2.8 for sulfamethoxazole, 0.061 to 1.1 for tetracycline, and 0.21 to 7.9 for trimethoprim. The overall percent difference in the concentrations of the antibiotics in the effluent and influent of these antibiotics differed between plants and ranged from 33% to 97%. In this thesis, three different processes were applied to two micropollutants (CIP and OFL) with using novel material; graphene. During synthesis of GO, individual sheets of GO can be viewed as graphene decorated with oxygen functional groups on both sides of the plane and around the edges (Lerf et al. 1998; Shahriary & Athawale, 2014). Magnetic Fe3O4 has the advantage for the usage as support material of composite Nano-GO/M composite because it can be easily separated by an external magnetic field (Dong et al., 2010). Iron oxide nanomaterials composited with GO as magnetic adsorbents were useful and do not need extra filtration or centrifugation (Mostofizadeh et al., 2011).

CIP and OFL treatment with Nano-GO/M has not been worked yet via adsorption and photooxidation. Different removal parameters realized in detail under different conditions to get optimum treatment condition. All of these methods were comprised; the optimum dose and optimum retention time and optimum pH for maximum yields were detected for both adsorption and photooxidation processes. In addition, cost analysis of treatment methods were investigated reusability of Nano-GO/M composite

was investigated; reuse of nanocomposite is eco-friendly approach and decreasing the treatment cost of both CIP and OFL.

# CHAPTER TWO
# FLOUROQUINOLONE ANTIBIOTICS AS MICROPOLLUTANT

Pharmaceuticals are often used on people and animals to treat infections and prevent diseases (Fink, Dror & Berkowitz, 2012). After being used on humans and animals, a considerable portion of the pharmaceuticals, which range from 10 to 90%, is to be found in urine and feces into sewage (Frade et al., 2014). Then they get into wastewater treatment plants (WWTPs) and are treated, along with other organic and inorganic compounds in the sewage (Frade et al., 2014; Ikehata, Naghashkar & El-Din, 2006). Antibiotics are one of the most important groups of pharmaceuticals. They often have no biodegradability (Kümmerer, Al-Ahmad & Mersch-Sundermann, 2000) and can have toxic effects on bacteria (Vasconcelos et al., 2009). They can also contribute to the development of resistant bacteria in aqueous systems (Kümmerer, 2009; Vasconcelos et al., 2009). Among widespread used antibiotics, FQs (ciprofloxacin, norfloxacin, levofloxacin, ofloxacin, clinafloxacin, etc.) the most common ones. CIP and OFL were patented in 1981 and 1982, respectively (Appelbaum & Hunter, 2000). The advantages of these compounds are that their spectrum includes Gram-positive species as well as Gram-negatives, and that they are well absorbed from the gastrointestinal tract, providing adequate blood levels to allow their use for systemic infections (Appelbaum & Hunter, 2000). In human medicine, CIP and OFL are among the most widely used quinolones in hospitals (Kümmerer, Al-Ahmad & Mersch-Sundermann, 2000). In these drugs, there are two types of ring structures, a naphthyridine nucleus, with a nitrogens at position 1 and 8, and a nucleus with only one nitrogen in position 1, referred to as a quinoline nucleus (Park, Kim & Bark, 2002). All compounds, both quinolones and naphthyridones, contain the keto oxygen at C-4 and carboxylic acid side chain at C-3, both of which have now been found to be essential to activity. Moreover, OFL, norfloxacin (NOR), enoxacin (ENO) etc. have a piperazinyl group at 7-carbon atom (Park, Kim & Bark, 2002). It has often been shown that the presence of charged groups is necessary for biological activity and solubility. However, the unionised form has a more favourable partition coefficient toward nonaqueous solvents (Park, Kim & Bark, 2002). The physicochemical properties of

micropollutants are important in the prediction of their environmental fate (Guney & Sponza, 2016). Physicochemical properties of CIP are given in Table 2.1.

Table 2.1 Physicochemical properties of CIP (Guney & Sponza, 2016) and OFL.

| IUPAC Name | Molecular Structure | CAS Number | Molecular Weight ($gmol^{-1}$) | Henry's law constant at 25°C ($atmm^3 mol^{-1}$) | Solubility in water ($mgL^{-1}$) | Dissociation constant pKa, pKa1, pKa2 | Octanol/ water partition coefficient log Kow | Apparent Log Kow at pH = 8.5 |
|---|---|---|---|---|---|---|---|---|
| CIP<br>1-Cyclopropyl-6-fluoro-1,4-dihydro-4-oxo-7-(1-piperazinyl)- 3-quinoline carboxylic acid | 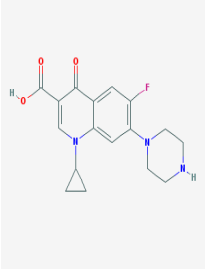 | 85721-33-1 | 331.35 | $5.1\times10^{-19}$ | 30.000 | 5.6, 6.2, 8.8 | 0.28 | −1.52 |
| OFL<br>(*RS*)-7-fluoro-2-methyl-6-(4-methylpiperazin-1-yl)-10-oxo-4-oxa-1-azatricyclo[7.3.1.$0^{5,13}$]trideca-5(13),6,8,11-tetraene-11-carboxylic acid | 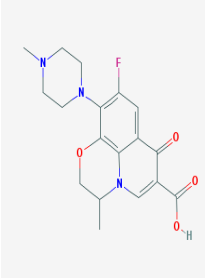 | 82419-36-1 | 361.37 | $4.98x10^{-20}$ | 28.300 | 5.23, 5.97, 9.28 | 0.36 | −0.39 |

FQs work against different pathogenic bacterial species, inhibiting bacterial DNA synthesis. Administered FQs are largely excreted as unchanged compounds in urine, and discharged into hospital or municipal sewage (Fink, Dror & Berkowitz, 2012). These FQs are not completely removed at WWTPs which explains their continuous presence in the environment resulting in FQs 'pseudo-persistent' compounds (Frade et al., 2014). The FQs, are included in water bodies and enter the soil and sediments, because of the adsorption on minerals and organic matter (Sturini et al., 2012). Along with their capability to grow resistance against antibiotics, FQs also have an unfit eco-toxicity tendency (Golet, Alder & Giger, 2002). In the environment, there are three possible end for any given drug: (1) it may be biodegradable, and turn into $CO_2$ and $H_2O$; (2) it may go through spesific metabolic processes or have a partial degradation. (3) Lastly, it may persist (Bila & Dezotti, 2003).

Most used wastewater and drinking water treatments are implemented within the frame work of biological degradation, coagulation, flocculation, sedimentation and filtration processes which are shown to be inadequate for removing/destroying pharmaceuticals, including antibiotics. Hence, it is required to improve new and more efficient processes (Balcioglu & Ötker, 2004).

In last literature surveys, there are several studies focused on FQs removal (An et al., 2010; Balcioglu & Ötker, 2004; Fink, Dror & Berkowitz, 2012; Guinea et al., 2009; Ge et al., 2010; Li, Niu & Wang, 2011; Sturini et al., 2012; Wang, He & Haung, 2010; Zhang & Huang, 2007).

## 2.1 Literature Review on the Treatment of CIP and OFL

Many different technologies were developed to remove pollutants from urban wastewaters, where they can be present at high concentrations of the order of μg/L to mg/L (Frade et al., 2014). WWTPs are regarded as the barrier for antibiotics from wastewater into aquatic environment (Duong et al., 2008). Nevertheless, former studies have shown that antibiotics are only partially eliminated in conventional WWTPs, with removal efficiencies ranging from 80 to 90% (Le-Minh et al., 2010). Consequently, antibiotics may consistently exist in effluents, and the concentrations

of some of them are even higher in effluents than in influents (Lin et al., 2009). Additional processes such as ozonation or membrane ultrafiltration, can reduce the concentrations of antibiotics in the effluents of WWTPs (Zorita, Martensson & Mathiasson, 2009). Lately, different studies have been realized to determine the most effective process and the most favorable conditions for the degradation of CIP and OFL. Some of these studies are listed below.

### *2.1.1 Literature Review for Adsorption Process*

#### *2.1.1.1 CIP*

Shaoling et al. (2013), researched the adsorption experiments with 10 mg of GO/calcium alginate fibers into conical flasks containing 20 mL of the aqueous solutions with CIP concentration of 9.8 mg/L. Maximum adsorption capacity of GO/calcium alginate fibers was 11.8 mg/g at a pH of 5.9, at 24 hours adsorption time and at room temperature.

Chen, Gao & Li (2015), studied the adsorption of CIP onto GO (20 mg/L). CIP concentrations were varying from 1 to 20 mg/L, at a pH of 5 and after 48 h retention time. The Langmuir maximum sorption capacity of CIP on GO was obtained 379 mg/g.

Rakshit et al. (2013) reported a study with nano sized magnetite to remove CIP. They studied on different solution properties such as pH (in the range of 3.4-8.4), ionic strengths (0.5, 0.1 and 0.01M), and initial CIP concentrations (in the range of 0.5–0.001 mM). For sorption studies, 10 g/L nano-Fe3O4(s) were used. Isotherm data were fitted with Freundlich isotherm with high R2 values (0.99, 0.97 and 0.98) for 0.5, 0.1 and 0.01M ionic strengths, respectively. In addition, they obtained that, the sorption of CIP on nano-Fe3O4(s) was strongly pH-dependent.

Another study reported by Tang et al. (2013). A maximum CIP adsorption capacity of 10.91 mg/g investigated (for 5 mg/L initial CIP concentration using 0.2 g/L reduced-GO/M concentration within 24 hours retention time, at a pH of 6.2 and at a temperature of 25°C).

Jiang et al. (2013), researched the CIP adsorption onto birnessite. The study for the isotherm of CIP adsorption on birnessite was performed by mixing 0.5 g wet birnessite with 10 mL CIP solution at initial concentrations of 0, 50, 100, 200, 400, 600, 800, and 1000 mg/L. Also increasing pH levels (2-11) were observed. The adsorption data was fitted to the Langmuir and Freundlich isotherms. The observed CIP adsorption capacity was about 71–72 mg/g. At pH=6 maximum adsorption efficiency was obtained.

*2.1.1.2 OFL*

Peng et al. (2012), investigated the adsorption of OFL (initial concentration was 10 mg/L) onto carbon nanotubes (CNTs- 200 mg/L) at different pHs (pH 2.0–12.0). According to them best results were obtained at pH=5 at 25 °C for 7 d to reach equilibrium.

Nurchi et al. (2015), studied batch sorption of OFL with using grape stalk (an amount of biomass of about 0.5 g). 40 mL of OFL solutions (OFL concentrations spanned from 0.5 mM to ~7 mM) at buffered pH values (4, 7, and 9) for 120 min. Experimental isotherms are fitted by the Langmuir equilibrium model. The maximum adsorption capacity of CNTs at different pHs (4, 7 and 9) were obtained as 137.3, 75.9 and 112 mg/g, respectively. The sorption at pH 7 is significantly lower than those at pH 4 and pH 9.

Another study remarked the sorption of OFL by cork at three pH values (4, 7 and 9) the OFL (at a concentration of 0.5-5mM) adsorption on 0.5 g/40 ml OFL sample within 24 hours retention time and at room temperature. They found a maximum adsorption capacity of 31.1, 26 and 24.9 mg/g at a pH of 4, 7 and 9, respectively (Crespo-Alonso et al., 2013).

Rodríguez et al. (2015), remarked that the OFL (at a concentration of 7.5-15 μM) adsorption on 0.1 g/L TiO2 OFL sample within 2 hours irradiation time and at room temperature at a pH of 7 under UV light. They found removal efficiency was to be 5%.

### *2.1.2 Literature Review for Photocatalytic Process*

*2.1.2.1 CIP*

Hassani, Khataee & Karaca (2015), were investigated the effects of pH (3-10), irradiation time and initial concentration of CIP (5–25 mg/L) on the photocatalytic degradation of CIP onto the TiO2 on montmorillonite (with 0.025–0.150 g/L TiO2/MMT). For maximum CIP removal (5 mg/L CIP) optimum TiO2/MMT concentration was found as 0.1 g/L. pH studies realized that the natural pH of CIP (pH=5) facilitated the adsorption of the CIP molecule and improved photocatalytic degradation and optimal irradiation time was selected as 120 min.

Zhang et al. (2015), remarked the visible light-induced degradation of CIP and was examined by using bismuth oxybromide (BiOBr) as photocatalyst. A 400 W halogen lamp was used as the light source. In experiments, 0.02 g BiOBr was used for 40 mL 5 mg/L CIP solution. Results showed that first-order kinetic model was reasonable and the rate constant was calculated to be 0.0272 min−1 with a correlation coefficient (R2) of 0.9954.

Yahya et al. (2014), investigated CIP-hydrochloride using electro-Fenton (EF) treatment with a constant current in the range 60–500 mA. They realized the EF experiments using cells with a carbon felt cathode and Pt anode. Effect of applied current and catalyst concentration on the kinetics of oxidative degradation and mineralization efficiency investigated. Degradation of CIP followed pseudo-first order reaction kinetics. They obtained the rate constant of the oxidation of CIP to be (1.01 ± 0.14) × 1010 M−1 s−1. An optimum current of 400 mA and a catalyst concentration of Fe2+ at 0.1 mM are found to be optimal for an effective degradation of CIP under operating conditions. Mineralization (>94%) was obtained at 6 h of treatment under these conditions.

Lin & Wu (2014), studied the degradation of CIP with UV/S2O82− process. The initial concentration of CIP in the aqueous solution was 10 mg/L and the original pH of the aqueous CIP (6.8–7.1) used for experiments. The degradation of ciprofloxacin by the UV/S2O82− process exhibited pseudo-first-order kinetics. With a Na2S2O8

concentration of 1.92 g/L, 95% of CIP was degraded in the absence of inorganic anions after 30 min irradiation time.

#### *2.1.2.2 OFL*

Hapeshi et al. (2010), conducted photocatalytic experiments with artificial irradiation in a photochemical reactor to remove OFL. 350 mL of 10 mg/L OFL aqueous solution were mixed with the TiO2 in the range 50–1500 mg/L. They also studied the effect of different pH leves (3, 6 and 10) at 25 °C after 240 min. Optimum catalyst dosage for maximum OFL (initial concentration 5 mg/L) removal (92%) was obtained as 250 mg/L at pH 3.

Hapeshi, Fotiou & Fatta-Kassinos (2013), determined the optimum operating parameters for the sonophotocatalytic degradation of OFL. For the study of the OFL degradation, the catalyst loading of TiO2 was varied in the range of 0.5–4 g/L, whereas the initial concentration of the pollutant was 10 mg/L. OFL degradation increased slightly with increasing the H2O2 concentration, with an optimum level of H2O2 concentration at 0.14 mM/L at 120 min irradiation. Optimum catalyst dosage for maximum OFL (initial concentration 10 mg/L) removal (≈100%) was obtained as 1000 mg/L.

## 2.2 Graphene Oxide (GO)

GO is a new form of carbon materials that has unique electrical, thermal and mechanical properties (Fakhri, Mahjoub & Khavar, 2016). As a novel two-dimensional (2D) material, graphene (G) and graphene oxide (GO) have drawn an increasing attention nowadays (Figure 2.1). GO can be obtained after oxidization of G and shares similar advantages with G. So, there are a lot of oxygen-containing surface functional groups such as epoxy (C–O–C), hydroxyl (OH) and carboxyl (COOH) on GO surfaces (Li, Sheng G. & Sheng J., 2014; Sheng et al., 2012; Zhao, Li, Ren, Chen & Wang, 2011). The existences of oxygen-containing functional groups make GO participate in various modifications, and thus lots of GO-based multifunctional

materials have been prepared and used for the removal of environmental contaminants (Li, Sheng G. & Sheng J., 2014).

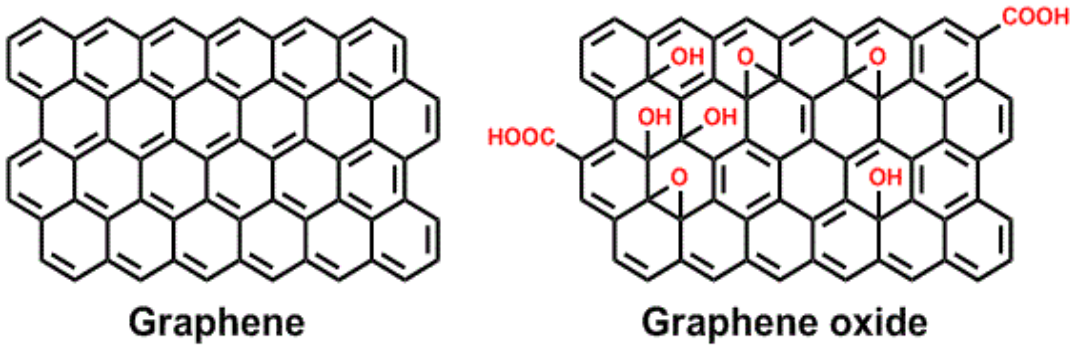


Figure 2.1 Structure of G and GO

Recently, a large number of studies have been published on the application of G/ metal oxide nanocomposites as photocatalysts and for water purification owing to its exceptional properties exhibited by the composites such as higher adsorptivity, conductivity, tunable optical behavior, stability and longevity (Upadhyay, Soin & Roy, 2013). Reduced GO (a derivative of graphene oxide) has been combined with variety of metal oxides such as TiO2 (Shi et al., 2012), ZnO (Fu, Han, Chang & Dong, 2012) and $Cu_2O$ (Wang, Huang, Tong, Li & Chen, 2013) found to be an excellent photocatalyst for the degradation of synthetic dyes (Upadhyay, Soin & Roy, 2013). Other than limiting the electron hole recombination, GO derivatives also prevent the corrosion and leaching of the metal oxide nanoparticles in to the water thereby enhancing the longevity of the photocatalyst. Also, the formation of π–π stacking between aromatic rings of graphene and organic pollutants also facilitates the adsorption of pollutants on the photocatalyst thereby enhancing the quenching of pollutants (Eunwoo, Jin-Yong, Haeyoung & Jyongsik, 2012; Upadhyay, Soin & Roy, 2013).

## 2.3 Magnetite ($Fe_3O_4$) Nanoparticles

Iron oxides exist in many forms in nature. Magnetite ($Fe_3O_4$), maghemite ($\gamma$-$Fe_2O_3$), and hematite ($\alpha$-$Fe_2O_3$) are the most common forms (Chan et al., 2004; Cornel &

Schwertmann, 1996; Xu et al., 2012). In recent years, the synthesis and utilization of iron oxide NPs (Figure 4.3) with novel properties and functions have been widely studied, due to their size in nano-range, high surface area to volume ratios and superparamagnetism (Afkhami, Saber-Tehrani & Bagheri, 2010; McHenry & Laughlin, 2000; Xu et al., 2012). Particularly, the easy synthesis, coating or modification, and the ability to control or manipulate matter on an atomic scale could provide unparalleled versatility (Dias, Hussain, Marcos & Roque, 201; Xu et al., 2012). In addition, iron oxide NPs with low toxicity, chemical inertness and biocompatibility show a tremendous potential (Xu et al., 2012).

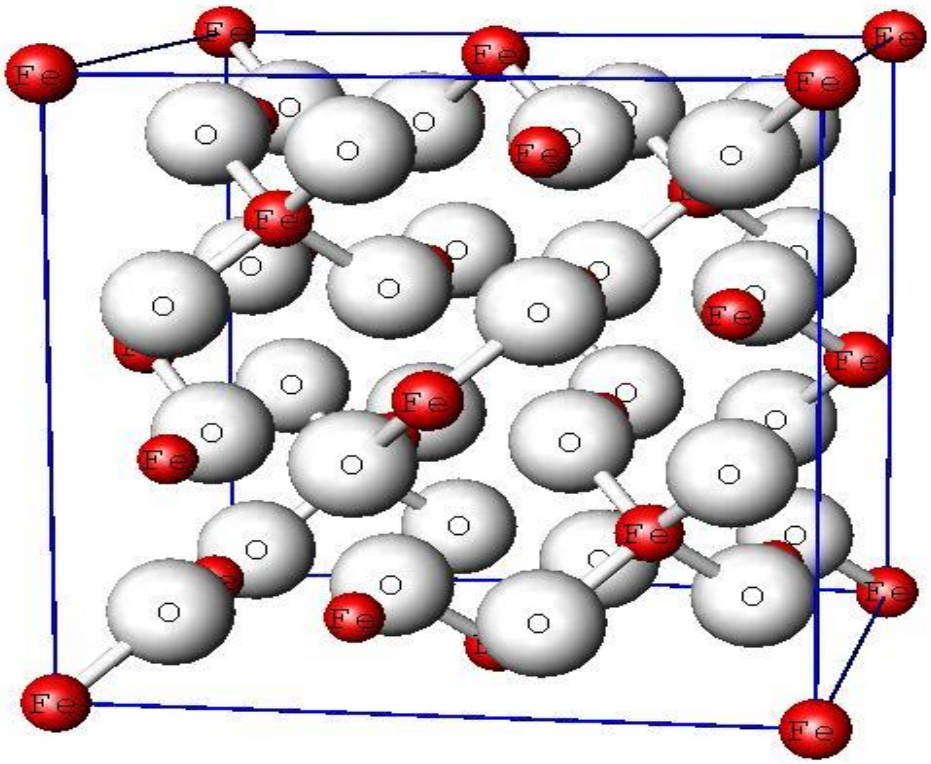

Figure 2.2 Chemical structure of magnetite

Current applications of iron oxide NPs in contaminated water treatment can be divided into two groups: (a) technologies which use iron oxide NPs as a kind of nanosorbent or immobilization carrier for removal efficiency enhancement (referred to here as adsorptive/immobilization technologies), and (b) those which use iron oxide NPs as photocatalysts to break down or to convert contaminants into a less toxic form (i.e. photocatalytic technologies) (Xu et al., 2012).

## 2.4 Graphene Literature Review

Dong et al. (2015), recently reported a study about removal of two pollutants namely levofloxacin (LEV) and lead (Pb) by using GO. 10 mL GO suspension (40 mg/L) was used as the adsorbent. 10 mL of LEV or Pb solutions of seven different concentrations (LEV: 1, 2, 5, 10, 20, 30, and 40 mg/L; and Pb: 1, 2, 5, 10, 20, 40, and 60 mg/L) were used for sorption experiments for 24 h retention time at 25°C. GO showed strong affinity for LEV and Pb in aqueous solutions with Langmuir maximum adsorption capacities of 256.6 and 227.2 mg/g, respectively.

Liu et al. (2012), reported the use of graphene as an adsorbent for removal of methylene blue (MB) from its aqueous solution. The dye uptake capacity increased from 153.5 mg/g to 204.08 mg/g with the rise in temperature from 293 K to 333 K while the maximum dye removal (~ 99.68%) was observed at pH 10.0. Adsorption equilibrium data fitted well to the Langmuir isotherm model than the Freundlich model.

Removal of MB using GO has also been reported by different researchers. Zhang et al. (2011), reported a maximum MB adsorption capacity of 1.939 mg/mg at pH 7 by GO. Li et al. (2013), found that adsorption of MB by GO was a pseudo-second-order reaction and followed the Langmuir adsorption isotherm. GO possessed a remarkably high adsorption capacity of 240.65 mg/g for MB. Initial dye concentration (40–120mg/L) and pH (2–9) on the removal of MB were studied in a batch mode of operation for 5h. 25mg adsorbent/50 mL sample was used for sorption studies.

Tayyebi, Outokesh, Moradi & Doram (2015), studied the removal of $Sr^{2+}$ and $Co^{2+}$ ions (50 mg/L initial concentration) by using magnetic GO (M-GO). 20 mg of adsorbent was added to vessels which contained 1000 mL of $Co^{2+}$or $Sr^{2+}$solution at pH 6.5. M–GO is saturated at the loading of 0.28 and 0.56 meq/g of $Sr^{2+}$ and $Co^{2+}$ ions, respectively. Adsorption isotherms of $Sr^{2+}$ and $Co^{2+}$ ions, which were fitted by Langmuir monolayer model.

Tang et al. (2013), reported CIP adsorption onto reduced-GO/M with a maximum CIP adsorption capacity of 10.91 mg/g for 0.2 g/L reduced-GO/M concentration within 24 hours retention time, at a pH of 6.2 and at a temperature of 25°C.

## 2.5 Treatment of CIP and OFL with Nano-GO/M

Important operating parameters on treatment of CIP and OFL with three different methods adsorption, photooxidation with UV and sunlight were studied. Effects of concentration of Nano-GO/M composite, contact time for adsorption, irradiation time for UV and sunlight irradiation and pH of CIP and OFL solution were investigated in this study.

### *2.5.1 Adsorption Process of CIP and OFL using Nano-GO/M*

Three different increasing concentrations of Nano-GO/M composite 0.5, 2 and 10 g/L were chosen to determine the optimum of Nano-GO/M composite concentration on the adsorption of CIP and OFL. All adsorption experiments were realized after 30 min for CIP and OFL adsorption (since the results of preliminary studies 30 min was the optimum contact time) at 21ºC and at original pH of CIP and OFL solutions (pH=6.5). Effect of contact time on the adsorption of CIP and OFL were investigated for the of Nano-GO/M composite concentration of 0.5 g/L, at original pH of CIP and OFL solutions (pH=6.5) and 21°C were illustrated in figures. Contact times were selected as 15, 30, 60 and 900 min also increasing temperatures (21, 40, 60 and 80ºC) were studied. The pHs of CIP and OFL solutions have important effect on adsorption capacity of Nano-GO/M. For that reason, different pH levels (4, 6.5 and 10) were studied to obtain optimum treatment pH. The maximum CIP (initial concentration of 1 mg/L) adsorption efficiency was obtained as 30% at 0.5 g/L of Nano-GO/M composite after 30 min contact time at original pH of CIP (6.5) and at $21^0$C. The maximum OFL (initial concentration of 1 mg/L) adsorption efficiency was obtained as 33% at 0.5 g/L of Nano-GO/M composite after 30 min contact time at original pH of OFL (6.5) and at 21°C.

### *2.5.2 Photocatalytic Process of CIP and OFL using Nano-GO/M*

In UV treatment studies, three different increasing concentrations of Nano-GO/M composite 0.5, 2 and 10 g/L were chosen to determine the optimum of Nano-GO/M composite concentration on the photodegradation of CIP and OFL. Effect of irradiation time on the removals of CIP and OFL were investigated for the Nano-GO/M composite concentration of 0.5 g/L, at original pH of CIP and OFL solutions (pH=6.5) and 21°C. All UV treatment experiments realized by using 0.5 g/L Nano-GO/M composite at original pH of CIP and OFL solutions (pH=6.5) and 21°C under 300 Watt UV power. 15, 30, 60 and 900 min irradiation times were studied to obtain the optimum irradiation time. The initial pH value of CIP and OFL plays key role in the photocatalytic degradation. Different pH levels (4, 6.5 and 10) were studied to obtain optimum treatment pH. Also we investigated effect of UV power (100, 300, 400 and 600 W) and increasing temperatures (21, 40, 60 and 80ºC). The maximum CIP (initial concentration of 1 mg/L) removal efficiency was obtained as 93% at 0.5 g/L of Nano-GO/M composite after 30 min irradiation time (300 W) at original pH of CIP solution (6.5) at 21ºC. The maximum OFL (initial concentration of 1 mg/L) removal efficiency was obtained as 96% at 0.5 g/L of Nano-GO/M composite after 60 min irradiation time (300 W) at original pH of OFL solution (6.5) at 21ºC.

In sunlight studies, Effects of 0.5 g/L, 2 g/L, 3.5 g/L, 5 g/L and 10 g/L Nano-GO/M composite concentrations on the removals of CIP and OFL with constant sunlight time (250 min for CIP removal, 350 min for OFL removal were chosen due to preliminary studies results) at original pH of CIP and OFL solution (pH=6.5) under sunlight irradiation with a power of 80 W at outdoor temperature (35°C ± 5°C). Effect of irradiation time on the removals of CIP and OFL were investigated for the Nano-GO/M composite concentration of 2 g/L, at original pH of CIP and OFL solutions (pH=6.5) and 21°C. All sunlight experiments realized by using 2 g/L Nano-GO/M composite at original pH of CIP and OFL solutions (pH=6.5) and 21°C under sunlight irradiation with a power of 80 W. In order to determine optimum irradiation time for maximum CIP and OFL removal yields, increasing irradiation (30 min, 120 min, 250 min, 350 min and 24h) times were used. The initial pH value of CIP and OFL plays key role in the photocatalytic degradation. Different pH levels (4, 6.5 and 10) were

studied to obtain optimum treatment pH. The maximum CIP (initial concentration of 1 mg/L) removal efficiency was obtained as 81% at 2 g/L of Nano-GO/M composite after 250 min irradiation time at original pH of CIP solution (6.5) at with a power of 80 W at outdoor temperature (35°C ± 5°C). The maximum OFL (initial concentration of 1 mg/L) removal efficiency was obtained as 82% at 2 g/L of Nano-GO/M composite after 350 min irradiation time at original pH of OFL solution (6.5) at with a power of 80 W at outdoor temperature (35°C ± 5°C).

# CHAPTER THREE
# ADSORPTION MECHANISM

Adsorption occurs whenever a solid surface is exposed to a gas or liquid: it is defined as the enrichment of material or increase in the density of the fluid in the vicinity of an interface (Rouquerol et al., 2014). The process of adsorption arises due to presence of unbalanced or residual forces at the surface of liquid or solid phase. These unbalanced residual forces have tendency to attract and retain the molecular species with which it comes in contact with the surface. Adsorption is essentially a surface phenomenon. Adsorption process involves two components Adsorbent and Adsorbate. Adsorbent is the substance on the surface of which adsorption takes place. Adsorbate is the substance which is being adsorbed on the surface of adsorbent. Adsorbate gets adsorbed (Figure 3.1). There are some important parameters that affecting adsorption behavior of adsorbent. Particle size and solubility have a converse effect to adsorption capacity of adsorbent while as the size of particles and temperature increased adsorption capacity also increased.

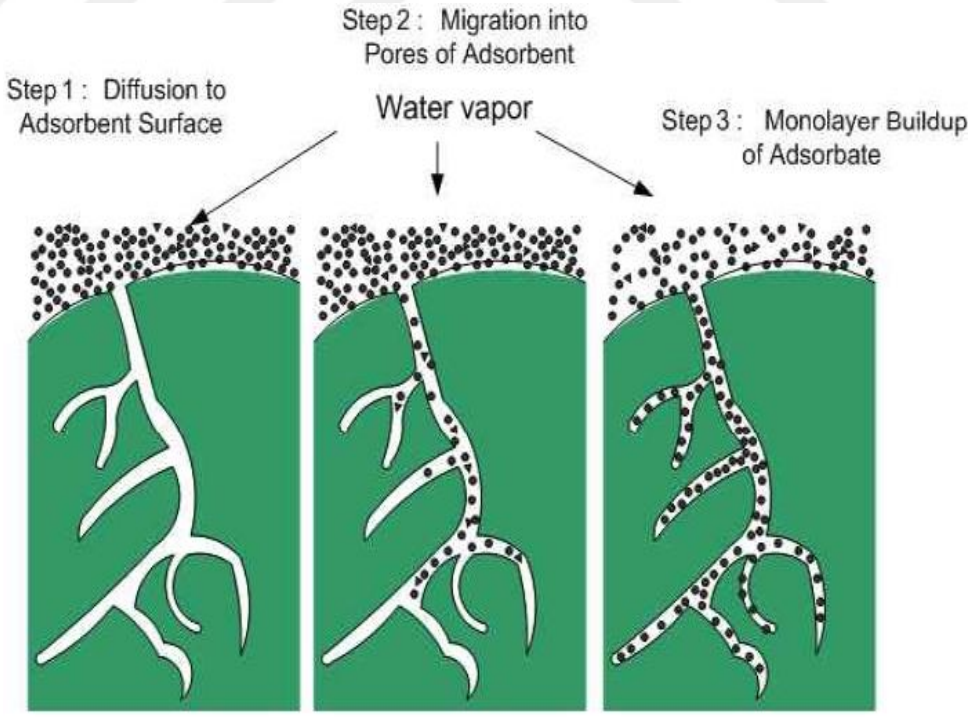


Figure 3.1 Mechanism of Adsorption (Kim & Chea, 2012)

It is mainly divided into three steps as follows:

Step 1: Molecule diffusion process into the thin layer of fluid (Called as fluid film) which is attached on the adsorbent.

Step 2: According to developing of diffusion, the surface diffusion process which attached the vapor or gas along the pores. It is called as mixed diffusion because there exist two diffusion of pore diffusion and surface diffusion.

Step 3: Adsorption process in the pore adsorption sites (Kim & Chea, 2012).

Modes of interaction of graphene/metal oxide composite with different type of pollutants are shown in Figure 3.2.

There are two types of adsorption; physical and chemical adsorptions. Chemisorption (or *chemical adsorption*) is adsorption in which the forces involved are valence forces of the same kind as those operating in the formation of chemical compounds. The problem of distinguishing between chemisorption and physisorption is basically the same as that of distinguishing between chemical and physical interaction in general. No absolutely sharp distinction can be made and intermediate cases exist, for example, adsorption involving strong hydrogen bonds or weak charge transfer (UIPAC, 2002).

Physisorption (or *physical adsorption*) is adsorption in which the forces involved are intermolecular forces (van der Waals forces) of the same kind as those responsible for the imperfection of real gases and the condensation of vapors, and which do not involve a significant change in the electronic orbital patterns of the species involved. The term *van der Waals adsorption* is synonymous with physical adsorption (UIPAC, 2002).

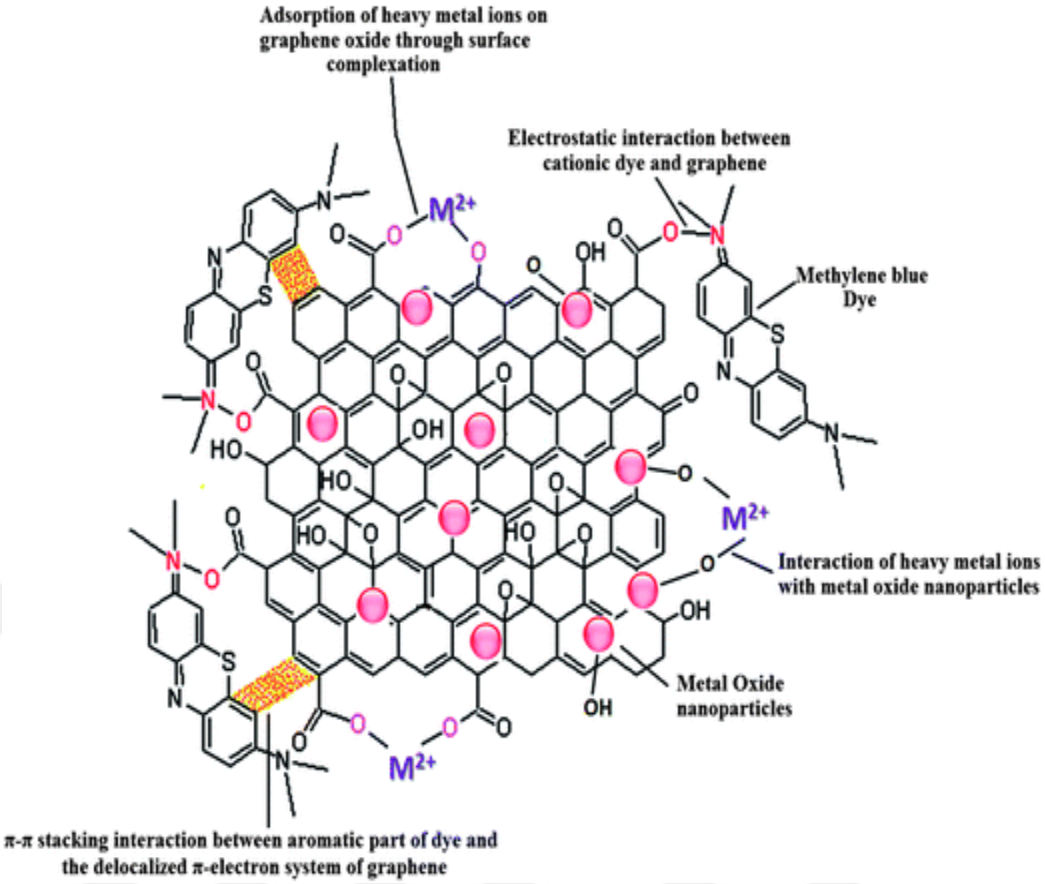


Figure 3.2 Different types of interactions in involved in the adsorption of pollutants on metal oxide/graphene oxide (Upadhyay, Soin & Roy, 2013).

# CHAPTER FOUR
# PHOTOCATALYTIC MECHANISM

Advanced oxidation processes (AOPs) are used to oxidize complex compounds in wastewater which are not degrading biologically. AOPs involve the generation of the hydroxyl radical ($HO^{\cdot}$) as oxidant to removal compounds. Photocatalytic oxidation is a type of AOP. Photocatalytic oxidation has recently become a common word and various products using photocatalytic functions have been commercialized (Hashimoto, Irie & Fujishima, 2005). Serpone & Emiline (2002), defined that photocatalysis, in its most simplistic description, is the acceleration of a photoreaction by action of a catalyst.

Among the AOPs, heterogeneous photocatalysis has attracted attention as a promising technique for solving environmental problems especially in the degradation of organic pollutants in water treatment (Ma, Xue, Zhou & Zhang, 2014; Umukoro, Peleyeju, Ngila & Arotiba, 2016). Heterogeneous photocatalysis is a process that occurs when a semiconductor absorbs a photon of energy greater than its band gap (the region between the electron-fill valance band and the empty conduction band of a semiconductor), and an electron is excited to the conduction band thereby creating a hole in the valence band. The generation of the electrons could lead to oxidation and reduction reactions on the surface of the semiconductor. In both reactions, hydroxyl radicals are produced and these radicals react with the molecules of the organic pollutants repeatedly to degrade and possibly mineralize them into less toxic and simpler substances such as $N_2$, $CO_2$ and $H_2O$ (Chan, Wu, Juan & Teh, 2011; Umukoro, Peleyeju, Ngila & Arotiba, 2016).

Metal oxides have been employed as a photocatalyst for the degradation of various water pollutants and have shown promising results (Chatterjee & Dasgupta, 2005; Upadhyay, Soin & Roy, 2013). In order to improve the photocatalytic efficiency of the metal oxides, combination of metal oxides with electron scavenging agents has been one the most popular and exploited approach to attenuate the effect of the large band gap and electron hole recombination on the photocatalytic performance. Graphene derivatives have acquired great interest as a support material

for the formation of nanocomposites with metal oxide because of availability of a large number of economical and facile synthesis approaches and possibility of surface which have been developed over the years *via* the work on other forms of carbon such as nanotubes and fullerenes. Figure 4.1. illustrates the mechanism involved in photocatalytic activity of graphene/metal oxide composite (Upadhyay, Soin & Roy, 2013).

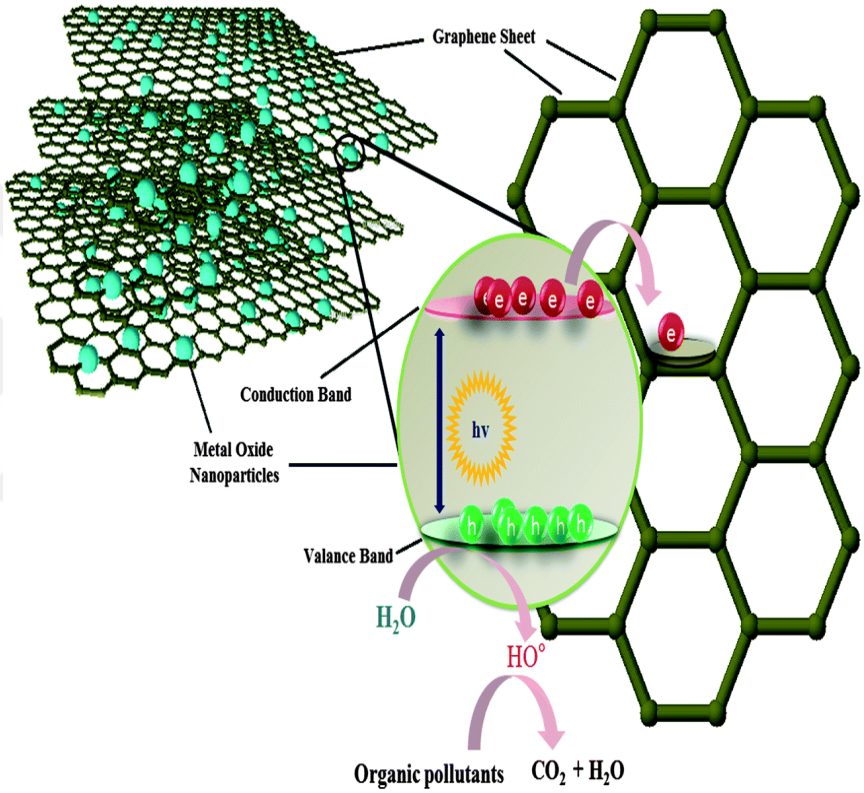


Figure 4.1 Electron transfer from conduction band of metal oxide to graphene through percolation mechanism (Upadhyay, Soin & Roy, 2013).

The efficiency of the photocatalytic process is related to the surface ionization state of the Nano-GO/M, as shown in equation (4.1-4.6);

$$Fe_3O_4 + h\nu \rightarrow Fe_3O_4\ (e^- + h^+) \quad (4.1)$$

$$CIP/OFL + h\nu \rightarrow CIP/OFL^* \quad (4.2)$$

$$Fe_3O_4 + \text{graphene} \rightarrow Fe_3O_4 + \text{graphene}\ (e^-) \quad (4.3)$$

$$\text{Graphene}\ (e^-) + O_2 \rightarrow \text{graphene} + O_2^{\cdot -} \quad (4.4)$$

$$Fe_3O_4\ (h^+) + OH^- \rightarrow Fe_3O_4 + {}^{\cdot}OH \quad (4.5)$$

$$CIP/OFL^* + {}^{\cdot}OH \rightarrow CO_2 + H_2O \quad (4.6)$$

Upon light irradiation, the $Fe_3O_4$ present on the GO sheet surface undergoes charge separation that leads to promotion of valence band (VB) electrons into the conduction band (CB), leaving a hole in the VB (4.1), whereas the OFL molecules are excited to cationic CIP/OFL radicals (CIP/OFL*) (4.2). These photo-generated electrons in the conduction band are instantaneously transferred to GO sheets (4.3), and are consequently captured by dissolved $O_2$ to generate reactive oxidation species such as ˙OH and $O_2^{\cdot -}$ (4.4). On the other hand, the photo induced holes are crucial for the oxidation process and adsorbents are effectively oxidized; usually the $Fe_3O_4$ (h+) can react with adsorbed $H_2O/OH^-$ to form strong hydroxyl radicals (˙OH) (4.5). Finally, these ˙OH radicals oxidize the CIP/OFL molecules adsorbed to $CO_2$ and $H_2O$ (4.6) via the π–π electrostatic interactions on the active sites of the Nano-GO/M composite (Peik-See et al., 2014).

# CHAPTER FIVE
# MATERIALS AND METHODS

## 5.1 Synthetic wastewater of CIP and OFL

Raw CIP and OFL stock solutions were prepared under laboratory conditions. CIP and OFL were diluted in ultrapure water and homogenized. Stock solutions of both CIP and OFL were prepared as 1000 mg/L. After that in order to obtain different concentrations of CIP and OFL during experiments (1, 3, 5, 25, 100 and 500 mg/L) dilution were performed for both CIP and OFL.

## 5.2 Reagents and Chemicals

CIP (>98%, Bayer AG, Germany) and its metabolites (M1- Desenthylenciprofloxacin (>98%, Bayer AG, Germany) and M3 - oxociprofloxacin (>98%, Bayer AG, Germany), OFL (>98%, Bayer AG, Germany) and its metabolites (POF- 9-piperazino ofloxacin (>98%, Bayer AG, Germany) and MOF- des-methyl ofloxacin (>98%, Bayer AG, Germany), Graphene (Ege Nanotek Kimya Sanayi Ltd. Şti.) and Magnetite were bought externally. Natural magnetite was purchased from Synergy Laboratory Products Ltd., Turkey. Demineralized water was used for preparation of reagents solutions. 0.1 M HCl and 0.1 M NaOH are used to adjust pH vales of CIP and OFL solutions.

## 5.3 Experimental Procedures

### *5.3.1 Batch Reactors for Adsorption Process*

The investigations were carried out in batch mode at different conditions of pH, Nano-GO/M concentrations, contacting time, increasing CIP and OFL concentrations and temperatures to obtain maximum yields of adsorption process. The adsorption experiments were carried out isothermally in static batch mode. The experiments were conducted by adding Nano-GO/M composite concentrations increasing from 0.5 g/L, 2 g/L and 10 g/L to the CIP and OFL presents in conical Teflon coated glass reactors with a volume of 250 mL. These reactors were placed on a rotating shaker at 150 rpm.

The pH of the CIP and OFL were adjusted between 4, 6.5 and 10 during the contact periods of 15, 30, 60 and 900 min. Samples were withdrawn at suitable intervals and were separated from the Nano-GO/M composite by an external magnetic field. The analyses were carried out in supernatants. All experiments were done duplicate.

The amount of maximum adsorption capacity of Nano-GO/M composite for the CIP and OFL removals were calculated according to Eq. (5.1):

$$q_e = \frac{(C0-Ce).V}{W} \tag{5.1}$$

where $q_e$ is the capacity of adsorbent (mg/g), $C_o$ and $C_e$ are the initial and equilibrium liquid concentrations (mg/L), respectively; V is the volume of solution (L); and W is the weight of adsorbent (g).

### *5.3.2 Quartz Glass Reactors for Photocatalytic Processes*

Photocatalytic experiments were conducted in a system which is well-sealed and constructed with stainless steel material. Quartz glass reactors coated with teflon and 10 UV lambs (each one has a power of 30 watt) were used for photocatalytic experiments. The dimensions of the silindirical quartz glass reactors were 38 and 3.5 cm. The experiments were performed at different temperatures, different UV powers, different initial concentration of CIP and OFL and the pH of the reaction mixture was adjusted from 4 to 6.5 and 10 using 1 mol/L of $H_2SO_4$ and NaOH solution. Photocatalytic experiments were carried out with a known quantity of Nano-GO/M composite varying between 0.5 g/L, 2 g/L and 10 g/L at different irradiations times (15, 30, 60 min, 900 min). Then, they were irradiated in a closed isolated device system. Figure 5.1 shows the device used for UV irradiation in an open condition.

Figure 2.1 the system used for UV irradiation

And also, photocatalytic degradation experiments were carried out under sunlight in the same quartz glass reactors which have the same dimensions. Experiments were carried out at different retention times of the day (30, 120, 250, 350 min and 24 h) and different initial concentration of CIP and OFL and the reactors were placed at an angle of 90 degrees to the sun at hours 08.00-17.00. The pH of the reaction mixture was adjusted from 4 to 6.5 and 10 using 1 mol/L of $H_2SO_4$ and NaOH solutions. Experiments were carried out at the same Nano-GO/M composite concentrations varying between 0.5 g/L, 2 g/L, 3.5 g/L, 5 g/L and 10 g/L. Samples were separated magnetically and were analyzed in HPLC. The sunlight power was measures as 80 W with a light-meter.

## 5.4 Synthesis of Nano-GO/M Composite under Laboratory Conditions

In a typical synthesis, 5 g purchased graphene was dispersed in 120 ml $H_2SO_4$ by adding 2.5 g of $NaNO_3$ in glass flasks coated by teflon on a magnetic stirrer for 30 min placed in a water bath at a temperature of 18°C. After stirring the aforementioned mixture at a rpm of 500g; 15 g of $KMnO_4$ was added gradually, and continued to stir the last mixture overnight, continuously at 18°C. Then, 150 ml $H_2O$ was slowly added and continued to mixing a day at 98°C. Finally, 50 mL of 30% $H_2O_2$ was added to the final mixture. The mixture was washed with 5% HCl and deionized water for several times and then, centrifuged and dried under vacuum for purification the GO which was obtained in a solid phase. The $Fe_3O_4$ Nano particles were dispersed in 25 mL water and added to 50 mL GO aqueous solution. This mixture contained 1 mg $Fe^{+3}$ /1mL GO and it was stirred at 60°C through 1 h. The nano-composite was collected by using a magnet from the outside of the glass reactor and washed with water three times (Nengsheng et al.,2014).

Figure 5.2 Picture of synthesized Nano-GO/M

## 5.5 Analytical Methods

*HPLC Equipment Specifications:* A HPLC Degasser (Agilent 1100), a HPLC Pump (Agilent 1100), a HPLC Auto-Sampler (Agilent 1100), a HPLC Column Oven (Agilent 1100) and a HPLC Diode-Array-Detector (DAD) (Agilent 1100) were used.

Figure 5.3 and 5.4 shows the molecular structure of CIP and OFL and their metabolites, respectively.

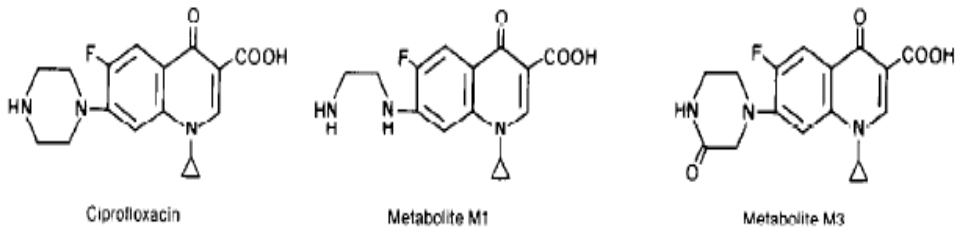


Figure 5.3 Molecular structures of CIP and its metabolites namely M1 (desenthylenciprofloxacin) and M3 (oxociprofloxacin).

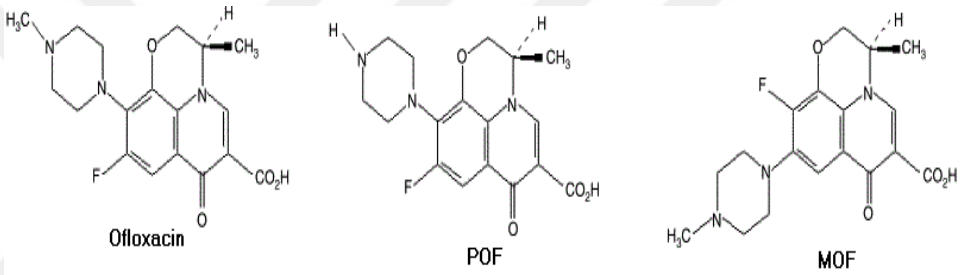


Figure 5.4 Molecular structures of OFL and its metabolites namely POF (9-piperazino ofloxacin) and MOF (des-methyl ofloxacin).

For quantization, an external standard method was utilized. Peak areas from the HPLC chromatogram were plotted against to the known concentrations of stock solutions at varying concentrations. Equations generated by linear regression were used to establish concentrations for CIP and OFL standard solutions.

### *5.5.1 Standard Solutions and Calibration Curves for CIP and Its Metabolites*

Linear range and the equations of linear regression were obtained through such a sequence of 100 mg/L, 50 mg/L, 20 mg/L, 10 mg/L. Mean areas generated from the standard solutions were plotted against concentration to establish calibration equations. CIP, M1 (desenthylenciprofloxacin) and M3 (oxociprofloxacin) peaks were seen at 7.342, 6.51 and 8.49 min.

The mobile phase consisted of $KH_2PO_4$ in aqueous solution and Acetonitrile (95:5, v/v). The flow rate was set at 1.5 mL/min and injection volume at 20 µL. C18 column was used for the analysis. The analyte was separated at ambient temperature. The detection wavelengths of DAD were set at: 210 nm.

$R^2$ values of calibration graphs of CIP, M1 (desenthylenciprofloxacin) and M3 (oxociprofloxacin) were found as 0.99 for both CIP and M1 and M3 (Figure 5.6, 5.7 and 5.8, respectively).

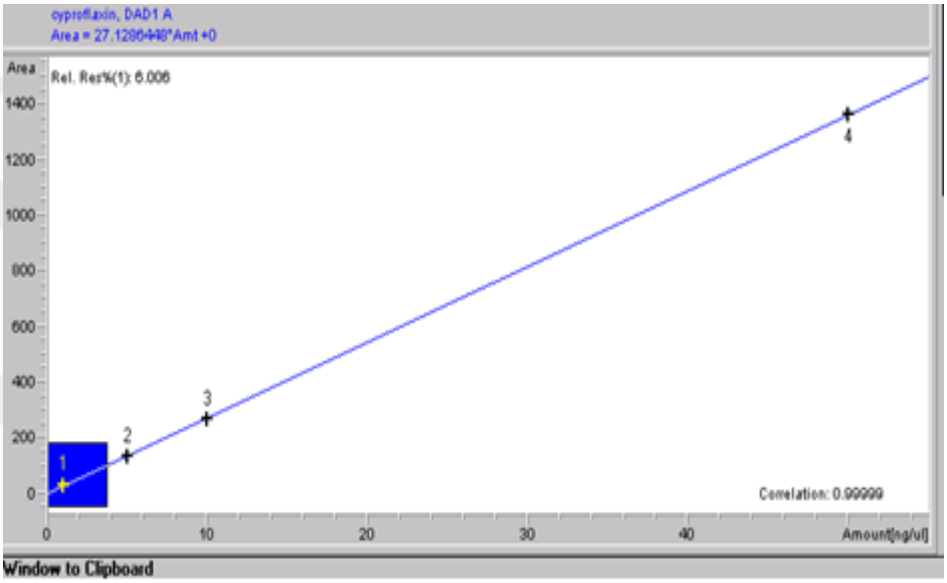


Figure 5.6 Calibration graph of CIP

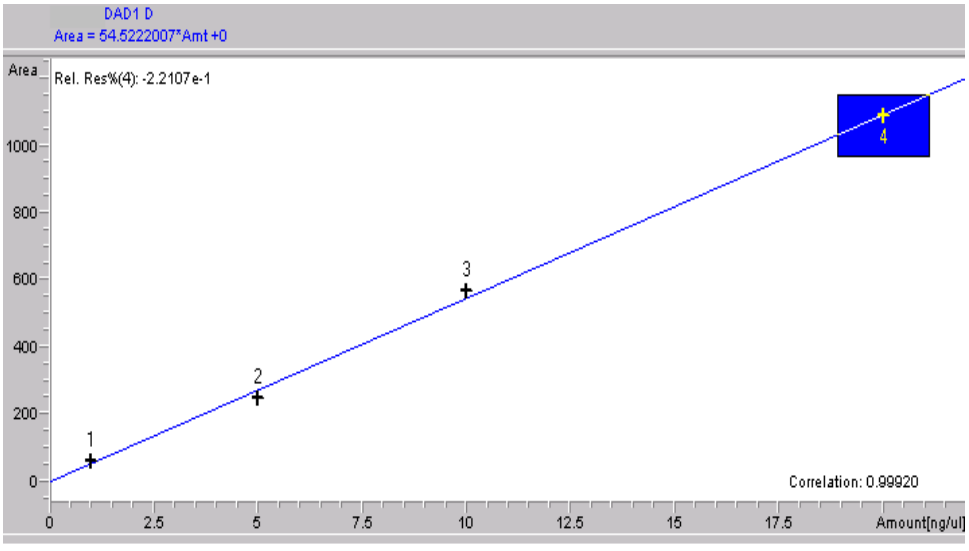


Figure 5.7 Calibration graph of M1 (desenthylenciprofloxacin)

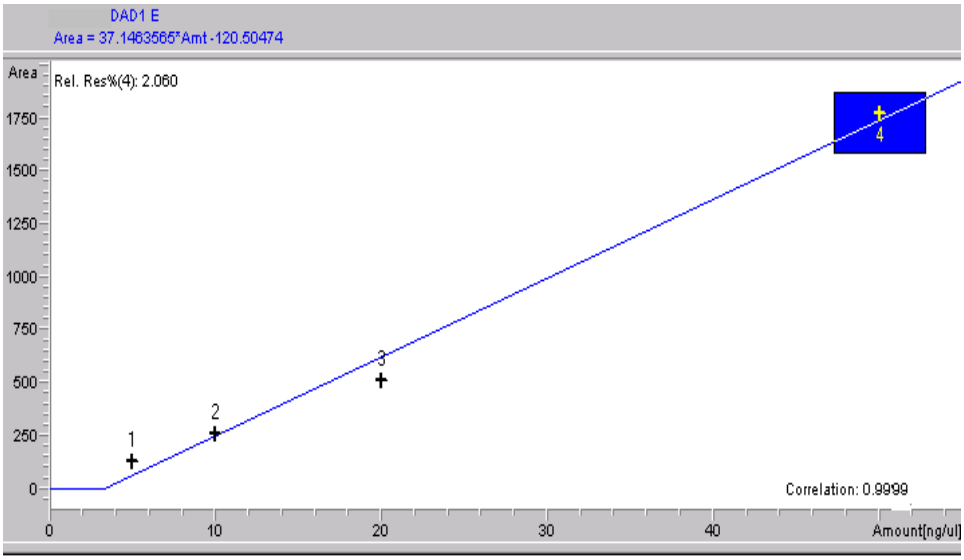


Figure 5.8 Calibration graph of M3 (oxociprofloxacin)

### *5.5.2 Standard Solutions and Calibration Curves for OFL and Its Metabolites*

All reagents were of HPLC grade. HPLC gradient grade acetonitrile, 85% orthophosphoric acid, and potassium perchlorate were purchased from Merck (Darmstadt, Germany).

Linear range and the equations of linear regression were obtained through such a sequence of 100 mg/L, 50 mg/L, 20 mg/L, 10 and 5 mg/L. Mean areas generated from the standard solutions were plotted against concentration to establish calibration equations. The mobile phase consisted of acetonitrile (18:82, v/v). The aqueous component of the mobile phase was prepared by dissolving 1.0 g of ammonium acetate and 1.75 g of potassium perchlorate by ultrasonic treatment in 325 mL of water and the pH was adjusted to 3.50 using 85% orthophosphoric acid. The column was equilibrated to stable baseline at a flow rate of 1.0 mL $min^{-1}$, maintaining the temperature of the column at 45 °C. Detection was at 294 nm (Zivanovic, Zigic & Zecevic, 2006). OFL, (9-piperazino ofloxacin) and MOF (des-methyl ofloxacin) metabolites peaks were seen at 10.01, 7.99 and 9.68 min. Also C8 column was used for the analysis.

$R^2$ values of calibration graphs of OFL, POF (9-piperazino ofloxacin) and MOF (des-methyl ofloxacin) metabolites were found as 0.99 for OFL, POF (9-piperazino ofloxacin) and MOF (des-methyl ofloxacin) (Figure 5.9, 5.10 and 5.11, respectively).

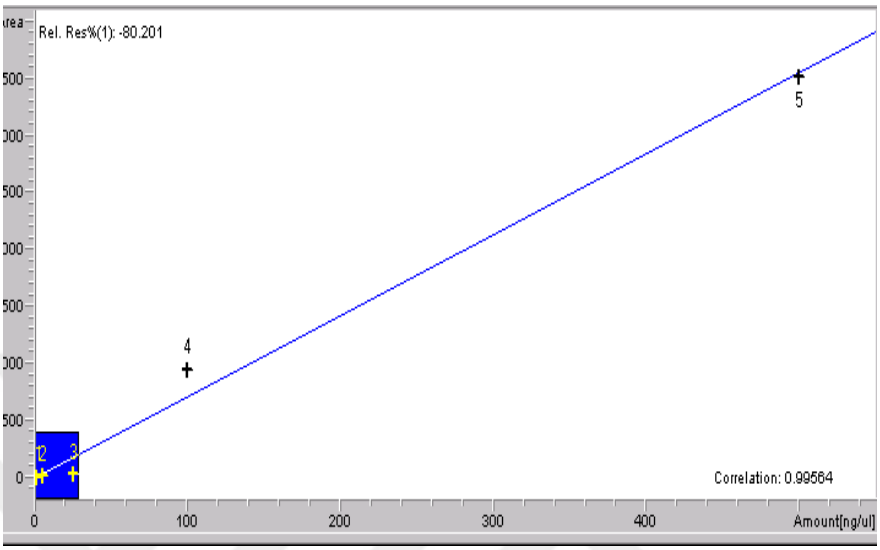


Figure 5.9 Calibration graph of OFL

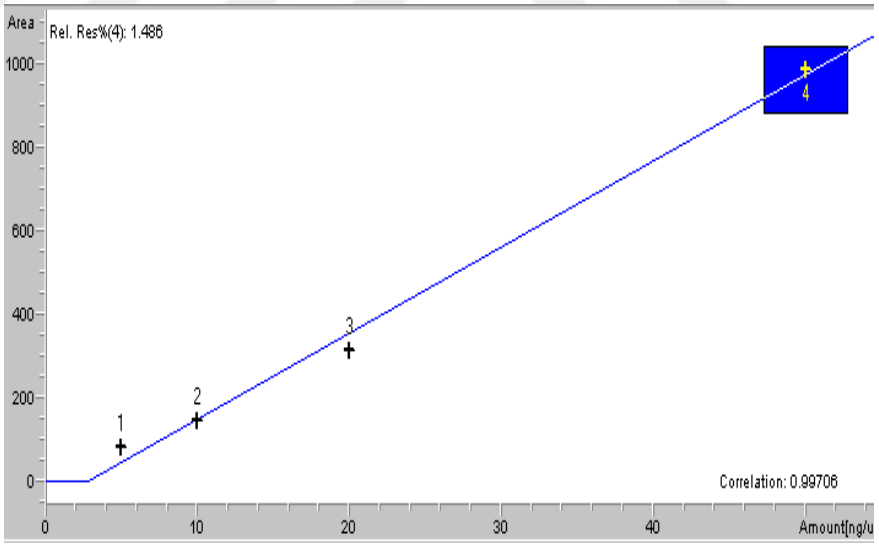


Figure 5.10 Calibration graph of POF (9-piperazino ofloxacin)

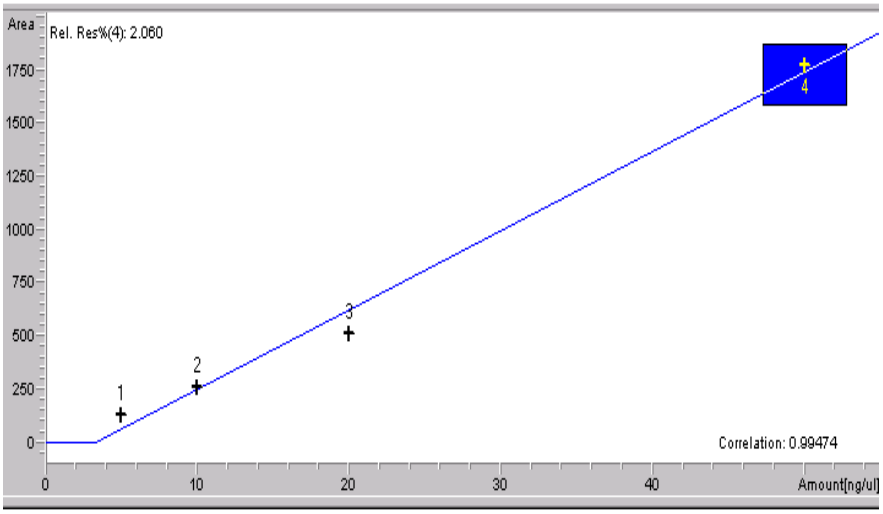


Figure 5.11 Calibration graph of MOF (des-methyl ofloxacin)

## 5.6 Instrumental Characterization

### *5.6.1 X-ray diffraction (XRD)*

XRD measurements were carried out with the D/max-2200 PC (Rigaku, Japan), using Cu-Ka radiation for photocatalytic processes.

### *5.6.2 Fourier transform infrared (FT-IR)*

FT- IR spectra's of Nano-GO/M after different conditions applied were measured with the Perkin Elmer FTIR System Spectrum BX with the KBr method for photocatalytic processes.

### *5.6.3 SEM*

The morphological and structural observation was made on a scanning electron microscope VegaII/LMU (Tescan, Czech Republic) for photocatalytic processes.

## 5.7 Kinetic Studies

Adsorption is defined as a process which specific components attached the surface or the interface between the two phases (adsorbate (CIP and OFL) and adsorbent (Nano-GO/M)). If the adsorbent and adsorbate are contacted enough equilibrium will

be established between the amount of adsorbate adsorbed and the amount of adsorbate in solution. The equilibrium relationship could be described with isotherms. These isotherms can then be used to predict the performance of the adsorption contact processes under a range of operating conditions. In this study, Langmuir isotherm, Freundlich isotherm, Temkin isotherm, Dubinin–Radushkevich and Flory-Huggins isotherm were used for the adsorption of CIP and OFL to Nano-GO/M composites.

### *5.7.1 Langmuir Isotherm*

The Langmuir adsorption isotherm is often expressed as equation (5.2);

$$q_e = \frac{qm.KL.Ce}{1+KL.Ce} \tag{5.2}$$

The Langmuir constants, $K_L$ and $q_m$ were calculated by the linearization of Eq. (5.2): This gives the Eq. (5.3)

$$\frac{C_e}{q_e} = \frac{1}{b.q_m} + \frac{C_e}{q_m} \tag{5.3}$$

where $q_e$ is the capacity of adsorbent (mg/g), $C_e$ is the initial and equilibrium liquid concentrations (mg/L), $q_m$ is the maximum capacity of adsorbent, respectively; $K_L$ is the Langmuir isotherm constant.

### *5.7.2 Freundlich Isotherm*

This model indicates that it is a special occasion for heterogenic surface energies as b turned into a function of $q_e$ (Freundlich &H.M.F, 1906). The linearized form of the Freundlich isotherm is given by the Eq. (5.4):

$$lnq_e = lnK_F + \frac{1}{n} lnC_e \tag{5.4}$$

$C_e$: Effluent CIP concentration (mg/L)

$q_e$: CIP amount adsorbed on unit adsorbent (mg/g)

$K_F$: Freundlich constant (unitlessss)

n: Adsorption intensity (unitlesss)

### *5.7.3 Temkin Isotherm*

According to Temkin isotherm reduction of adsorption temperature is linear while binding energy is homogenous (Temkin & Pyzhev, 1940) This isotherm was developed by considering adsorption temperature of all molecules in solution. Temkin isotherm equation is expressed as follows:

$$q_e = \frac{RT}{b}(lnAC_e) \tag{5.5}$$

The linearized form of the Temkin isotherm is given by the Eq. (5.6):

$$q_e = BlnA + BlnC_e \tag{5.6}$$

where B= RT/b is related to heat of adsorption, $q_e$ (mg/g) and $C_e$ (mg/L) are the amount of adsorbed CIP per unit weight of adsorbent and un-adsorbed CIP concentration in solution at equilibrium, A (L/mg) and B (J/mol) are the Temkin constants. The Temkin isotherm parameters were obtained by plotting $q_e$ versus $lnC_e$, respectively. The isotherm data were calculated from the least squares methods.

### *5.7.4 Dubinin-Radushkevich Isotherm*

The Dubinin–Radushkevich (D–R) equation can be explained based on Polanyi's potential theory of physical adsorption (Dubinin & Radushkevich, 1947). The D–R equation can include the effect of temperature as well as the properties of both adsorbent and adsorbate (Wood 2002). The linearized form of the D-R isotherm is given by the Eq. (5.7):

$$lnq_e = \ln X'_m - K'\varepsilon^2 \tag{5.7}$$

where;

$\varepsilon$ = RT ln (1+$\frac{1}{C_e}$) (Polanyi potential),

$X'_m$= adsorption capacity (mg/g),

K′= adsorption energy constant (mol$^2$ kJ$^{-2}$),

R= ideal gas constant (8.3145 J/ (mol K))

T= temperature (K)

### *5.7.5 Flory–Huggins Isotherm*

This model helps to account the degree of surface coverage characteristics of the CIP on the Nano-GO/M. The Flory-Huggins model is represented by Eq. (5.8) (Aniekeme-Abasi, Okon, Saviour & Ubong, 2013):

$$\log\frac{\theta}{C_0} = \log Ka + n\log(1-\theta) \tag{5.8}$$

Where θ is the degree of surface coverage (unitless), n is the number of CIP/OFL ions occupying sorption sites, Ka is the equilibrium constant of adsorption (L/g) and C is equilibrium CIP/OFL ion concentration (mg/L). A plot of log θ/$C_0$ against log (1 - θ) is linear if the adsorption process conforms to this model. The equilibrium constant Ka and n are obtained from the intercept and slope of the plot respectively. The θ in Eq. (5.9) was calculated from the relation below:

$$\theta = 1 - \frac{C_e}{C_0} \tag{5.9}$$

## 5.8 Investigation of Photocatalytic Degradation Kinetic of CIP and OFL Using Nano-GO/M Composite

### *5.8.1 Zero-Order Reaction Kinetics*

A zero order reaction has a rate that is independent of the concentration of the reactants. Increasing the concentration of the reacting species will not speed up the rate of the reaction i.e. the amount of substance reacted is proportional to the time. Zero order reactions are typically found when a material that is required for the

reaction to proceed, such as a surface or a catalyst, is saturated by the reactants. The rate law for a zero order reaction is:

$$r = k \tag{5.10}$$

where r is the reaction rate and k is the reaction rate coefficient with units of concentration or time. If, and only if, this zeroth order reaction;
1) occurs in a closed system,
2) there is no net build-up of intermediates,
3) there are no other reactions occurring, it can be shown by solving a mass balance equation for the system that:

$$r = -\frac{d[A]}{dt} = k$$

If this differential equation is integrated, it gives an equation often called the integrated zero order rate law.

$$[A]_t = -kt + [A]_0 \tag{5.11}$$

where $[A]_t$ represents the concentration of the chemical of interest at a particular time, and $[A]_0$ represents the initial concentration (Wikipedia, 2016a).
(5.11) is in the form y = mx+b where slope = m = -k and the y-intercept = b = $[A]_0$

where $A_0$ is the influent concentration of CIP/OFL and A is the effluent concentration of CIP/OFL (mg/L) at any time t (min), respectively and $k_0$ is the constant of pseudo-zero-order reaction ($min^{-1}$).

### *5.8.2 First-order Reaction Kinetics*

A first order reaction depends on the concentration of only one reactant (a unimolecular reaction). Other reactants can be present, but each will be zero order. The rate law for a reaction that is first order with respect to a reactant A is;

$$\frac{-d[A]}{dt} \equiv r = k[A] \quad (5.12)$$

*k* is the first order rate constant, which has units of 1/s. The integrated first order rate law is:

$$\ln [A] = -kt + \ln[A]_0 \quad (5.13)$$

A plot of $\ln[A]_0$ vs. time *t* gives a straight line with a slope of -k (Wikipedia, 2016a).

where $A_0$ is the influent concentration of CIP/OFL and A is the effluent concentration of CIP/OFL (mg/L) at any time t (min), respectively and $k_1$ is the constant of pseudo-firs-order reaction ($min^{-1}$).

### *5.8.3 Second-Order Reaction Kinetics*

A second order reaction depends on the concentrations of one second order reactant, or two first order reactants (Wikipedia, 2016a).
Its reaction rate is given by:

$$\frac{1}{[A]} = \frac{1}{[A]_0} + kt \quad (5.14)$$

where $A_0$ is the influent concentration of CIP/OFL and A is the effluent concentration of CIP/OFL (mg/L) at any time t (min), respectively and $k_2$ is the constant of pseudo-second- order reaction ($min^{-1}$).

## 5.9 Statistical Analysis

Regression analysis is widely used for prediction and forecasting, where its use has substantial overlap with the field of machine learning. Regression analysis is used to understand which among the independent variables are related to the dependent variable, and to explore the forms of these relationships. In restricted circumstances, regression analysis can be used to infer causal relationships between the independent

and dependent variables (Wikipedia, 2016b). Regression analysis were performed using MS Office 2010 Excell program.

**Analysis of variance** (**ANOVA**) is a collection of statistical models used to analyze the differences among group means and their associated procedures (such as "variation" among and between groups). In the ANOVA setting, the observed variance in a particular variable is partitioned into components attributable to different sources of variation. In its simplest form, ANOVA provides a statistical test of whether or not the means of several groups are equal, and therefore generalizes. ANOVAs are useful for comparing the analysis result for statistical significance. The *F* statistic is a ratio of a numerator to a denominator. Consider randomly selected subjects that are subsequently randomly assigned to groups A, B, and C. Under the truth of the null hypothesis, the variability (or sum of squares) of scores on some dependent variable will be the same within each group. When divided by the degrees of freedom (i.e., based on the number of subjects per group), the denominator of the *F* ratio is obtained. Under the truth of the null hypothesis, the sampling distribution of the F ratio depends on the degrees of freedom for the numerator and the denominator. Alpha (α) level is the significance of the ANOVA statistic. In the study α was accepted as 0.05. F value of analysis were performed using MS Office 2010 Excell program.

# CHAPTER SIX
# RESULT AND DISCUSSION

## 6.1 Physicochemical Properties of Nano-GO/M

### *6.1.1 Fourier Transform Infrared (FTIR) Analyses Results*

The produced nano particles (raw Nano-GO/M composite) and treated samples of CIP and OFL with UV and sunlight were characterized using Fourier transform infrared spectroscopy (FTIR). UV experiments were realized after 30 min (CIP) and 60 min (OFL) irradiation times, with 0.5 g/L Nano-GO/M composite, at original pH of solutions (6.5 for both CIP and OFL), at 21ºC and under 300 W UV light. Sunlight experiments were conducted after 250 min (CIP) and 350 min (OFL) irradiation times, with 2 g/L Nano-GO/M composite, at original pH of solutions (6.5 for both CIP and OFL), at 35ºC±5ºC and under 80 W sunlight. Figure 6.5, 6.6 and 6.7 shows the FTIR analysis of GO, $Fe_3O_4$ and Nano-GO/M composites, respectively. From Figure 6.1, it can be seen that the most characteristic features in the FTIR spectrum of GO are the adsorption bands corresponding to the C=O carbonyl stretching at 1714 $cm^{-1}$, the C–OH stretching at 1188 $cm^{-1}$, and the C–O stretching at 1041 $cm^{-1}$ (Stankovich et al., 2006). The presence of these oxygen containing groups reveals that the graphite has been oxidized. The polar groups, especially the surface hydroxyl groups, result in the formation of hydrogen bonds between graphite and water molecules. These properties explain the hydrophilic nature of graphene oxide (Shahriary & Athawale, 2014).

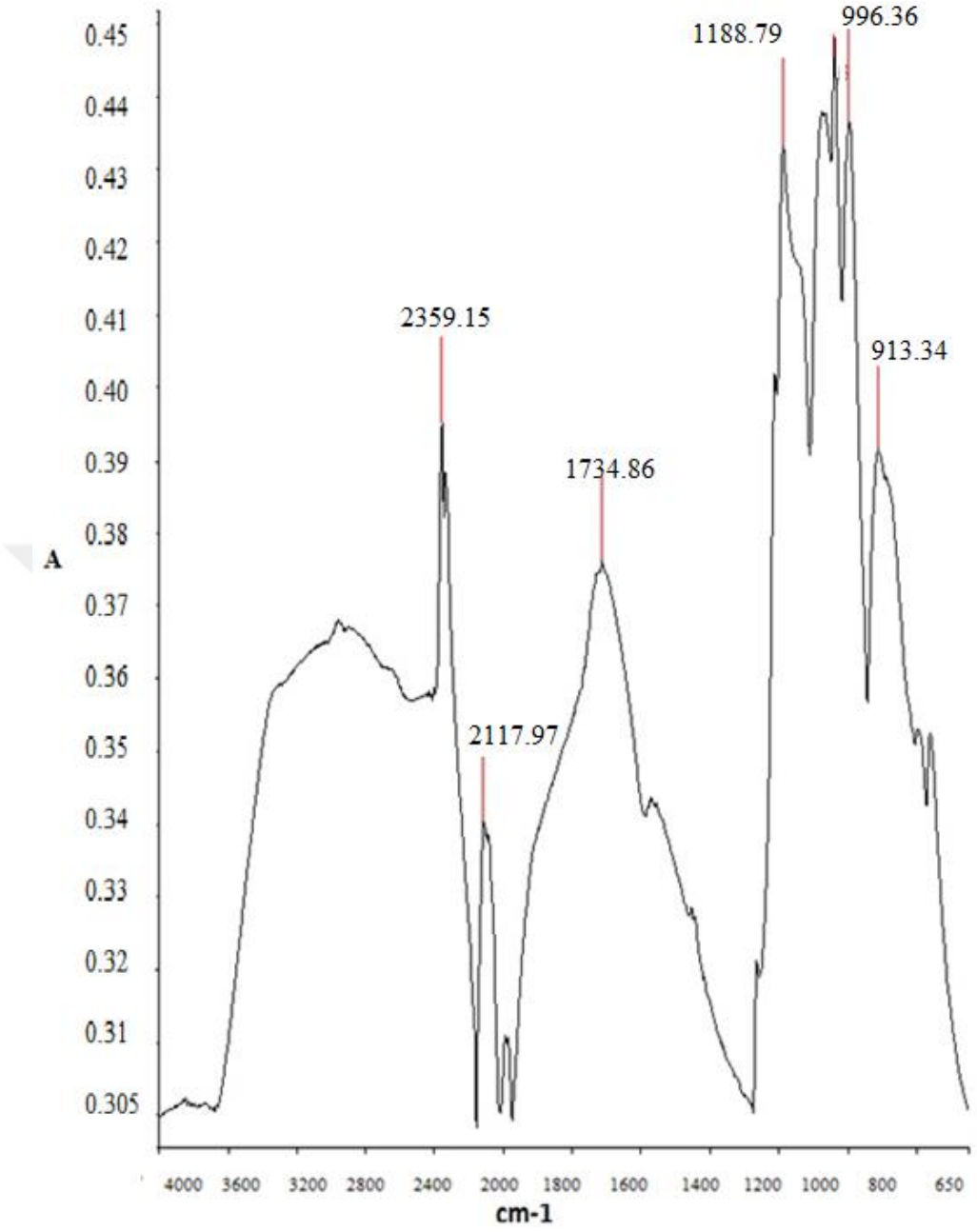


Figure 6.1 FTIR analysis of synthesized GO ($cm^{-1}$: wave number and A-%: percent transmittance)

Figure 6.2 shows the FTIR spectra of $Fe_3O_4$. The peaks at 3536.53 $cm^{-1}$ and 562.26 $cm^{-1}$ were related to O-H stretching and Fe-O stretching band, respectively. The FT-IR spectrum of modified magnetite nano-particles verifies the existence of C-H and S-H groups at 2919.70 $cm^{-1}$ and 2193.74 $cm^{-1}$, respectively (Panahi & Alaei, 2014).

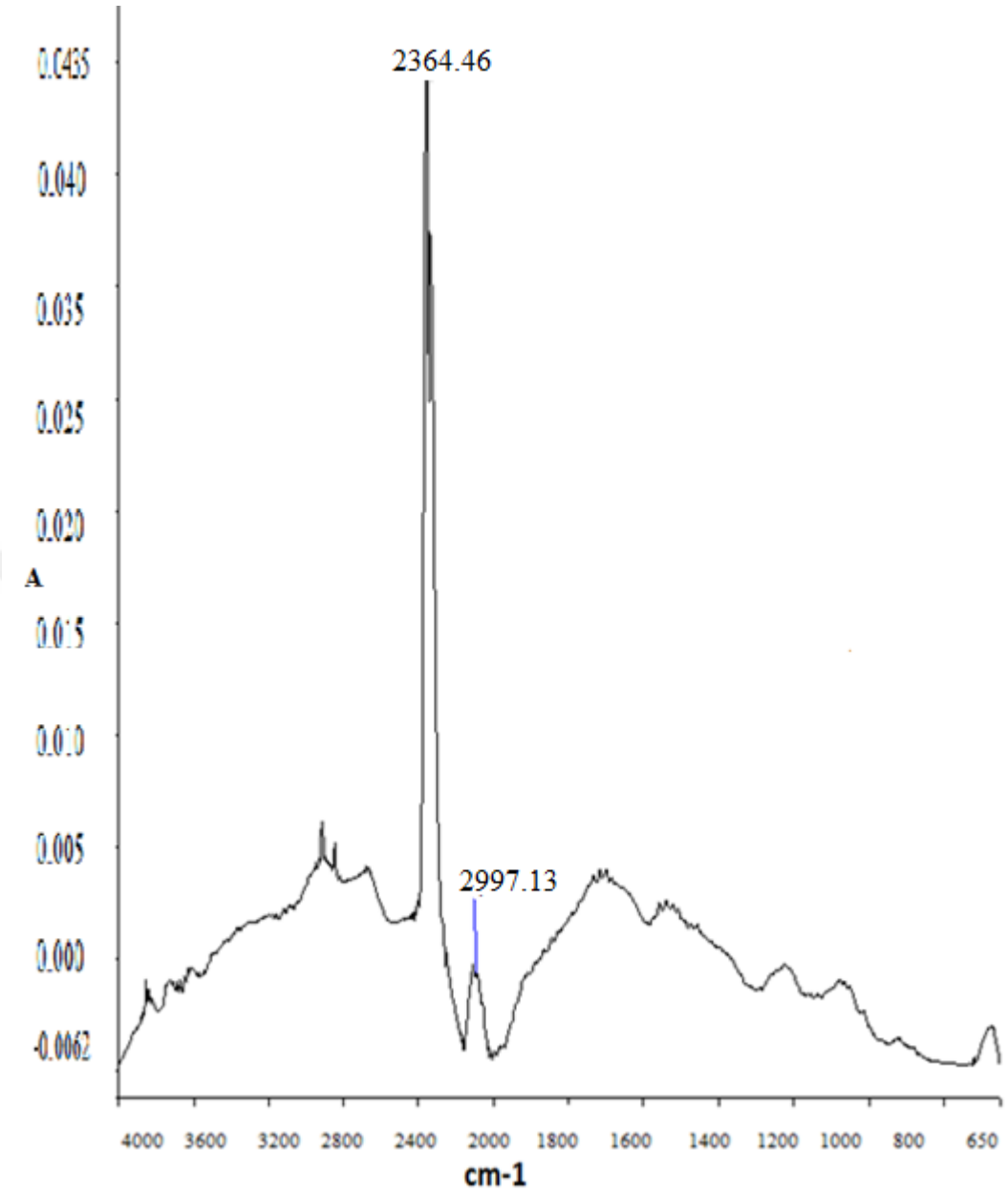


Figure 6.2 FTIR analysis of raw $Fe_3O_4$ ($cm^{-1}$: wave number and A-%: percent transmittance)

Figure 6.3 shows the peaks of GO plotted between wave number $(cm)^{-1}$ and percent transmittance (A-%). In the spectrum of Nano-GO/M, the peaks at 2359, 1568 $cm^{-1}$ are the characteristics spectrum of benzene ring of Nano-GO/M while the peak at 1073 $cm^{-1}$ is the characteristic spectrum of the C–OH rings of Nano-GO/M. This confirms the presence of graphene oxide peak at 600 $cm^{-1}$ which is the characteristics of $Fe_3O_4$ giving an evidence of the successful preparation of the Nano-GO/M as reported by Huamin et al., (2012).

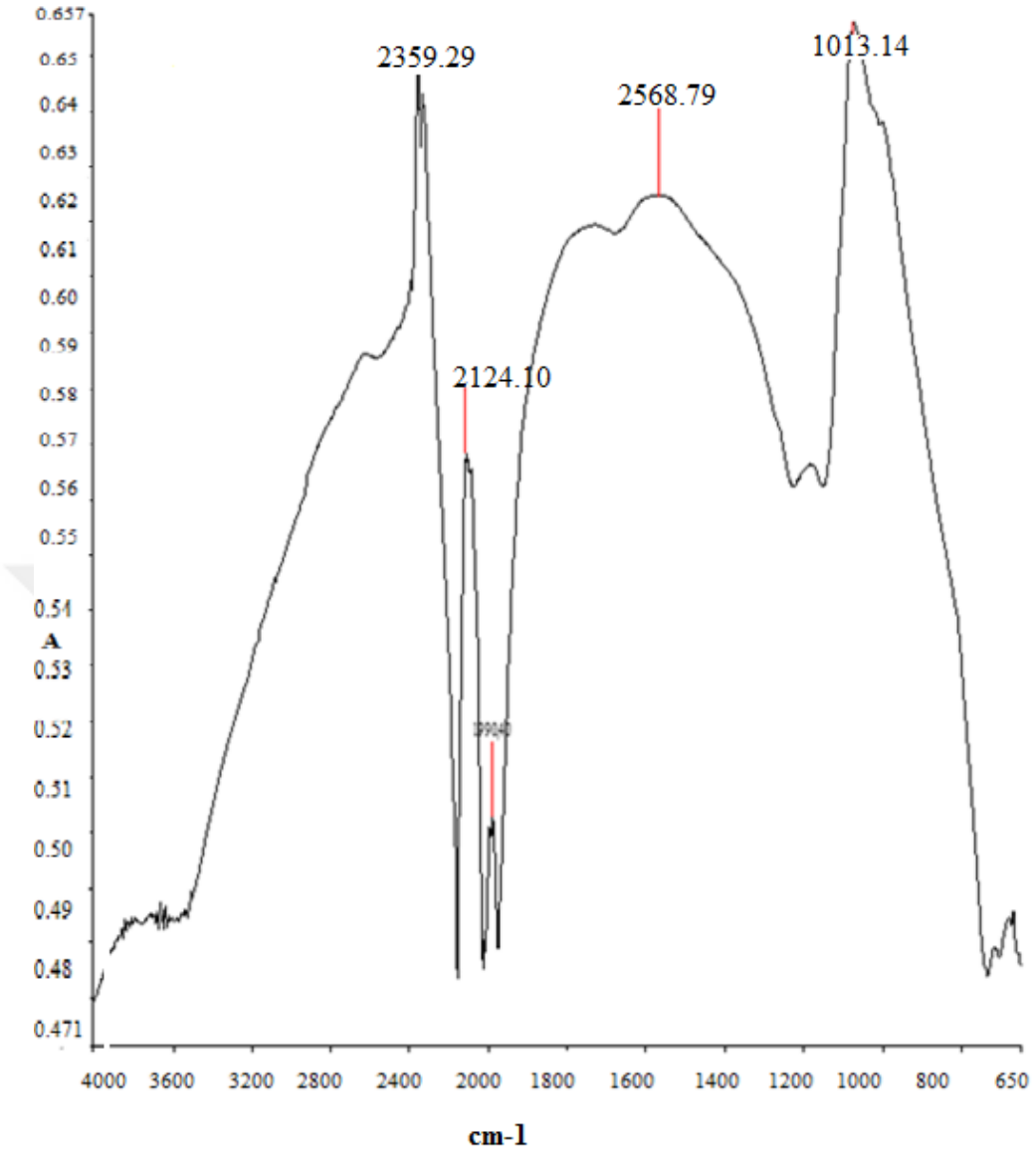


Figure 6.3 FTIR analysis of raw Nano-GO/M ($cm^{-1}$: wave number and A-%: percent transmittance)

### *6.1.1.1 FTIR spectrum of CIP under UV light and Sunlight*

CIP photooxidation experiments were conducted in optimal conditions. In UV oxidation process, experiments were realized at optimum Nano-GO/M concentration (0.5 g/L), for initial 100 mg/L CIP concentration, at a pH of 6.5 and under 300 W UV light after 30 min irradiation time at 21ºC. In sunlight oxidation process, experiments were realized at optimum Nano-GO/M concentration (2 g/L), for initial 100 mg/L CIP concentration, at a pH of 6.5 and under 80 W sunlight after 250 min irradiation time and at 35ºC±5. Figure 6.4 shows the FTIR analysis of Nano-GO/M composite after CIP treatment with UV. The maximum peaks obtained in this figure are similar to the

nano composite before UV treatment. Condensation of Nano-GO/M composite remained almost the same after UV treatment. This shows that Nano-GO/M composite can be recovered and can be used again for the treatment CIP with UV. From figure 6.5, it can be seen that the CIP binds to the surface of Nano-GO/M composite after sunlight irradiation. As a result, the peak number in the Nano-GO/M composite decreases in the amorphous shape.

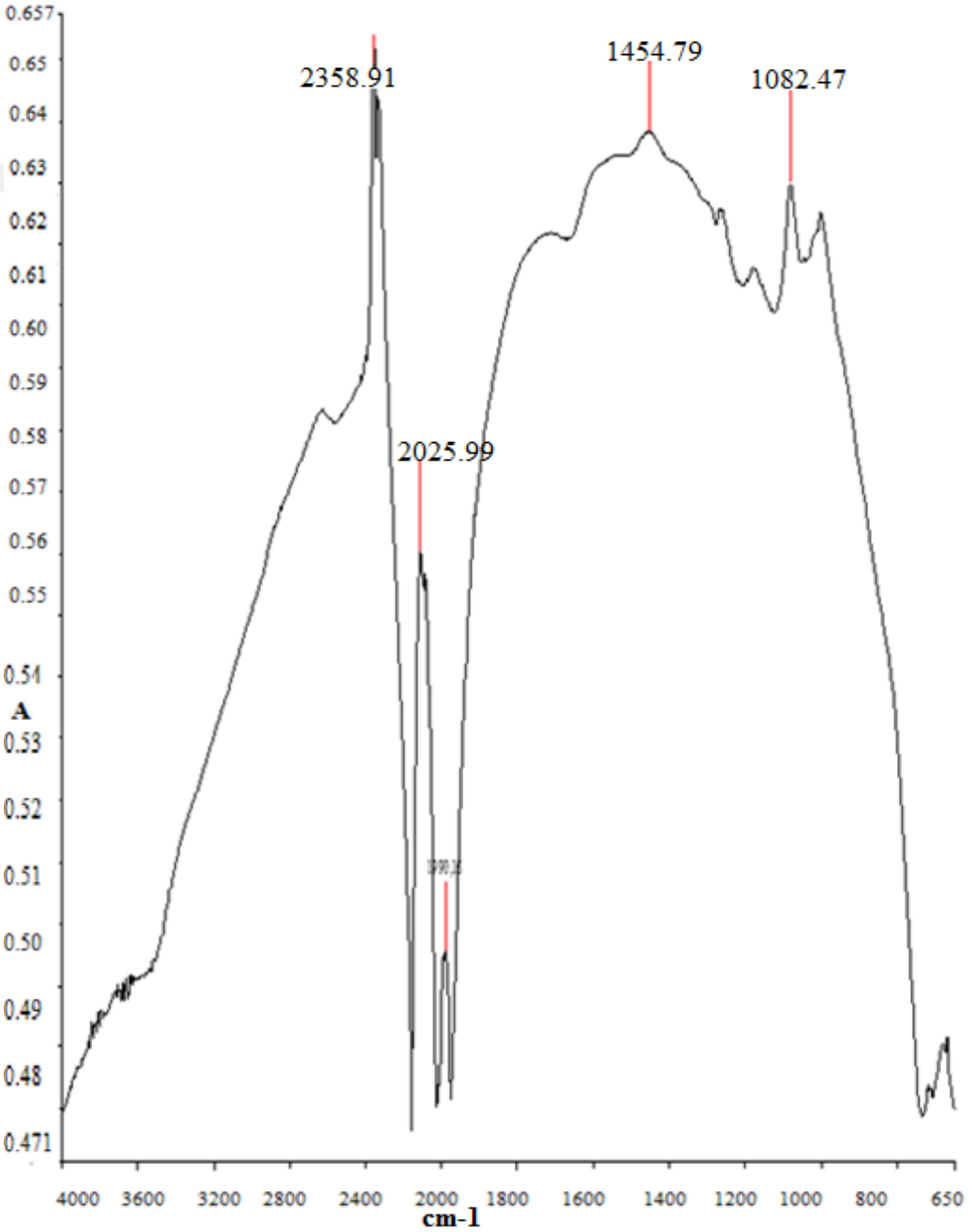


Figure 6.4 FTIR analysis of Nano-GO/M (0.5 g/L) after UV treatment (300 W) of CIP (100 mg/L), at pH=6.5, at 21ºC after 30 min irradiation time ($cm^{-1}$: wave number and A-%: percent transmittance)

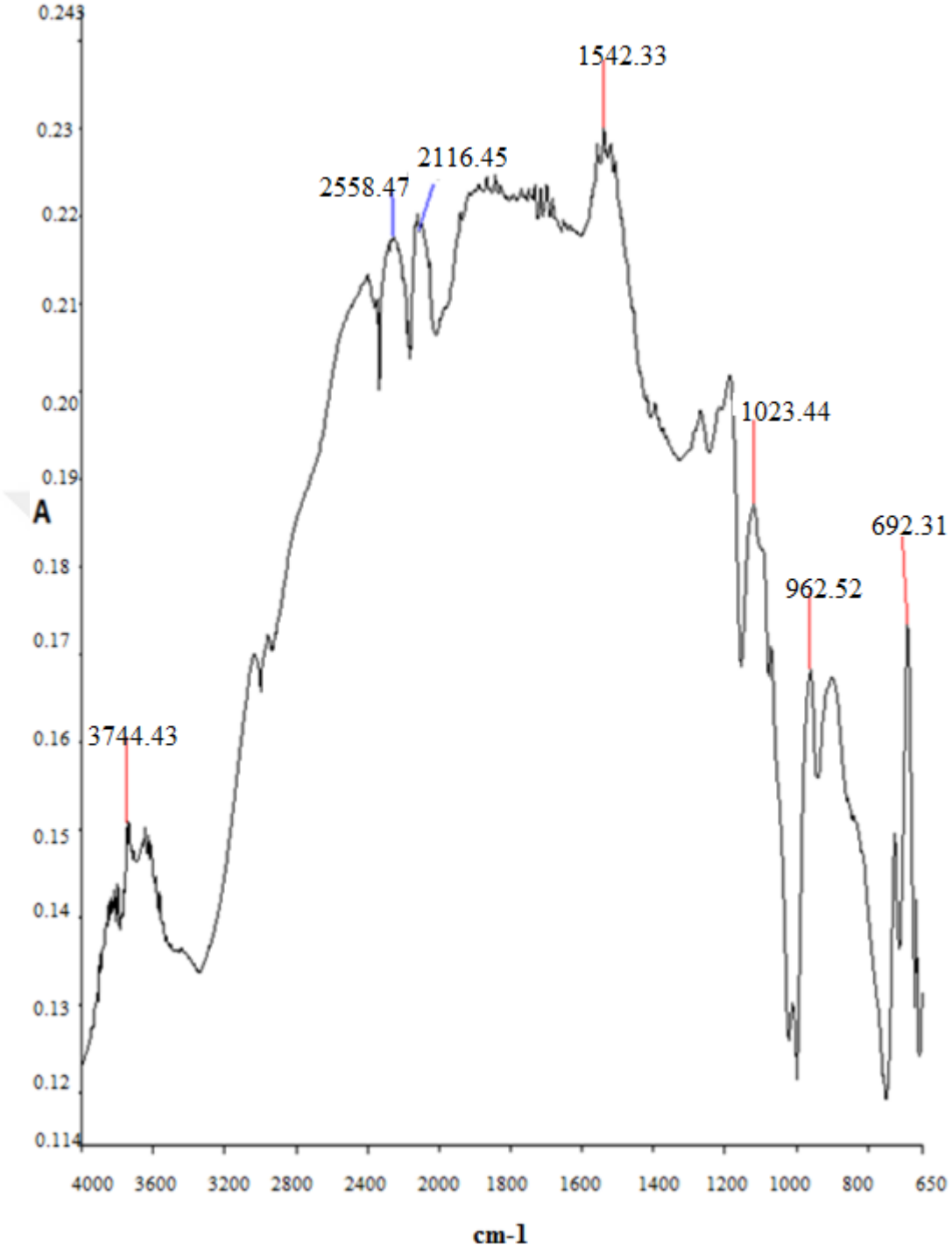


Figure 6.5 FTIR analysis of Nano-GO/M (2 g/L) after sunlight treatment (80 W) of CIP (100 mg/L), at pH=6.5, at 35ºC±5 after 250 min irradiation time ($cm^{-1}$: wave number and A-%: percent transmittance)

### *6.1.1.2 FTIR spectrum of OFL under UV light and Sunlight*

OFL photooxidation experiments were conducted in optimal conditions. In UV oxidation process, experiments were realized at optimum Nano-GO/M concentration

(0.5 g/L), for initial 100 mg/L OFL concentration, at a pH of 6.5 and under 300 W UV light after 60 min irradiation time at 21ºC. In sunlight oxidation process, experiments were realized at optimum Nano-GO/M concentration (2 g/L), for initial 100 mg/L OFL concentration, at a pH of 6.5 and under 80 W sunlight after 350 min irradiation time and at 35ºC±5. Figure 6.6 shows the FTIR analysis of Nano-GO/M composite after OFL treatment with UV. The maximum peaks obtained in this figure are similar to the nano composite before UV treatment. Condensation of Nano-GO/M composite remained almost the same after UV treatment. After sunlight experiments, Nano-GO/M structure has turned to amorphous shape (Figure 6.7). It may be due to sunlight has wide spectrum in comparison to UV light and thus, sunlight might be changed the structure of Nano-GO/M.

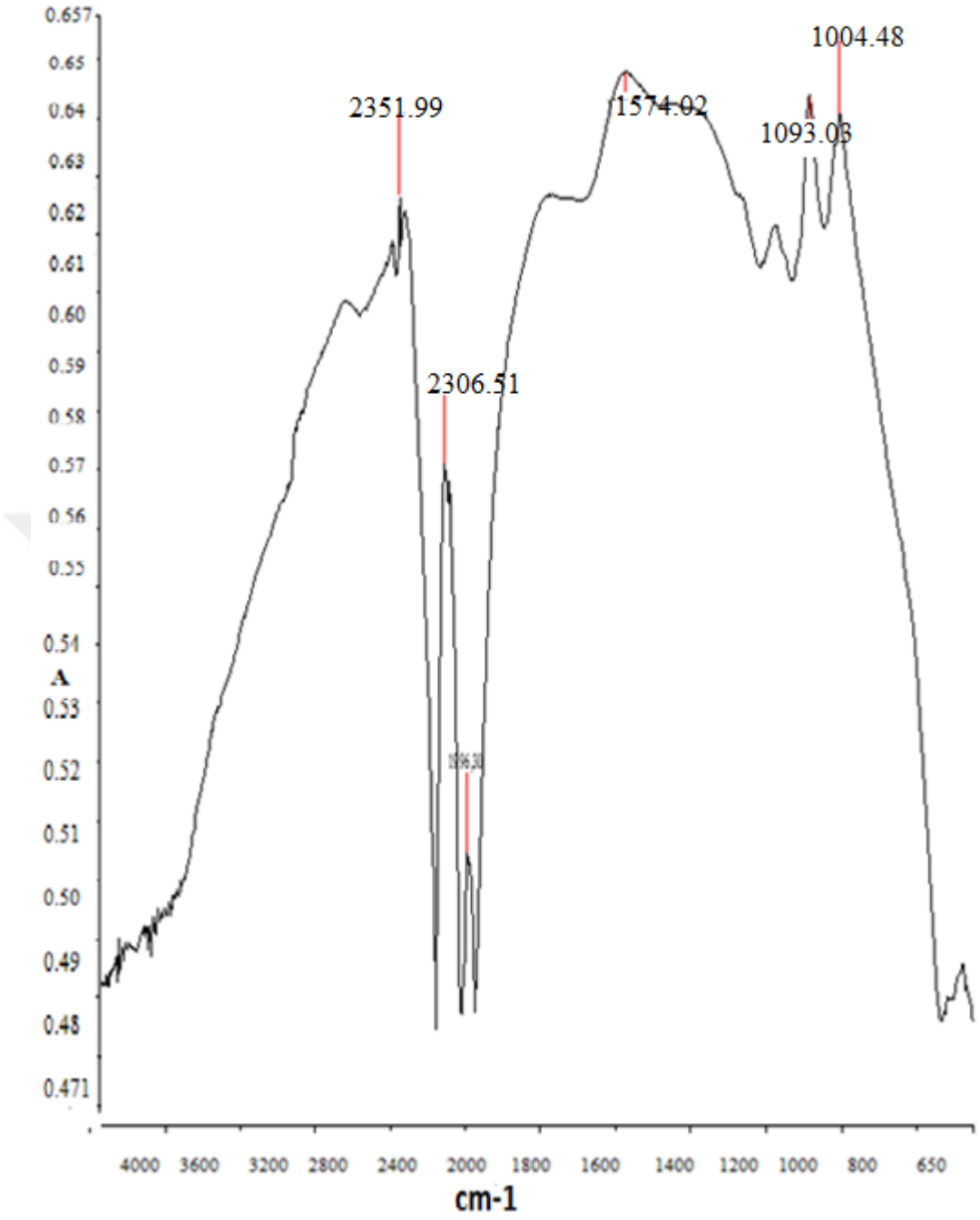


Figure 6.6 FTIR analysis of Nano-GO/M (0.5 g/L) after UV treatment (300 W) of OFL (100 mg/L), at pH=6.5, at 21ºC after 60 min irradiation time ($cm^{-1}$: wave number and A-%: percent transmittance)

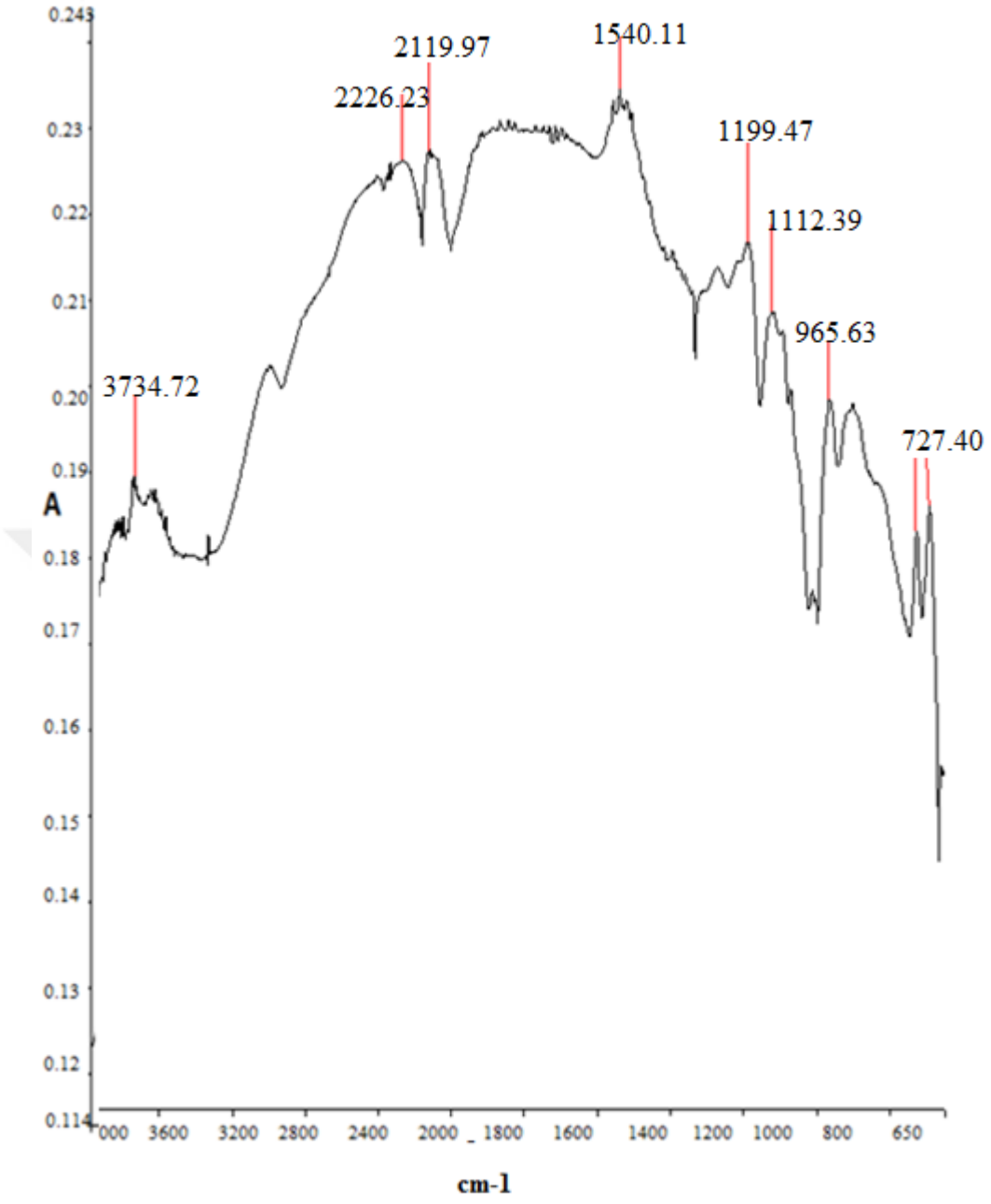


Figure 6.7 FTIR analysis of Nano-GO/M (2 g/L) after sunlight treatment (80 W) of OFL (100 mg/L), at pH=6.5, at 35ºC±5 after 350 min irradiation time ($cm^{-1}$: wave number and A-%: percent transmittance)

### *6.1.2 Scanning Electron Microscope (SEM) Analysis Results*

The SEM images of synthesized GO, $Fe_3O_4$ nanoparticles, raw and treated 0.5 g/L Nano-GO/M composites under UV for photodegradation of 100 mg/L CIP after 30 min irradiation under 300 W UV power at 21°C. Figure 6.8, shows the GO structure

which was in a sheet form. $Fe_3O_4$ nanoparticles are as small dots onto GO sheets (Figure 6.9). The $Fe_3O_4$ sample composed of spherical particles with a size of approximately 20 nm and GO was composed wrinkled sheets (Zhang et al., 2015). Many $Fe_3O_4$ microspheres were firmly anchored on both sides of the wrinkled graphene sheets (Figure 6.10). The graphene layers might contribute to hinder the $Fe_3O_4$ microspheres forming aggregation as reported by Tang et al. (2013) (Figure 6.9). The $Fe_3O_4$ particles disperse on GO and there are some interspaces among them (Figure 6.10). After assembly, Nano-GO/M composites maintained their's spherical morphology. $Fe_3O_4$ and GO dispersed densely and evenly on the surface of the Nano-GO/M composites and it have a core shell structure (Figure 6.10).

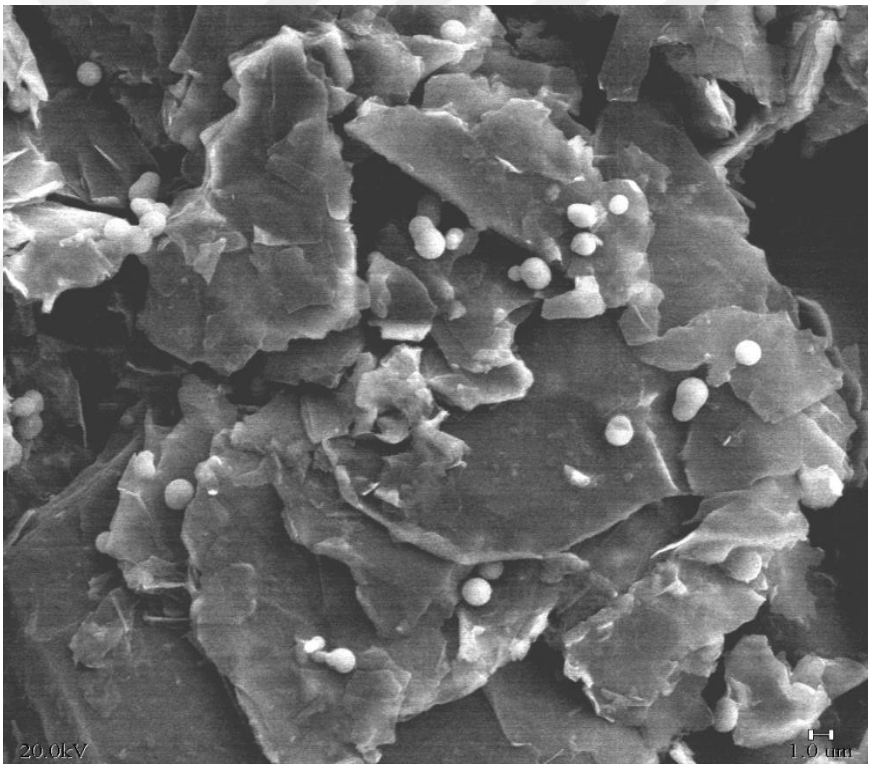


Figure 6.8 SEM imagine of synthesized GO (1 μm)

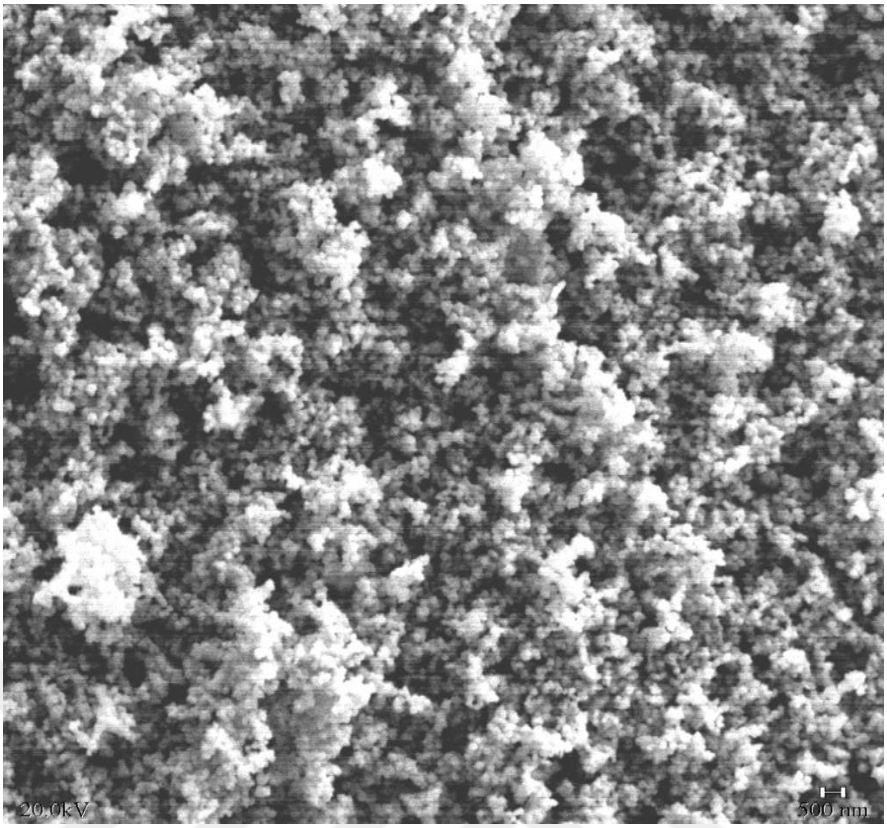


Figure 6.9 SEM imagine of $Fe_3O_4$ (500 nm)

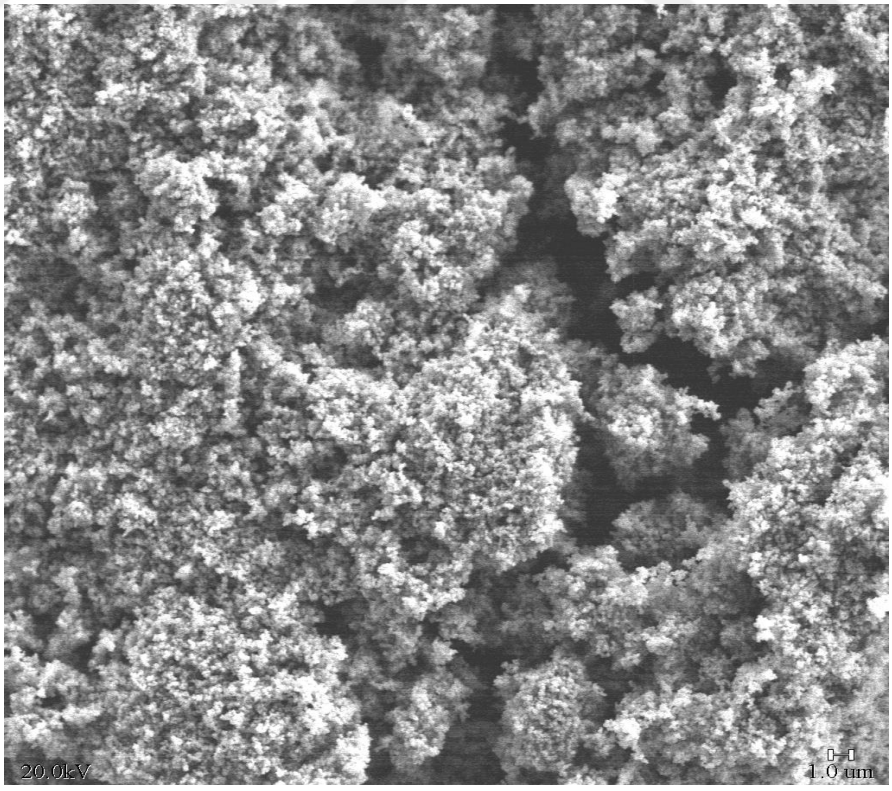


Figure 6.10 SEM imagine of raw Nano-GO/M (1 μm)

### *6.1.2.1 SEM Imagines of Nano-GO/M after UV and Sunlight Irradiation with CIP*

CIP photooxidation experiments were conducted in optimal conditions. In UV oxidation process, experiments were realized at optimum Nano-GO/M concentration (0.5 g/L), for initial 100 mg/L CIP concentration, at a pH of 6.5 and under 300 W UV light after 30 min irradiation time at 21ºC. In sunlight oxidation process, experiments were realized at optimum Nano-GO/M concentration (2 g/L), for initial 100 mg/L CIP concentration, at a pH of 6.5 and under 80 W sunlight after 250 min irradiation time and at 35ºC±5. Figure 6.11 shows the SEM imagine of Nano-GO/M composite after CIP treatment with UV. Figure 6.12. represents the SEM imagine of Nano-GO/M composite after CIP treatment with sunlight irradiation. Color of Nano-GO/M composite turns to grey after treatment of CIP under UV and sunlight irradiation and surface of composite fills with CIP as illustrated in Figure 6.15 and Figure 6.16. The average particle size was measured about 400 nm and 200 μm for Nano-GO/M composite and UV irradiated Nano-GO/M composite, respectively. After sunlight irradiation average particle size was measured about 350 μm.

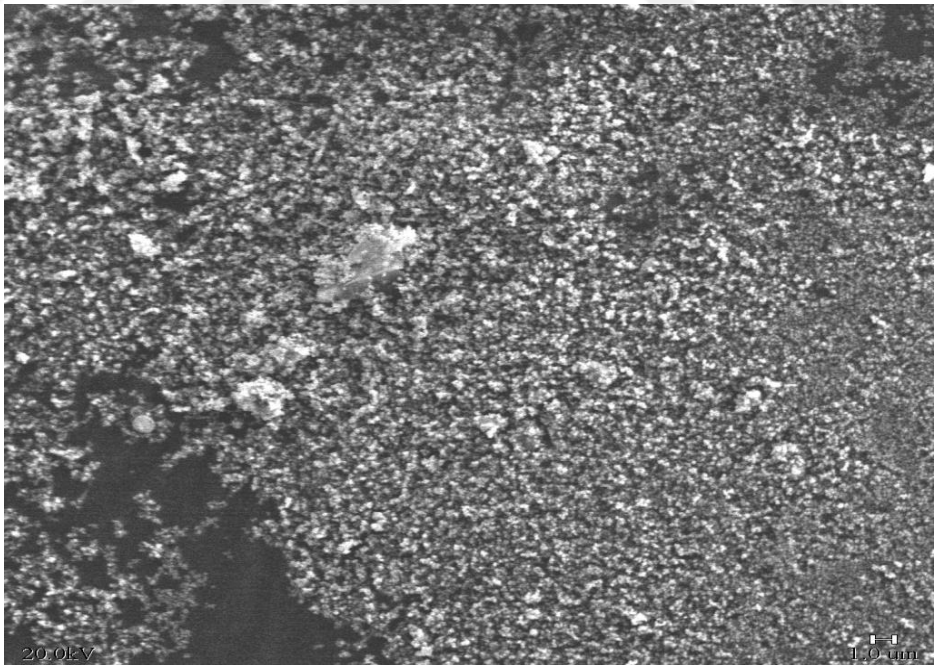


Figure 6.11 SEM imagine of Nano-GO/M (0.5 g/L) after UV treatment (300 W) of CIP (100 mg/L), at pH=6.5, at 21ºC after 30 min irradiation time (1 μm)

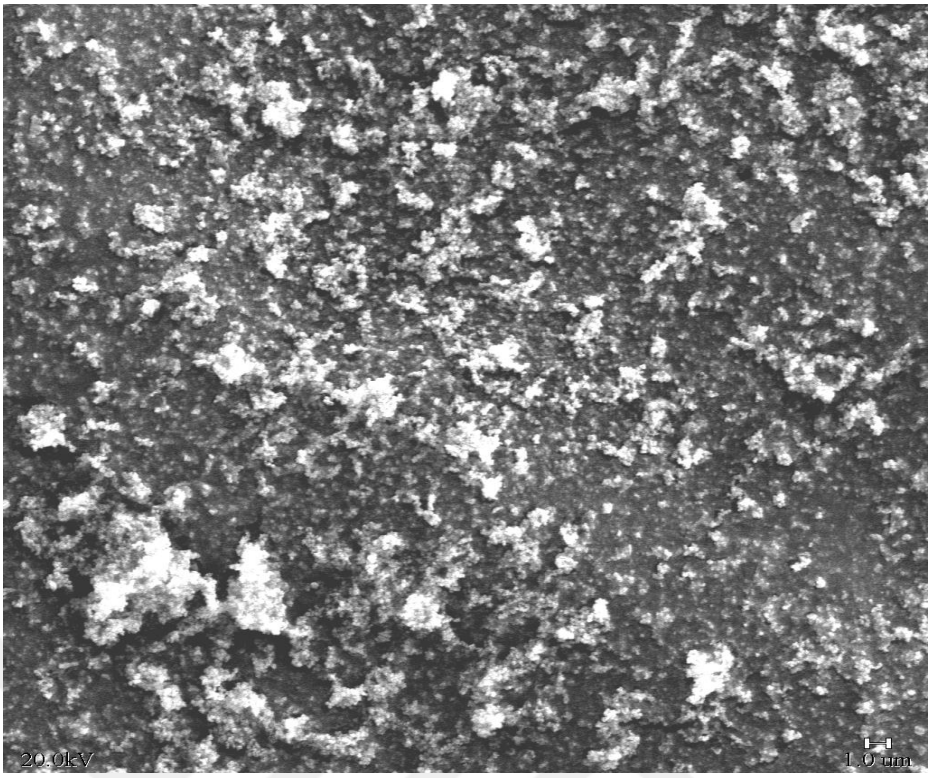


Figure 6.12 SEM imagine of Nano-GO/M (2 g/L) after sunlight treatment (80 W) of CIP (100 mg/L), at pH=6.5, at 35ºC±5 after 250 min irradiation time (1 µm)

### *6.1.2.2 SEM Imagines of Nano-GO/M after UV and Sunlight Irradiation with OFL*

OFL photooxidation experiments were conducted in optimal conditions. In UV oxidation process, experiments were realized at optimum Nano-GO/M concentration (0.5 g/L), for initial 100 mg/L OFL concentration, at a pH of 6.5 and under 300 W UV light after 60 min irradiation time at 21ºC. In sunlight oxidation process, experiments were realized at optimum Nano-GO/M concentration (2 g/L), for initial 100 mg/L OFL concentration, at a pH of 6.5 and under 80 W sunlight after 350 min irradiation time and at 35ºC±5. Figure 6.13. shows the SEM imagine of Nano-GO/M composite after OFL treatment with UV. Color of Nano-GO/M composite turns to grey after treatment of CIP under UV and sunlight treatment surface of composite fills with OFL as illustrated in Figure 6.13 and Figure 6.14. The average particle size was measured about 400 nm and 250 µm for Nano-GO/M composite and UV irradiated Nano-GO/M composite, respectively. After sunlight irradiation average particle size was measured about 400 µm.

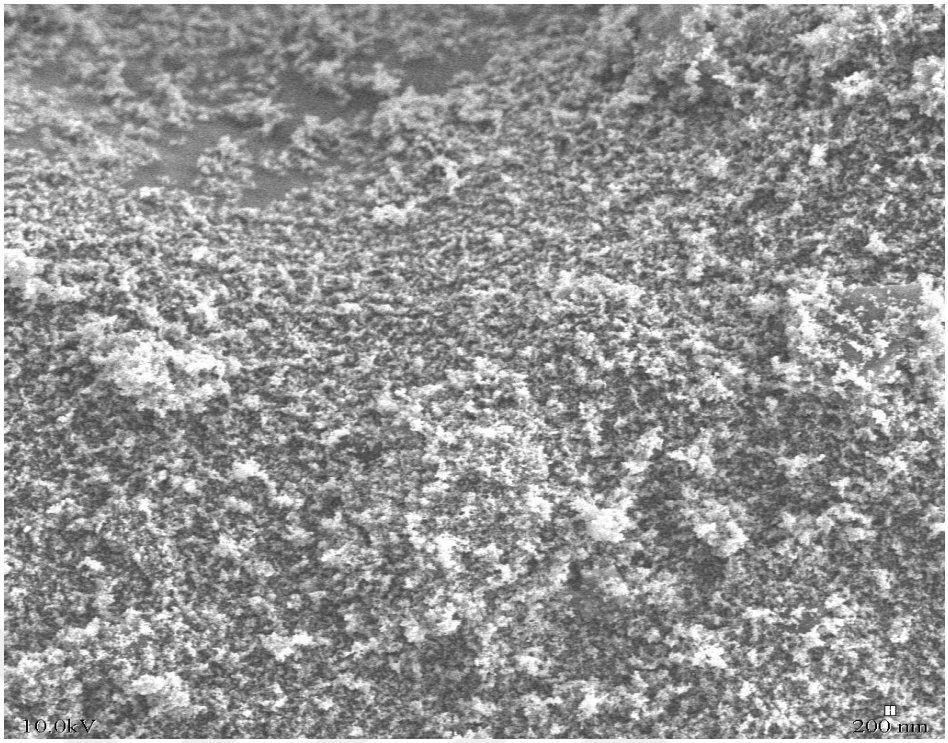


Figure 6.13 SEM imagine of Nano-GO/M (0.5 g/L) after UV treatment (300 W) of OFL (100 mg/L), at pH=6.5, at 21ºC after 60 min irradiation time (200 nm)

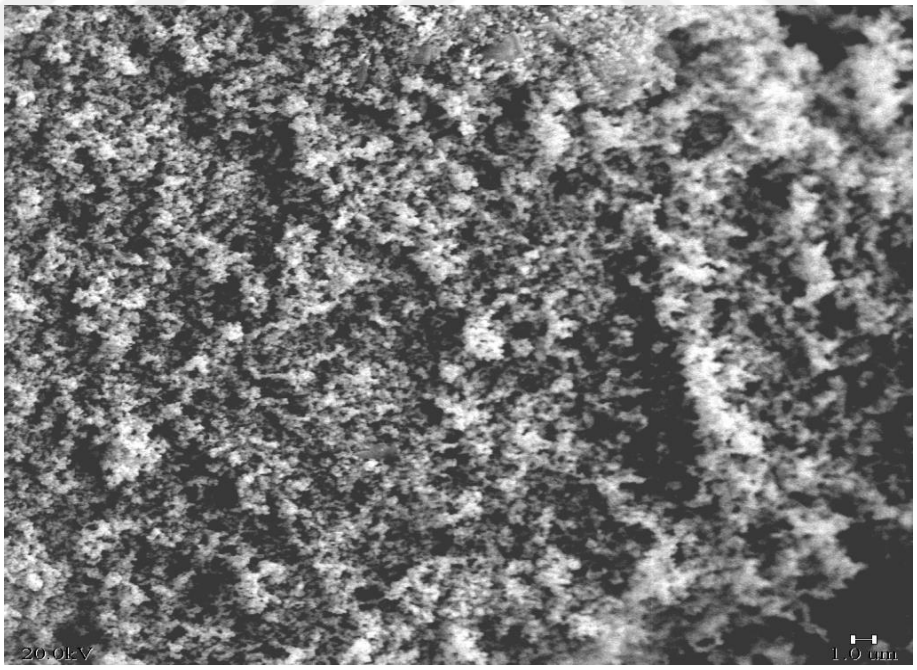


Figure 6.14 SEM imagine of Nano-GO/M (2 g/L) after sunlight treatment (80 W) of OFL (100 mg/L), at pH=6.5, at 35ºC±5 after 350 min irradiation time (1 µm).

### *6.1.3 X-Ray Diffraction (XRD) Analysis Results*

XRD analysis was used to study the composition of GO, magnetite, Nano-GO/M composite and Nano-GO/M composite which was used for UV treatment and sunlight treatment of both CIP and OFL.

#### *6.1.3.1 CIP Analysis*

The XRD spectra of magnetite nanoparticles, GO, raw Nano-GO/M composite and Nano-GO/M composite after CIP treatment under UV irradiation with 100 mg/L CIP concentration are shown in Figure 6.15. $Fe_3O_4$ and GO exhibited their characteristic diffraction peaks (Chandra et al., 2010). All of the diffraction peaks in the XRD pattern can be indexed as a pure cubic spine crystal structure of magnetite. The broadening diffraction peaks with high intensity indicated that the particles were highly crystalline and small in size. Furthermore, no obvious diffraction peak attributed to graphite was observed, which indicated that the stacking of graphene sheets remained disordered (Cong et al., 2009). As shown in this Figure series of characteristic peaks at the ranges at $2\theta$ = 30-32°, 35-37°, 43-45°, 53-55°, 57-59°, and 62-64° versus intensities (cps) were observed. These peaks were well matched of the crystal planes of $Fe_3O_4$. Results showed that Nano-GO/M composite was obtained successfully and the crystalline structure of $Fe_3O_4$ did not change during the synthesis as reported by Nengsheng et al., (2014). Experiments were realized at optimum Nano-GO/M concentration (0.5 g/L), for initial 100 mg/L CIP concentration, at a pH of 6.5 and under 300 W UV light after 30 min irradiation time.

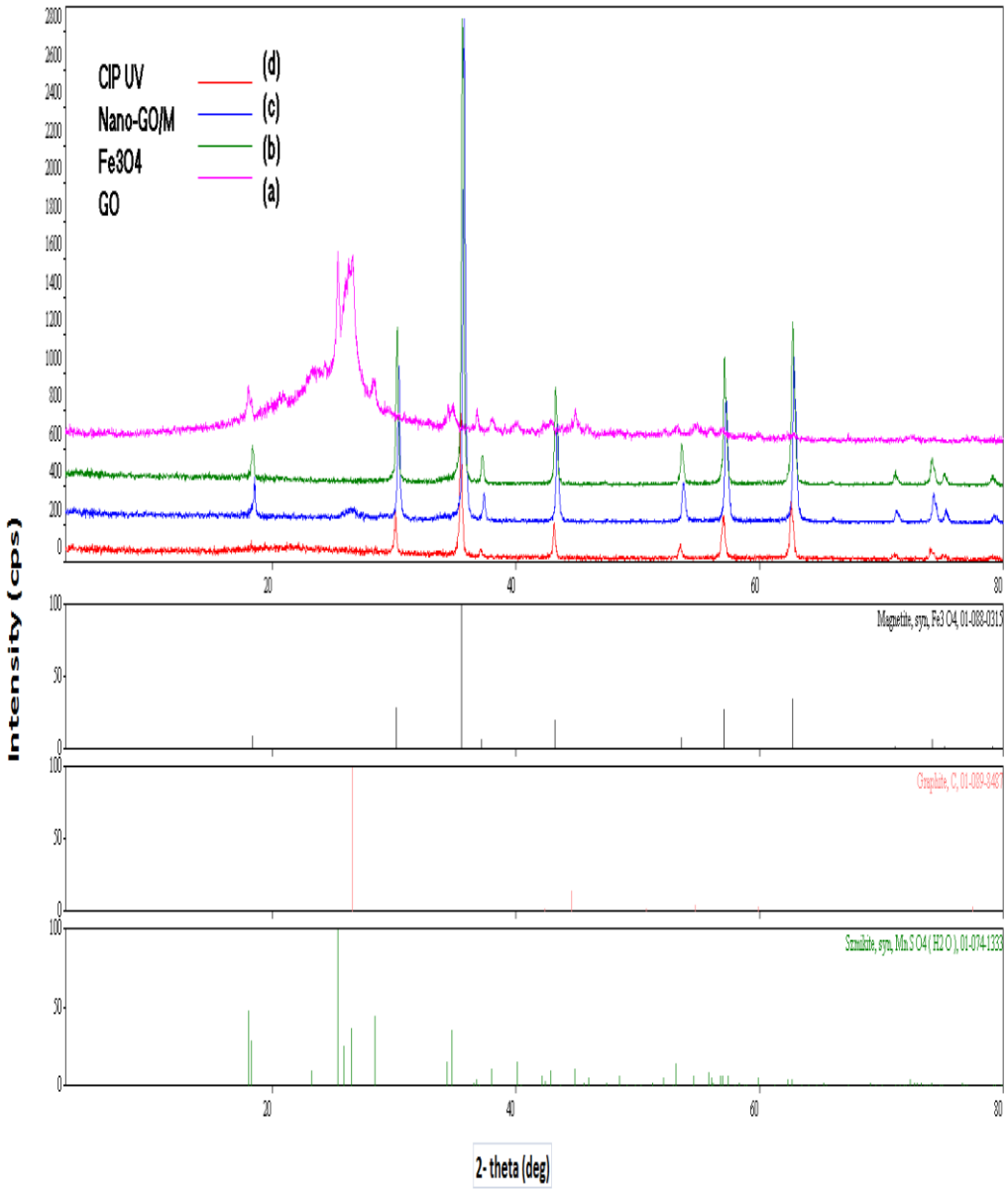


Figure 6.15 XRD analysis of GO (a), $Fe_3O_4$ (b) and Nano-GO/M composite before(c) and Nano-GO/M composite (0.5 g/L) composite after UV irradiation (30 min-300 W), with 100 mg/L CIP concentration (d) at pH=6.5

The comparison of XRD spectra of raw Nano-GO/M composite and Nano-GO/M composite after CIP treatment under UV irradiation (30 min- 300 W) and sunlight (250 min- 80 W) with 100 mg/L CIP concentration. As shown in Figure 6.16 series of characteristic peaks at the ranges at 2θ = 30-32°, 35-37°, 43-45°, 53-55°, 57-59°, and 62-64° versus intensities (cps) were observed. After UV and sunlight irradiations the crystal planes of $Fe_3O_4$ remained almost same. The structure of Nano-GO/M composite did not change considerably. UV experiments were realized at optimum Nano-GO/M

concentration (0.5 g/L), for initial 100 mg/L CIP concentration, at a pH of 6.5 and under 300 W UV light after 30 min irradiation time. Sunlight experiments were realized at optimum Nano-GO/M concentration (2 g/L), for initial 100 mg/L CIP concentration, at a pH of 6.5 and under 80 W UV light after 250 min irradiation time.

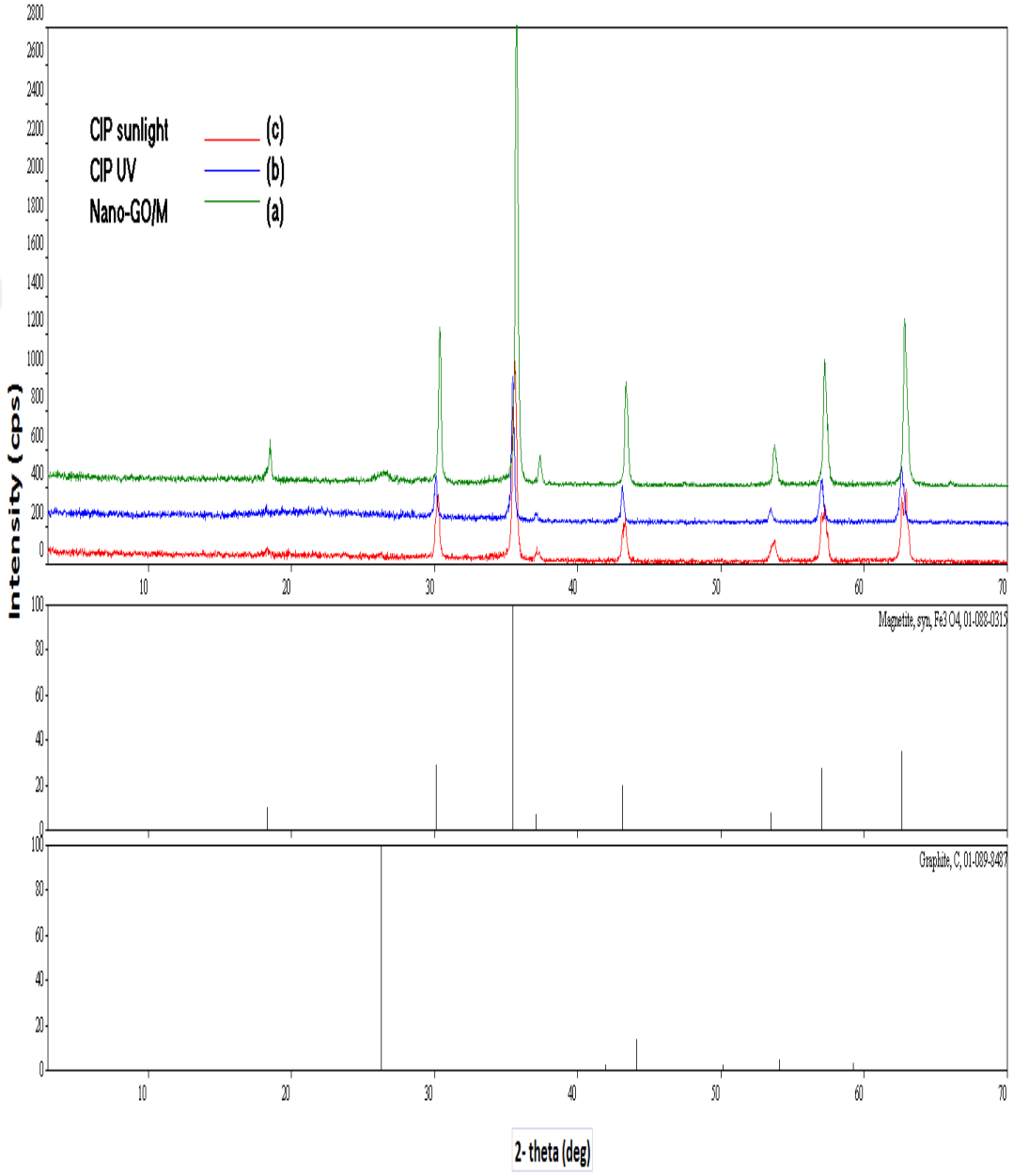


Figure 6.16 XRD analysis raw Nano-GO/M composite (a), Nano-GO/M (0.5 g/L) composite after UV irradiation (30 min-300 W) (b), Nano-GO/M (2 g/L) composite after sunlight (250 min- 80 W) with 100 mg/L CIP concentration (c) at pH=6.

*6.1.3.2 OFL Analysis*

The XRD spectra of magnetite nanoparticles, GO, raw Nano-GO/M composite and Nano-GO/M composite after OFL treatment under UV irradiation with 100 mg/L OFL concentration. As shown in Figure 6.17 series of characteristic peaks at the ranges at 2θ = 18-20°, 30-32°, 35-37°, 43-45°, 53-55°, 57-59°, and 62-64° versus intensities (cps) were observed. These peaks were well matched of the crystal planes of $Fe_3O_4$. Experiments were realized at optimum Nano-GO/M concentration (0.5 g/L), for initial 100 mg/L OFL concentration, at a pH of 6.5 and under 300 W UV light after 60 min irradiation time. The characteristic peaks of Nano-GO/M did not change considerably after UV irradiation. In this aspect, Nano-GO/M composite can be used again and again.

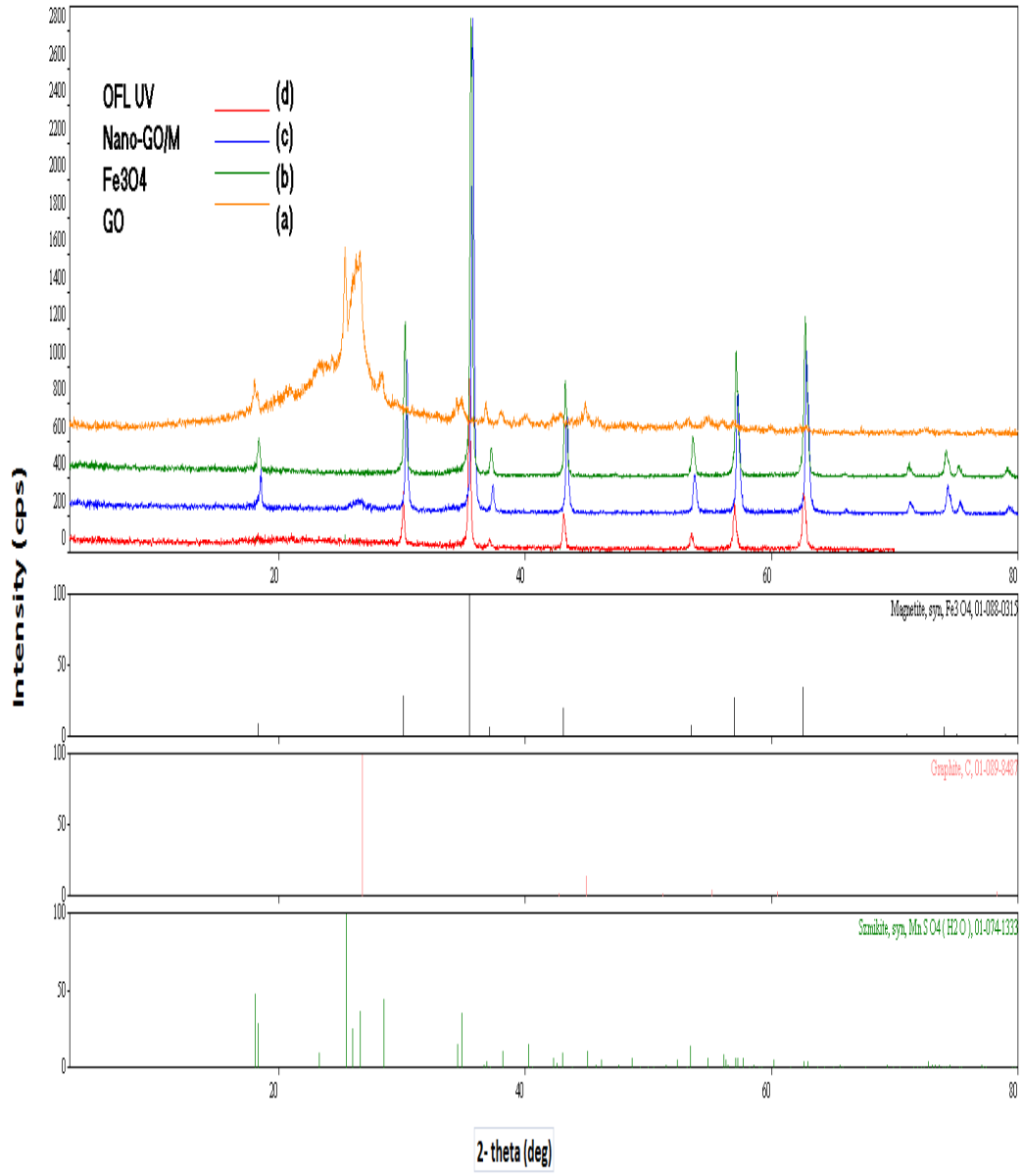


Figure 6.17 XRD analysis of GO (a), $Fe_3O_4$ (b) and Nano-GO/M composite before(c) and Nano-GO/M (0.5 g/L) composite after UV irradiation (60 min-300 W), with 100 mg/L OFL concentration (d) at pH=6.5

The comparison of XRD spectra of raw Nano-GO/M composite and Nano-GO/M composite after OFL treatment under UV irradiation (60 min- 300 W) and sunlight (350 min- 80 W) with 100 mg/L OFL concentration are shown in Figure 6.18. After UV and sunlight irradiations the crystal planes of $Fe_3O_4$ remained almost same. The structure of Nano-GO/M composite did not change considerably. UV experiments were realized at optimum Nano-GO/M concentration (0.5 g/L), for initial 100 mg/L OFL concentration, at a pH of 6.5 and under 300 W UV light after 60 min irradiation

time. Sunlight experiments were realized at optimum Nano-GO/M concentration (2 g/L), for initial 100 mg/L OFL concentration, at a pH of 6.5 and under 80 W UV light after 350 min irradiation time. The characteristic peaks of Nano-GO/M did not change considerably after UV and sunlight irradiation.

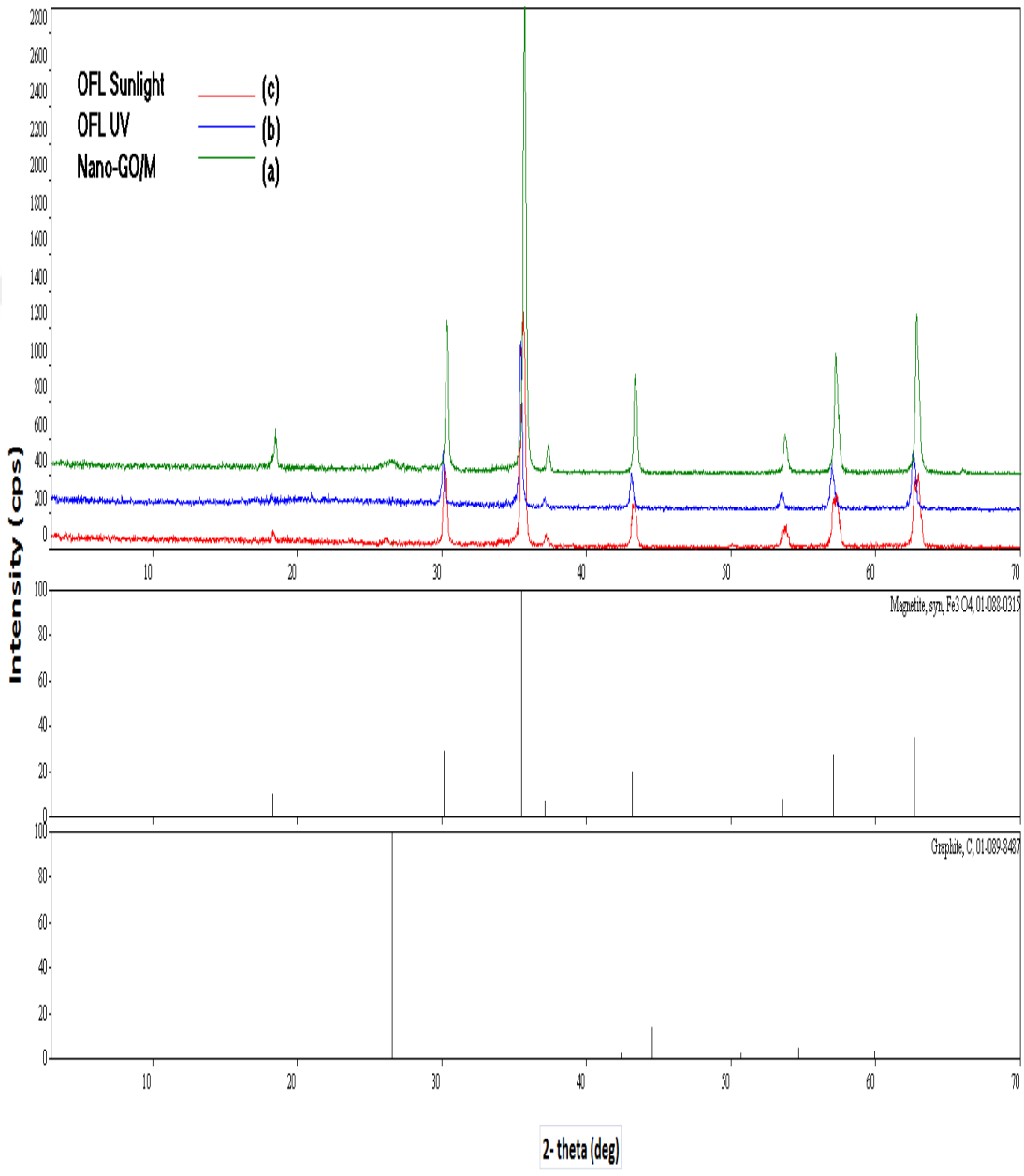


Figure 6.18 XRD analysis raw Nano-GO/M composite (a), Nano-GO/M (0.5 g/L) composite after UV irradiation (60 min-300 W) (b), Nano-GO/M (2 g/L) composite after sunlight (350 min- 80 W) with 100 mg/L OFL concentration (c) at pH=6.5.

## 6.2 Batch Adsorption Studies

### *6.2.1 Batch Adsorption Studies of CIP*

*6.2.1.1 Effects of Nano-GO/M Composite Concentrations on the Adsorption of CIP*

Nano particles concentration is an important parameter for the treatment of CIP. In order to determine the maximum adsorption efficiencies of CIP, 0.5 g/L, 2g/L, 10g/L Nano-GO/M composite concentrations were researched. Preliminary experiments showed that among the adsorption times that are tested, the maximum CIP removal was obtained after 30 min adsorption time (data not shown). Therefore, all experiments were realized after 30 min adsorption time, at 21°C (room temperature) and at original pH (6.5) of CIP solution. Figure 6.19 summarizes the adsorption efficiencies of CIP at 0.5 g/L Nano-GO/M, at increasing CIP concentrations (1, 3, 5, 25, 100, 500 and 1000 mg/L). CIP adsorption efficiencies were found as 30 %, 29%, 28%, 20%, 16%, 13% and 9% for 1, 3, 5, 25, 100, 500 and 1000 mg/L CIP concentrations, respectively. According to this results it can be concluded that the CIP adsorption removals were high (30-29%) at low CIP concentrations (1-3 mg/L). As the CIP concentrations were increased, the adsorption efficiencies decreased. The reason of this can be explained as follows: at high CIP concentrations the surface of Nano-GO/M was not enough high to adsorb all the CIP concentrations. Therefore, the adsorption efficiency is low at high CIP concentrations. In other words, the Nano-GO/M adsorb small amount of CIP at high CIP concentrations as reported by Hong et al. (2009).

The maximum CIP adsorption efficiency obtained is (30%) at 0.5 g/L Nano-GO/M concentration at 1 mg/L influent CIP concentration while the other high maximum CIP adsorption yield was calculated as 29% at 3 mg/L CIP concentration.

A linear relationship between CIP adsorption efficiencies and influent CIP concentration was obtained (R=0.83) and this regression is significant (ANOVA $p=0.01<\alpha$ (0.05) and F=10.64)

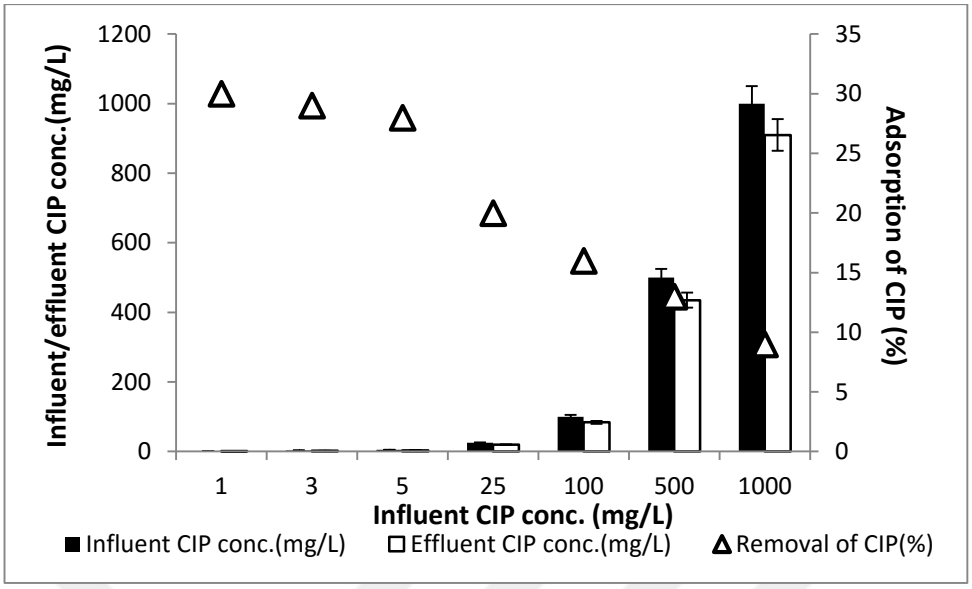


Figure 6.19 Effect of increasing CIP concentration on the yields of CIP adsorption at a Nano-GO/M concentration of 0.5 g/L at pH=6.5, at 21°C and 30 min contacting time (<α (0.05)).

In recent years, GO, a type of two-dimensional carbon nanomaterials can be used for the treatment of some chemical substances (Ji, Chen, Duan & Zhu, 2009). GO with large amounts of oxygen atoms on the surface are observed in the forms of epoxy, hydroxyl, and carboxyl groups. These functional groups turn GO into hydrophilic type and therefore it is convenient to be an adsorbent (Gao et al., 2012). A study done recently remarked that carbon based materials are able to remove CIP from aqueous solutions (Li, Zhang, Han & Xing, 2014). Nano-GO/M compared to GO may be due to the more functional groups and micro-channels formed by Nano-GO/M which increase their surface complexation capability and ion exchange capacity of between CIP molecules and Nano-GO/M (Shaoling et al. 2013).

Figure 6.20 shows the adsorption efficiencies of CIP at increasing CIP concentrations (1, 3, 5, 25, 100, 500 and 1000 mg/L) were found as 30 %, 29%, 28%, 20%, 16%, 13% and 9% at 2 g/L Nano-GO/M, respectively. As the CIP concentrations were increased, the adsorption efficiencies decreased. The maximum CIP removal efficiency is 30% at 2 g/L Nano-GO/M concentration at 1 mg/L influent CIP concentration. According to this results it can be concluded that the CIP adsorption removals were high (30-29%) at low CIP concentrations (1-3 mg/L) As the CIP concentrations were increased, the adsorption efficiencies decreased. The reason of

this can be explained as follows: at high CIP concentrations the surface of Nano-GO/M was not enough high to adsorb all the CIP concentrations. Therefore, the adsorption efficiency is low at high CIP concentrations. In other words, the Nano-GO/M adsorb small amount of CIP at high CIP concentrations as reported by Hong et al. (2009).

The maximum CIP adsorption efficiency obtained is (30%) at 2 g/L Nano-GO/M concentration at 1 mg/L influent CIP concentration while the other high maximum CIP adsorption yield was calculated as 29% at 3 mg/L CIP concentration.

A linear relationship between CIP adsorption efficiencies and influent CIP concentration was obtained (R=0.82) and this regression is significant (ANOVA $p=0.02<\alpha$ (0.05) and F=10.64).

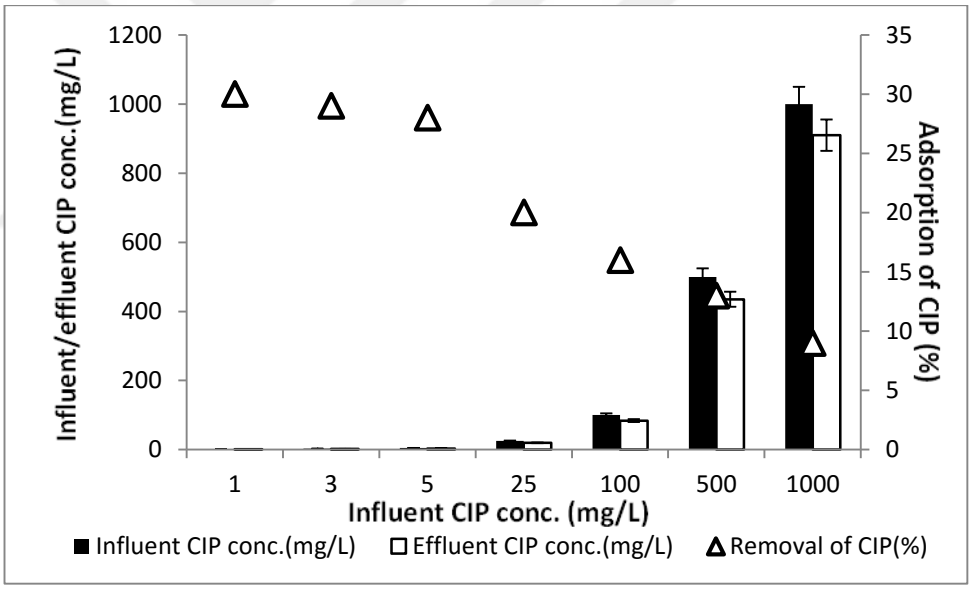


Figure 6.20 Effect of increasing CIP concentration on the yields of CIP adsorption at a Nano-GO/M concentration of 2 g/L at pH=6.5, at 21°C and 30 min contacting time (<α (0.05)).

Figure 6.21 shows the adsorption efficiencies of CIP at increasing CIP concentrations (1, 3, 5, 25, 100, 500 and 1000 mg/L) for 10 g/L Nano-GO/M. According these CIP concentrations, the adsorption yields were 25%, 24%, 23%, 18%, 11%, 7% and 3%, respectively. As the CIP concentrations were increased, the adsorption efficiencies decreased. The maximum CIP removal efficiency is 25% at 10 g/L Nano-GO/M concentration for 1 mg/L influent CIP concentration. According to

this results it can be concluded that the CIP adsorption removals were high (30-29%) at low CIP concentrations (1-3 mg/L). As the CIP concentrations were increased, the adsorption efficiencies decreased. The reason of this can be explained as follows: at high CIP concentrations the surface of Nano-GO/M was not enough high to adsorb all the CIP concentrations. Therefore, the adsorption efficiency is low at high CIP concentrations. In other words, the Nano-GO/M adsorb small amount of CIP at high CIP concentrations as reported by Hong et al. (2009).

A linear relationship between CIP adsorption efficiencies and influent CIP concentration was obtained (R =0.87) and this regression is significant (ANOVA $p=0.01<\alpha$ (0.05) and F=14.93).

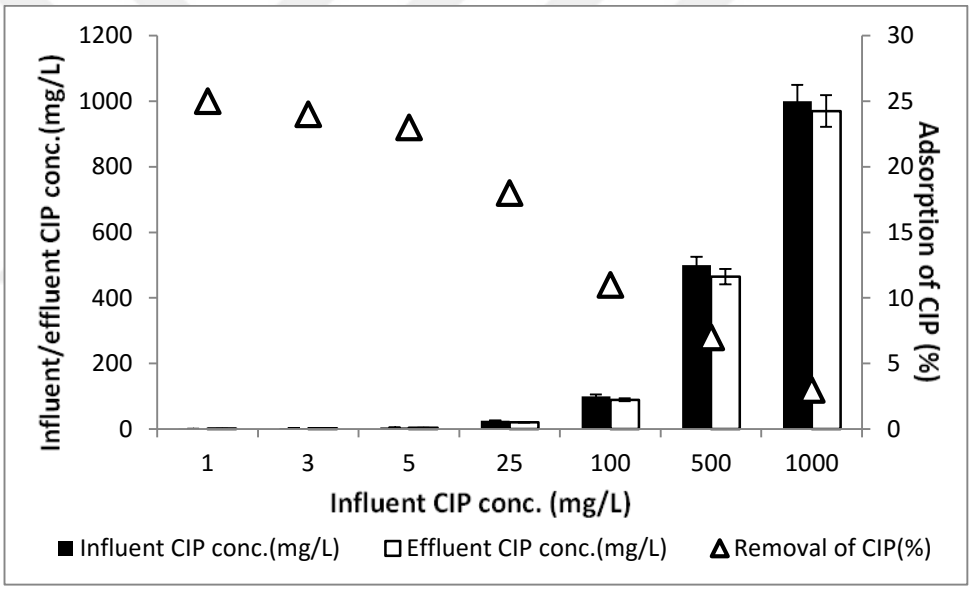


Figure 6.21 Effect of increasing CIP concentration on the yields of CIP removal at a Nano-GO/M concentration of 10 g/L at pH=6.5, at 21°C and 30 min contacting time (<α (0.05)).

Figure 6.22 summarizes the effects of increasing Nano-GO/M concentrations (0.5, 2 and 10g/L) on CIP adsorption yields at a CIP concentration of 5 mg/L after 30 min adsorption time at pH=6.5 and at 21°C. Increasing the concentration of Nano-GO/M from 0.5 g/L to 2 g/L did not change the CIP adsorption yields (30%) but slightly lower adsorption efficiency (25%) was obtained with 10 g/L Nano-GO/M composite concentration at the same operational conditions. Among these 3 different (0.5, 2 and 10 g/L) concentrations of Nano-GO/M, the maximum CIP adsorption yields was found

as 28% for 5 mg/L initial CIP concentration. The optimum Nano-GO/M concentration was chosen as 0.5 g/L in order to reduce the operational cost of adsorption process. It was not found a significant correlation between CIP adsorption yields and Nano-GO/M concentrations.

A linear relationship between maximum CIP adsorption efficiencies and Nano-GO/M composite was obtained (R=0.93) and this regression is significant (ANOVA p=0.079> α (0.05) and F=7.39).

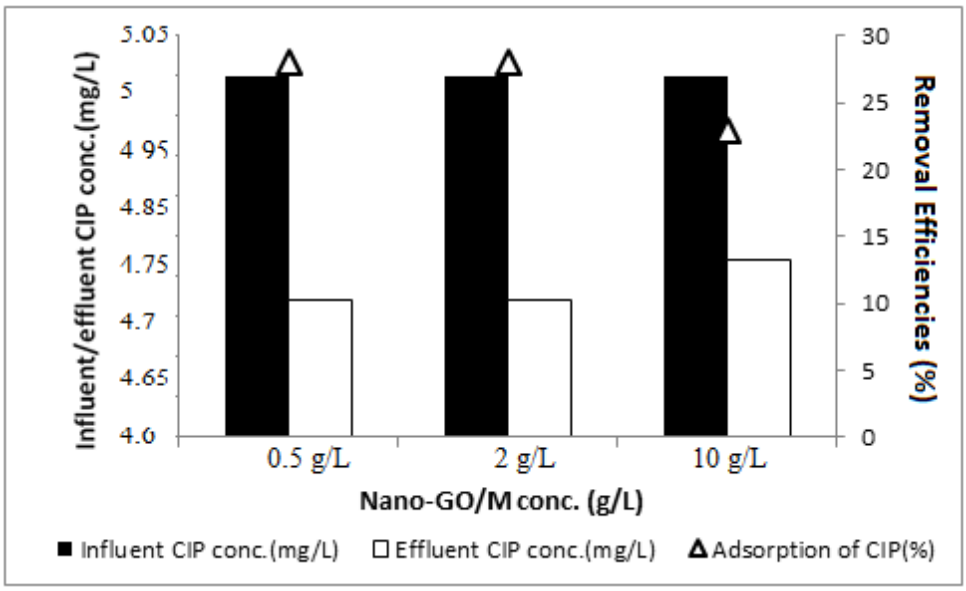


Figure 6.22 Comparison of increasing concentration of Nano-GO/M (0.5, 2 and 10 g/L) on the yields of CIP adsorption for constant CIP concentration (5 mg/L) at pH=6.5, at 21°C and 30 min contacting time (<α (0.05)).

At lower Nano-GO/M composite concentration (0.5, 2 g/L) slightly higher CIP adsorption yields (30%) was obtained while slightly lower CIP adsorption removals was obtained at higher Nano-GO/M concentration (10 g/L) at pH 6.5 (Figure 1d.). This can be attributed to that partial active sites are not entirely exposed and utilized at lower Nano-GO/M composite concentrations, which leads to slightly higher adsorption capacity. Lower active surface area on the Nano-GO/M decrease the adsorption yield as reported by Li et al. (2013).

Adsorption of CIP with Nano-GO/M is a newly found study area. There are a few similar studies on adsorption of CIP: Tang et al. (2013), reported a maximum CIP adsorption capacity of 10.91 mg/g with a yield of 25% for 0.2 g/L reduced-GO/M concentration within 24 hours retention time, at a pH of 6.2 and at a temperature of 25°C. This yield and adsorption time are lower than that our study with a maximum CIP yield of 30% at 30 min. Another study remarked the CIP adsorption on 10 g/L nano-$Fe_3O_4$ within 24 hours retention time, at a pH of 6.03, at room temperature. They found a maximum adsorption capacity of 0.043 mmol/g with a CIP yield of 30% (Rakshit et al., 2013). On the other hand, there are some studies reported about adsorption of CIP with different adsorbents. Shaoling et al. (2013) researched the adsorption experiments with 10 mg of GO/calcium alginate fibers into conical flasks containing 20 mL of the aqueous solutions with CIP concentration of 9.8 mg/L. Maximum adsorption capacity of GO/calcium alginate fibers was 11.8 mg/g at a pH of 5.9, at 24 hours adsorption time and at room temperature. Carabineiro et al. (2011), found maximum CIP adsorption capacities of varying between 60 to 300 mg/g at CIP concentrations of 3-30 mg/L, with 50 mg/L carbon concentration after 72 hours adsorption time at 25°C, at a pH of 5 after 3 day's equilibrium studies.

*6.2.1.2 Effect of Contacting Time on the Adsorption of CIP*

After determining the optimum concentration of Nano-GO/M (0,5 g/L), it was decided to investigate the effect of contact time on the adsorption of 5 mg/L CIP at increasing retention times (15, 30 and 60 min) at pH = 6.5, at a temperature of 21°C. As the contacting time was increased from 15 min to 30 min and 60 min the CIP removals increased slightly from 20% to 28% and to 29% for initial CIP concentration of 5 mg/L (Figure 6.23). Further increase in contact time from 60 min to 900 min decreased the CIP adsorption yield significantly from 29% to 8%. There was no significant difference between adsorption efficiency of CIP and increasing time (from 15 to 30 and 60 min). As a result, in this study the optimum contact time for maximum CIP removal (28%) was found to be 30 min. Tang et al. (2013), reported that the CIP adsorption reached equilibrium on 0.2 g/L reduced-GO/M within 24 hours retention time, at a pH of 6.2, at a temperature of 25°C. In our study, at very short adsorption time (30 min) 28% CIP removal yield was obtained for 5 mg/L influent CIP

concentration. This short retention time reduces the cost for adsorption of CIP to Nano-GO/M extremely.

A linear relationship between adsorption yields and adsorption times were obtained up to a contacting time of 900 min, and this regression is significant (R=0.86, p= 0,15>α (0.05) and F= 3.01).

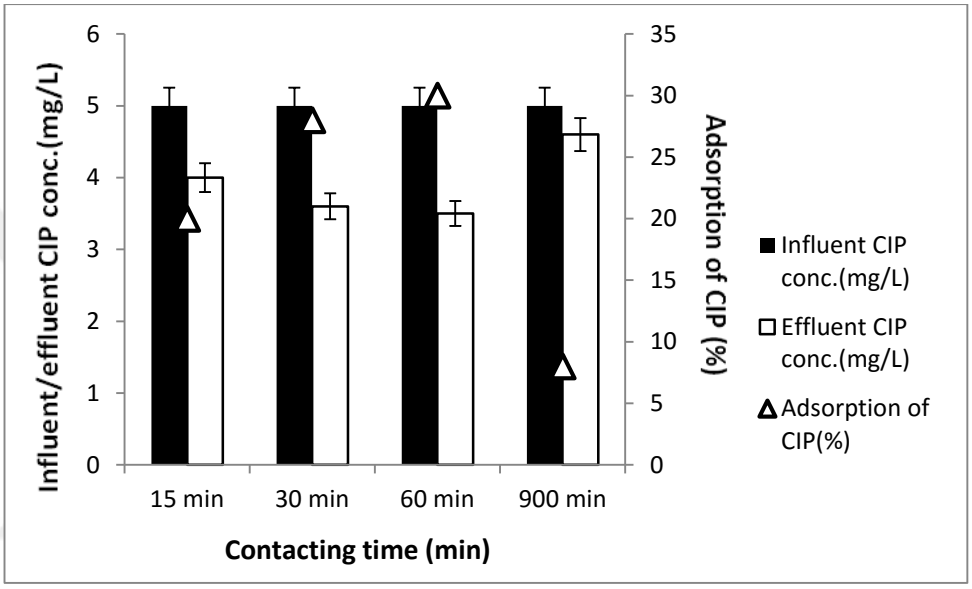


Figure 6.23 Effect of contacting time on the yields of constant CIP concentration (5 mg/L), at a constant Nano-GO/M concentration (0.5 g/L), at a pH of 6.5 and at 21°C (<α (0.05))

According to the results obtained in step of the study it was found that at very short irradiation time (15 min) and very long irradiation times (900 min) low CIP adsorption yields was obtained. The decreased adsorption efficiency may be explained as the reduction of the remaining active adsorption sites of Nano-GO/M (Shaoling et al. 2013).

*6.2.1.3 Effect of Increasing CIP concentrations on the CIP Adsorption yields*

At this step of this study, the effects of increasing CIP concentrations (1 mg/L, 3 mg/L, 5 mg/L, 25 mg/L, 100 mg/L, 500 mg/L, 1000 mg/L) on the CIP removals were studied at a Nano-GO/M concentration of 0.5 g/L, after 30 min contacting time, at pH= 6.5 and at a temperature of 21°C (Figure 6.24). Results showed that increasing in the

CIP concentration reduced the removal efficiency of CIP at a Nano-GO/M concentration of 0.5 g/L. For 1 mg/L initial CIP concentration the maximum CIP removal efficiency was found as 30% while the removal efficiency of 1000 mg/L CIP was found almost 9%. This increase in the CIP concentrations after adsorption process results in decrease in the adsorption efficiencies of CIP. Thus, for the maximum adsorption yield of CIP (30%) the optimum CIP concentration was found to be 1 mg/L. The CIP ions around absorbent sites of Nano-GO/M increased in number with the increase of initial CIP concentration.

As the influent CIP concentration increased the CIP adsorption yields decreased. A linear relationship between CIP adsorption efficiencies and influent CIP concentration was obtained (R=0.83) and this regression is significant (ANOVA p=0.01<α (0.05) and F=10.64).

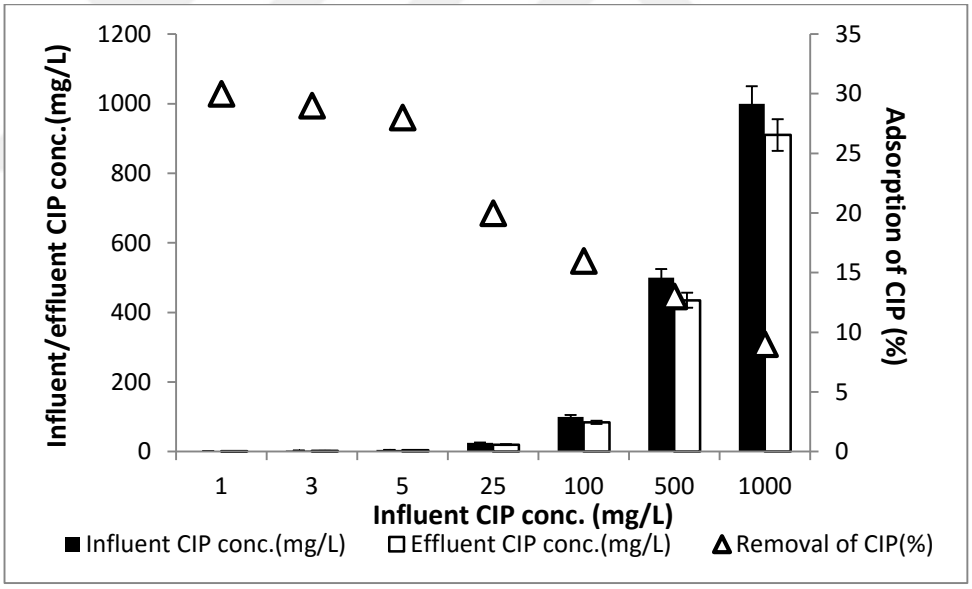


Figure 6.24 Effect of increasing CIP concentration on the yields of CIP adsorption at a Nano-GO/M concentration of 0.5 g/L at pH=6.5, at 21°C and 30 min contacting time (<α (0.05)).

*6.2.1.4 Effect of pH on the Adsorption of CIP with Nano-GO/M composite*

The pH value is among the most important parameters that has an impact on adsorption capacity of Nano-GO/M. CIP has two proton-binding sites, carboxyl and piperazinyl group (Rakshit et al., 2013).

The effects of pH on the adsorption of increasing CIP concentrations (1, 3, 5, 25, 100, 500 and 1000 mg/L) were studied under acidic, neutral and alkaline pHs (4, 6.5 and 10) at an adsorption time of 30 min, at a Nano-GO/M concentration of 0.5 g/L and at 21°C. Table 6.1 represents the effects of different pHs on the adsorption efficiency of CIP at 21°C. Adsorption of CIP on Nano-GO/M was relatively high at pH 6.5.

Table 6.1 shows the adsorption efficiencies of increasing CIP at acidic, neutral and alkaline pHs (4, 6.5 and 10) at 21°C and at 0.5 g/L constant Nano-GO/M concentration.

| **CIP concentrations (mg/L)** | **1** | **3** | **5** | **25** | **100** | **500** | **1000** |
|---|---|---|---|---|---|---|---|
| **Adsorption efficiency (%) at pH= 4** | 25 | 24 | 23 | 18 | 10 | 5 | 2 |
| **Adsorption efficiency (%) at pH= 6.5** | 30 | 29 | 28 | 20 | 16 | 13 | 9 |
| **Adsorption efficiency (%) at pH= 10** | 20 | 19 | 18 | 13 | 8 | 4 | 1 |

In this study, the maximum adsorption efficiency was found as 30% at pH=6.5 at 1 mg/L CIP concentration and 0.5 g/L Nano-GO/M concentration. As the pH values decreased from 6.5 to 4 the CIP adsorption yields decreased to 25% at pH=4 at 1mg/L CIP concentration and constant Nano-GO/M concentration (0.5 g/L). Under alkaline conditions the adsorption yields exhibited decrease to 20%. As the CIP concentrations were increased from 1 to 1000 mg/L the adsorption yields decreased significantly to 2%, 9% and 1% at pH 4, 6.5 and 10, respectively.

CIP has positively charged (cationic; pH=3), negatively charged (anionic; pH=7.5), and/or zwitterionic (pH=10) species at pHs due to different pKas of 6.1 and 8.7, respectively (Gu & Karthikeyan, 2005). At pH < 6.1, CIP molecules mainly exist as cations ($CIP^+$) because of the protonation of the amine group in the piperazine moiety (Wang et al., 2010). At pH > 8.7, CIP molecules exist as anions ($CIP^-$) due to the loss of a proton from the carboxylic group (Jalil, Baschini & Sapag, 2015). In the pH range 6.1–8.7, the pH values are higher than p*K*a1 of the carboxylic group, thus deprotonating the carboxylic group to the negatively charged carboxylate (Jalil, Baschini & Sapag, 2015). However, the amine group stays protonated and positively charged as this pH range is still lower than p*K*a2 of the amine group (Drakopoulos & Ioannou, 1997). Accordingly, in the above mentioned pH range, zwitterionic species of CIP molecules dominate in the aqueous solution. This behavior

can be explained by the relationship between the surface charge of Nano-GO/M and the CIP total charge and by the presence of the cationic form (CIP) that favors a strong adsorption on the negative surface of the Nano-GO/M. These results suggest that there is a cation exchange of this species for the natural cation within the Nano-GO/M interlayer. The adsorption decrease gradually after a pH of 6.5. This behavior could be related to the presence of the negative molecule form (CIP), which can exhibit repulsive interactions with the Nano-GO/M negative surface.(Jalil, Baschini & Sapag, 2015).

Shaoling et al. (2013), were investigated the effect of pH on the adsorption of CIP onto the fibers of graphene oxide/calcium alginate. They researched the adsorption experiments with 10 mg of GO/calcium alginate fibers into conical flasks containing 20 mL of the aqueous solutions with CIP concentration of 9.8 mg/L at different pH values between 3.0 and 9.3 for 24 hours adsorption time at room temperature. Results show that the adsorption capacity of calcium alginate fibers increases with the rise in pH from 3.5 to 7.3 and reaches the maximum value of 4.4 mg/g at pH 7.3. Then, the adsorption capacity decreases gradually with decreasing pH value. GO/Calcium Alginate fibers show that the adsorption capacity increases with the initial from 3.0 to 5.9 and reaches the maximum value of 11.8 mg/g at pH 5.9.

Figure 6.25 summarizes the adsorption yields versus pH levels and CIP concentrations. Consequently, the maximum CIP (initial CIP concentration was 1 mg/L) adsorption yield was obtained at pH 6.5 (30%), but at alkaline pH lowest CIP adsorption yield (20%) was obtained whilst at acidic pH lower CIP adsorption yield was obtained (25%).

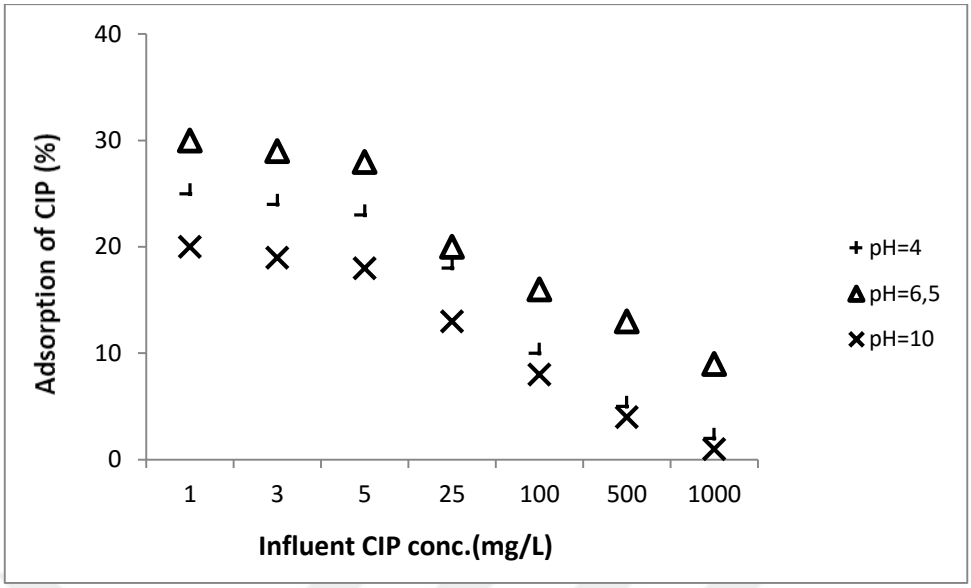


Figure 6.25 Effect of different pHs (4, 6.5 and 10) on the yield of CIP adsorption at a Nano-GO/M concentration of 0.5 g/L at pH=6.5, at 21°C and 30 min contacting time (<α (0.05)).

Table 6.2 represents the effects of different pHs on the adsorption efficiency of CIP (for 1 mg/L initial CIP concentration) at 21°C. Adsorption of CIP on nano-GO-M was relatively high at pH 6.5.

Table 6.2 Shows the maximum adsorption efficiencies of CIP (1mg/L) at acidic, neutral and alkaline pHs (4, 6.5 and 10) at 21°C and at 0.5 g/L constant Nano-GO/M concentration.

| pH | Adsorption efficiencies (%) |
|---|---|
| 4 | 25 |
| 6.5 | 30 |
| 10 | 20 |

A linear relationship between pH and maximum CIP adsorption efficiencies (for 1 mg/L initial CIP concentration) was obtained (R=0.58) and this regression is not significant (ANOVA p=0.43>α (0.05) and F=0.51).

As the pH increases from 4.0 to 6.5the interaction between CIP and positively charged Nano-GO/M became more feasible. Above pH 6.5, both CIP and Nano-GO/M became increasingly negatively charged with increasing pH, resulting in decreased adsorption (Rakshit et al., 2013).

*6.2.1.5 Effect of Temperature on the Adsorption of CIP with Nano-GO/M composite*

Temperature is an important parameter for the adsorption process. To investigate the effect of temperature, CIP adsorption was studied under different temperatures (21°C, 40°C, 60°C and 80°C). For maximum CIP adsorption optimum Nano-GO/M concentration (0.5 g/L) and optimum adsorption time (30 min) were determined in the preliminary studies as mentioned above. Therefore, all experiments were realized after 30 min adsorption time, at increasing CIP concentrations (1, 3, 5, 25, 100, 500 and 1000 mg/L) and at original pH (6.5) of CIP solution at 0.5 g/L Nano-GO/M. Figure 6.26 summarizes the adsorption efficiencies of CIP at 21°C, with 0.5 g/L constant Nano-GO/M, at increasing CIP concentrations (1, 3, 5, 25, 100, 500 and 1000 mg/L). CIP adsorption efficiencies were found as 30 %, 29%, 28%, 20%, 16%, 13% and 9% for 1, 3, 5, 25, 100, 500 and 1000 mg/L CIP concentrations, respectively. As a consequence, the CIP adsorption efficiencies were high (30-29%) at low CIP concentrations (1-3 mg/L).

A linear relationship between CIP adsorption efficiencies and influent CIP concentration was obtained (R=0.83) and this regression is significant (ANOVA $p=0.01<\alpha$ (0.05) and F=10.64).

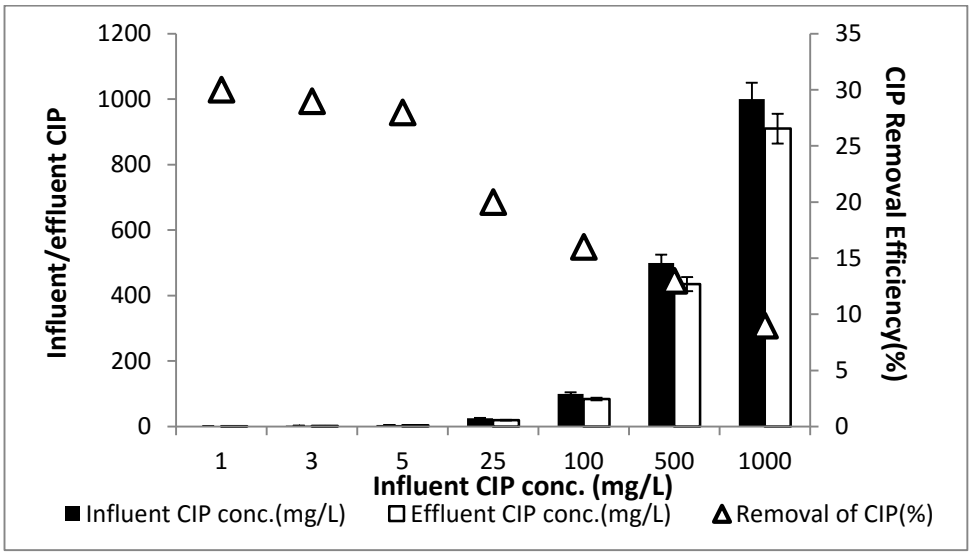


Figure 6.26 Effect of increasing CIP concentration on the yields of CIP adsorption at a Nano-GO/M concentration of 0.5 g/L at pH=6.5, at 21°C and 30 min contacting time (<α (0.05)).

Figure 6.27 shows the adsorption efficiencies of CIP at 40°C, with 0.5 g/L constant Nano-GO/M, at increasing CIP concentrations (1, 3, 5, 25, 100, 500 and 1000 mg/L). The adsorption efficiencies of CIP were found as 20 %, 19%, 18%, 13%, 9%, 5% and 3%, respectively. As the CIP concentrations were increased, the adsorption efficiencies decreased. The maximum CIP removal efficiency is 20% at 40°C, with 0.5 g/L constant Nano-GO/M concentration for 1 mg/L influent CIP concentration. According to this results it can be concluded that the CIP adsorption removals were not so high (20-19%) at low CIP concentrations (1-3 mg/L) at 40°C.

A linear relationship between CIP adsorption efficiencies and influent CIP concentration was obtained (R=0.84) and this regression is significant (ANOVA $p=0.01<\alpha$ (0.05) and F=12.33).

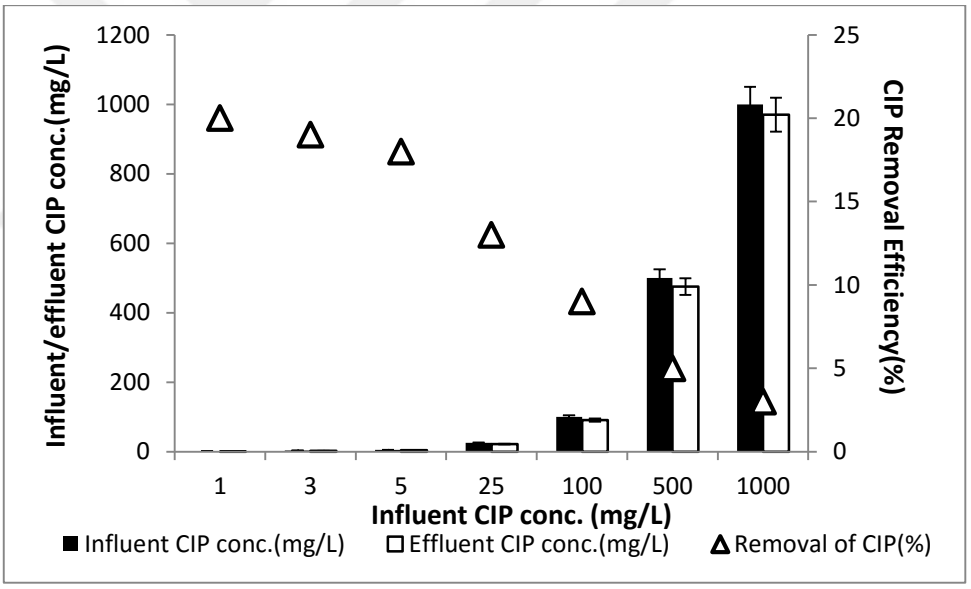


Figure 6.27 Effect of increasing CIP concentration on the yields of CIP adsorption at a Nano-GO/M concentration of 0.5 g/L at pH=6.5, at 40°C and 30 min contacting time (<α (0.05)).

Figure 6.28 shows the adsorption efficiencies of CIP at increasing CIP concentrations (1, 3, 5, 25, 100, 500 and 1000 mg/L) for 60°C at 0.5 g/L constant Nano-GO/M and at pH of 6.5. According these CIP concentrations, the adsorption yields were 16%, 15%, 14%, 10%, 7%, 4% and 2%, respectively. As the CIP concentrations were increased, the adsorption efficiencies decreased. The maximum CIP removal efficiency is 16% at 60°C for 1 mg/L influent CIP concentration.

According to this results it can be concluded that the CIP adsorption removals were lower (16-15%) at low CIP concentrations (1-3 mg/L) at 60°C.

A linear relationship between CIP adsorption efficiencies and influent CIP concentration was obtained (R=0.85) and this regression is significant (ANOVA p=0.02<α (0.05) and F=12.50).

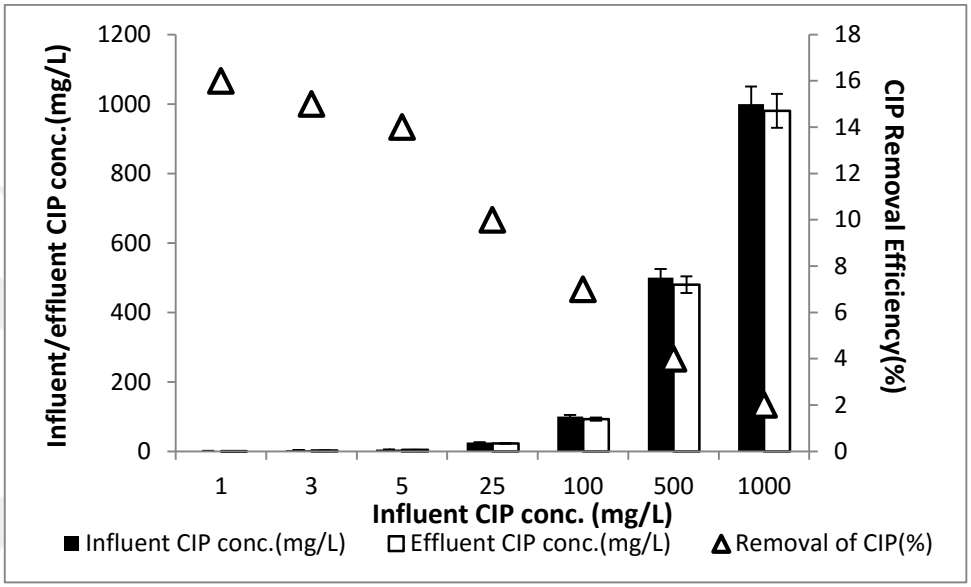


Figure 6.28 Effect of increasing CIP concentration on the yields of CIP adsorption at a Nano-GO/M concentration of 0.5 g/L at pH=6.5, at 60°C and 30 min contacting time (<α (0.05)).

Figure 6.29 shows the adsorption efficiencies of CIP at increasing CIP concentrations (1, 3, 5, 25, 100, 500 and 1000 mg/L) for 80°C at 0.5 g/L constant Nano-GO/M. According these CIP concentrations, the adsorption yields were 12%, 11%, 10%, 7%, 5%, 3% and 1%, respectively. As the CIP concentrations were increased, the adsorption efficiencies decreased. The maximum CIP removal efficiency is 12% at 80°C for 1 mg/L influent CIP concentration. According to this results it can be concluded that the CIP adsorption removals were lower (12-11%) at low CIP concentrations (1-3 mg/L) at 80°C. As the CIP concentrations were increased, the adsorption efficiencies decreased. The reason of this can be explained as follows: at high CIP concentrations the surface of Nano-GO/M was not enough high to adsorb all the CIP concentrations. Therefore, the adsorption efficiency is low at high CIP

concentrations. In other words, the Nano-GO/M adsorb small amount of CIP at high CIP concentrations as reported by Hong et al. (2009).

A linear relationship between CIP adsorption efficiencies and influent CIP concentration was obtained (R=0.85) and this regression is significant (ANOVA $p=0.016<\alpha$ (0.05) and F=12.59).

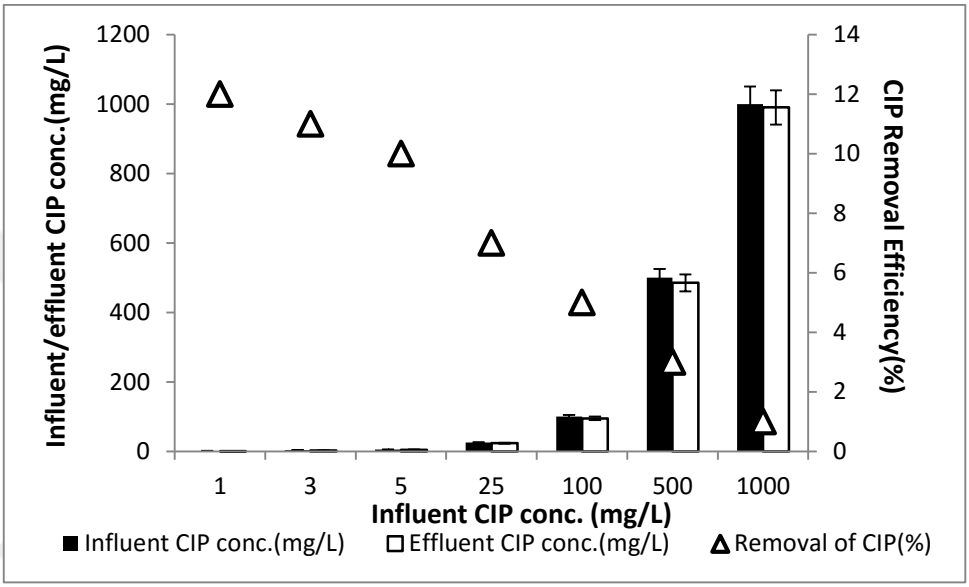


Figure 6.29 Effect of increasing CIP concentration on the yields of CIP adsorption at a Nano-GO/M concentration of 0.5 g/L at pH=6.5, at 80°C and 30 min contacting time (<α (0.05)).

Figure 6.30 summarizes the effects of increasing temperatures (21°C, 40°C, 60°C and 80°C) on CIP adsorption yields at a CIP concentration of 5 mg/L after 30 min adsorption time at pH=6.5 and at constant Nano-GO/M concentration (0.5 g/L). Increasing the temperature from 21°Cto 40-60-80°C yielded a decrease on the adsorption efficiencies of CIP.

Among these four different temperatures (21°C, 40°C, 60°C and 80°C), the maximum CIP adsorption yields was found as 28% for 5 mg/L initial CIP concentration at 21°C. This low temperature reduced the operational cost of adsorption process.

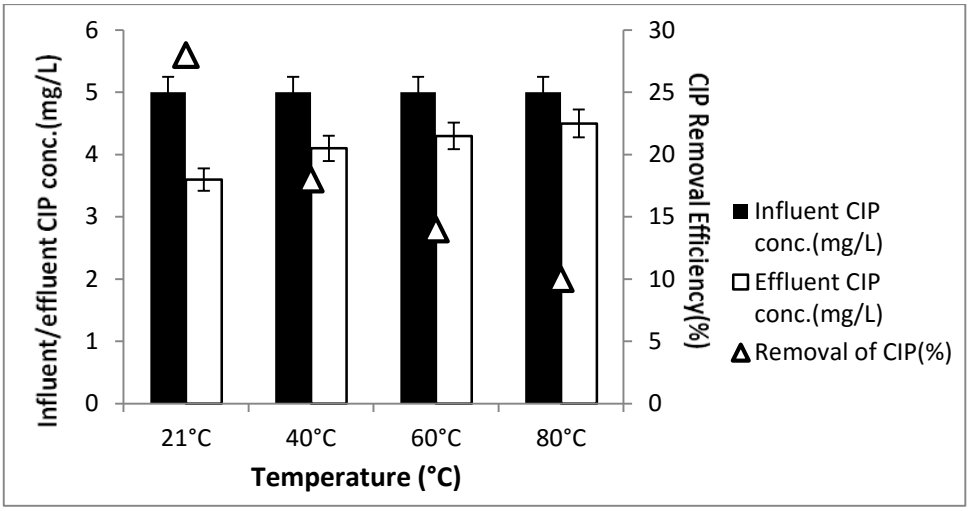


Figure 6.30 Effect of contacting time on the yields of constant CIP concentration (5 mg/L), at a constant nano GO/M concentration (0,5 g/L), at a pH of 6.5 and at 21°C, 40°C, 60°C and 80°C (<α (0.05)).

Table 6.3 represents the effects of different temperatures on the adsorption efficiency of CIP for 1 mg/L initial CIP concentration. Adsorption of CIP on Nano-GO/M was high at 21°C.

Table 6.3 Shows the maximum adsorption efficiencies of CIP (1mg/L) at 21°C, 40°C, 60°C and 80°C and at 0.5 g/L constant Nano-GO/M concentration.

| Temperature (°C) | Adsorption efficiencies (%) |
|---|---|
| 21 | 30 |
| 40 | 20 |
| 60 | 16 |
| 80 | 12 |

A linear relationship between temperature and maximum CIP adsorption efficiencies (for 1 mg/L initial CIP concentration) was obtained (R=0.96) and this regression is significant (ANOVA p=0.33 >α (0.05) and F=28.12).

### *6.2.1.6 Calculation of Maximum Adsorption Capacity of Nano-GO/M*

CIP adsorption kinetics on 0.5 g/L Nano-GO/M was performed with the increasing CIP concentrations (1, 3, 5, 25, 100, 500 and 1000 mg/L) at pH 6.5, at Nano-GO/M

concentration of 0.5 g/L at 21°C after 30 min adsorption time. After magnetic separation, the adsorption amounts, $q_e$ (mg/g), were calculated by Eq. (5.1).

Table 6.4 represents the maximum adsorption capacities calculated with Eq. (6.1). The maximum adsorption capacity of CIP was found as 180 mg/g for 1000 mg/L CIP concentration while minimum value of adsorption capacity was found as 0.6 mg/g for 1 mg/L CIP concentration at 0.5 g/L Nano-GO/M. At high CIP concentration higher CIP adsorption capacities were obtained while low CIP adsorption capacities were obtained at low CIP concentrations. This adsorption capacity increased as the CIP concentrations increased. The results showed that the CIP amount adsorbed increase with the increase of CIP concentration but the percent of CIP adsorption decrease at high concentration. The increase in adsorption with the increase in CIP concentration is due to the driving force that initial concentration provides to overcome the mass transfer resistance between the aqueous and solid phases (Al-Heetimi, Kadhum & Alkhazrajy, 2014).

Table 6.4 The maximum adsorption capacities of increasing concentration of CIP at 0.5 g/L Nano-GO/M, at a pH of 6.5 and 21°C.

| **Influent CIP conc.(mg/L)** | 1 | 3 | 5 | 25 | 100 | 500 | 1000 |
|---|---|---|---|---|---|---|---|
| **Effluent CIP conc.(mg/L)** | 0.7 | 2.13 | 3.6 | 20 | 8 | 35 | 910 |
| **$q_e$ (mg/g)** | 0.6 | 1.74 | 2.8 | 10 | 32 | 130 | 180 |

For the maximum CIP adsorption capacity (180 mg/g) the optimum Nano-GO/M concentration, adsorption time and temperature were 0.5 g/L 30 min and at 21°C (room temperature), respectively, at original pH (6.5).

#### *6.2.1.7 Adsorption Isotherms of CIP on Nano-GO/M*

The adsorption isotherm indicates how the adsorbed molecules distribute between the liquid phase and the solid phase when the adsorption process reaches an equilibrium state. The analysis of the isotherm data by fitting them to different isotherm models is an important step in finding a suitable model that can be used for design purpose. The adsorption capacity of this system was investigated with

Langmuir, Freundlich, Temkin, Dubinin–Radushkevich, Flory–Huggins adsorption isotherms (Al-Heetimi, Kadhum & Alkhazrajy, 2014).

The experimental adsorption data were exposed to different adsorption isotherms to determine the adsorption capacity of Nano-GO/M. In this thesis five different adsorption isotherms were used for CIP adsorption on Nano-GO/M.

*6.2.1.7.1 Langmuir Isotherm.* Figure 6.31 represents the Langmuir isotherm slopes for adsorption of CIP on Nano-GO/M. In Langmuir isotherm the $R^2$ value of the linear line was 0.86, while b and $q_m$ values were calculated as 0.003 L/mg and 12.05 mg/g, respectively from the Eq. (5.3).

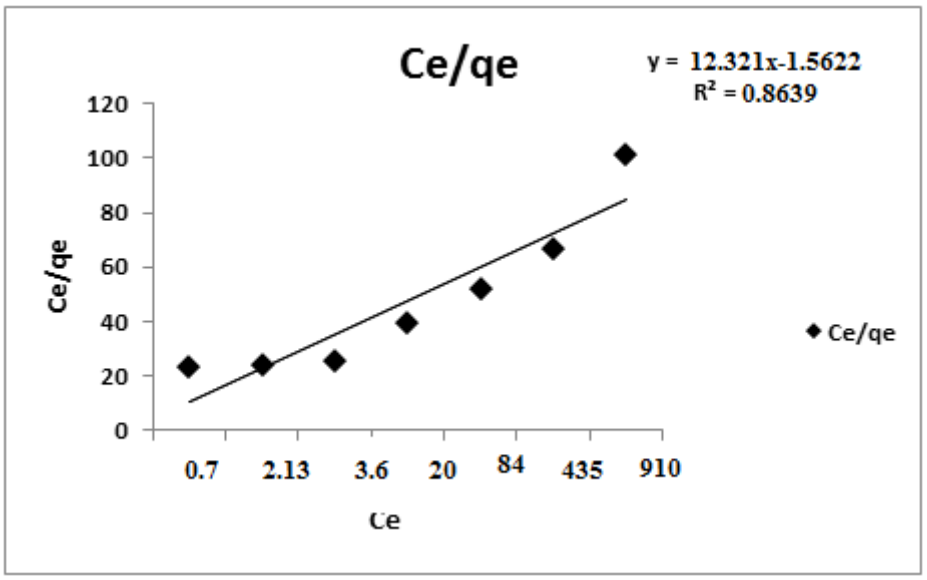


Figure 6.31 Langmuir isotherm for CIP adsorption at increasing CIP concentration, at a Nano-GO/M concentration of 0.5 g/L at pH=6.5, at 21°C and 30 min contacting time.

The $R_L$ values indicate the type of isotherm: to be favorable $0 < R_L < 1$, linear ($R_L = 1$) or irreversible ($R_L = 0$). In this study $R_L$ value was found as 0.25 (unitlesss) that indicated the description of adsorption process by mean of Langmuir model is favorable.

*6.2.1.7.2 Freundlich Isotherm.* This equation predicts multilayer adsorption on heterogeneous surface, characterized by an exponential distribution of active sites. The

Freundlich coefficients $K_F$ (unitlessss) and n (unitlessss) which are the Freundlich constant and adsorption intensity were obtained from the intercepts and slopes of linear plots between $\ln q_e$ against $\ln C_e$ (Figure 6.32) (Eba et al. 2010). In Freundlich isotherm the $R^2$ value of the linear line was 0.98, $K_F$ and n were calculated as 1.31(unitlessss) and 1.38(unitlessss), respectively from the Eq. (5.4).

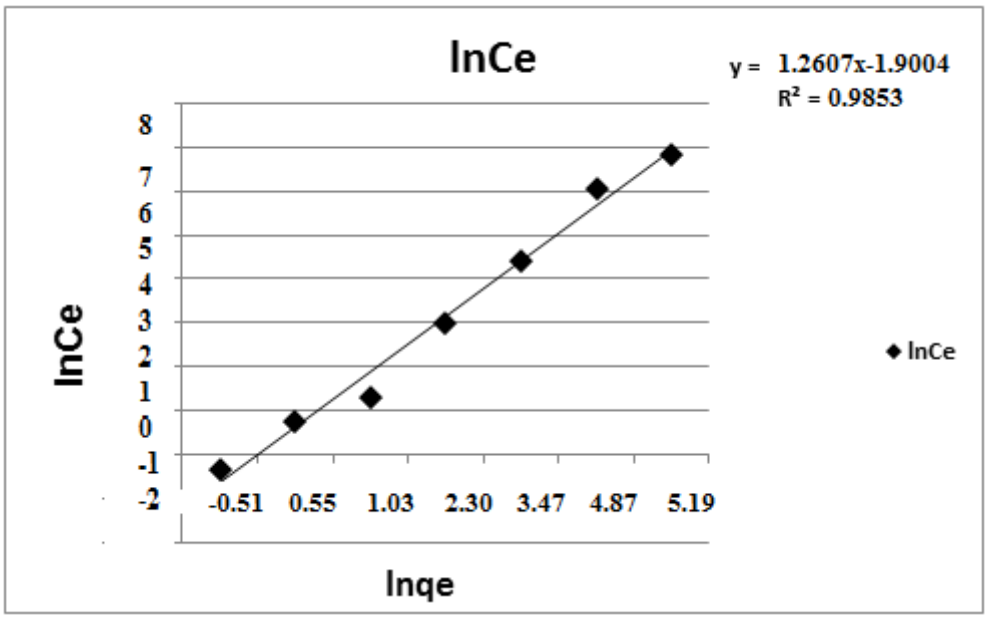


Figure 6.32 Freundlich isotherm of CIP at increasing CIP concentration, at a Nano-GO/M concentration of 0.5 g/L at pH=6.5, at 21°C and 30 min contacting time.

The values of the adsorption intensity obtained in conformity with the requirement $n > 1$ for physical adsorption process (Olakitan, Mi-Hwa & Dong, 2009), characterized the nature favorable of the adsorption of CIP onto Nano-GO/M described by the Freundlich isotherm.

*6.2.1.7.3 Temkin Isotherm.* The Temkin isotherm parameters were obtained by plotting $q_e$ versus $\ln C_e$, respectively. The isotherm data were calculated from the least squares methods.

Figure 6.33 represents the Temkin adsorption isotherm of CIP on Nano-GO/M. In the Temkin isotherm the $R^2$ value of the linear line was 0.75, A (L/mg) and B (J/mol) calculated as 0.66 L/mg and 1.03 J/mol, respectively from the Eq. (5.6).

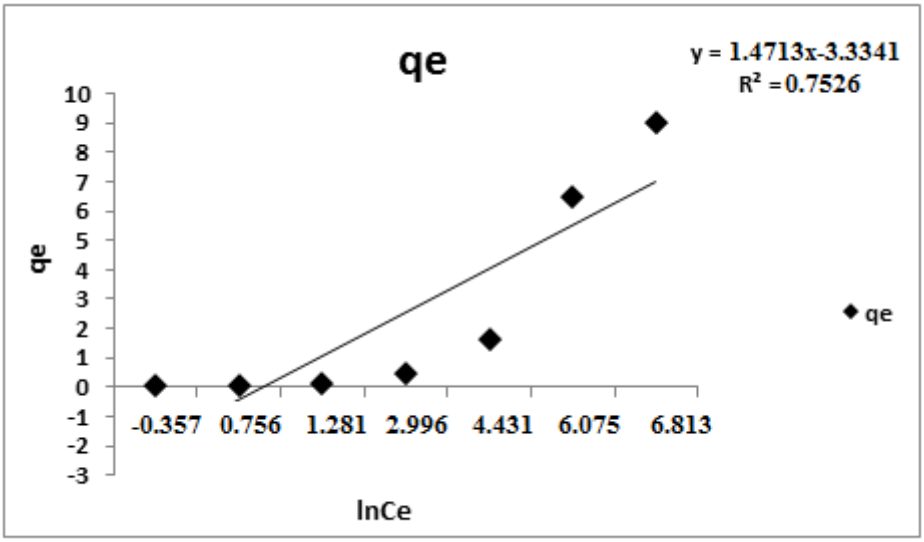


Figure 6.33 Temkin isotherm of CIP at increasing CIP concentration, at a Nano-GO/M concentration of 0.5 g/L at pH=6.5, at 21°C and 30 min contacting time.

*6.2.1.7.4 Dubinin-Radushkevich Isotherm.* Figure 6.34 represents the D-R adsorption isotherm of CIP on Nano-GO/M. The D-R parameters $X'_m$ and K′ were obtained from the intercepts and slopes of linear plots between $\ln q_e$ against $\varepsilon^2$. In the D-R isotherm the $R^2$ value of the linear line was calculated as 0.98. K′ and $X'_m$ were calculated as 8,73895E-06($mol^2\ kJ^{-2}$) and 0.030(mg/g), respectively from the Eq. (5.7). In addition, adsorption energy (E; J/mol) was calculated which gave information about physical or chemical characteristic of adsorption.

As a result, E was calculated as 0,239197 J/mol. If the E value IS between 8-16 kJ/mol the adsorption mechanism is chemically occurred. If the E value <8 kJ/mol this indicated that adsorption mechanism is physical. In this study calculated e value showed that a physical adsorption mechanism between CIP and Nano-GO/M was observed.

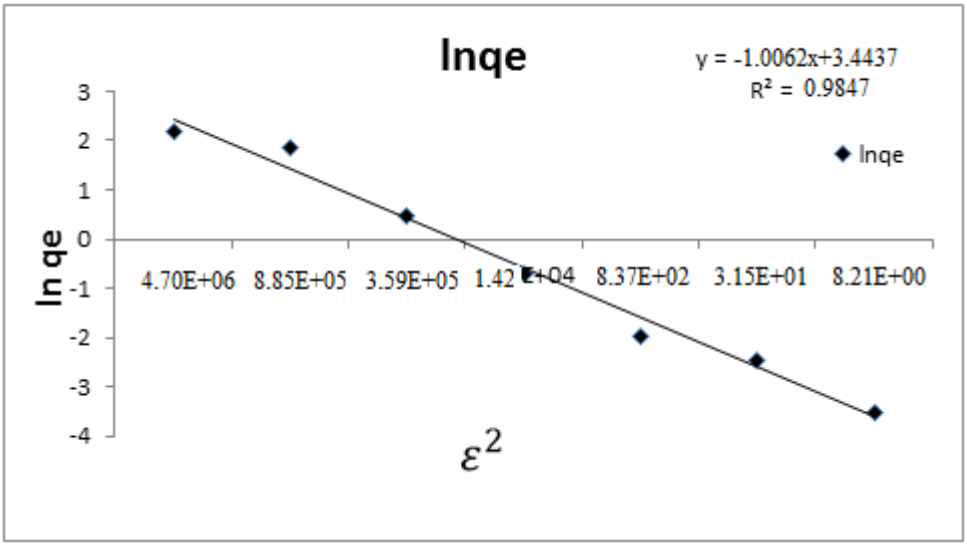


Figure 6.34 D-R isotherm of CIP at increasing CIP concentration, at a Nano-GO/M concentration of 0.5 g/L at pH=6.5, at 21°C and 30 min contacting time.

*6.2.1.7.5 Flory–Huggins Isotherm.* A plot of log $\theta/C_0$ against log (1 - θ) is linear if the adsorption process conforms to this model. The equilibrium constant Ka (0.328 L/g) and n (0.18) are obtained from the intercept and slope of the plot respectively from the Eq. (5.8). The θ in Eq. (5.8) was calculated from the Eq. (5.9).

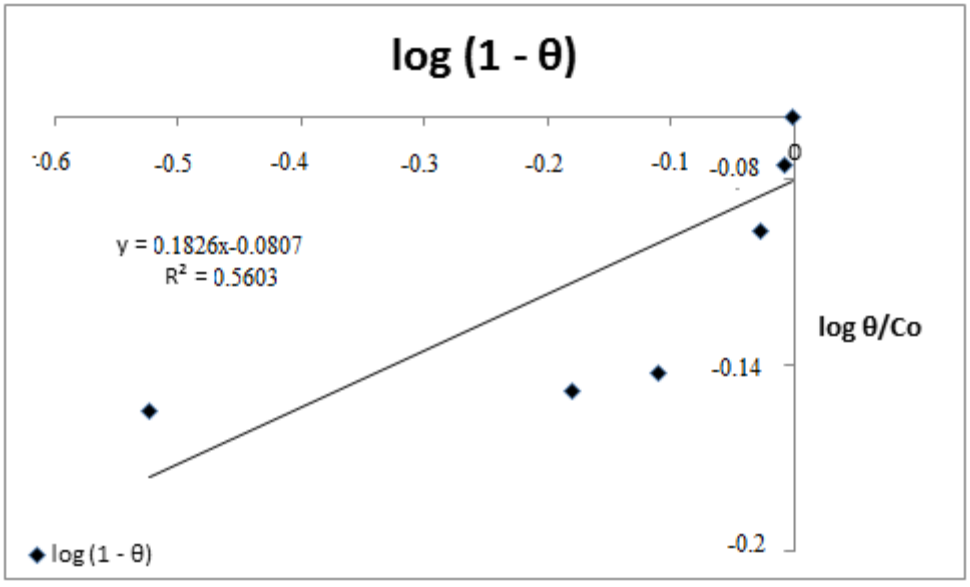


Figure 6.35 Flory-Huggins isotherm of CIP at increasing CIP concentration, at a Nano-GO/M concentration of 0.5 g/L at pH=6.5, at 21°C and 30 min contacting time.

The apparent Gibbs free energy of sorption $\Delta G_0$, which is a fundamental criterion of spontaneity, was evaluated using the following equation (Wankasi & Tarawou, 2008) (Eq. (6.1));

$$\Delta Go = RT \ln Ce \quad (6.1)$$

Where R is the universal gas constant (8.314 J/molK) and T is absolute temperature (K). Ka is obtained from the Flory-Huggins isotherms in Eq.5.8. The ΔGo (-2725.76) value for CIP adsorption onto Nano-GO/M is calculated and shown to be negative hence the process is spontaneous.

Among the five adsorption isotherms used in this study (Langmuir, Freundlich, Temkin, D-R and Flory-Huggins) the higher $R^2$ value (0,9853) vas obtained in the Freundlich isotherm with meaningful kinetic constants indicating the low adsorption capacity of Nano-GO/M ($K_F$ and n were calculated as 1.31 (unitless) and 1.38 (unitless), respectively. This showed that the adsorptions of CIP to the Nano-GO/M can be explained with Freundlich isotherm. The Flory-Huggins isotherm represents the poorest fit of experimental data than the other isotherm equations according to $R^2$ values of the plots (0.8639, 0.9853 and 0.7526, 0.9847 and 0.5603, respectively) with not significant kinetic constants values. Al-Heetimi et al. (2014), researched adsorption of CIP on porcelinaite. They calculated $K_F$ and n values as 1.7(unitless) and 0.59 (unitless) ($R^2$=0.9889). In our study $K_F$ value was lower than Al-Heetimi et al. (2014) while n value vas higher. The value of 1/n (0.73 in our study) is <1, indicating that adsorption of CIP onto Nano-GO/M is a favorable adsorption (Han et al. 2011).

### *6.2.2 Batch Adsorption Studies of OFL*

*6.2.2.1 Effects of Nano-GO/M Composite Concentrations on the Adsorption of OFL*

In order to determine the maximum adsorption efficiencies of OFL, 0.5 g/L, 2 g/L, 10 g/L Nano-GO/M composite concentrations were researched. Preliminary experiments showed that among the adsorption times that are tested, the maximum OFL removal was obtained after 30 min adsorption time (data not shown). Therefore, all experiments were realized after 30 min adsorption time, at 21°C (room temperature)

and at original pH (6.5) of OFL solution. Figure 6.36 summarizes the adsorption efficiencies of OFL at 0.5 g/L Nano-GO/M, at increasing OFL concentrations (1, 3, 5, 25, 100, 500 and 1000 mg/L). OFL adsorption efficiencies were found as 35 %, 34%, 33%, 23%, 18%, 14% and 10% for 1, 3, 5, 25, 100, 500 and 1000 mg/L OFL concentrations, respectively. According to these results it can be concluded that the OFL adsorption removals were high (35-34%) at low OFL concentrations (1-3 mg/L). As the OFL concentrations were increased, the adsorption efficiencies decreased. The reason of this can be explained as follows: at high OFL concentrations the active centers in holes of the surface of Nano-GO/M was not enough high to adsorb all the OFL concentrations. Therefore, the adsorption efficiency is low at high OFL concentrations.

A linear relationship between OFL adsorption efficiencies and influent OFL concentration was obtained (R=0.82) and this regression is significant (ANOVA $p=0.025<\alpha$ (0.05) and F=10.05).

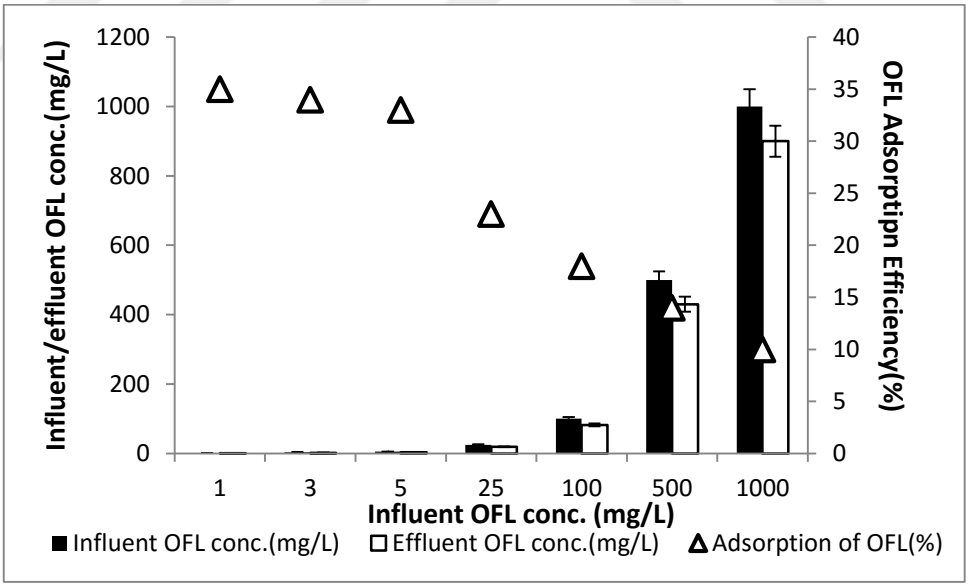


Figure 6.36 Effect of increasing OFL concentration on the yields of OFL adsorption at a Nano-GO/M concentration of 0.5 g/L at pH=6.5, at 21°C and 30 min contacting time (<α (0.05)).

Figure 6.37 shows the adsorption efficiencies of OFL at increasing OFL concentrations (1, 3, 5, 25, 100, 500 and 1000 mg/L) were found as 33 %, 32%, 31%, 24%, 15%, 10% and 6% at 2 g/L Nano-GO/M, respectively. As the OFL

concentrations were increased, the adsorption efficiencies decreased. The maximum OFL removal efficiency is 33% at 2 g/L Nano-GO/M concentration at 1 mg/L influent OFL concentration. According to this results it can be concluded that the OFL adsorption removals were high (33-32%) at low OFL concentrations (1-3 mg/L). As the OFL concentrations were increased, the adsorption efficiencies decreased. The reason of this can be explained as follows: at high OFL concentrations the surface of Nano-GO/M was not enough high to adsorb all the OFL concentrations. Therefore, the adsorption efficiency is low at high OFL concentrations.

A linear relationship between OFL adsorption efficiencies and influent OFL concentration was obtained (R=0.85) and this regression is significant (ANOVA $p=0.015<\alpha$ (0.05) and F=12.84).

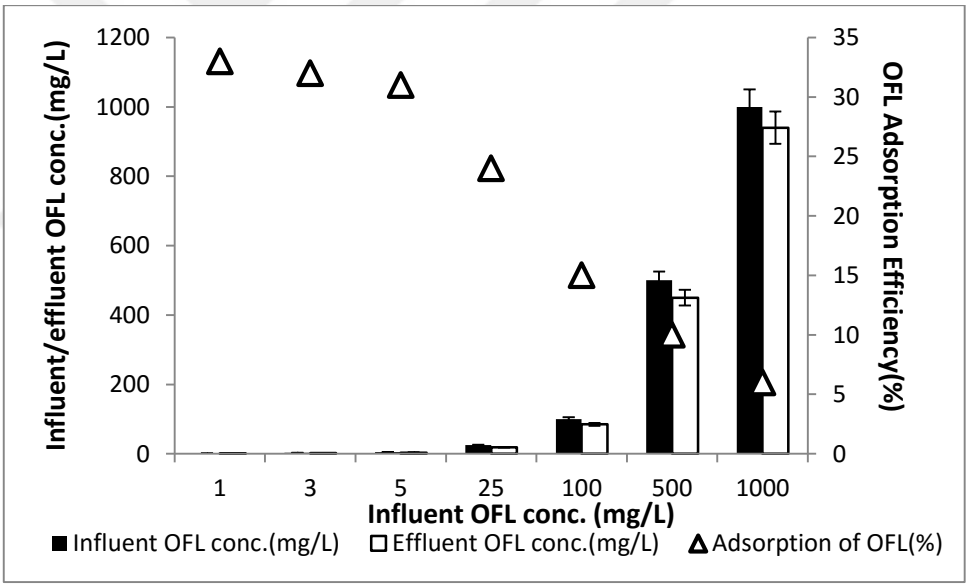


Figure 6.37 Effect of increasing OFL concentration on the yields of OFL adsorption at a Nano-GO/M concentration of 2 g/L at pH=6.5, at 21°C and 30 min contacting time (<α (0.05)).

Figure 6.38 shows the adsorption efficiencies of OFL at increasing OFL concentrations (1, 3, 5, 25, 100, 500 and 1000 mg/L) for 10 g/L Nano-GO/M. According these OFL concentrations the adsorption yields were 29%, 28%, 27%, 20%, 13%, 6% and 3%, respectively. As the OFL concentrations were increased, the adsorption efficiencies decreased. The maximum OFL removal efficiency is 29% at 10 g/L Nano-GO/M concentration for 1 mg/L influent OFL concentration. According

to this results it can be concluded that the OFL adsorption removals were high (29-28%) at low OFL concentrations (1-3 mg/L).

A linear relationship between OFL adsorption efficiencies and influent OFL concentration was obtained (R=0.86) and this regression is significant (ANOVA $p=0.013 < \alpha\ (0.05)$ and F=14.35).

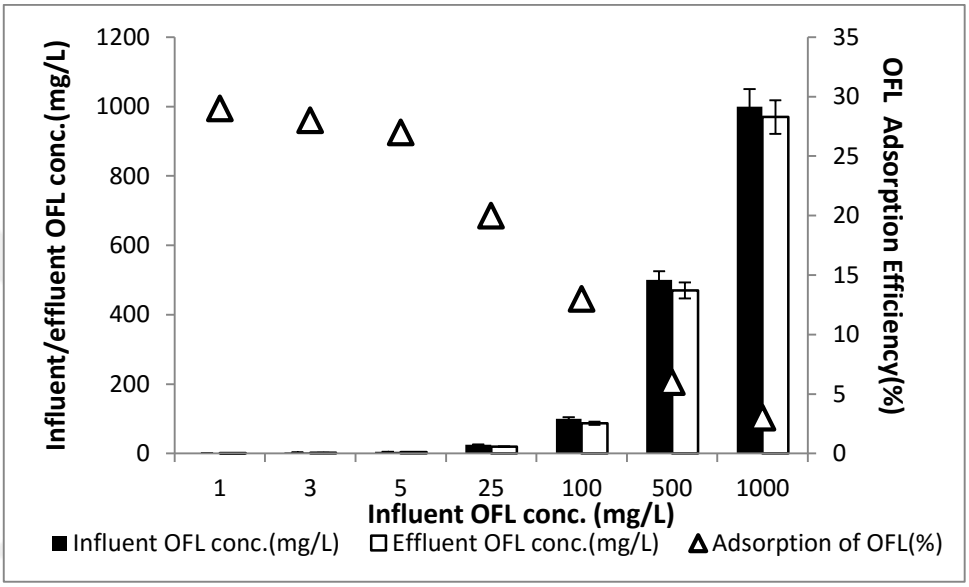


Figure 6.38 Effect of increasing OFL concentration on the yields of OFL removal at a Nano-GO/M concentration of 10 g/L at pH=6.5, at 21°C and 30 min contacting time ($<\alpha\ (0.05)$).

Figure 6.39 summarizes the effects of increasing Nano-GO/M concentrations (0.5, 2 and 10g/L) on OFL adsorption yields at an OFL concentration of 5 mg/L after 30 min adsorption time at pH=6.5 and at 21°C. Increasing the concentration of Nano-GO/M from 0.5 g/L to 2 g/L did not change the OFL adsorption yields significantly (35% and 33%, respectively) but slightly lower adsorption efficiency (29%) was obtained with 10 g/L Nano-GO/M composite concentration at the same operational conditions. Among these 3 different (0.5, 2 and 10 g/L) concentrations of Nano-GO/M, the maximum OFL adsorption yields was found as 33% for 5 mg/L initial OFL concentration. The optimum Nano-GO/M concentration was chosen as 0.5 g/L in order to reduce the operational cost of adsorption process.

At lower Nano-GO/M concentration (0.5, 2 g/L) slightly higher OFL adsorption yields (35% and 33%, respectively) was obtained while slightly lower OFL adsorption

removals was obtained at higher Nano-GO/M concentration (10 g/L) at pH 6.5 (Figure 6.39). This can be attributed to that partial active sites are not entirely exposed and utilized at lower Nano-GO/M concentrations, which leads to slightly higher adsorption capacity. Lower active surface area on the Nano-GO/M decrease the adsorption yield as reported by Li et al. (2013).

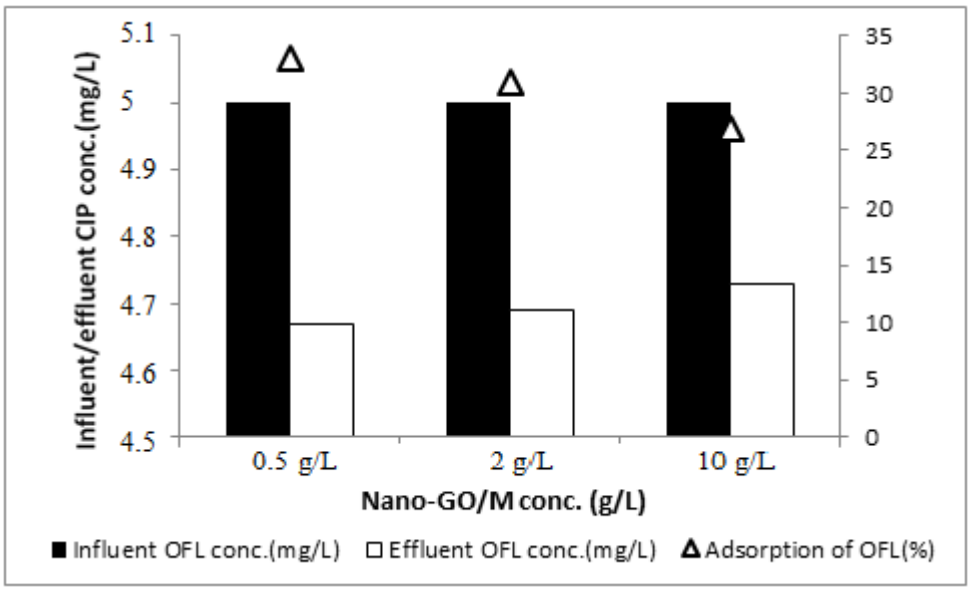


Figure 6.39 Comparison of increasing concentration of Nano-GO/M (0.5, 2 and 10 g/L) on the yields of OFL adsorption for constant OFL concentration (5 mg/L) at pH=6.5, at 21°C and 30 min contacting time (<α (0.05)).

Table 6.5 represents the effects of different Nano-GO/M concentrations on the adsorption efficiency of OFL for 1 mg/L initial OFL concentration. Adsorption of OFL on Nano-GO/M composite was high at 0.5 g/L.

Table 6.5 Shows the maximum adsorption efficiencies of OFL (1mg/L) at 21°C, and at 0.5, 2 and 10 g/L Nano-GO/M concentration, at a pH of 6.5.

| Nano-GO/M concentrations (g/L) | Adsorption efficiencies (%) |
|---|---|
| 0.5 | 35 |
| 2 | 33 |
| 10 | 29 |

A linear relationship between Nano-GO/M concentrations and maximum OFL adsorption efficiencies (for 1 mg/L initial OFL concentration) was obtained (R=0.97) and this regression is significant (ANOVA p=0.12>α (0.05) and F=28.21).

There are a few studies on adsorption of OFL: Nurchi et al. (2015), found maximum OFL adsorption capacities of 137.3, 75.9 and 112 mg/g with different pHs (4, 7 and 9, respectively) for 12.5g/L biomass (grape stalk) concentration within 120 min retention time and at a room temperature. Initial OFL concentration varying between 0.5 to 7 mM. Another study remarked the OFL (at a concentration of 0.5-5mM) adsorption on 0.5 g/40 ml OFL sample within 24 hours retention time and at room temperature. They found a maximum adsorption capacity of 31.1, 26 and 24.9 mg/g at a pH of 4, 7 and 9, respectively (Crespo-Alonso et al. 2013). In our study, for each pH (4, 6.5 and 10) the maximum OFL adsorption capacities were calculated as 20, 36 and 16.5 mg/g, respectively. The maximum OFL adsorption capacities were higher than Crespo-Alonso et al. 2013.

#### *6.2.2.2 Effect of Contacting Time on the Adsorption of OFL*

After determining the optimum concentration of Nano-GO/Min preliminary studies (0,5 g/L Nano-GO/M, data not shown), it was decided to investigate the effect of contact time on the adsorption of 5 mg/L OFL at increasing retention times (15, 30 and 60 min) at pH = 6.5, at a temperature of 21°C. As the contacting time was increased from 15 min to 30 min and 60 min the OFL removals increased from 19% to 33% and to 36% for initial OFL concentration of 5 mg/L (Figure 6.40). Further increase in contact time from 60 min to 900 min decreased the OFL adsorption yield from 39% to 22%. There was no significant difference between adsorption efficiency of OFL and increasing time (from 15 to 30 and 60 min). As a result, in this study the optimum contact time for maximum OFL removal (33%) was found to be 30 min. This short retention time reduces the cost for adsorption of OFL to Nano-GO/M extremely.

A linear relationship between adsorption yields and adsorption times were obtained up to a contacting time of 900 min, and this regression is significant (R=0.85, p= 0,34>α (0.05) and F= 2.69).

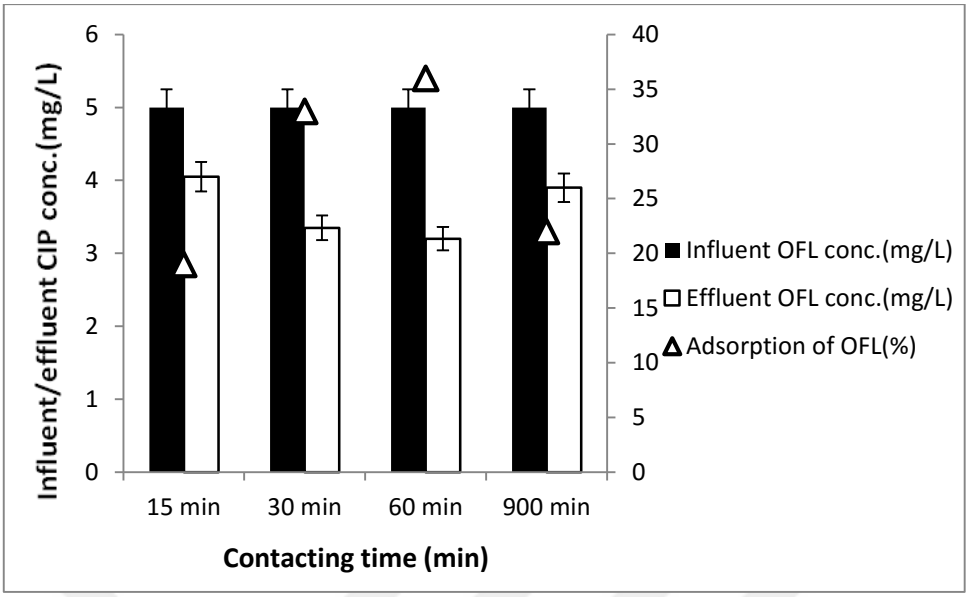


Figure 6.40 Effect of contacting time on the yields of constant OFL concentration (5 mg/L), at a constant Nano-GO/M concentration (0.5 g/L), at a pH of 6.5 and at 21°C (<α (0.05)).

According to the results obtained in step of the study it was found that at very short irradiation time (15 min) and very long irradiation times (900 min) low OFL adsorption yields was obtained. The decreased adsorption efficiency may be explained as the reduction of the remaining active adsorption sites of Nano-GO/M (Shaoling et al., 2013).

### *6.2.2.3 Effect of Increasing OFL concentrations on the OFL Adsorption yields*

At this step of this study, the effects of increasing OFL concentrations (1 mg/L, 3 mg/L, 5 mg/L, 25 mg/L, 100 mg/L, 500 mg/L, 1000 mg/L) on the OFL removals were studied at a Nano-GO/M concentration of 0.5 g/L, after 30 min contacting time, at pH= 6.5 and at a temperature of 21°C (Figure 6.41). Results showed that increasing in the OFL concentration reduced the removal efficiency of OFL at a Nano-GO/M concentration of 0.5 g/L. For 1 mg/L initial OFL concentration the maximum OFL removal efficiency was found as 35% while the removal efficiency of 1000 mg/L OFL was found almost 10%. This increase in the OFL concentrations after adsorption process results in decrease in the adsorption efficiencies of OFL. Thus, for the maximum adsorption yield of OFL (35%) the optimum OFL concentration was found

to be 1 mg/L. The OFL ions around absorbent sites of Nano-GO/M composite increased in number with the increase of initial OFL concentration.

A significant correlation between OFL adsorption yields and influent OFL concentration was obtained (R=0.82). ANOVA test statistics showed that a significant regression between adsorption yields and CIP yields was obtained ($p=0.024<\alpha$ (0.05) and F=10.04).

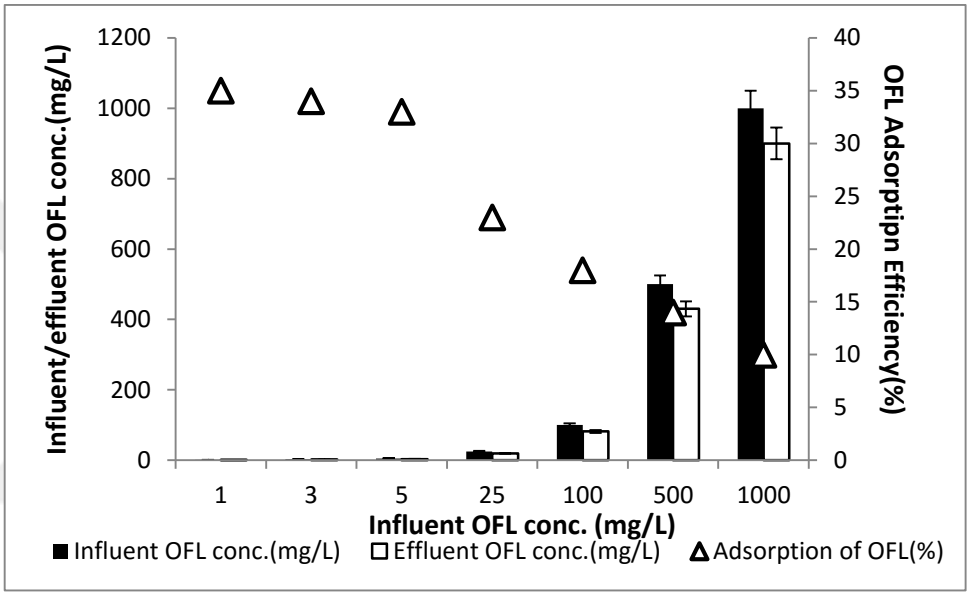


Figure 6.41 Effect of increasing OFL concentration on the yields of OFL adsorption at a Nano-GO/M concentration of 0.5 g/L at pH=6.5, at 21°C and 30 min contacting time (<α (0.05)).

### *6.2.2.4 Effect of pH on the Adsorption of OFL with Nano-GO/M composite*

The pH value is among the most important parameters that has an impact on adsorption capacity of Nano-GO/M. The effects of pH on the adsorption of increasing OFL concentrations (1, 3, 5, 25, 100, 500 and 1000 mg/L) were studied under acidic, neutral and alkaline pHs (4, 6.5 and 10) at an adsorption time of 30 min, at a Nano-GO/M concentration of 0.5 g/L and at 21°C. Table 6.6 represents the effects of different pHs on the adsorption efficiency of OFL at 21°C. Adsorption of OFL on Nano-GO/M was relatively high at pH 6.5.

Table 6.6 Shows the adsorption efficiencies of increasing OFL at acidic, neutral and alkaline pHs (4, 6.5 and 10) at 21°C and at 0.5 g/L constant Nano-GO/M concentration.

| **OFL concentrations (mg/L)** | **1** | **3** | **5** | **25** | **100** | **500** | **1000** |
|---|---|---|---|---|---|---|---|
| **Adsorption efficiency (%) at pH= 4** | 27 | 26 | 25 | 18 | 10 | 6 | 3 |
| **Adsorption efficiency (%) at pH= 6.5** | 35 | 34 | 33 | 23 | 18 | 14 | 10 |
| **Adsorption efficiency (%) at pH= 10** | 19 | 18 | 17 | 12 | 8 | 5 | 2 |

In this study, the maximum adsorption efficiency was found as 35% at pH=6.5 at 1 mg/L OFL concentration and 0.5 g/L Nano-GO/M concentration. As the pH values decreased from 6.5 to 4 the CIP adsorption yields decreased to 27% at pH=4 at 1mg/L OFL concentration and constant Nano-GO/M concentration (0.5 g/L). Under alkaline conditions the adsorption yields exhibited decrease to 19%. As the OFL concentrations were increased from 1 to 1000 mg/L the adsorption yields decreased significantly to 3%, 10% and 2% at pH 4, 6.5 and 10, respectively.

OFL can interaction the surface of Nano-GO/M with its quinoline aromatic moiety; and with neutral and positively charged piperazine groups present in the chemical structure (Crespo-Alonso et al., 2013). At pH 6.5 the prevalent species of OFL is the zwitterionic form and Nano-GO/M surface is negatively charged, so a strong interaction occurs between the positively charged piperazine ring and the negatively charged solid surface (Crespo-Alonso et al., 2013). Similar considerations hold at pH 10, taking into account that about 20% of OFL is still in the zwitterionic form. At any rate, these electrostatic interactions seem to play a secondary role in the antibiotic interaction with the whole Nano-GO/M, which seems to the stacking interactions of quinoline and piperazione moieties as reported above (Crespo-Alonso et al., 2013). The adsorption decrease gradually after a pH of 6.5. This behavior could be related to the presence of the negative molecule form OFL, which can exhibit repulsive interactions with the Nano-GO/M negative surface (Jalil, Baschini & Sapag, 2015).

Figure 6.42 summarizes the adsorption yields versus pH levels and OFL concentrations. Consequently, the maximum OFL (initial OFL concentration was 1 mg/L) adsorption yield was obtained at pH 6.5 (35%), but at alkaline pH lowest OFL

adsorption yield (19%) was obtained whilst at acidic pH lower OFL adsorption yield was obtained (27%).

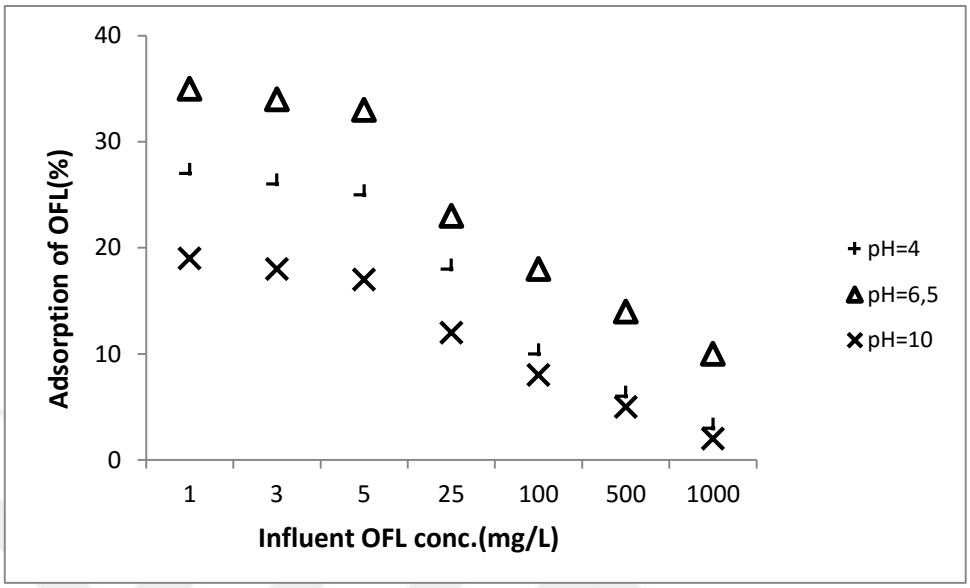


Figure 6.42 Effect of different pHs (4, 6.5 and 10) on the yield of OFL adsorption at a Nano-GO/M concentration of 0.5 g/L at pH=6.5, at 21°C and 30 min contacting time (<α (0.05)).

Table 6.7 represents the effects of different pHs on the maximum adsorption efficiency of OFL for 1 mg/L initial OFL concentration at 21°C. Adsorption of OFL on Nano-GO/M was relatively high at pH 6.5.

Table 6.7 shows the maximum adsorption efficiencies of OFL (1mg/L) at acidic, neutral and alkaline pHs (4, 6.5 and 10) at 21°C and at 0.5 g/L constant Nano-GO/M concentration.

| pH | Adsorption efficiencies (%) |
|---|---|
| 4 | 27 |
| 6.5 | 35 |
| 10 | 19 |

A linear relationship between pH and maximum OFL adsorption efficiencies (for 1 mg/L initial OFL concentration) was obtained (R=0.58) and this regression is not significant (ANOVA p=0.61>α (0.05) and F=0.51).

As the pH increases from 4.0 to 6.5 the interaction between OFL and positively charged Nano-GO/M became more feasible. Above pH 6.5, both OFL and Nano-GO/M became increasingly negatively charged with increasing pH, resulting in decreased adsorption (Rakshit et al., 2013).

#### *6.2.2.5 Effect of Temperature on the Adsorption of OFL with Nano-GO/M Composite*

Temperature is an important parameter for the adsorption process. To investigate the effect of temperature, OFL adsorption was studied under different temperatures (21°C, 40°C, 60°C and 80°C). For maximum OFL adsorption the optimum Nano-GO/M concentration (0.5 g/L) and optimum adsorption time (30 min) were determined in the preliminary studies as mentioned above. Therefore, all experiments were realized after 30 min adsorption time, at increasing OFL concentrations (1, 3, 5, 25, 100, 500 and 1000 mg/L) and at original pH (6.5) of OFL solution at 0.5 g/L Nano-GO/M. Figure 6.43 summarizes the adsorption efficiencies of OFL at 21°C, with 0.5 g/L constant Nano-GO/M, at increasing OFL concentrations (1, 3, 5, 25, 100, 500 and 1000 mg/L). OFL adsorption efficiencies were found as 35 %, 3%, 33%, 23%, 18%, 14% and 10% for 1, 3, 5, 25, 100, 500 and 1000 mg/L OFL concentrations, respectively. Therefore, the OFL adsorption efficiencies were high (35-34%) at low OFL concentrations (1-3 mg/L).

A linear relationship between OFL adsorption efficiencies and influent OFL concentration was obtained (R=0.82) and this regression is significant (ANOVA $p=0.025<\alpha$ (0.05) and F=10.04).

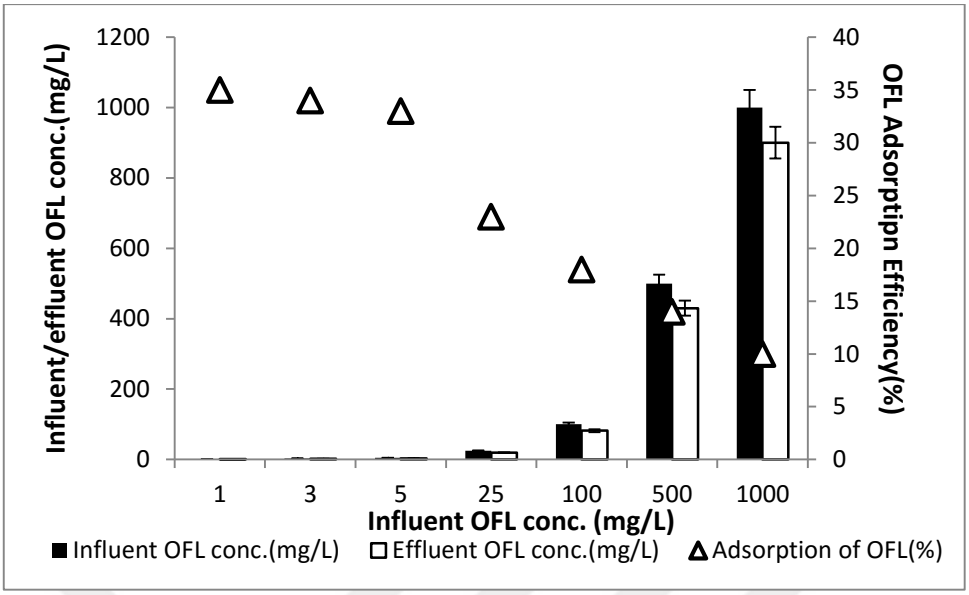


Figure 6.43 Effect of increasing OFL concentration on the yields of OFL adsorption at a Nano-GO/M concentration of 0.5 g/L at pH=6.5, at 21°C and 30 min contacting time (<α (0.05)).

Figure 6.44 shows the adsorption efficiencies of OFL at 40°C, with 0.5 g/L constant Nano-GO/M, at increasing OFL concentrations (1, 3, 5, 25, 100, 500 and 1000 mg/L). The adsorption efficiencies of OFL were found as 27 %, 26%, 25%, 16%, 10%, 5% and 3%, respectively. As the OFL concentrations were increased, the adsorption efficiencies decreased. The maximum OFL removal efficiency is 27% at 40°C, with 0.5 g/L constant Nano-GO/M concentration for 1 mg/L influent OFL concentration. According to this results it can be concluded that the OFL adsorption removals were not so high (27-26%) at low OFL concentrations (1-3 mg/L) at 40°C.

A linear relationship between OFL adsorption efficiencies and influent OFL concentration was obtained (R=0.81) and this regression is significant (ANOVA p=0.027>α (0.05) and F=9.48).

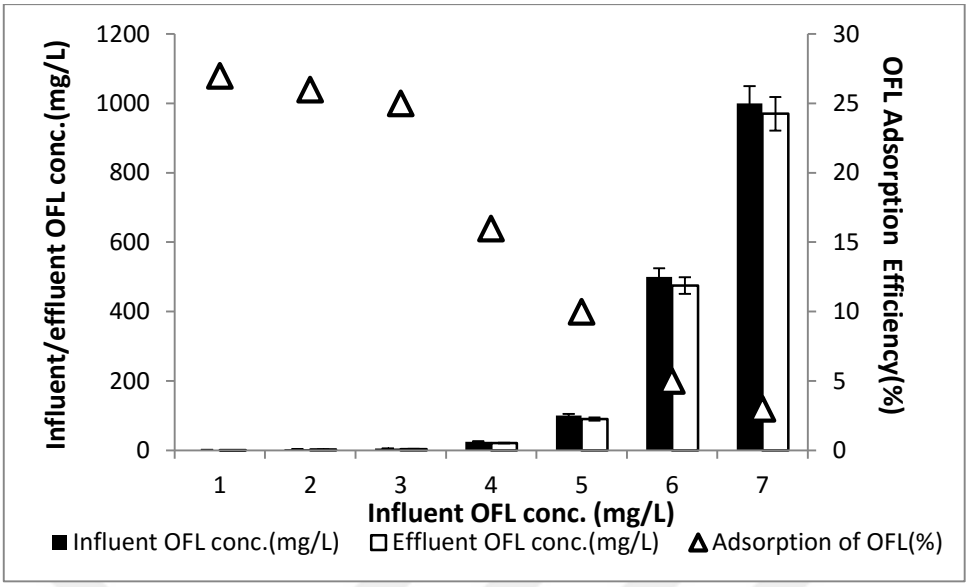


Figure 6.44 Effect of increasing OFL concentration on the yields of OFL adsorption at a Nano-GO/M concentration of 0.5 g/L at pH=6.5, at 40°C and 30 min contacting time (<α (0.05)).

Figure 6.45 shows the adsorption efficiencies of OFL at increasing OFL concentrations (1, 3, 5, 25, 100, 500 and 1000 mg/L) for 60°Cat 0.5 g/L constant Nano-GO/M and at pH of 6.5. According these OFL concentrations the adsorption yields were 20%, 19%, 18%, 12%, 7%, 4% and 2%, respectively. As the OFL concentrations were increased, the adsorption efficiencies decreased. The maximum OFL removal efficiency is 20% at 60°C for 1 mg/L influent OFL concentration. According to this results it can be concluded that the OFL adsorption removals were lower (20-19%) at low OFL concentrations (1-3 mg/L) at 60°C.

A linear relationship between OFL adsorption efficiencies and influent OFL concentration was obtained (R=0.81) and this regression is significant (ANOVA p=0.027<α (0.05) and F=9.63).

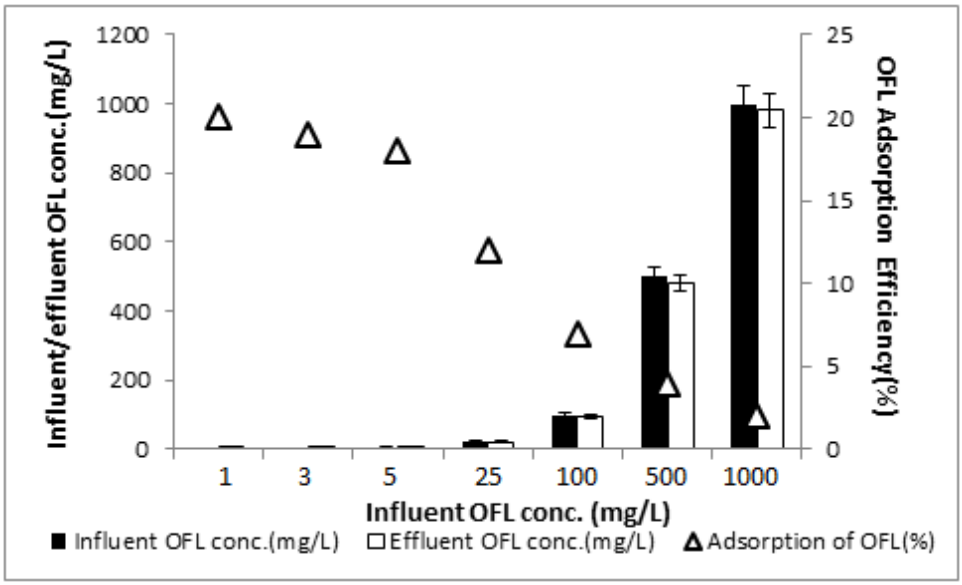


Figure 6.45 Effect of increasing OFL concentration on the yields of OFL adsorption at a Nano-GO/M concentration of 0.5 g/L at pH=6.5, at 60°C and 30 min contacting time (<α (0.05)).

Figure 6.46 shows the adsorption efficiencies of OFL at increasing OFL concentrations (1, 3, 5, 25, 100, 500 and 1000 mg/L) for 80°C at 0.5 g/L constant Nano-GO/M. According these OFL concentrations the adsorption yields were 14%, 13%, 12%, 8%, 6%, 3% and 1%, respectively. As the OFL concentrations were increased, the adsorption efficiencies decreased. The maximum OFL removal efficiency is 14% at 80°C for 1 mg/L influent OFL concentration. According to this results it can be concluded that the OFL adsorption removals were lower (14-13%) at low OFL concentrations (1-3 mg/L) at 80°C.

A linear relationship between OFL adsorption efficiencies and influent OFL concentration was obtained (R=0.85) and this regression is significant (ANOVA p=0.016<α (0.05) and F=12.78).

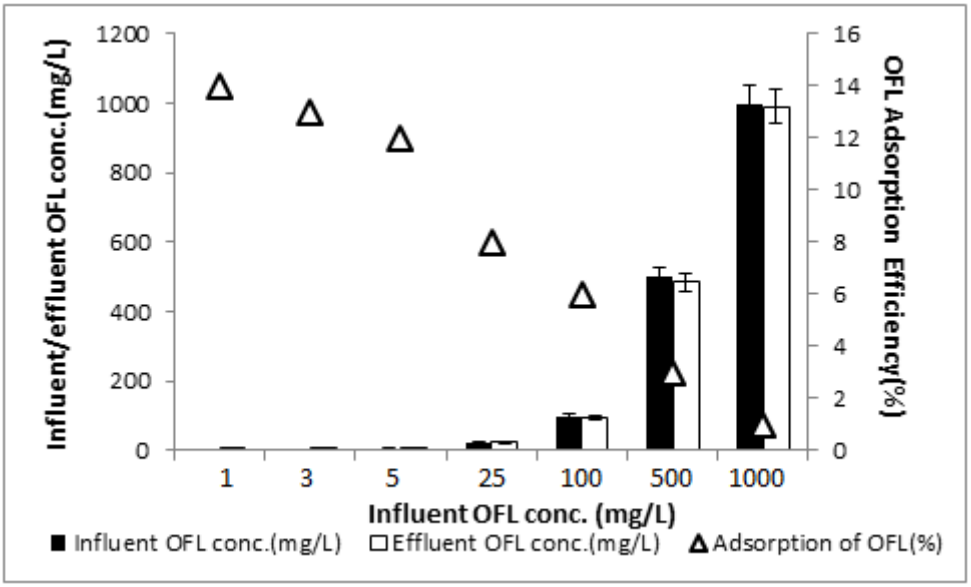


Figure 6.46 Effect of increasing OFL concentration on the yields of OFL adsorption at a Nano-GO/M concentration of 0.5 g/L at pH=6.5, at 80°C and 30 min contacting time (<α (0.05)).

Figure 6.47 summarizes the effects of increasing temperatures (21°C, 40°C, 60°C and 80°C) on OFL adsorption yields at a OFL concentration of 5 mg/L after 30 min adsorption time at pH=6.5 and at constant Nano-GO/M concentration (0.5 g/L). Increasing the temperature from 21°Cto 40-60-80°C yielded a decrease on the adsorption efficiencies of OFL.

Among these four different temperatures (21°C, 40°C, 60°C and 80°C), the maximum OFL adsorption yields was found as 33% for 5 mg/L initial OFL concentration at 21°C. This low temperature reduced the operational cost of adsorption process.

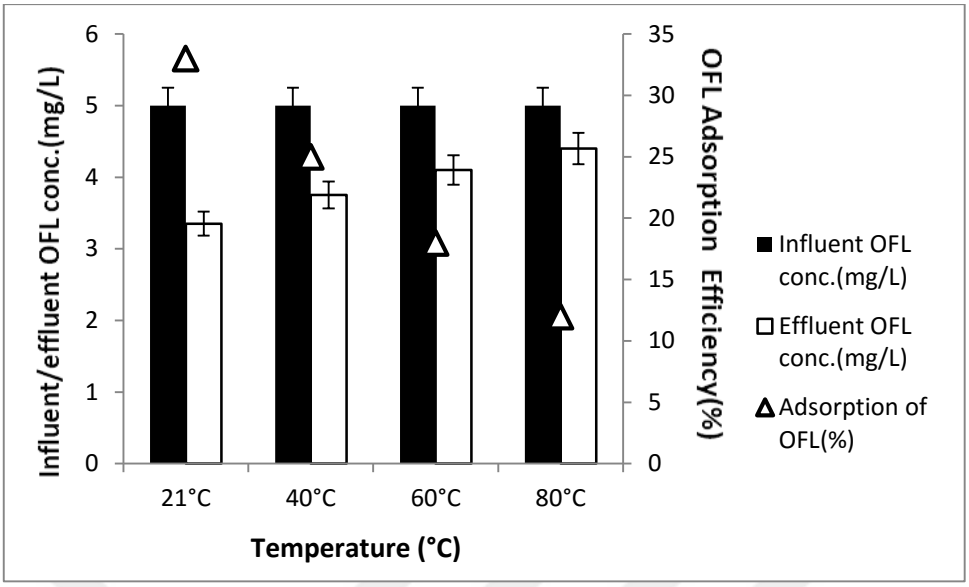


Figure 6.47 Effect of contacting time on the yields of constant OFL concentration (5 mg/L), at a constant Nano-GO/M concentration (0.5 g/L), at a pH of 6.5 and at 21°C, 40°C, 60°C and 80°C (<α (0.05)).

Table 6.8 represents the effects of different temperatures on the adsorption efficiency of OFL for 1 mg/L initial OFL concentration. Adsorption of OFL on Nano-GO/M was high at 21°C.

Table 6.8 Shows the maximum adsorption efficiencies of OFL (1mg/L) at 21°C, 40°C, 60°C and 80°C and at 0.5 g/L constant Nano-GO/M concentration.

| Temperature (°C) | Maximum Adsorption efficiencies (%) |
|---|---|
| 21 | 35 |
| 40 | 27 |
| 60 | 20 |
| 80 | 14 |

A linear relationship between temperature and maximum OFL adsorption efficiencies (for 1 mg/L initial OFL concentration) was obtained (R=0.97) and this regression is significant (ANOVA p=0.003<α (0.05) and F=35.18).

#### *6.2.2.6 Calculation of Maximum Adsorption Capacity of Nano-GO/M*

OFL adsorption kinetics on 0.5 g/L Nano-GO/M was performed with the increasing OFL concentrations (1, 3, 5, 25, 100, 500 and 1000 mg/L) at pH 6.5, at Nano-GO/M concentration of 0.5 g/L at 21°C after 30 min adsorption time. After magnetic separation, the adsorption amounts, $q_e$ (mg/g), were calculated by Eq. (5.1).

Table 6.9 represents the maximum adsorption capacities calculated with Eq. (5.1). The maximum adsorption capacity of OFL was found as 200 mg/g for 1000 mg/L OFL concentration while minimum value of adsorption capacity was found as 0.7 mg/g for 1 mg/L OFL concentration at 0.5 g/L Nano-GO/M. At high OFL concentration higher OFL adsorption capacities were obtained while low OFL adsorption capacities were obtained at low OFL concentrations. This increase in adsorption capacity the OFL concentrations after adsorption process resulting in increase in the maximum adsorption capacities of OFL by Nano-GO/M composite. The results showed that the OFL amount adsorbed on to surface of Nano-GO/M increase with the increase of OFL concentration while the removal percentage of OFL adsorbed on Nano-GO/M removal decreases at high OFL concentrations. This can be explained as follows: the maximum ads capacity was calculated per mass of nanocomposite while the adsorption yields were calculated from the removals of OFL. Since at low OFL concentrations the adsorption yields were high the studies were performed at low OFL levels.

Table 6.9 The maximum adsorption capacities of increasing concentration of OFL at 0.5 g/L Nano-GO/M, at a pH of 6.5 and at 21°C after 30 min adsorption time.

| **Influent OFL conc.(mg/L)** | 1 | 3 | 5 | 25 | 100 | 500 | 1000 |
|---|---|---|---|---|---|---|---|
| **Effluent OFL conc.(mg/L)** | 0.65 | 1.98 | 3.35 | 19.25 | 82 | 430 | 900 |
| **$q_m$ (mg/g)** | 0.7 | 2.04 | 3.3 | 11.5 | 36 | 140 | 200 |

#### *6.2.2.7 Adsorption Isotherms of OFL on Nano-GO/M*

The experimental adsorption data were exposed to different adsorption isotherms to determine the adsorption capacity of Nano-GO/M. Five different adsorption isotherms also were used for OFL adsorption on Nano-GO/M.

For maximum OFL adsorption capacity (200 mg/g) the optimum Nano-GO/M concentration (0.5 g/L) and optimum adsorption time (30 min), at 21°C (room temperature) and at original pH (6.5) were used for all adsorption isotherms. OFL concentrations were increased from 1 mg/L, to 3, 5, 25, 100, 500 and 1000 mg/L.

*6.2.2.7.1 Langmuir Isotherm.* The Langmuir coefficients b and qm representing the adsorption equilibrium constant and maximum adsorption capacity, respectively. These constants were obtained from the intercepts and slopes of the plots Ce versus qe exhibiting a linear plot (Eba et al. 2010).

Figure 6.48 represents the Langmuir isotherm slopes for adsorption of OFL on Nano-GO/M. In Langmuir isotherm the $R^2$ value of the linear line was 0.87, while b and $q_m$ values were calculated as 0.0049 L/mg and 245.35 mg/g, respectively from the Eq. (5.3).

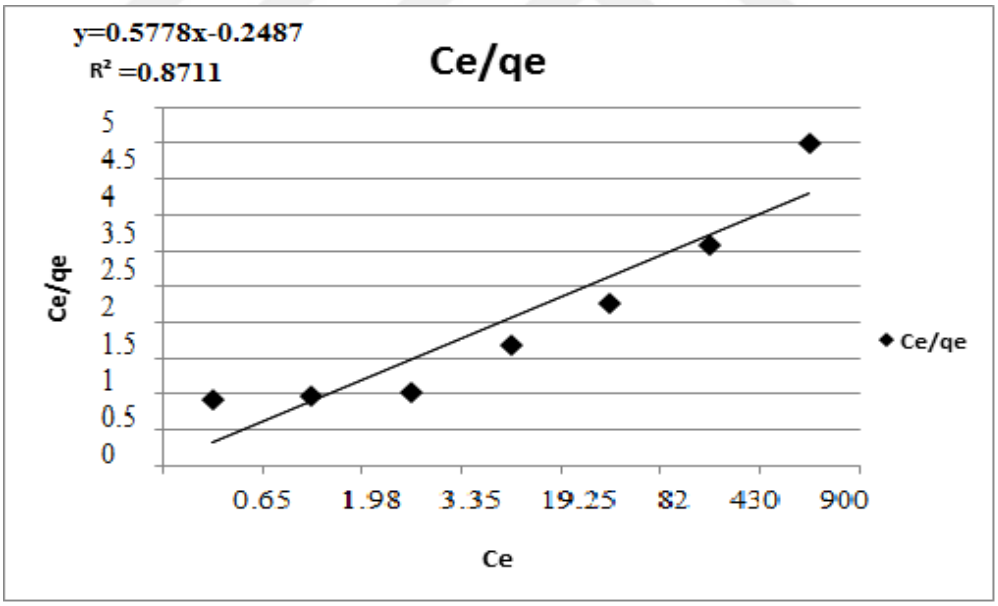


Figure 6.48 Langmuir isotherm for OFL adsorption at increasing concentration of OFL, at 0.5 g/L Nano-GO/M, at a pH of 6.5 and at 21°C after 30 min adsorption time.

The $R_L$ values indicate the type of isotherm which can to be favourable $0 < R_L < 1$, linear ($R_L=1$) or irreversible ($R_L = 0$). In this study $R_L$ value was found as 0.97 (unitless) indicating the adsorption process by mean of Langmuir model is favorable.

*6.2.2.7.1 Freundlich Isotherm.* This equation predicts multilayer adsorption on heterogeneous surface, characterized by an exponential distribution of active sites. The Freundlich coefficients $K_F$ and n which are the Freundlich constant and adsorption intensity were obtained from the intercepts and slopes of linear plots between $\ln q_e$ against $\ln C_e$ (Figure 6.49) (Eba et al., 2010). In Freundlich isotherm the $R^2$ value of the linear line was 0.98, $K_F$ and n were calculated as 1.30 (unitless) and 1.35 (unitless), respectively from the Eq. (5.4).

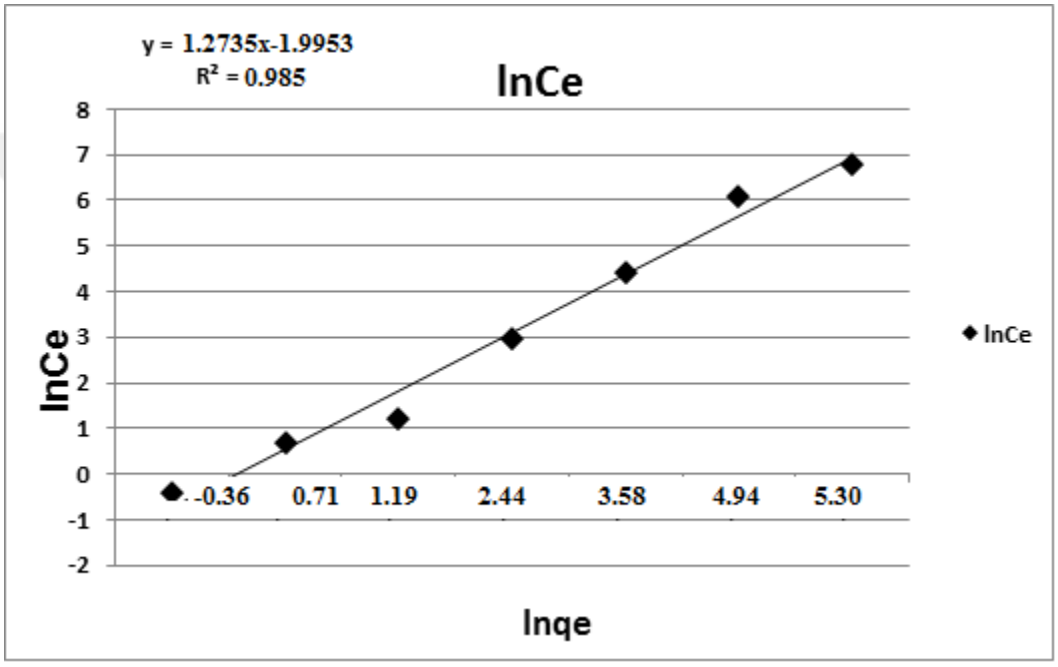


Figure 6.49 Freundlich isotherm of OFL at increasing concentration of OFL, at 0.5 g/L Nano-GO/M, at a pH of 6.5 and at 21°C after 30 min adsorption time.

The values of the adsorption intensity obtained in conformity with the requirement n>1 for physical adsorption process (Olakitan, Mi-Hwa & Dong, 2009), characterized by the adsorption of OFL onto Nano-GO/M described is favorable by the Freundlich isotherm.

*6.2.2.7.2 Temkin Isotherm.* The Temkin isotherm parameters were obtained by plotting $q_e$ versus $\ln C_e$, respectively. The isotherm data were calculated from the least squares methods.

Figure 6.50 represents the Temkin adsorption isotherm of OFL on Nano-GO/M. In the Temkin isotherm the $R^2$ value of the linear line was 0.79, A (L/mg) and B (J/mol) calculated as 0.030 L/mg and 1.38 J/mol, respectively from the Eq. (5.6).

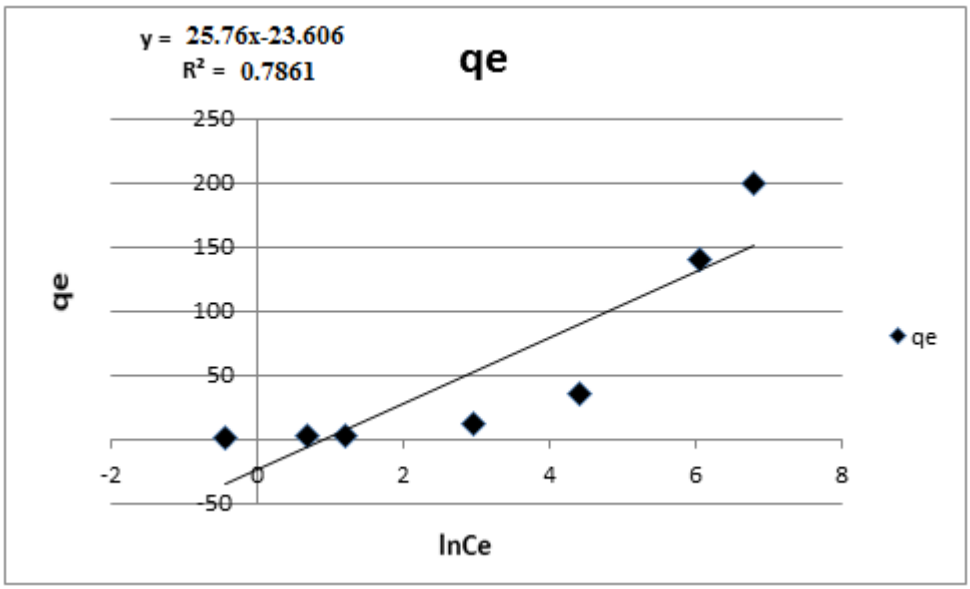


Figure 6.50 Temkin isotherm of OFL at increasing concentration of OFL, at 0.5 g/L Nano-GO/M, at a pH of 6.5 and at 21°C after 30 min adsorption time.

*6.2.2.7.3 Dubinin-Radushkevich Isotherm.* Figure 6.51 represents the D-R adsorption isotherm of OFL on Nano-GO/M. The D-R parameters $X'_m$ and K′ were obtained from the intercepts and slopes of linear plots between ln $q_e$ against $\varepsilon^2$. In the D-R isotherm the $R^2$ value of the linear line was calculated as 0.986. K′ and $X'_m$ were calculated as 8.84E-07($mol^2$ $kJ^{-2}$) and 0.7 mg/g, respectively from the Eq. (5.7). In addition, adsorption energy (E; J/mol) was calculated which gave information about physical or chemical characteristic of adsorption. As a result, E was calculated as 0.7519 J/mol. If the E value is between 8 and 16 kJ/mol the adsorption mechanism is chemically occurred. If the E value is <8 kJ/mol this indicated that adsorption mechanism is physical. In this study calculated E value showed that a physical adsorption mechanism between OFL and Nano-GO/M was observed.

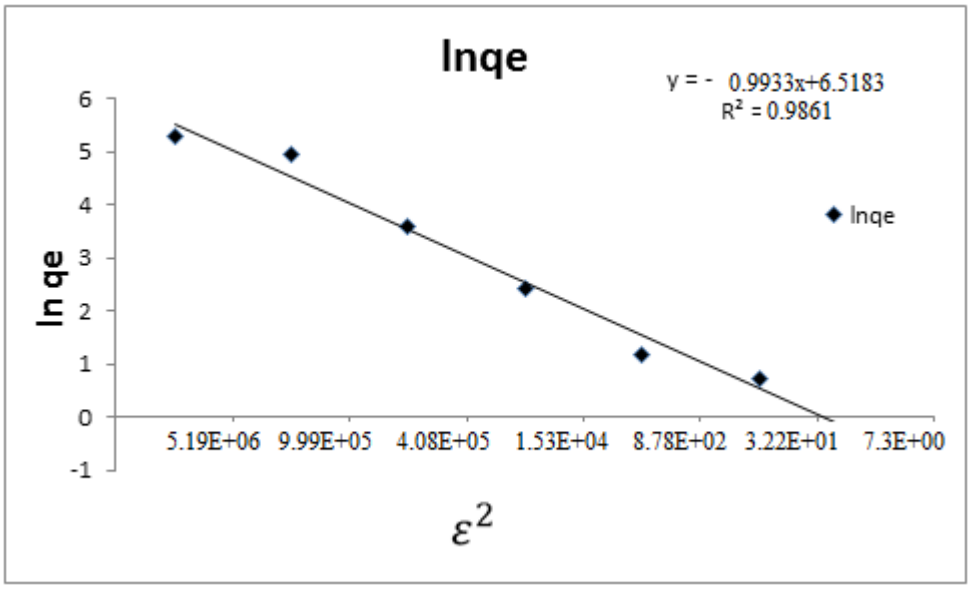


Figure 6.51 D-R isotherm of OFL at increasing concentration of OFL, at 0.5 g/L Nano-GO/M, at a pH of 6.5 and at 21°C after 30 min adsorption time.

*6.2.2.7.4 Flory–Huggins Isotherm.* A plot of log $\theta/C_0$ against log (1 - θ) is linear if the adsorption process conforms to this model. The equilibrium constant Ka (0.349 L/g) and n (3.21) are obtained from the intercept and slope of the plot, respectively from the Eq. (5.8). The θ in Eq. (5.8) was calculated from the Eq. (5.9).

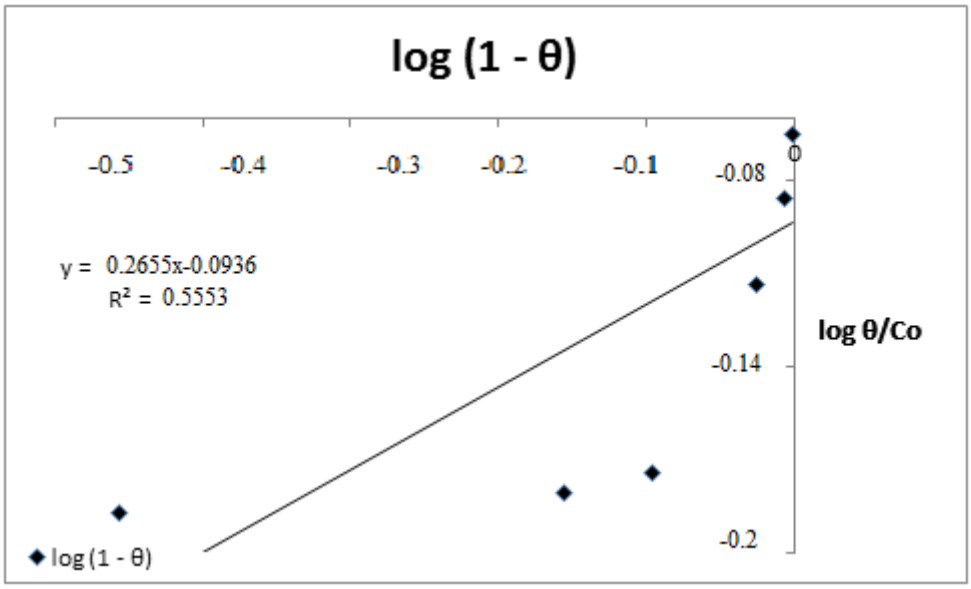


Figure 6.52 Flory-Huggins isotherm of OFL at increasing concentration of OFL, at 0.5 g/L Nano-GO/M, at a pH of 6.5 and at 21°C after 30 min adsorption time.

The apparent Gibbs free energy of sorption $\Delta G_0$, which is a fundamental criterion of spontaneity, was evaluated using the equation Eq. (6.1) (Wankasi &Tarawou, 2008).

Where R is the universal gas constant (8.314 J/molK) and T is absolute temperature (K). Ka is obtained from the Flory-Huggins isotherms. The ΔGo (-2547.60) value for OFL adsorption onto Nano-GO/M is calculated and shown to be negative hence the process is spontaneous.

Among the five adsorption isotherms used in this study (Langmuir, Freundlich, Temkin, D-R and Flory-Huggins) the higher $R^2$ (0.986) value vas obtained in the D-R isotherm with meaningful kinetic constants (K′ and $X'_m$ were calculated as 8.84E-07($mol^2$ $kJ^{-2}$), and 0.7 mg/g respectively). The Flory-Huggins isotherm represents the poorest fit ($R^2$= 0.555) of experimental data than the other isotherm equations according to $R^2$ values of the plots (0,871, 0,985 and 0,786, 0.986 and 0.555, respectively) and kinetic constants values indicating the low adsorption capacity of Nano-GO/M composite.

## 6.3 Photocatalytic Treatment Process

### *6.3.1 Removal of CIP under Photocatalytic Studies*

#### *6.3.1.1 Effects of Nano-GO/M Composite Concentrations on the Photocatalytic Treatment of CIP*

In this step of this study CIP was treated via photodegradation under UV light power in the presence of a nano composite (Nano-GO/M*)* generated under laboratory conditions.

Nano particles concentration is an important parameter for the photo-treatment of CIP. In order to determine the maximum photocatalytic treatment efficiencies of CIP, 0.5 g/L, 2 g/L, 10 g/L Nano-GO/M composite concentrations were researched. Preliminary experiments showed that among the irradiation times that are tested, the maximum CIP removal was obtained after 30 min irradiation time (data not shown). Therefore, all experiments were realized after 30 min irradiation time, at 21°C (room temperature) and at original pH (6.5) of CIP solution. Also the effects of increasing

UV light powers on the CIP yields were tested and the maximum CIP removal was obtained with 300 W UV light in the preliminary studies (data not shown). Figure 6.53 summarizes the photocatalytic treatment efficiencies of CIP at 0.5 g/L Nano-GO/M, at increasing CIP concentrations (1, 3, 5, 25, 100, 500 and 1000 mg/L). CIP photocatalytic treatment efficiencies were found as 93 %, 92%, 91%, 87%, 81%, 73% and 64% for 1, 3, 5, 25, 100, 500 and 1000 mg/L CIP concentrations, respectively. According to this results it can be concluded that the CIP photocatalytic treatment efficiencies were high (93-92%) at low CIP concentrations (1-3 mg/L).

The maximum CIP photocatalytic treatment efficiency obtained as 93% at 0.5 g/L Nano-GO/M concentration at 1 mg/L influent CIP concentration while the other high maximum CIP photocatalytic treatment efficiencies was calculated as 92% at 3 mg/L CIP concentration. At highest CIP concentration (1000 mg/L) the photocatalytic treatment efficiency obtained as 64% at 0.5 g/L Nano-GO/M concentration. As can be seen in Figure 6.53, the photocatalytic treatment efficiency was decreased from 93% to 64% with an increase in the initial CIP concentration from 1 mg/L to 1000 mg/L. When the initial CIP concentration is low, the probability of the reaction between CIP and oxidizing species was increased, leading to an improvement of photocatalytic treatment efficiency. However, the excess CIP concentration reduced photocatalytic treatment efficiency because only some parts of CIP molecules could interact with active holes of Nano-GO/M. All active holes on the surface of Nano-GO/M composite are full of the low concentration of CIP enabling photooxidation to exist with high efficiency. Consequently, the photocatalytic treatment efficiency of CIP was high. However, with increasing the CIP in the aqueous solution, there was a surplus for CIP molecules. In this case, only a part of CIP could interact with limited active sites on the Nano-GO/M surface, thereby causing lower photocatalytic treatment efficiency of CIP at higher initial CIP concentration. In addition, according to the Beer-Lambert law, as the initial CIP concentration was increased, the path length of photons entered the solution decrease, thereby resulting in lower photon adsorption on catalyst particles and consequently decreasing the generation of hydroxyl radical (Khataee et al., 2015). Thus, the photocatalytic treatment efficiency was gradually decreased as a result of increasing CIP concentration.

A linear relationship between CIP photocatalytic treatment efficiencies and influent CIP concentration was obtained (R=0.95) and this regression is significant (ANOVA $p=0.001<\alpha$ (0.05) and F=47.13).

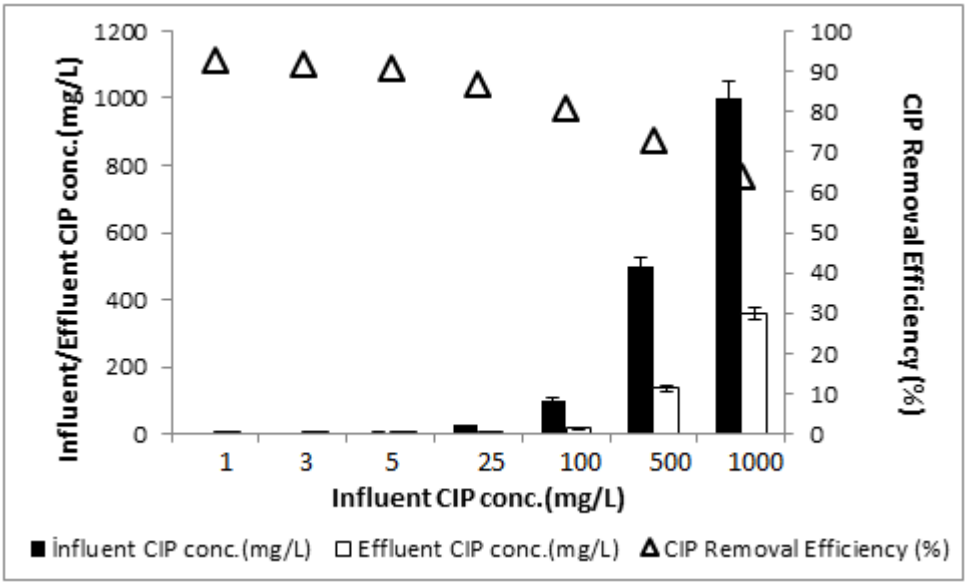


Figure 6.53 Effect of increasing CIP concentration on the yields of CIP photocatalytic treatment at a Nano-GO/M concentration of 0.5 g/L at pH=6.5, at 21°C and 30 min irradiation time and with a power of 300 W UV light ($<\alpha$ (0.05)).

Figure 6.54 shows the photocatalytic treatment efficiencies of CIP at increasing CIP concentrations (1, 3, 5, 25, 100, 500 and 1000 mg/L). The CIP yields were found as 91 %, 90%, 89%, 83%, 79%, 71% and 62% at 2 g/L Nano-GO/M, respectively**.** As the CIP concentrations were increased from 1 mg/L to 1000 mg/L, the photocatalytic treatment efficiencies decreased from 91% to 62%, respectively. The maximum CIP removal efficiency is 91% at 2 g/L Nano-GO/M concentration at 1 mg/L influent CIP concentration. According to this results it can be concluded that the CIP photocatalytic treatment efficiency were high (91-90%) at low CIP concentrations (1-3 mg/L). At highest CIP concentration (1000 mg/L) the photocatalytic treatment efficiency was obtained as 62% at 2g/L Nano-GO/M concentration. The reason of this may be explained by the only parts of CIP could interact with limited active sites on the Nano-GO/M surface, thereby causing lower photocatalytic treatment efficiency of CIP at higher initial CIP concentration.

A linear relationship between CIP photocatalytic treatment efficiencies and influent CIP concentration was obtained (R=0.94) and this regression is significant (ANOVA p=0.001<α (0.05) and F=39.79).

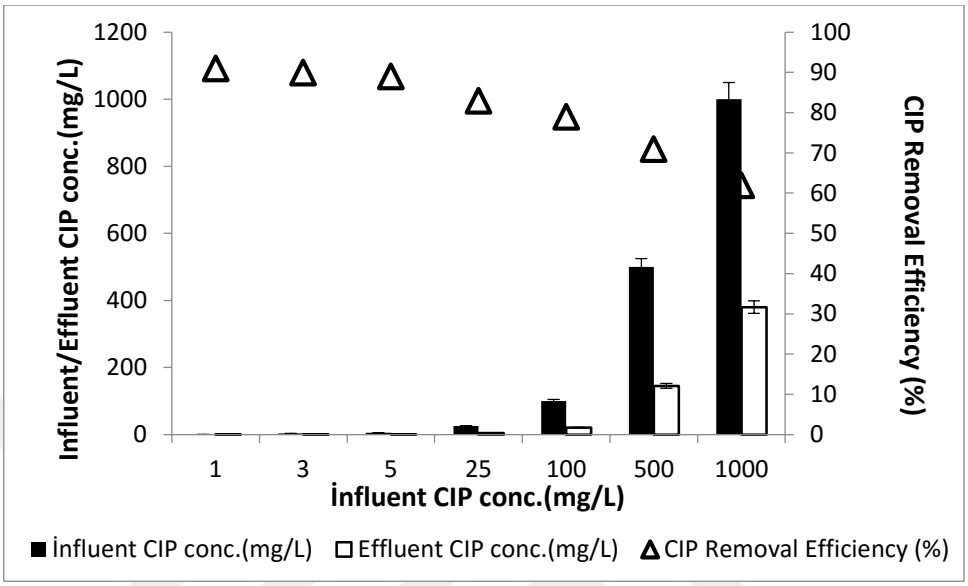


Figure 6.54 Effect of increasing CIP concentration on the yields of CIP photocatalytic treatment at a Nano-GO/M concentration of 2 g/L at pH=6.5, at 21°C and 30 min irradiation time and with a power of 300 W UV light (<α (0.05)).

Figure 6.55 shows the photocatalytic treatment efficiencies of CIP at increasing CIP concentrations (1, 3, 5, 25, 100, 500 and 1000 mg/L) for 10 g/L Nano-GO/M. According these CIP concentrations, the removal yields were 90%, 89%, 88%, 82%, 78%, 70% and 60%, respectively. The maximum CIP removal efficiency is 90% at 10 g/L Nano-GO/M concentration for 1 mg/L influent CIP concentration. According to this results it can be concluded that the CIP removals were high (90-89%) at low CIP concentrations (1-3 mg/L) while CIP removals were lower (70-60%) at high CIP concentrations (500-1000 mg/L). The photocatalytic treatment efficiency is low at high CIP concentrations. In other words, the Nano-GO/M remove small amount of CIP at high CIP concentrations as reported by Hong et al. (2009).

A linear relationship between CIP photocatalytic treatment efficiencies and influent CIP concentration was obtained (R =0.95) and this regression is significant (ANOVA p=0.0011<α (0.05) and F=44.39).

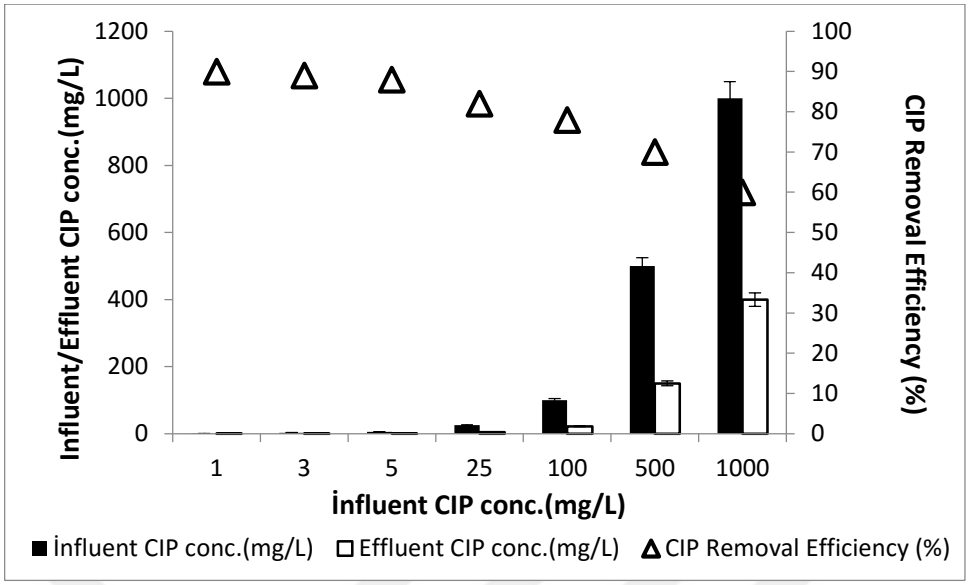


Figure 6.55 Effect of increasing CIP concentration on the yields of CIP photocatalytic treatment at a Nano-GO/M concentration of 10 g/L at pH=6.5, at 21°C and 30 min irradiation time and with a power of 300 W UV light (<α (0.05)).

Figure 6.56 summarizes the effects of increasing Nano-GO/M concentrations (0.5, 2 and 10g/L) on CIP removal yields at a CIP concentration of 5 mg/L after 30 min irradiation time at pH=6.5 and at 21°C and with a power of 300 W UV light.

Increasing the concentration of Nano-GO/M from 0.5 g/L to 2 g/L and to 10 g/L the removal yields slightly decreased. The CIP removal yields were obtained as 91%, 89% and 88% at 0.5, 2 and 10g/L Nano-GO/M composite concentration, respectively for 5 mg/L CIP concentration, at the same operational conditions. The optimum Nano-GO/M concentration was chosen as 0.5 g/L in order to reduce the operational cost of photocatalytic treatment process.

A linear relationship between maximum CIP removal efficiencies and Nano-GO/M composite was obtained (R=0.84) and this regression is significant (ANOVA p=0.06<α (0.05) and F=2.47).

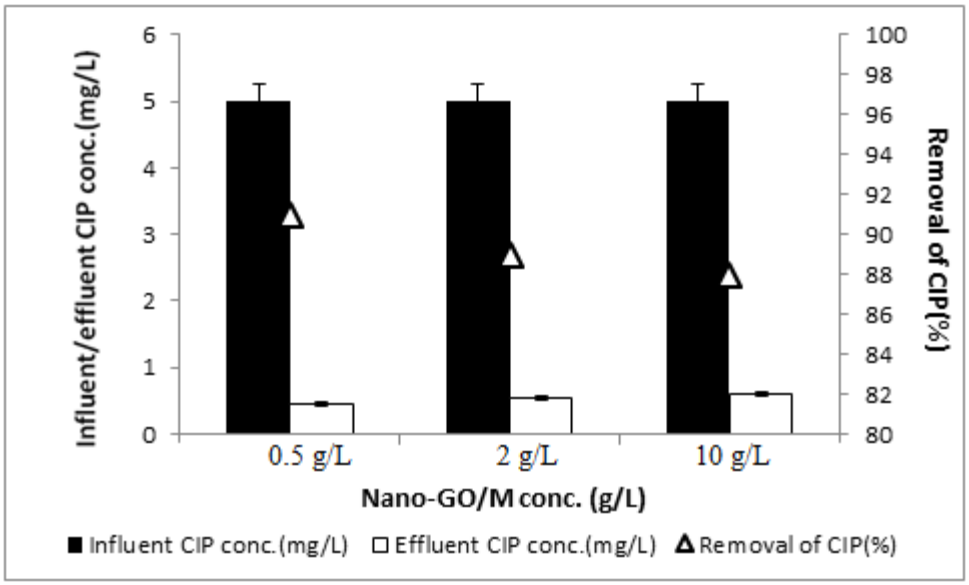


Figure 6.56 Effect of increasing concentration of Nano-GO/M (0.5, 2 and 10 g/L) on the yields of CIP removal for constant CIP concentration (5 mg/L) at pH=6.5, at 21°C and 30 min irradiation time and with a power of 300 W UV light (<α (0.05)).

At lower Nano-GO/M concentration (0.5 g/L) slightly higher CIP removal yields (93%) was obtained while slightly lower CIP removal yields (91 and 90%) was obtained at higher Nano-GO/M concentration (2 and 10 g/L, respectively) at pH 6.5 and with a power of 300 W UV light (Figure 22d).

Catalyst dosage is an important parameter in heterogeneous photocatalytic reaction. The photocatalytic treatment efficiency was increased with an increase in Nano-GO/M dosage up to 0.5 g/L and slightly decreased thereafter. Increasing the amount of photocatalyst from 0.5 g/L to 10 g/L resulted in decreasing the photocatalytic treatment efficiency from 93% to 90% at the irradiation time of 30 min for 1 mg/L of CIP initial solution, respectively. By increasing the catalyst dosage, the surface area was increased, leading to an increase in the production of reactive species (Pelaez et al., 2012). However, more Nano-GO/M dosage would also induce greater aggregation of the catalyst and decrease the total active surface area, thereby leading to a reduction in the photocatalytic treatment efficiency. Moreover, due to an increase in the turbidity of the solution, reduction in the degree of light penetration through the solution could take place (Zhe-Qi et al., 2015). Therefore, other experiments were carried out with 0.5 g/L Nano-GO/M to avoid the excessive usage of the catalyst.

Photocatalytic treatment of CIP with nanoparticles is a very new study area. There are a few studies on photocatalytic treatment of CIP: Xinlin et al. (2014), reported a maximum CIP (initial CIP conc. was 10 g/L) photocatalytic treatment efficiency of 70.90% for 0.1 g/L NaCl/$TiO_2$ concentration within 60 min irradiation time, at a temperature of 30 °C. Another study remarked the CIP (initial CIP conc. was 10 g/L) removal by photocatalytic treatment using 2 g/L reduced-GO/$BiVO_4$ within 60 min irradiation time, at 30 °C with a photocatalytic treatment efficiency of 68.2% (Yan et al., 2013). These yields were slightly lower than our study in the research performed by Yan et al., 2013 which these results are obtained at an irradiation time 60 min which is two times higher than our study. Therefore, in this study the short optimum irradiation time (30 min) reduced the operational cost of the CIP treatment.

Recently, graphene-based nano-materials as photocatalyst have been utilized to enhance the photocatalytic efficiencies such a supporting matrix with excellent electric conductivity and super-high surface area can sufficiently contact with water or target pollutants (Jia, Wang, Huang, Xu & Yu, 2011). That provide plenty of reactive sites as well as efficiently accelerate the electrons transfer process that from the inside of photocatalyst particles to reactive sites to suppress the recombination of photo-induced electron–hole pairs (Jia, Wang, Huang, Xu & Yu, 2011; Zhang, Li, Cui & Lin, 2010). Under UV irradiation, the Nano-GO/M nanoparticles generate an excitation of electrons in valence band into the conduction band (electron–hole separation). The generated electron (hole) transfer to the adsorbed CIP on the Nano-GO/M surface has always been considered as the first step of the photocatalytic action of nanoparticles (Wang, Von, Volman & Neckers, 1995). Photo-generated holes as well as hydroxyl radicals oxidize the CIP adsorbed at Nano-GO/M surface. The high oxidative potential of holes can lead to direct and indirect oxidation of CIP. In the indirect oxidation process of CIP molecules, hole at the valence band generates the hydroxide reactive radicals ($OH^{\bullet}$) via reaction with water and/or hydroxide anions ($OH^-$). Primary photoproducts resulting from interfacial electron (hole) transfer, i.e. radical ions, undergo further transformations, leading to the formation of final photoproducts. The photodegradation of CIP probably involves (Sponza & Oztekin, 2014):

• adsorption of efficient photons by Nano-GO/M composite

• oxygen adsorption followed by generation of superoxide radicals,
• generation of [H] atoms through photoelectrons,
• formation of hydroxyl radicals (OH●) from transient hydrogen peroxide ($H_2O_2$) and
• oxidation of organic molecule via successive attack of OH● radicals.

#### *6.3.1.2 Effect of Irradiation Time on the Photocatalytic Treatment of CIP*

After determining the optimum concentration of Nano-GO/M (0,5 g/L), it was decided to investigate the effect of irradiation time on the photocatalytic treatment of 5 mg/L CIP at increasing irradiation times (15, 30 and 60 min) at pH = 6.5, at a temperature of 21°C and at a power of 300 W UV light. As the irradiation time was increased from 15 min to 30 min and 60 min the CIP photo removals increased slightly from 82% to 93% and to 98% for initial CIP concentration of 5 mg/L (Figure 6.57). Further increase in irradiation time from 60 min to 900 min decreased the CIP removal yield slightly from 98% to 95% as reported by Lin & Wu (2014). They showed that CIP was degraded as a function of time at a $Na_2S_2O_8$ concentration of 1.92 g/L. The efficiency of photo-degradation of CIP (initial concentration 10 mg/L) reached 70% after 5 min and then increased with time and the maximum CIP yield was recorded as 90%. They also reported that after 30 min irradiation time the degradation efficiency did not show a significant increase compared to our study.

A linear relationship between photocatalytic removal yields and irradiation times were obtained up to a contacting time of 900 min, and this regression is significant ($R=0.92$, $p= 0,06<\alpha$ (0.05) and $F= 5.49$).

Yan et al. (2013), reported that the CIP photodegradation efficiency was 68.2% at 60 min irradiation time with 20 mg reduced-GO-$BiVO_4$ composite photocatalyst and 10 mg/L of 100 mL CIP solution at 33°C in a photochemical reactor under visible light with a 300 W xenon lamp. In our study, at short irradiation time (30 min) compared to the study of Yan et al. (2013) (to times higher of our irradiation time-60 min) 93% CIP removal yield was obtained for 5 mg/L influent CIP concentration. According to the results obtained in step of the study it was found that at very short irradiation time (15 min) and very long irradiation times (900 min) slightly lower CIP removal yields was

obtained. This short retention time reduces the cost for photocatalytic removal of CIP to Nano-GO/M extremely.

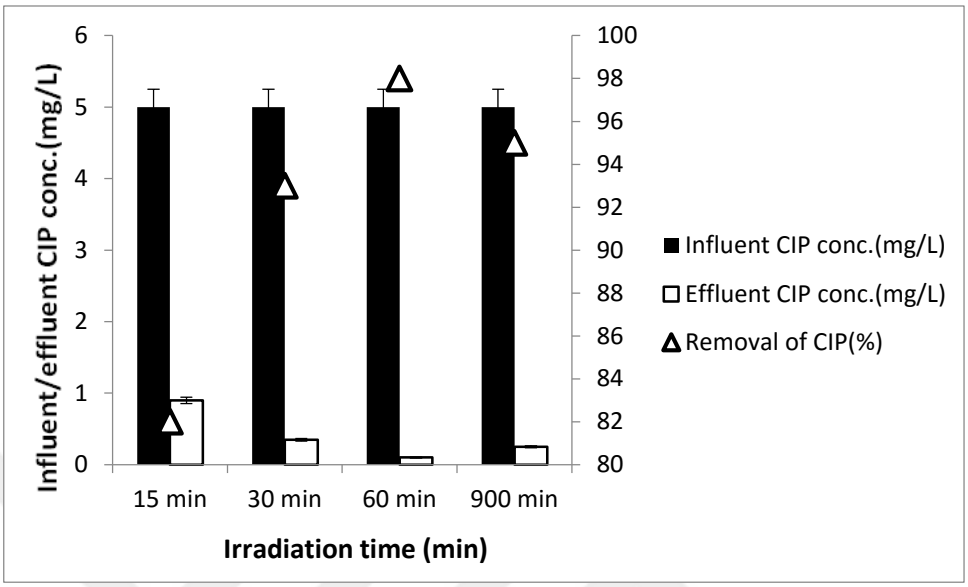


Figure 6.57 Effect of irradiation time on the yields of constant CIP concentration (5 mg/L), at a constant Nano-GO/M concentration (0.5 g/L), at a pH of 6.5 and at 21°C and with a power of 300 W UV light (<α (0.05)).

#### *6.3.1.3 Effect of Increasing CIP Concentrations on the CIP Photocatalytic Treatment Yields*

At this step of this study, the effects of increasing CIP concentrations (1 mg/L, 3 mg/L, 5 mg/L, 25 mg/L, 100 mg/L, 500 mg/L and 1000 mg/L) on the CIP removals were studied at a Nano-GO/M concentration of 0.5 g/L, after 30 min irradiation time, at pH= 6.5 and at a temperature of 21°C with a power of 300 W UV light (Figure 6.58). Results showed that increasing in the CIP concentration reduced the removal efficiency of CIP at a Nano-GO/M concentration of 0.5 g/L. For 1 mg/L initial CIP concentration the maximum CIP removal efficiency was found as 93% while the removal efficiency of 1000 mg/L CIP was found 64%. This increase in the CIP concentrations after photocatalytic process results in decrease in the removal efficiencies of CIP. This can be a result of blocking of the photocatalytically active sites on the Nano-GO/M and reducing the interaction of photons with these sites as reported by Lin & Wu (2014). Besides, the light absorbed by Nano-GO/M is more than

that at higher concentration of CIP, which can reduce the photocatalytic degradation efficiency to a certain extent (Hassani, Khataee & Karaca, 2015).

As the influent CIP concentration increased the CIP removal yields decreased. A linear relationship between CIP removal efficiencies and influent CIP concentration was obtained (R=0.95) and this regression is significant (ANOVA p=0.0007<α (0.05) and F=47.13).

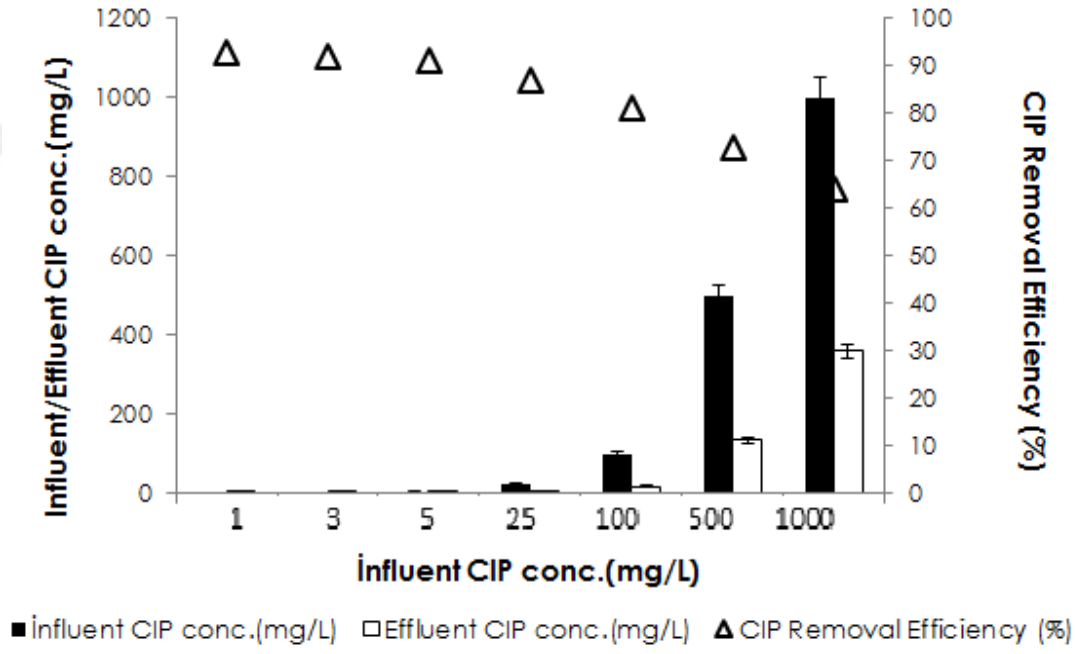


Figure 6.58 Effect of increasing CIP concentration on the yields of CIP removal at a Nano-GO/M concentration of 0.5 g/L at pH=6.5, at 21°C and 30 min irradiation time and with a power of 300 W UV light (<α (0.05)).

### *6.3.1.4 Effect of pH on the Photocatalytic Removal of CIP with Nano-GO/M composite*

Due to the chemical nature of fluoroquinolones, pH is the parameter ruling the photodegradation of CIP onto the catalyst surface. The pH value is among the most important parameters that has an impact on the photocatalytic capacity of Nano-GO/M.

The effects of pH on the on the increasing CIP concentrations (1, 3, 5, 25, 100, 500 and 1000 mg/L) were studied under acidic, neutral and alkaline pHs (4, 6.5 and 10) at

an irradiation time of 30 min, at a Nano-GO/M concentration of 0.5 g/L and at 21°C. Table 6.10 represents the effects of different pHs on the removal efficiency of CIP at 21°C. Photocatalytic removal efficiency of CIP on Nano-GO/M was relatively high at pH 6.5.

Table 6.10 Shows the photocatalytic removal efficiencies of increasing CIP at acidic, neutral and alkaline pHs (4, 6.5 and 10) at 21°C and at 0.5 g/L constant Nano-GO/M concentration.

| **CIP concentrations (mg/L)** | **1** | **3** | **5** | **25** | **100** | **500** | **1000** |
|---|---|---|---|---|---|---|---|
| **Removal efficiency (%) at pH= 4** | 72 | 71 | 70 | 62 | 56 | 49 | 38 |
| **Removal efficiency (%) at pH= 6.5** | 93 | 92 | 91 | 87 | 81 | 73 | 64 |
| **Removal efficiency (%) at pH= 10** | 57 | 56 | 55 | 49 | 42 | 33 | 25 |

In this study, the maximum removal efficiency was found as 93% at pH=6.5 at 1 mg/L CIP concentration and 0.5 g/L Nano-GO/M concentration. As the pH values decreased from 6.5 to 4 the CIP removal yields decreased to 72% at pH=4 at 1mg/L CIP concentration and constant Nano-GO/M concentration (0.5 g/L). Under alkaline conditions photodegradation yields decrease to 57%. As the CIP concentrations were increased from 1 to 1000 mg/L the removal yields decreased significantly to 38%, 64% and 25% at pH 4, 6.5 and 10, respectively.

CIP has two proton-binding sites, carboxyl and piperazinyl group (Rakshit et al., 2013). Explaining the pH effect on the photocatalytic process is a very laborious task because of its multiple roles such as electrostatic interactions between the catalyst surface and charged radicals formed during the photocatalytic reaction process. CIP has positively charged (cationic; pH=3), negatively charged (anionic; pH=7.5), and/or zwitterionic (pH=10) species at pHs due to different pKas of 6.1 and 8.7, respectively (Gu & Karthikeyan, 2005). At pH < 6.1, CIP molecules mainly exist as cations ($CIP^+$) because of the protonation of the amine group in the piperazine moiety (Wang et al., 2010). At pH > 8.7, CIP molecules exist as anions ($CIP^-$) due to the loss of a proton from the carboxylic group (Jalil, Baschini & Sapag, 2015). In the pH range 6.1–8.7, the pH values are higher than p*K*a1 of the carboxylic group, thus deprotonating the carboxylic group to the negatively charged carboxylate (Jalil, Baschini & Sapag, 2015). However, the amine group stays protonated and positively charged as this pH range is still lower than p*K*a2 of the amine group (Drakopoulos & Ioannou, 1997).

Accordingly, in the above mentioned pH range, zwitterionic species of CIP molecules dominate in the aqueous solution. This behavior can be explained by the relationship between the surface charge of Nano-GO/M and the CIP total charge and by the presence of the cationic form (CIP) that favors a strong removal on the negative surface of the Nano-GO/M.

The low photodegradation efficiency at more acidic pH (for example, at 4) may be related to the decomposition and corrosion of catalyst in acidic medium (Daneshvar et al., 2007). On the other hand, both Nano-GO/M and CIP were negatively charged in basic conditions, leading to electrostatic repulsion between them and the lower photodegradation efficiency of CIP. In the case of pH 6.5 (the natural pH of CIP), photocatalytic removal efficiency was the highest and the surface of Nano-GO/M was still in the positive form and the CIP was in its neutral form (Jalil, Baschini & Sapag, 2015).

Hassani, Khataee & Karaca. (2015), were investigated the effect of pH on the photocatalytic degradation of CIP onto the $TiO_2$ on montmorillonite. They researched the degradation experiments with 0.1 g/L of $TiO_2$ on montmorillonite with 20 mg/L initial concentration of CIP at different pH values between 3.0 and 10 for 120 min irradiation time at room temperature. Results show that the degree of photodegradation efficiency was increased with increasing the solution pH up to 5 and then decreased. These results are similar to our study.

Figure 6.59 summarizes the photocatalytic removal yields versus pH levels and CIP concentrations. Consequently, the maximum CIP (initial CIP concentration was 1 mg/L) photocatalytic removal yield (93%) was obtained at pH 6.5, but at alkaline and acidic pHs lowest CIP photocatalytic removal yields (57% and 72%, respectively) was obtained.

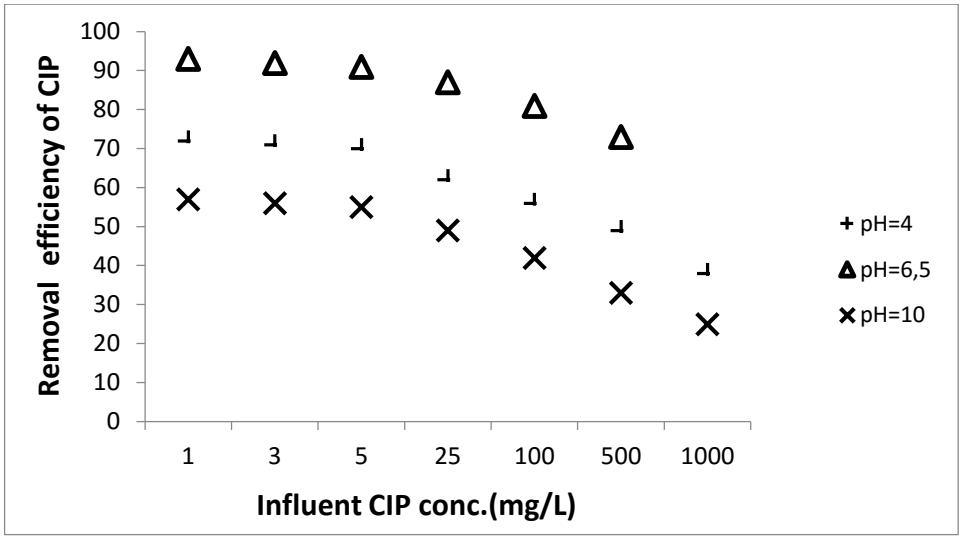


Figure 6.59 Effect of different pHs (4, 6.5 and 10) on the yield of CIP photocatalytic removal efficiency at a Nano-GO/M concentration of 0.5 g/L, at 21°C and 30 min irradiation time and with a power of 300 W UV light (<α (0.05)).

Table 6.11 summarizes shortly the effects of different pHs on the photocatalytic removal efficiency of CIP (for 1 mg/L initial CIP concentration) at 21°C. Photocatalytic removal of CIP on Nano-GO/M was relatively high at pH 6.5.

Table 6.11 Shows the maximum photocatalytic removal efficiencies of CIP (1mg/L) at acidic, neutral and alkaline pHs (4, 6.5 and 10) at 21°C and at 0.5 g/L constant Nano-GO/M concentration.

| pH | Removal efficiencies (%) |
|---|---|
| 4 | 72 |
| 6.5 | 93 |
| 10 | 57 |

A linear relationship between pH and maximum CIP photocatalytic removal efficiencies (for 1 mg/L initial CIP concentration) was not obtained (R=0.60) and this regression is not significant (ANOVA p=0.43>α (0.05) and F=0.33).

As the pH increases from 4.0 to 6.5 the correlation between CIP and positively charged Nano-GO/M became more feasible. Above pH 6.5, both CIP and Nano-GO/M became increasingly negatively charged with increasing pH, resulting in decreased photocatalytic removal (Rakshit et al., 2013).

#### *6.3.1.5 Effect of Temperature on the Photocatalytic Removal of CIP with Nano-GO/M Composite*

Temperature is an important parameter for the photocatalytic process. To investigate the effect of temperature, CIP removal was studied under different temperatures (21°C, 40°C, 60°C and 80°C). For maximum CIP removal the optimum Nano-GO/M concentration (0.5 g/L) and the optimum irradiation time (30 min) were determined in the preliminary studies as mentioned above. Therefore, all experiments were realized after 30 min irradiation time, at increasing CIP concentrations (1, 3, 5, 25, 100, 500 and 1000 mg/L) and at original pH (6.5) at 0.5 g/L Nano-GO/M. Figure 6.60 summarizes the photocatalytic removal efficiencies of CIP at 21°C, with 0.5 g/L constant Nano-GO/M, at increasing CIP concentrations (1, 3, 5, 25, 100, 500 and 1000 mg/L). CIP photocatalytic efficiencies were found as 93 %, 92%, 91%, 87%, 81%, 73% and 64% for 1, 3, 5, 25, 100, 500 and 1000 mg/L CIP concentrations, respectively. As a consequence, the CIP photocatalytic removal efficiencies were high (93-92%) at low CIP concentrations (1-3 mg/L). This can be a result of blocking of the photocatalytically active sites on the Nano-GO/M and reducing the interaction of photons with these sites as reported by Lin & Wu (2014). Besides, the light absorbed by Nano-GO/M is more than that at higher concentration of CIP, which can reduce the photocatalytic degradation efficiency to a certain extent (Hassani, Khataee & Karaca, 2015).

A linear relationship between CIP photocatalytic removal efficiencies and influent CIP concentration was obtained (R =0.95) and this regression is significant (ANOVA $p=0.001<\alpha$ (0.05) and F=47.13) and this regression is significant.

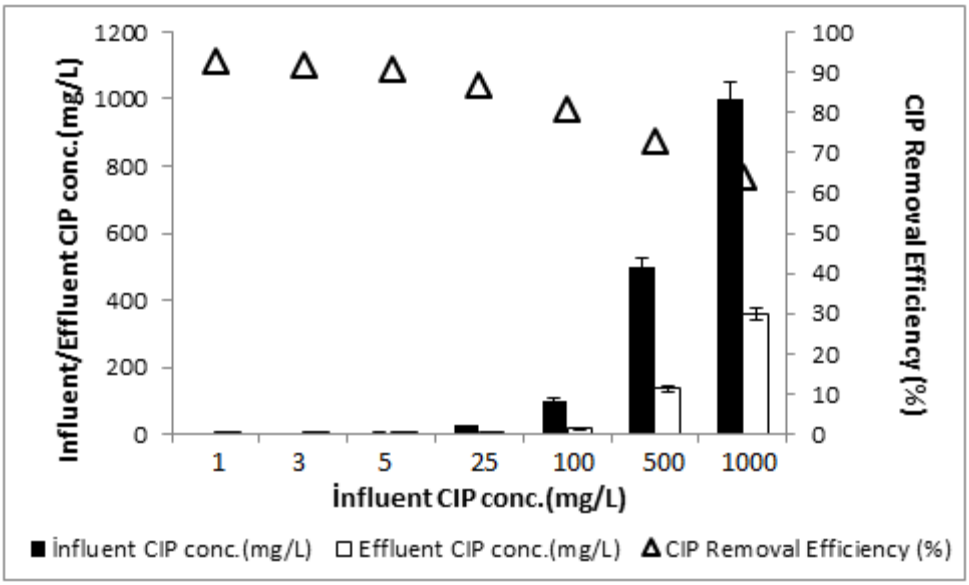


Figure 6.60 Effect of increasing CIP concentration on the yields of CIP removal at a Nano-GO/M concentration of 0.5 g/L at pH=6.5, at 21°C and 30 min irradiation time and at a power of 300 W UV light (<α (0.05)).

Figure 6.61 shows the photocatalytic removal efficiencies of CIP at 40°C, with 0.5 g/L constant Nano-GO/M, at increasing CIP concentrations (1, 3, 5, 25, 100, 500 and 1000 mg/L). The photocatalytic removal efficiencies of CIP were found as 82%, 81%, 80%, 72%, 63%, 52% and 44%, respectively. As the CIP concentrations were increased, the photocatalytic removal efficiencies decreased. The maximum CIP removal efficiency is 82% at 40°C, with 0.5 g/L constant Nano-GO/M concentration for 1 mg/L influent CIP concentration. The photodegradation efficiency was gradually decreased as a result of increasing CIP concentration. When the initial CIP concentration was decreased, the probability of the reaction between CIP and oxidizing species was increased, leading to an improvement of photodegradation efficiency. However, the excess CIP concentration reduced photodegradation efficiency. According to this results it can be concluded that the CIP photocatalytic removals were high (82-81%) at low CIP concentrations (1-3 mg/L) at 40°C.

A linear relationship between CIP photocatalytic removal efficiencies and influent CIP concentration was obtained (R=0.91) and this regression is significant (ANOVA p=0.004<α (0.05) and F=25.05).

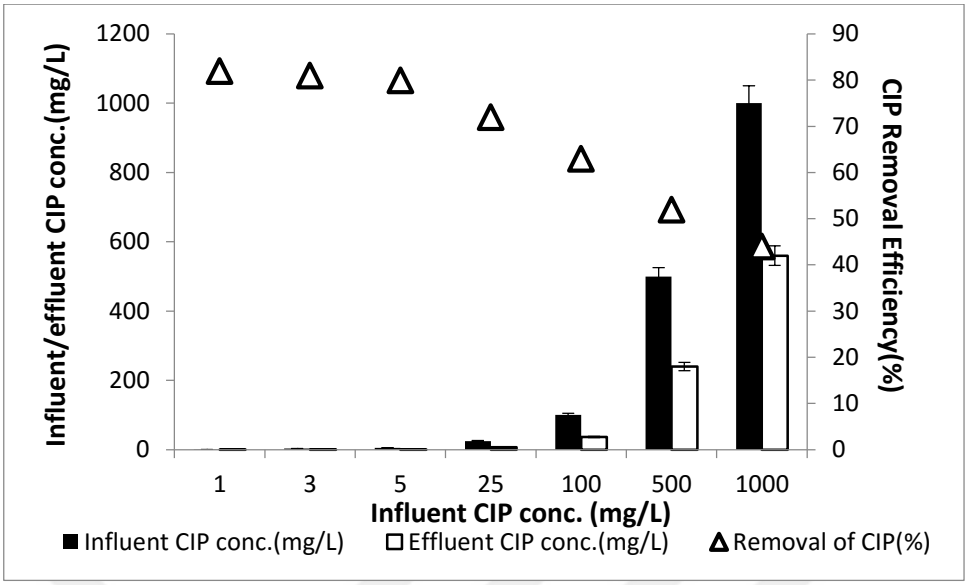


Figure 6.61 Effect of increasing CIP concentration on the yields of CIP removal at a Nano-GO/M concentration of 0.5 g/L at pH=6.5, at 40°C and 30 min irradiation time and at a power of 300 W UV light (<α (0.05)).

Figure 6.62 shows the photocatalytic removal efficiencies of CIP at increasing CIP concentrations (1, 3, 5, 25, 100, 500 and 1000 mg/L) for 60°C at 0.5 g/L constant Nano-GO/M and at pH of 6.5. According these CIP concentrations, the photocatalytic removal yields were 70%, 69%, 68%, 56%, 49%, 40% and 34%, respectively. As the CIP concentrations were increased, the photocatalytic removal efficiencies decreased. The maximum CIP removal efficiency is 70% at 60°C for 1 mg/L influent CIP concentration. According to this results it can be concluded that the CIP photocatalytic removals were lower (70-69%) at low CIP concentrations (1-3 mg/L) at 60°C.

A linear relationship between CIP photocatalytic removal efficiencies and influent CIP concentration was obtained (R=0.87) and this regression is significant (ANOVA p=0.01<α (0.05) and F=14.95)

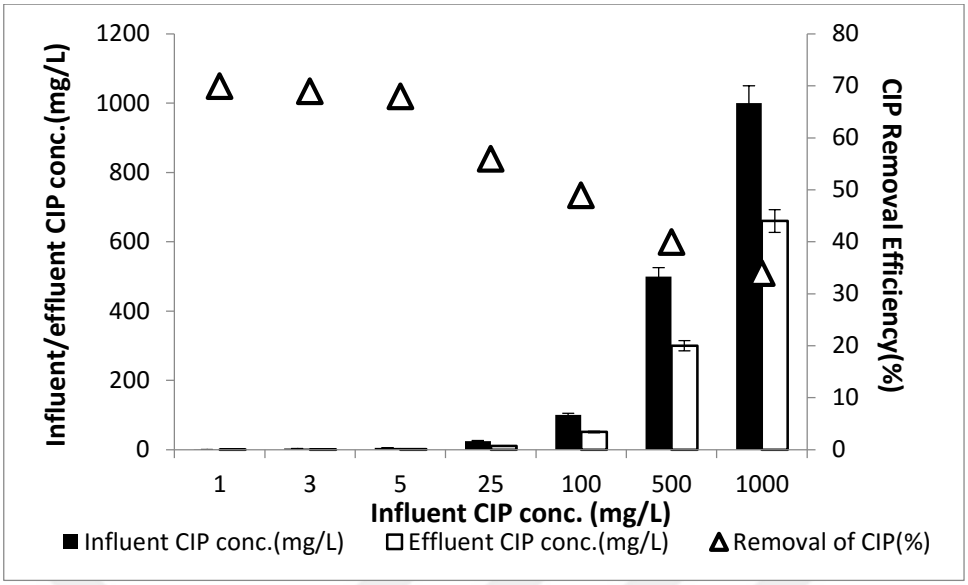


Figure 6.62 Effect of increasing CIP concentration on the yields of CIP removal at a Nano-GO/M concentration of 0.5 g/L at pH=6.5, at 60°C and 30 min irradiation time and at a power of 300 W UV light (<α (0.05)).

Figure 6.63 shows the photocatalytic removal efficiencies of CIP at increasing CIP concentrations (1, 3, 5, 25, 100, 500 and 1000 mg/L) for 80°C at 0.5 g/L constant Nano-GO/M. According these CIP concentrations, the photocatalytic removal yields were 62%, 61%, 60%, 52%, 43%, 31% and 23%, respectively. As the CIP concentrations were increased, the photocatalytic removal efficiencies decreased. The maximum CIP removal efficiency is 62% at 80°C for 1 mg/L influent CIP concentration. According to these results it can be concluded that the CIP adsorption removals were lowest (62-61%) at low CIP concentrations (1-3 mg/L) at 80°C. The photodegradation efficiency was gradually decreased as a result of increasing CIP concentration. When the initial CIP concentration was decreased, the probability of the reaction between CIP and oxidizing species was increased, leading to an improvement of photodegradation efficiency. However, the excess CIP concentration reduced photodegradation efficiency.

A linear relationship between CIP photocatalytic removal efficiencies and influent CIP concentration was obtained (R=0.92) and this regression is significant (ANOVA p=0.003<α (0.05) and F=26.21).

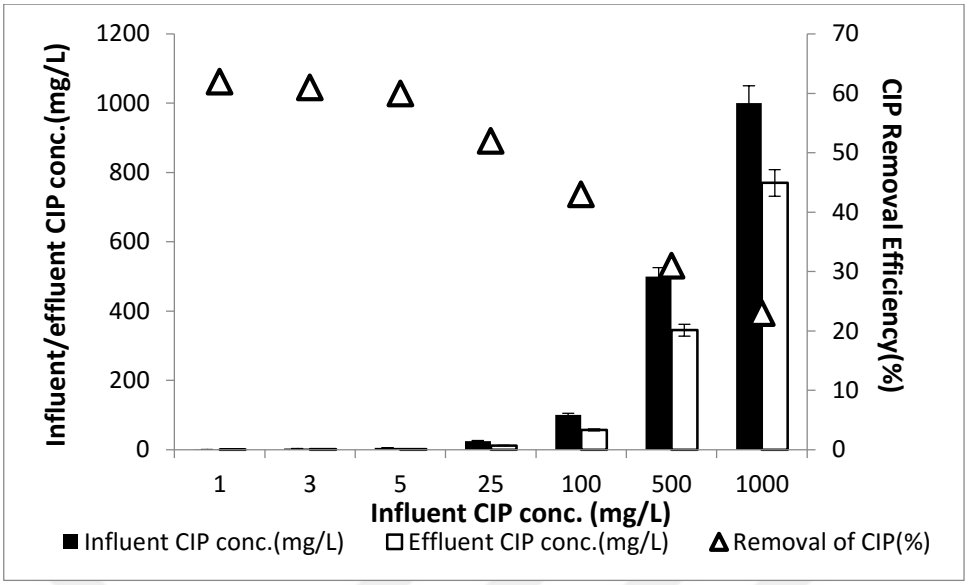


Figure 6.63 Effect of increasing CIP concentration on the yields of CIP removal at a Nano-GO/M concentration of 0.5 g/L at pH=6.5, at 80°C and 30 min irradiation time and at a power of 300 W UV light (<α (0.05)).

Figure 6.64 summarizes the effects of increasing temperatures (21°C, 40°C, 60°C and 80°C) on CIP photocatalytic removal yields at a CIP concentration of 5 mg/L after 30 min irradiation time at pH=6.5 and at constant Nano-GO/M concentration (0.5 g/L). Increasing the temperature from 21°C to 40-60-80°C yielded a decrease on the photocatalytic removal efficiencies of CIP.

Among these four different temperatures (21°C, 40°C, 60°C and 80°C), the maximum CIP photocatalytic removal yields were found as 91% for 5 mg/L initial CIP concentration at 21°C. This low temperature reduced the operational cost of photocatalytic process.

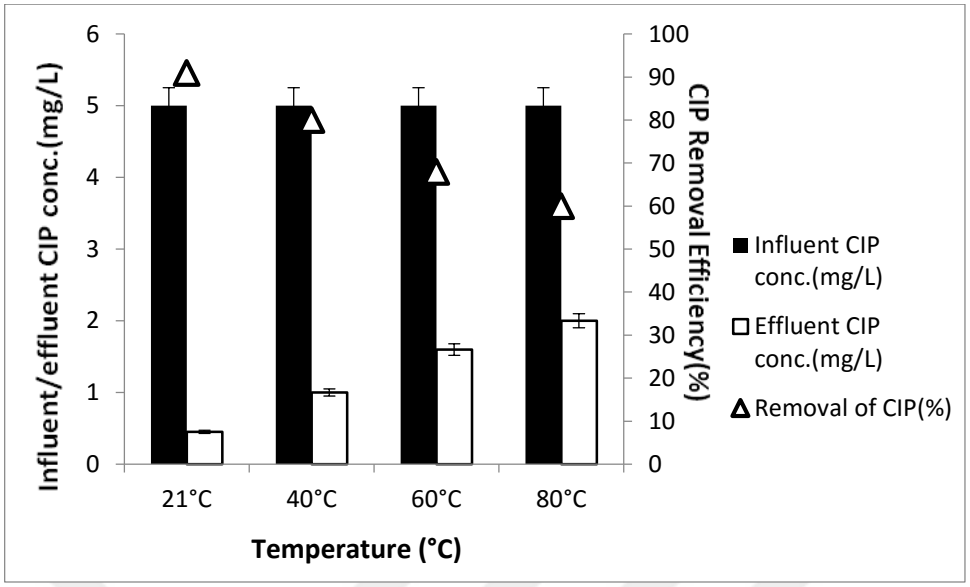


Figure 6.64 Effect of temperature time on the yields of constant CIP concentration (5 mg/L), at a constant Nano-GO/M (0,5 g/L), at a pH of 6.5 and at 21°C, 40°C, 60°C and 80°C and at a power of 300 W UV light (<α (0.05)).

Table 6.12 represents the effects of different temperatures on the photocatalytic removal efficiency of CIP for 1 mg/L initial CIP concentration. Photocatalytic removal of CIP on Nano-GO/M was high at 21°C.

Table 6.12 Shows the maximum photocatalytic removal efficiencies of CIP (1mg/L) at 21°C, 40°C, 60°C and 80°C and at 0.5 g/L constant Nano-GO/M concentration and at a power of 300 W UV light.

| Temperature (°C) | Removal efficiencies (%) |
|---|---|
| 21 | 93 |
| 40 | 82 |
| 60 | 70 |
| 80 | 62 |

A linear relationship between temperature and maximum CIP photocatalytic removal efficiencies (for 1 mg/L initial CIP concentration) was obtained (R=0.99) and this regression is significant (ANOVA p=0.003<α (0.05) and F=62.42).

#### *6.3.1.6 Effect of UV Power on the Photocatalytic Removal of CIP with Nano-GO/M Composite*

UV power is another important parameter for the photocatalytic process. To investigate the effect of UV power, CIP removal was studied under different UV powers (100 W, 300 W, 400 W and 600 W). For maximum CIP removal the optimum Nano-GO/M concentration (0.5 g/L) and the optimum irradiation time (30 min) were determined in the preliminary studies as mentioned above. Therefore, all experiments were realized after 30 min irradiation time, at increasing CIP concentrations (1, 3, 5, 25, 100, 500 and 1000 mg/L) and at original pH (6.5) at 0.5 g/L Nano-GO/M. Figure 6.65 summarizes the photocatalytic removal efficiencies of CIP at 21°C, with 0.5 g/L constant Nano-GO/M, at increasing CIP concentrations (1, 3, 5, 25, 100, 500 and 1000 mg/L) and with a power of 100 W UV light. CIP photocatalytic efficiencies were found as 88%, 87%, 86%, 80%, 71%, 66% and 59% for 1, 3, 5, 25, 100, 500 and 1000 mg/L CIP concentrations, respectively. Consequently, the CIP photocatalytic removal efficiencies were high (88-87%) at low CIP concentrations (1-3 mg/L). The percentage of photodegradation decreased with increasing of initial concentration of CIP. When initial concentration increase, more substances are adsorbed on the surface of Nano-GO/M. Therefore, there are only a fewer active sites for adsorption of hydroxyl ions so the generation of hydroxyl radicals will be reduced. Further, as the concentration of CIP solution increase, the photons get intercepted before they can reach the catalyst surface, hence the adsorption of photons by the catalyst decreases, and consequently the degradation percent is reduced (Chakrabarti & Dutta, 2004; Shankar et al., 2004).

A linear relationship between CIP photocatalytic removal efficiencies and influent CIP concentration was obtained (R=0.89) and this regression is significant (ANOVA $p=0.007<\alpha$ (0.05) and F=19.01) and this regression is significant.

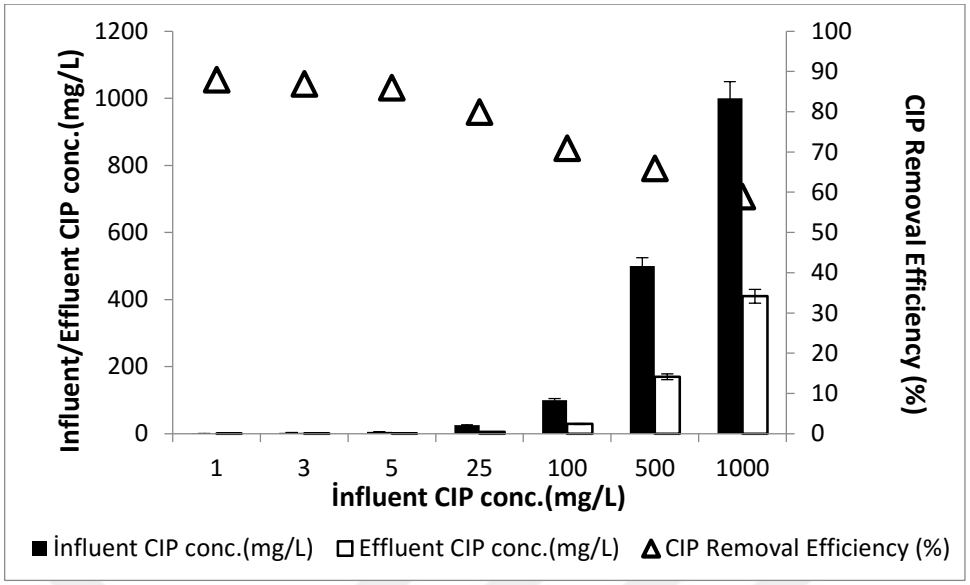


Figure 6.65 Effect of increasing CIP concentration on the yields of CIP removal at a Nano-GO/M concentration of 0.5 g/L at pH=6.5, with a power of 100 W UV light and 30 min irradiation time (<α (0.05)).

Figure 6.66 shows the photocatalytic removal efficiencies of CIP with 0.5 g/L constant Nano-GO/M, at increasing CIP concentrations (1, 3, 5, 25, 100, 500 and 1000 mg/L) and with a power of 300 W UV light. The photocatalytic removal efficiencies of CIP were found as 93%, 92%, 91%, 87%, 81%, 73% and 64% for 1, 3, 5, 25, 100, 500 and 1000 mg/L CIP concentrations, respectively. According to this results it can be concluded that the CIP photocatalytic treatment efficiencies removals were high (93-92%) at low CIP concentrations (1-3 mg/L). As the CIP concentrations were increased, the photocatalytic removal efficiencies decreased. The photodegradation efficiency was gradually decreased as a result of increasing CIP concentration. When the initial CIP concentration was decreased, the probability of the reaction between CIP and oxidizing species was increased, leading to an improvement of photodegradation efficiency. However, the excess CIP concentration reduced photodegradation efficiency. Therefore, there are only a fewer active sites for adsorption of hydroxyl ions so the generation of hydroxyl radicals will be reduced. Further, as the concentration of CIP solution increase, the photons get intercepted before they can reach the catalyst surface, hence the adsorption of photons by the catalyst decreases, and consequently the degradation percent is reduced (Chakrabarti & Dutta, 2004; Shankar et al., 2004).

A linear relationship between CIP photocatalytic treatment efficiencies and influent CIP concentration was obtained (R=0.95) and this regression is significant (ANOVA p=0.001<α (0.05) and F=47.13).

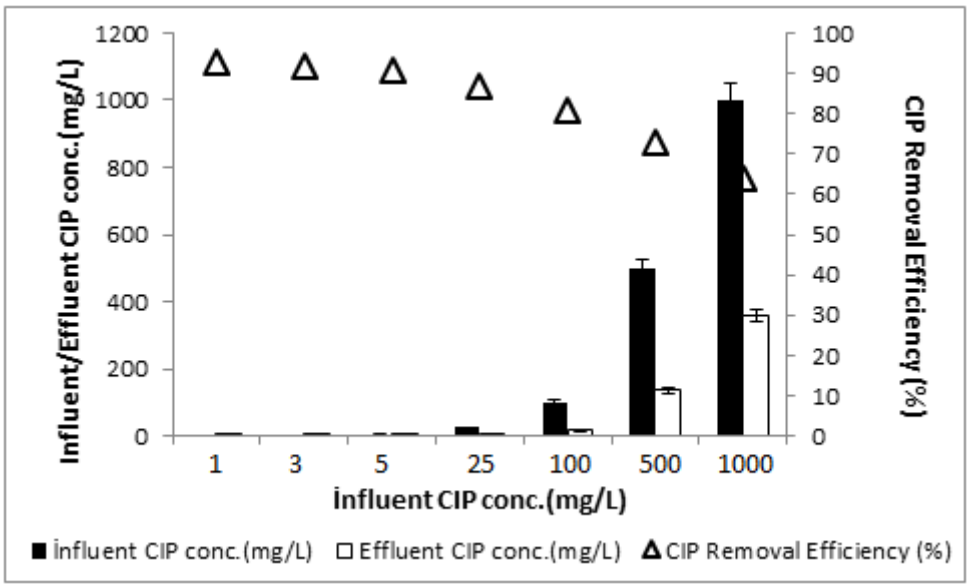


Figure 6.66 Effect of increasing CIP concentration on the yields of CIP photocatalytic treatment at a Nano-GO/M concentration of 0.5 g/L at pH=6.5, at 21°C and 30 min irradiation time and with a power of 300 W UV light (<α (0.05)).

Figure 6.67 shows the photocatalytic removal efficiencies of CIP with 0.5 g/L constant Nano-GO/M, at increasing CIP concentrations (1, 3, 5, 25, 100, 500 and 1000 mg/L) and with a power of 400 W UV light. The photocatalytic removal efficiencies of CIP were found as 95%, 94%, 93%, 88%, 82%, 74% and 66% for 1, 3, 5, 25, 100, 500 and 1000 mg/L CIP concentrations, respectively. According to this results it can be concluded that the CIP photocatalytic treatment efficiencies removals were high (95-94%) at low CIP concentrations (1-3 mg/L). The photodegradation efficiency was gradually decreased as a result of increasing CIP concentration. When the initial CIP concentration was decreased, the probability of the reaction between CIP and oxidizing species was increased, leading to an improvement of photodegradation efficiency. However, the excess CIP concentration reduced photodegradation efficiency. Therefore, there are only a fewer active sites for adsorption of hydroxyl ions so the generation of hydroxyl radicals will be reduced. Further, as the concentration of CIP solution increase, the photons get intercepted before they can reach the catalyst

surface, hence the adsorption of photons by the catalyst decreases, and consequently the degradation percent is reduced (Chakrabarti & Dutta, 2004; Shankar et al., 2004).

A linear relationship between CIP photocatalytic treatment efficiencies and influent CIP concentration was obtained (R=0.94) and this regression is significant (ANOVA $p=0.001<\alpha$ (0.05) and F=35.66).

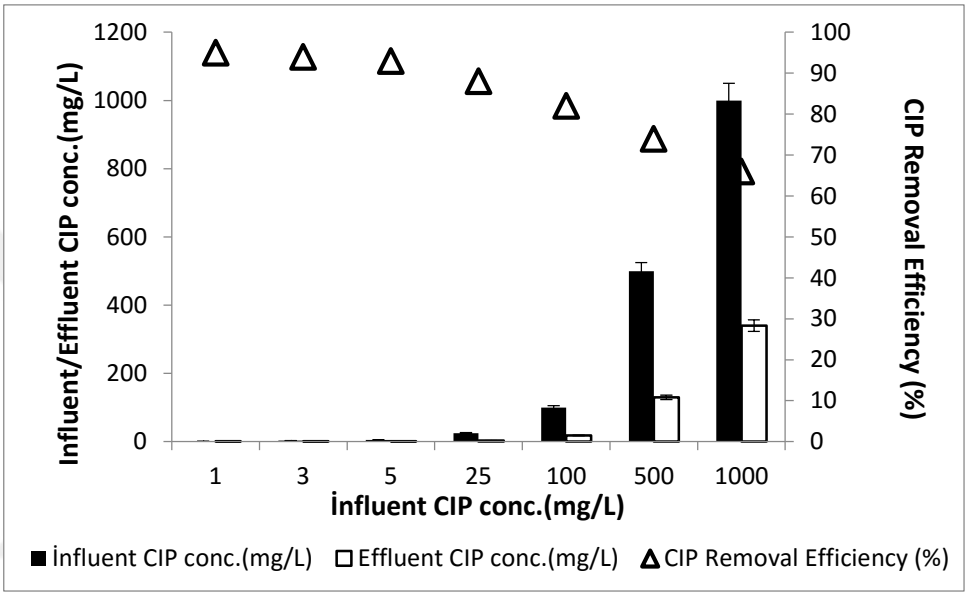


Figure 6.67 Effect of increasing CIP concentration on the yields of CIP photocatalytic treatment at a Nano-GO/M concentration of 0.5 g/L at pH=6.5, at 21°C and 30 min irradiation time and with a power of 400 W UV light ($<\alpha$ (0.05)).

Figure 6.68 shows the photocatalytic removal efficiencies of CIP with 0.5 g/L constant Nano-GO/M, at increasing CIP concentrations (1, 3, 5, 25, 100, 500 and 1000 mg/L) and with a power of 600 W UV light. The photocatalytic removal efficiencies of CIP were found as 96%, 95%, 94%, 89%, 83%, 75% and 67% for 1, 3, 5, 25, 100, 500 and 1000 mg/L CIP concentrations, respectively. According to this results it can be concluded that the CIP photocatalytic treatment efficiencies removals were high (96-95%) at low CIP concentrations (1-3 mg/L). The photodegradation efficiency was gradually decreased as a result of increasing CIP concentration. When the initial CIP concentration was decreased, the probability of the reaction between CIP and oxidizing species was increased, leading to an improvement of photodegradation efficiency. However, the excess CIP concentration reduced photodegradation efficiency.

Therefore, there are only a fewer active sites for adsorption of hydroxyl ions so the generation of hydroxyl radicals will be reduced. Further, as the concentration of CIP solution increase, the photons get intercepted before they can reach the catalyst surface, hence the adsorption of photons by the catalyst decreases, and consequently the degradation percent is reduced (Chakrabarti & Dutta, 2004; Shankar et al., 2004).

A linear relationship between CIP photocatalytic treatment efficiencies and influent CIP concentration was obtained (R=0.94) and this regression is significant (ANOVA $p=0.001<\alpha$ (0.05) and F=35.66).

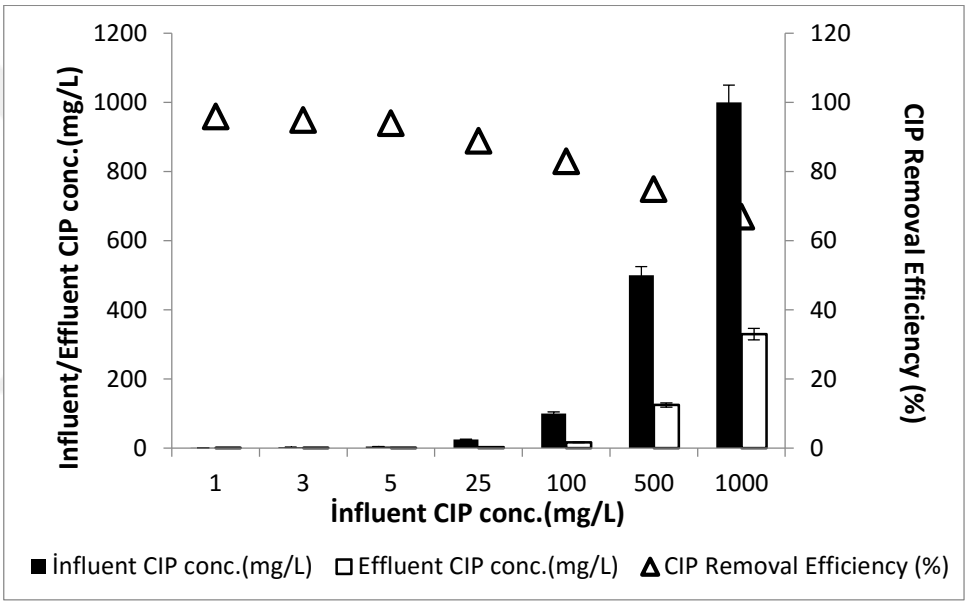


Figure 6.68 Effect of increasing CIP concentration on the yields of CIP photocatalytic treatment at a Nano-GO/M concentration of 0.5 g/L at pH=6.5, at 21°C and 30 min irradiation time and with a power of 600 W UV light ($<\alpha$ (0.05)).

Figure 6.69 represents the effect of UV powers on the photocatalytic removal of CIP with 0.5 g/L constant Nano-GO/M (at pH=6.5, at 21°C and 30 min irradiation time). CIP concentration was chosen as 5 mg/L to compare the effects of each UV power. As the UV power increased, the CIP yields also increased. This can be explained by the fact that UV power provided more energy, so large amounts of HO• were formed, and more CIP molecules in aqueous solution were therefore degraded (Lin C., Lin H. & Hsu, 2016). The maximum CIP (for 1 mg/L initial CIP

concentration) yields obtained as 88%, 93%, 95% and 96% for 100 W, 300 W, 400 W and 600 W UV power, respectively.

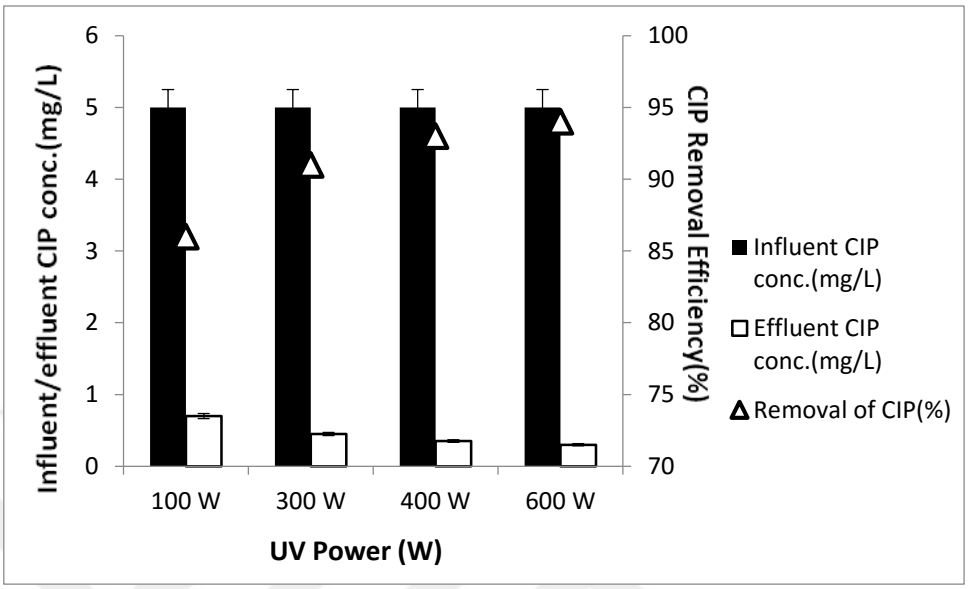


Figure 6.69 Effect of increasing CIP concentration on the yields of CIP photocatalytic treatment at a Nano-GO/M concentration of 0.5 g/L at pH=6.5, at 21°C and 30 min irradiation time and with increasing UV power (100, 300, 400 and 600 W) (<α (0.05)).

Table 6.13 represents the effects of different UV light powers on the photocatalytic removal efficiency of CIP for 1 mg/L initial CIP concentration. Our results reveal that the photooxidation increases between 100 W and 600 W but this increase is not significant in the range of 300–600 W. In the present work, we have used 300 W UV light power as optimum for photooxidation of CIP.

Table 6.13 Shows the maximum photocatalytic removal efficiencies of CIP (1mg/L) at 21°C and at 0.5 g/L constant Nano-GO/M concentration and at increasing power of (100 W, 300 W, 400 W and 600 W) UV light.

| UV Power (W) | Removal efficiencies (%) |
|---|---|
| 100 | 88 |
| 300 | 93 |
| 400 | 95 |
| 600 | 96 |

A linear relationship between temperature and maximum CIP photocatalytic removal efficiencies (for 1 mg/L initial CIP concentration) was obtained (R=0.94) and this regression is significant (ANOVA $p=0.005<\alpha$ (0.05) and F=162.64).

The UV power determines the amount of photons absorbed by the catalyst. In the photocatalytic treatment process with Nano-GO/M, at increased light power electron-hole pair separation competes with recombination, causing less effect on the reaction efficiency (Konstantinou & Albanis, 2004). With the increase of the UV power, the catalyst absorbs more photons, producing more electron-hole pairs in the catalyst surface, and this increases the concentration of hydroxyl radicals and consequently increases the removal percent. Earlier studies on the effect of UV light power have shown the almost same results. Farzadkia et al., (2014), studied that metronidazole (MNZ) removal with ZnO nanoparticles after 180 min UV irradiation. Results showed that UV power has significant effect for removal MNZ. They reported that removal efficiency of MNZ was increased with increasing UV light power. For initial 80 mg/L MNZ concentration maximum MNZ removal efficiency was 27.83% for 8 W UV power and for 125 W the removal efficiency was 95.42% after 180 min irradiation time. Muruganandham & Swaminathan (2004), researched the influence of UV power on the decolourisation of reactive orange 4 (RO4) has been investigated by varying the UV power from 16 W to 64 W. Results showed increase of UV power from 16 W to 64 W increases the decolourisation from 56.81% to 81.36% at 20 min for initial RO4 concentration of $5x10^{-4}$ M.

*6.3.1.7 CIP Metabolites*

In this study we also investigated two different metabolites (M1: desethyleneciprofloxacin and M3: oxociprofloxacin) of CIP which are released during photocatalytic processes. In order to measure metabolites of CIP (initial CIP conc. 100 mg/L), all experiments were realized after 30 min irradiation time, at room temperature at an original pH (6.5) of CIP solution with 0.5 g/L Nano-GO/M. Results showed that, after photocatalytic treatment from 100 mg/L CIP 83 mg/L CIP was photodegraded (Table 6.14). The CIP was photodegraded with a yield of 83%. 17 mg/L CIP was remained in the effluent and cannot be photodegraded with UV and Nano-GO/M. CIP

was photodegraded to two metabolites namely M1 and M3. From 83 mg/L CIP; 20.22 mg/L M1 and 3.4 mg/L M2 were produced (Table 6.14). 20.22 mg/L M1 was degraded with a yield of 24.36% while 3.4 mg/L M3 was degraded with a yield of 4.096%. As a result, from 83 mg/L CIP; totally 23.62 mg/L metabolites were discharged and removed. The rest of CIP (83 mg/L – 23.62 mg/L= 59.38 mg/L) was completely transformed to $CO_2$ and $H_2O$. Table 6.14 shows the percentage of removed or transformed products.

Table 6.14 Influent/effluent and removed/transformed CIP, M1 (desethyleneciprofloxacin) and M3 (oxociprofloxacin) (operational conditions: 30 min, pH 6.5, 0.5 g/L Nano-GO/M, 21°C and 300 W UV power).

| | Influent (mg/L) | Effluent (mg/L) | Removed concentration (mg/L) |
|---|---|---|---|
| CIP | 100 | 17.0135 | 83 |
| M1(desethyleneciprofloxacin) | 0 | 20.22 | 20.22 |
| M3 (oxociprofloxacin) | 0 | 3.4 | 3.4 |
| Total metabolites | 0 | 23.62 | 23.62 |
| Rest of CIP | 100 | 59.38 | 59.38 |

Figure 6.70 shows the HPLC analysis of CIP and its metabolites. M1 and M3 were obtained as 20.22 and 3.4 mg/L, respectively.

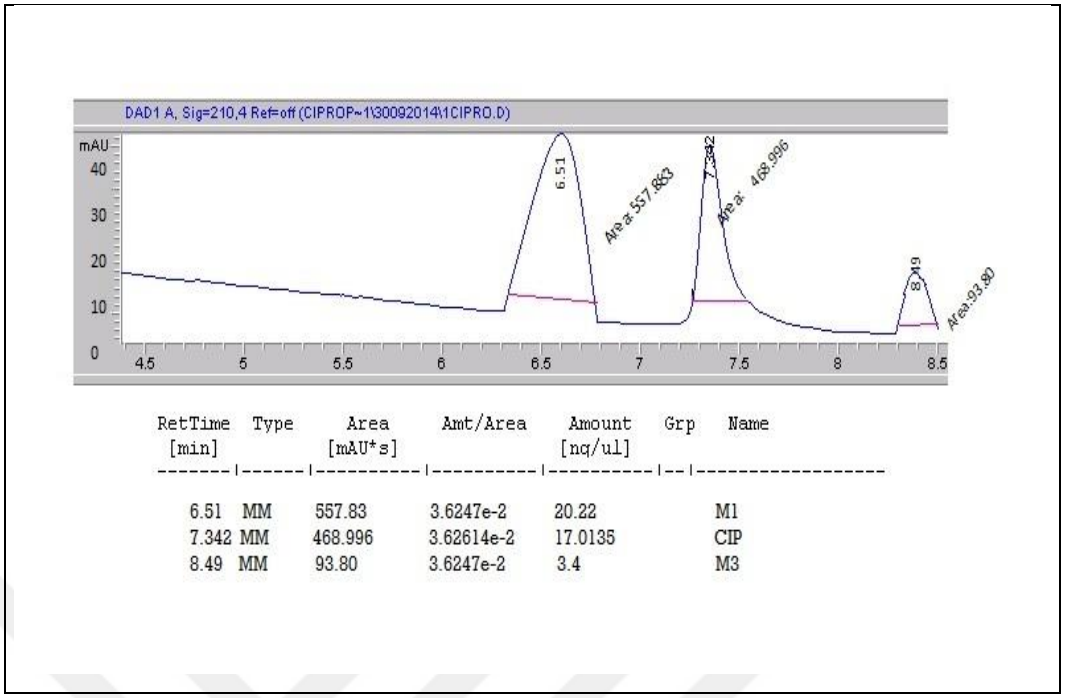


| RetTime [min] | Type | Area [mAU*s] | Amt/Area | Amount [ng/ul] | Grp | Name |
|---|---|---|---|---|---|---|
| 6.51 | MM | 557.83 | 3.6247e-2 | 20.22 | | M1 |
| 7.342 | MM | 468.996 | 3.62614e-2 | 17.0135 | | CIP |
| 8.49 | MM | 93.80 | 3.6247e-2 | 3.4 | | M3 |

Figure 6.70 HPLC analyses of 100 mg/L CIP after UV treatment (300W) with 0.5 g/L Nano-GO/M at 30 min retention time and at a pH of 6.5.

### *6.3.1.8 Investigation of Photocatalytic Degradation Kinetic of CIP Using Nano-GO/M Composite*

In this step of the study, zero-order kinetic, first-order kinetic and second-order kinetic models were discussed to indicate the removal kinetics of CIP on the surface of Nano-GO/M composite throughout photodegradation under UV.

*6.3.1.8.1. Zero-Order Kinetics.* The $R^2$ value for pseudo-zero-order reaction was found as 0.955 for CIP in the photocatalytic studies performed with Nano-GO/M (Figure 6.71). Pseudo-zero-order reaction's the zero order rate kinetic constant is $k_0$. The $k_0$ values evaluated from Pseudo-zero-order reaction plots were found as 0.393 $min^{-1}$ for CIP from the Eq. (5.11).

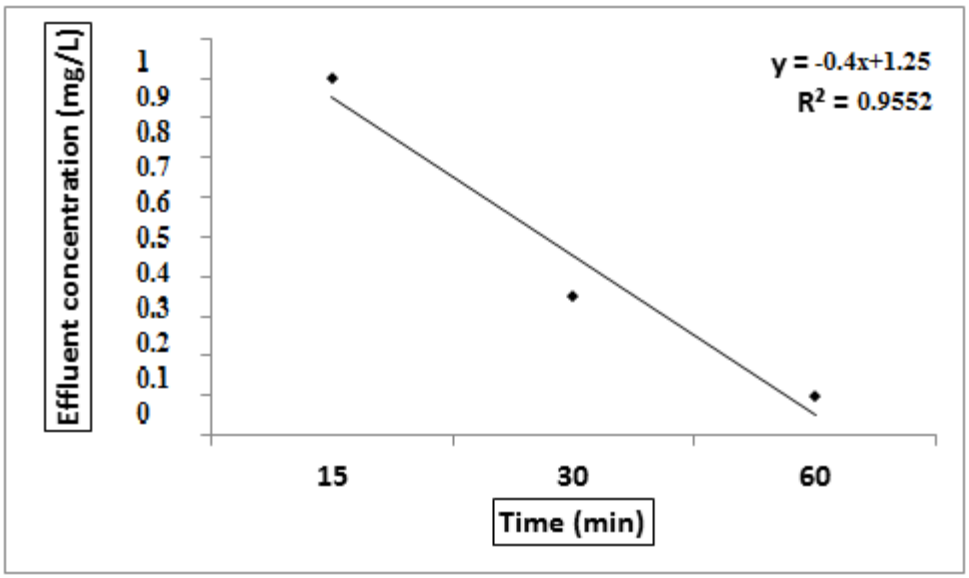


Figure 6.71 Pseudo-zero-order reaction of CIP (CIP: 5 mg/L, T: room temperature, irradiation time: 30 min., concentration of Nano-GO/M: 0.5 g/L, 300 watt UV light).

*6.3.1.8.2. First-Order Reaction Kinetics.* The $R^2$ value for first-order reaction was obtained as 1 for CIP in the photocatalytic studies performed with Nano-GO/M (Figure 6.72). First-order reaction's in the first order rate kinetic constant is $k_1$. The $k_1$ values was calculated from the first-order reaction plots as 0.8047 $min^{-1}$ for CIP from the Eq. (5.13).

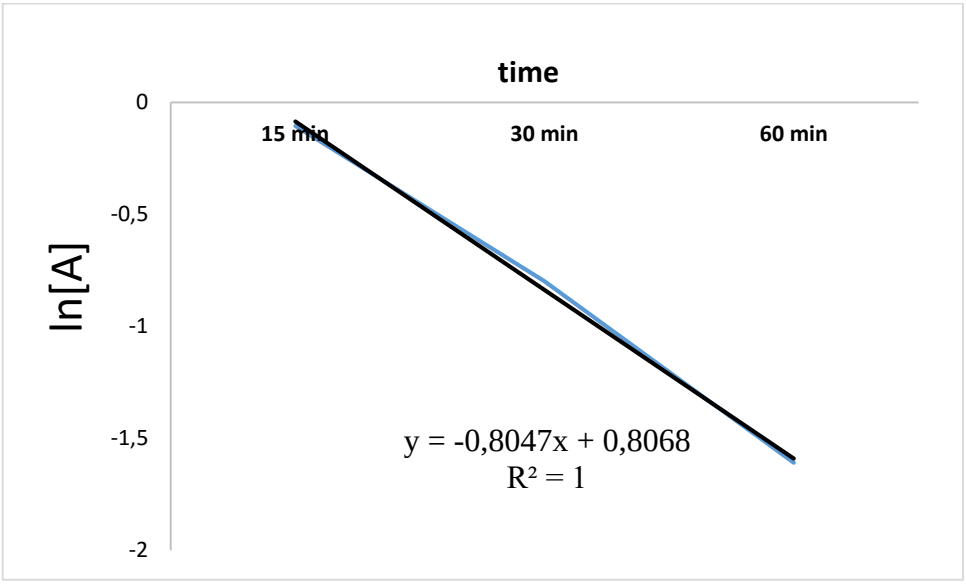


Figure 6.72 First-order reaction of CIP (CIP concentration: 5 mg/L, T: room temperature, irradiation time: 15 min., concentration of Nano-GO/M: 0.5 g/L, 300 watt UV light).

*6.3.1.8.3. Second-Order Kinetics.* The $R^2$ value for second-order reaction was found as 0.8031 for CIP in the photocatalytic studies performed with Nano-GO/M (Figure 6.73). Second-order reaction's in the second order rate kinetic constant is $k_2$. The $k_2$ values were calculated from the second-order reaction plots as 4.43 $min^{-1}$ for CIP from the Eq. (5.14).

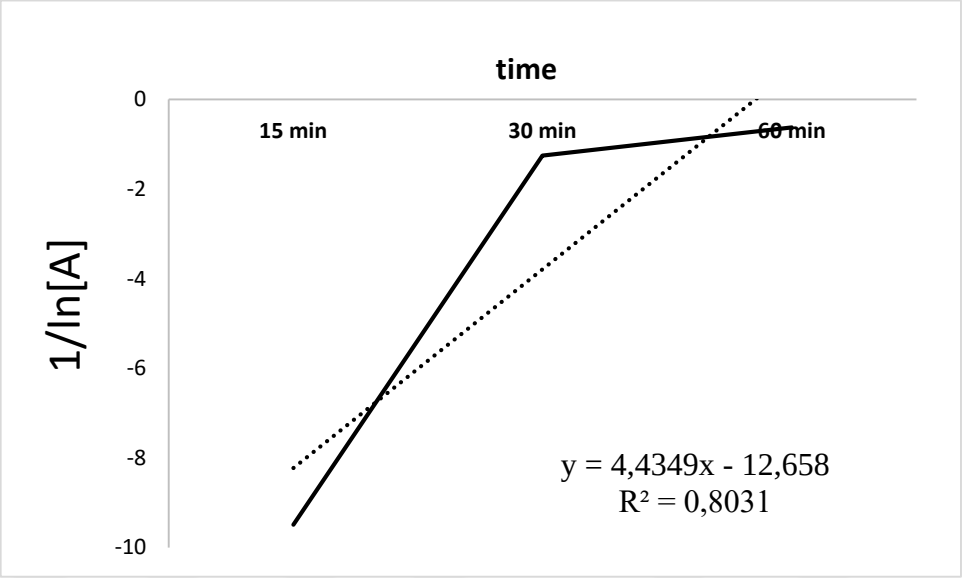


Figure 6.73 Second-order reaction of CIP (CIP concentration: 5 mg/L, T: room temperature, irradiation time: 30min., concentration of Nano-GO/M: 0.5 g/L, 300 watt UV light).

As a results of kinetic studies it was found that the CIP was photodegraded according to first order reaction kinetic since the $k_1$ value calculated is meaningful than that calculated in the first order and second order reaction kinetics with highest $R^2$ value (1). From the first order reaction plots $k_1$ value for CIP photodegradation was found to be 0.8047 $min^{-1}$. In the other words, CIP was removed under 300 W UV irradiation according to first order reaction kinetics.

### *6.3.1.9 UV Absorption Spectra of CIP*

The UV–visible spectra of the CIP were measured with a spectro-photometer in the wave lengths range varying from 190 nm to 1100 nm. UV absorption spectra of raw CIP and treated CIP under UV irradiation can be seen in Figures 6.74 and 6.75, respectively. The maximum absorbance peaks were seen at between 260 nm at

wavelengths between 190 nm and 400 nm as 4.331 A in raw CIP. After the CIP was treated under UV light with 0.5 g/L Nano-GO/M composite, the measured absorbance values were illustrated in Figure 6.75. The maximum absorbance peaks slightly decreased after UV irradiation. This can be attributed to the production of some CIP metabolites under UV after photodegradation of CIP ending with ultimate mineralization to $CO_2$ and $H_2O$.

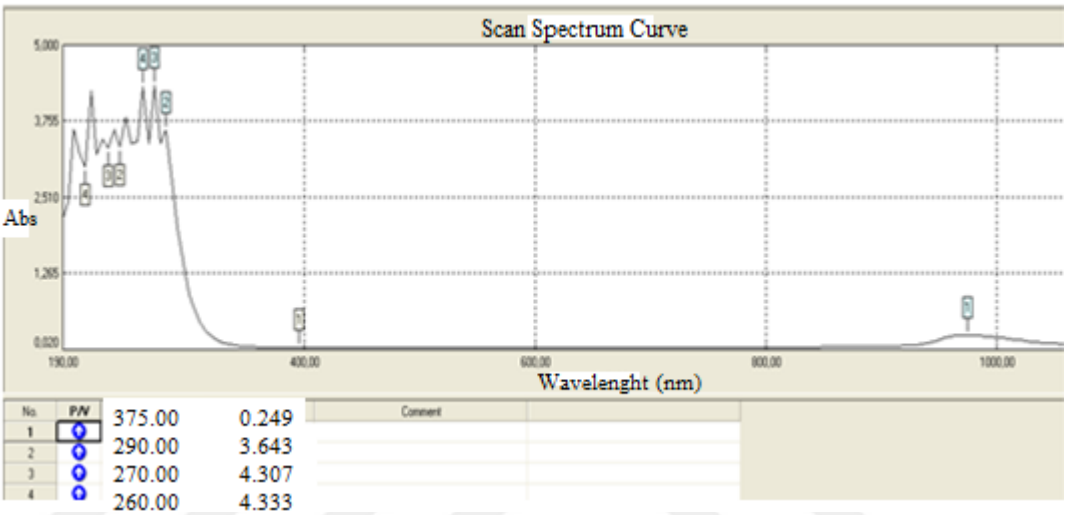


Figure 6.74 UV absorption spectra of raw CIP (100 mg/L).

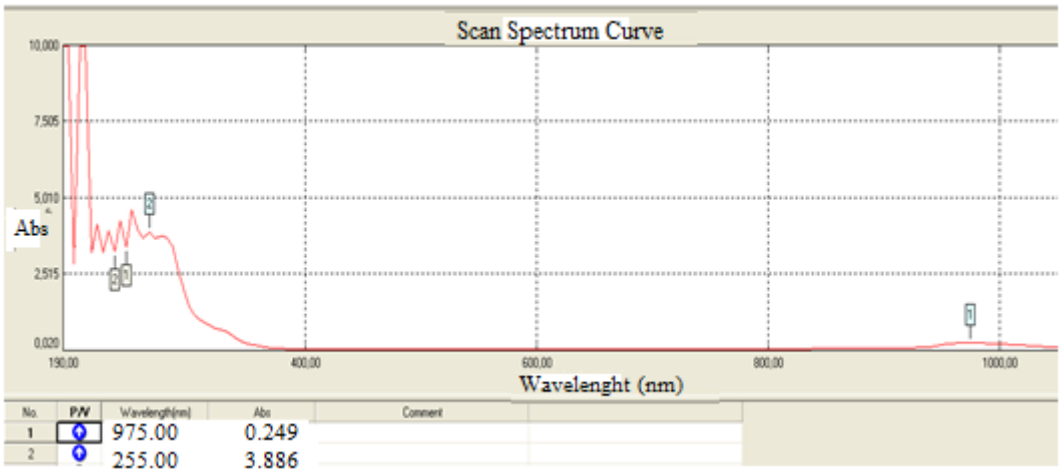


Figure 6.75 UV absorption spectra of the treated CIP under UV irradiation (T: room temperature, irradiation time: 30 min, concentration of Nano-GO/M: 0.5 g/L, 300 watt UV light).

### *6.3.2 Removal of OFL Under Photocatalytic Studies*

#### *6.3.2.1 Effects of Nano-GO/M Composite Concentrations on the Photocatalytic Treatment of OFL*

In this step of this study OFL were treated via photodegradation under UV light power in the presence of a nano composite (Nano-GO/M*)* generated under laboratory conditions. Nano particles concentration is an important parameter for the treatment of OFL. In order to determine the effects of increasing Nano-GO/M concentrations on the treatment of 1, 3, 5, 25, 100, 500 and 1000 mg/L OFL; the effects of 0.5 g/L, 2 g/L, 10 g/L Nano-GO/M composite concentrations were researched. Preliminary experiments showed that among the irradiation times that are tested, the maximum OFL removal was obtained after 60 min irradiation time (data not shown). Therefore, all experiments were realized after 60 min irradiation time, at 21°C (room temperature) and at original pH (6.5) of OFL solution and with a power of 300 W UV light. Figure 6.76 summarizes the photocatalytic treatment efficiencies of OFL at 0.5 g/L Nano-GO/M, at increasing OFL concentrations (1, 3, 5, 25, 100, 500 and 1000 mg/L). OFL photocatalytic treatment efficiencies were found as 96 %, 95%, 94%, 87%, 82%, 76% and 65% for 1, 3, 5, 25, 100, 500 and 1000 mg/L OFL concentrations, respectively. According to this results it can be concluded that the OFL photocatalytic treatment efficiencies removals were high (96-95%) at low OFL concentrations (1-3 mg/L).

The maximum OFL photocatalytic treatment efficiency obtained is (96%) at 0.5 g/L Nano-GO/M concentration at 1 mg/L influent OFL concentration while the other high maximum OFL photocatalytic treatment efficiencies was calculated as 95% at 3 mg/L OFL concentration. It is clear that the photodegradation of OFL decreases with increasing concentration of the OFL. By increasing the concentration of OFL, more OFL molecules are adsorbed on the surface of Nano-GO/M composite, resulting in occupation of the active sites of the catalyst. Thus, $OH^0$ radicals produced on the surface of the Nano-GO/M composite decreased during photocatalysis. Furthermore, the large amount of the adsorbed OFL is thought that can be inhibit the reaction between the OFL molecules and photogenerated holes or the hydroxyl radicals (Barjasteh-Moghaddam & Habibi-Yangjeh, 2010).

A linear relationship between OFL photocatalytic treatment efficiencies and influent OFL concentration was obtained (R=0.93) and this regression is significant (ANOVA p=0.0001<α (0.05) and F=33.22).

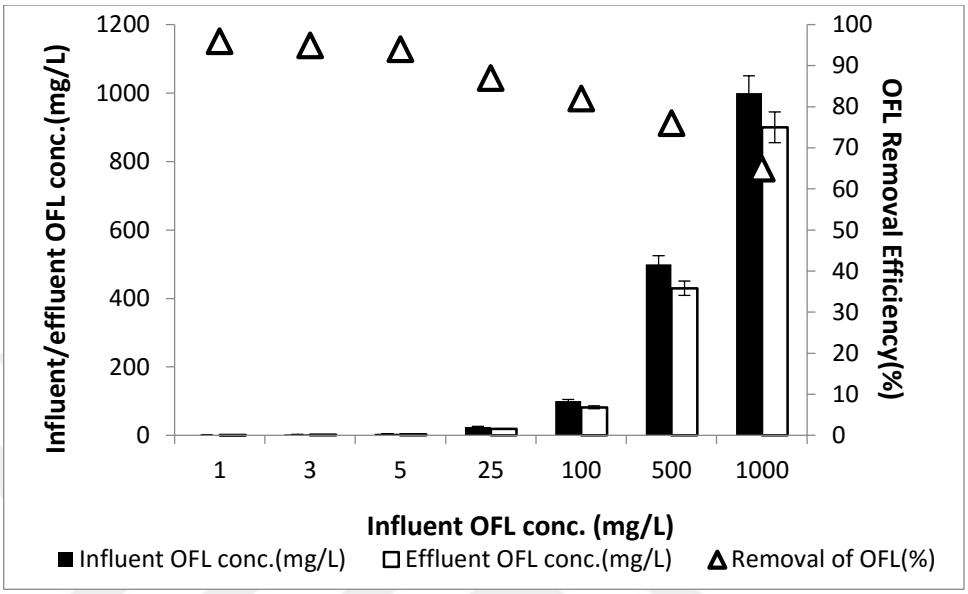


Figure 6.76 Effect of increasing OFL concentration on the yields of OFL photooxidation at a Nano-GO/M concentration of 0.5 g/L at pH=6.5, at 21°C and 60 min irradiation time and with a power of 300 W UV light (<α (0.05)).

Figure 6.77 shows the photocatalytic treatment efficiencies of OFL at increasing OFL concentrations (1, 3, 5, 25, 100, 500 and 1000 mg/L) were found as 94 %, 93%, 92%, 85%, 80%, 73% and 64% at 2 g/L Nano-GO/M, respectively. As the OFL concentrations were increased, the photocatalytic treatment efficiencies decreased. The maximum OFL removal efficiency is 94% at 2 g/L Nano-GO/M concentration at 1 mg/L influent OFL concentration. According to this results it can be concluded that the OFL photocatalytic treatment efficiency were high (94-93%) at low OFL concentrations (1-3 mg/L). By increasing the concentration of OFL, more OFL molecules are adsorbed at the Nano-GO/M surface, resulting in occupation of the catalyst active sites.

A linear relationship between OFL photocatalytic treatment efficiencies and influent OFL concentration was obtained (R=0.93) and this regression is significant (ANOVA p=0.0001<α (0.05) and F=29.69).

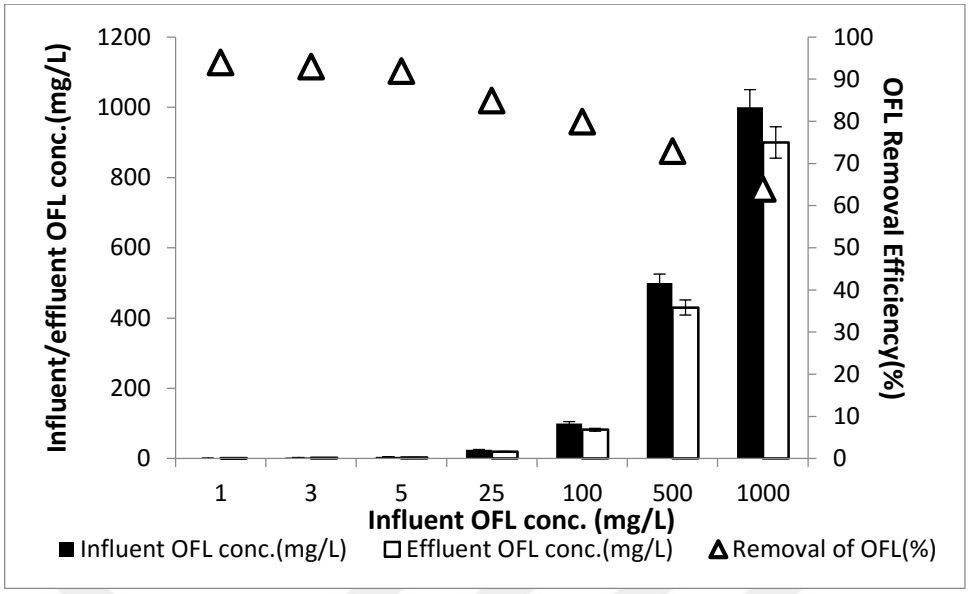


Figure 6.77 Effect of increasing OFL concentration on the yields of OFL photooxidation at a Nano-GO/M concentration of 2 g/L at pH=6.5, at 21°C and 60 min irradiation time (<α (0.05)).

Figure 6.78 shows the photocatalytic treatment efficiencies of OFL at increasing OFL concentrations (1, 3, 5, 25, 100, 500 and 1000 mg/L) for 10 g/L Nano-GO/M. According these OFL concentrations the removal yields were 91%, 90%, 89%, 83%, 77%, 70% and 61%, respectively. The maximum OFL removal efficiency is 91% at 10 g/L Nano-GO/M concentration for 1 mg/L influent OFL concentration. According to this results it can be concluded that the OFL removals were high (91-90%) at low OFL concentrations (1-3 mg/L).

A linear relationship between OFL photocatalytic treatment efficiencies and influent OFL concentration was obtained (R=0.93) and this regression is significant (ANOVA p=0.00011<α (0.05) and F=32.09).

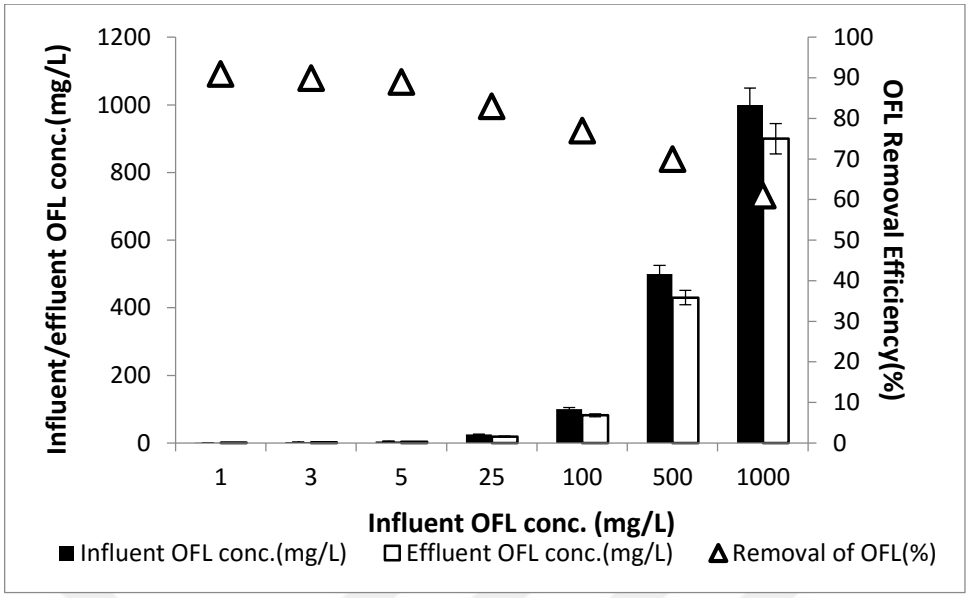


Figure 6.78 Effect of increasing OFL concentration on the yields of OFL photooxidation at a Nano-GO/M concentration of 10 g/L at pH=6.5, at 21°C and 60 min irradiation time (<α (0.05)).

Figure 6.79 summarizes the effects of increasing Nano-GO/M concentrations (0.5, 2 and 10g/L) on OFL removal yields at an OFL concentration of 5 mg/L after 60 min irradiation time at pH=6.5 and at 21°C and with a power of 300 W UV light. Increasing the concentration of Nano-GO/M from 0.5 g/L to 2 g/L and to 10 g/L the removal yields slightly decreased. The OFL removal yields were obtained as 94%, 92% and 89% at 0.5, 2 and 10g/L Nano-GO/M composite concentration, respectively for 5 mg/L OFL concentration, at the same operational conditions. The optimum Nano-GO/M concentration was chosen as 0.5 g/L in order to reduce the operational cost of photocatalytic treatment process.

A linear relationship between maximum OFL removal efficiencies and Nano-GO/M composite was obtained (R=0.97) and this regression is significant (ANOVA $p=0.005<\alpha$ (0.05) and F=13.99).

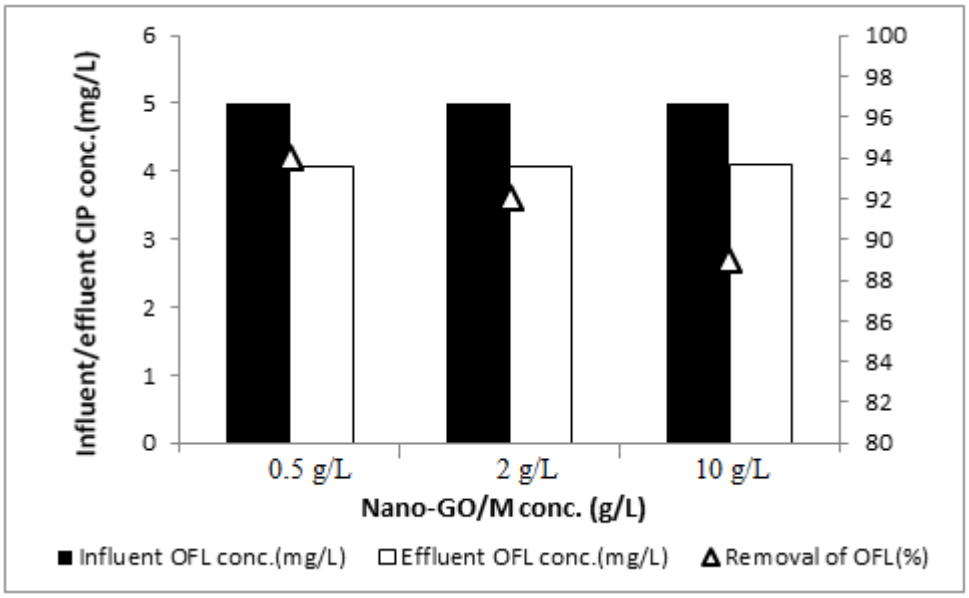


Figure 6.79 Effect of increasing concentration of Nano-GO/M (0.5, 2 and 10 g/L) on the yields of OFL removal via photooxidation for constant OFL concentration (5 mg/L) at pH=6.5, at 21°C and 60 min irradiation time (for ANOVA <α (0.05)).

At lower Nano-GO/M concentration (0.5 g/L) slightly higher OFL removal yields (94%) was obtained while slightly lower OFL removal yields (92 and 89%) was obtained at higher Nano-GO/M concentration (2 and 10 g/L, respectively) at pH 6.5 for 5 mg/L OFL concentration (Figure 6.79). Increase in Nano-GO/M concentration reduces the specific activity of the Nano-GO/M because of agglomeration of Nano-GO/M particles and light scattering and screening effect, thus leading to the decreased photocatalytic treatment efficiency (Zhe-Qi et al., 2015).

Increasing the amount of photocatalyst from 0.5 g/L to 10 g/L resulted in decreasing the photocatalytic treatment efficiency from 96% to 91% at the irradiation time of 60 min for 1 mg/L of OFL initial solution, respectively. By increasing the catalyst dosage, the surface area was increased, leading to an increase in the production of reactive species (Pelaez et al., 2012). However, more Nano-GO/M dosage would also induce greater aggregation of the catalyst and decrease the total active surface area, thereby leading to a reduction in the photocatalytic treatment efficiency. Moreover, due to an increase in the turbidity of the solution, reduction in the degree of light penetration through the solution could take place (Zhe-Qi et al., 2015). Therefore,

other experiments were carried out with 0.5 g/L Nano-GO/M to avoid the excessive usage of the catalyst.

*6.3.2.2 Effect of Irradiation Time on the Photocatalytic Treatment of OFL*

After determining the optimum concentration of Nano-GO/M (0.5 g/L), it was decided to investigate the effect of irradiation time on the photocatalytic treatment of 5 mg/L OFL at increasing irradiation times (15, 30, 60 and 900 min) at pH = 6.5, at a temperature of 21°C and with a power of 300 W UV light. As the irradiation time was increased from 15 min to 30 min and 60 min the OFL removals increased slightly from 86% to 90% and to 94% for initial OFL concentration of 5 mg/L (Figure 6.80). Further increase in irradiation time from 60 min to 900 min decreased the OFL removal yield slightly from 94% to 92%. As a result, in this study the optimum irradiation time for maximum OFL removal (94%) was found to be 60 min. Decreasing the removal efficiencies with the increasing the irradiation time can be associated with the metabolite of OFL molecules such as POF (9-piperazino ofloxacin) and MOF (des-methyl ofloxacin) formed during photooxidation during long irradiation time. These compounds were measured and the results were given in detail in the section 6.3.2.7.

In last literature surveys, there are only a few studies about removal of OFL via nanoparticles. One of them is reported by Rodriguez et al., (2015). They remarked that the OFL (at a concentration of 7.5-15 μM) adsorption on 0.1 g/L $TiO_2$ OFL sample occurs within 2 hours irradiation time and at room temperature at a pH of 7 under UV light. Their maximum removal efficiency was only 5%. In our study, the maximum OFL removal efficiency was calculated as 96% for 1 mg/L initial OFL concentration at 60 min. In our study, the maximum OFL removal efficiency was higher than that found by Rodriguez et al., (2015).

A linear relationship between photocatalytic removal yields and irradiation times were obtained up to an irradiation time of 900 min, and this regression is significant up to 900 min. ($R=0.98$, $p= 0{,}009<\alpha$ (0.05) and $F= 27$).

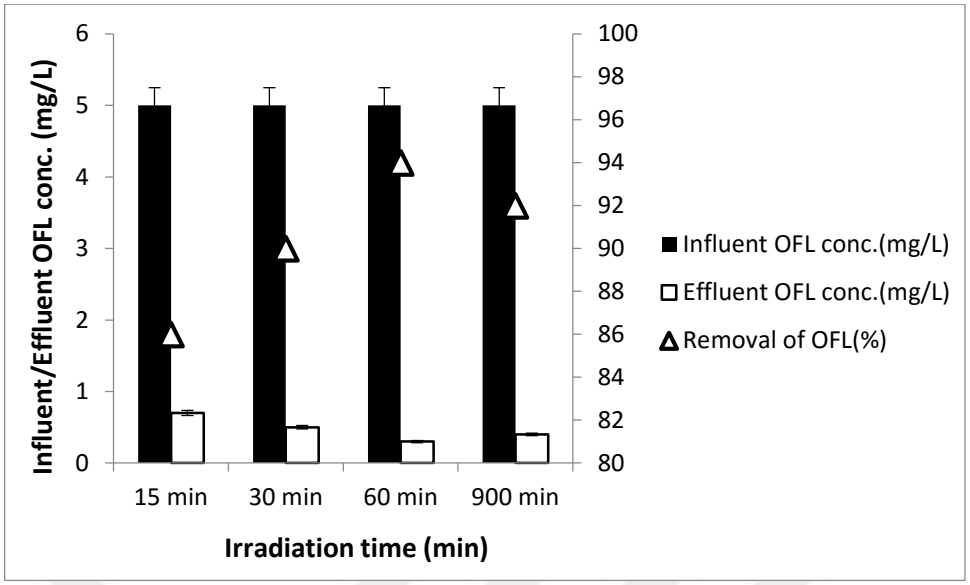


Figure 6.80 Effect of irradiation time on the yields of constant OFL concentration (5 mg/L), at a constant Nano-GO/M concentration (0.5 g/L), at a pH of 6.5 and at 21°C and with a power of 300 W UV light (<α (0.05)).

### *6.3.2.3 Effect of Increasing OFL concentrations on the OFL Photocatalytic Treatment yields*

At this step of this study, the effects of increasing OFL concentrations (1 mg/L, 3 mg/L, 5 mg/L, 25 mg/L, 100 mg/L, 500 mg/L, 1000 mg/L) on the OFL removals were studied at a Nano-GO/M concentration of 0.5 g/L, after 60 min irradiation time, at pH= 6.5 and at a temperature of 21°C and with a power of 300 W UV light (Figure 6.81). Results showed that increasing in the OFL concentration reduced the removal efficiency of OFL at a Nano-GO/M concentration of 0.5 g/L. For 1 mg/L initial OFL concentration the maximum OFL removal efficiency was found as 96% while the removal efficiency of 1000 mg/L OFL was found 65%. This increase in the OFL concentrations after photocatalytic process results in decrease in the removal efficiencies of OFL. Thus, for the maximum removal yield of OFL (96%) the optimum OFL concentration was found to be 1 mg/L. This can be as a result of blocking of the photocatalytically active sites on the Nano-GO/M and reducing the interaction of photons with these sites.

Figure 6.81 summarizes the photocatalytic treatment efficiencies of OFL at 0.5 g/L Nano-GO/M, at increasing OFL concentrations (1, 3, 5, 25, 100, 500 and 1000 mg/L).

OFL photocatalytic treatment efficiencies were found as 96 %, 95%, 94%, 87%, 82%, 76% and 65% for 1, 3, 5, 25, 100, 500 and 1000 mg/L OFL concentrations, respectively. According to this results it can be concluded that the OFL photocatalytic treatment efficiencies removals were high (96-95%) at low OFL concentrations (1-3 mg/L).

The maximum OFL photocatalytic treatment efficiency obtained is (96%) at 0.5 g/L Nano-GO/M concentration at 1 mg/L influent OFL concentration while the other high maximum OFL photocatalytic treatment efficiencies was calculated as 95% at 3 mg/L OFL concentration.

A linear relationship between OFL photocatalytic treatment efficiencies and influent OFL concentration was obtained (R=0.93) and this regression is significant (ANOVA p=0.0001<α (0.05) and F=33.22).

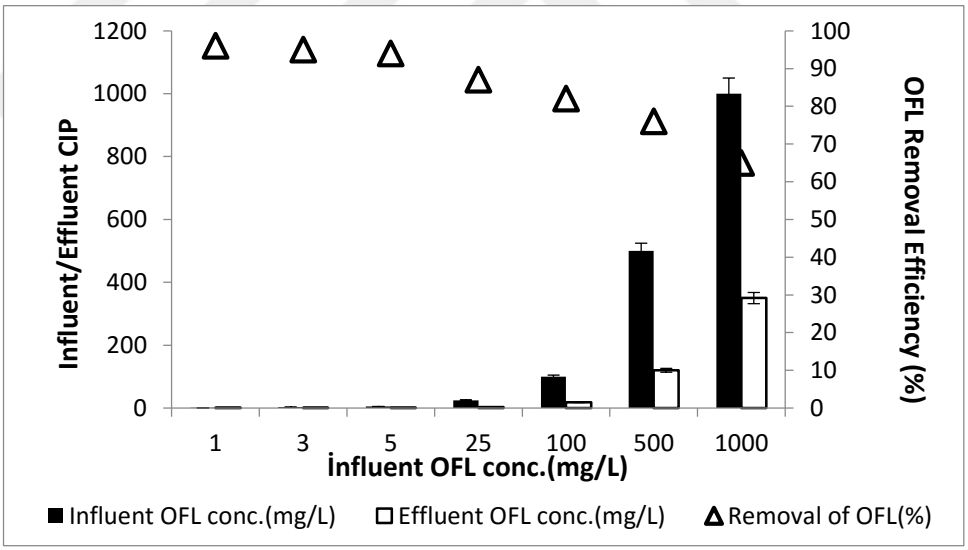


Figure 6.81 Effect of increasing OFL concentration on the yields of OFL photooxidation at a Nano-GO/M concentration of 0.5 g/L at pH=6.5, at 21°C and 60 min irradiation time and with a power of 300 W UV light (<α (0.05)).

#### *6.3.2.4 Effect of pH on the Photocatalytic Treatment of OFL with Nano-GO/M composite*

pH is an important parameter that can affect photocatalytic reactions. In this study the degradation of OFL was evaluated at different pH values (4, 6.5, and 10) as shown in Figure 36. The effects of pH on the removal of increasing OFL concentrations (1, 3, 5, 25, 100, 500 and 1000 mg/L) were studied under acidic, neutral and alkaline pHs (4, 6.5 and 10) at an irradiation time of 60 min, at a Nano-GO/M concentration of 0.5 g/L and at 21°C. Table 6.15 represents the effects of different pHs on the removal efficiency of OFL at 21°C. Photocatalytic removal efficiency of OFL on Nano-GO/M was relatively high at pH 6.5.

Table 6.15 Shows the photocatalytic removal efficiencies of increasing OFL at acidic, neutral and alkaline pHs (4, 6.5 and 10) at 21°C and at 0.5 g/L constant Nano-GO/M concentration at 60 min irradiation time under 300 W UV light.

| **OFL concentrations (mg/L)** | **1** | **3** | **5** | **25** | **100** | **500** | **1000** |
|---|---|---|---|---|---|---|---|
| **Removal efficiency (%) at pH= 4** | 79 | 78 | 77 | 65 | 50 | 44 | 34 |
| **Removal efficiency (%) at pH= 6.5** | 96 | 95 | 94 | 87 | 82 | 76 | 65 |
| **Removal efficiency (%) at pH= 10** | 60 | 59 | 58 | 48 | 40 | 31 | 23 |

In this study, the maximum removal efficiency was found as 96% at pH=6.5 at 1 mg/L OFL concentration and 0.5 g/L Nano-GO/M concentration. As the pH values decreased from 6.5 to 4 the OFL adsorption yields decreased to 79% at pH=4 at 1mg/L OFL concentration and constant Nano-GO/M concentration (0.5 g/L). Under alkaline conditions the removal yields exhibited decrease to 60%. As the OFL concentrations were increased from 1 to 1000 mg/L the removal yields decreased significantly to 34%, 65% and 23% at pH 4, 6.5 and 10, respectively.

The efficiency of the photocatalytic process is related to the surface ionization state of the Nano-GO/M, as shown in equation (6.28-33);

$$Fe_3O_4 + h\nu \rightarrow Fe_3O_4\ (e^- + h^+) \quad (6.28)$$

$$OFL + h\nu \rightarrow OFL^* \quad (6.29)$$

$$Fe_3O_4 + \text{graphene} \rightarrow Fe_3O_4 + \text{graphene}\ (e^-) \quad (6.30)$$

$$\text{Graphene } (e^-) + O_2 \rightarrow \text{graphene} + O_2^{\cdot -} \quad (6.31)$$

$$Fe_3O_4\ (h^+) + OH^- \rightarrow Fe_3O_4 + {}^{\cdot}OH \quad (6.32)$$

$$OFL^* + {}^{\cdot}OH \rightarrow CO_2 + H_2O \quad (6.33)$$

Upon light irradiation, the $Fe_3O_4$ present on the GO sheet surface undergoes charge separation that leads to promotion of valence band (VB) electrons into the conduction band (CB), leaving a hole in the VB (6.28), whereas the OFL molecules are excited to cationic OFL radicals (OFL*) (6.29). These photo-generated electrons in the conduction band are instantaneously transferred to GO sheets (6.30), and are consequently captured by dissolved $O_2$ to generate reactive oxidation species such as ˙OH and $O_2^{\cdot -}$ (6.31). On the other hand, the photo induced holes are crucial for the oxidation process and adsorbents are effectively oxidized; usually the $Fe_3O_4$ (h+) can react with adsorbed $H_2O/OH^-$ to form strong hydroxyl radicals (˙OH) (6.32). Finally, these ˙OH radicals oxidize the OFL molecules adsorbed to $CO_2$ and $H_2O$ (6.33) via the π–π electrostatic interactions on the active sites of the Nano-GO/M composite (Peik-See et al., 2014).

pH changes can influence OFL molecule adsorption on the Nano-GO/M surface, which is decisive for the occurrence of photocatalytic oxidation reactions. The zero charge point of ($pH_{pzc}$) Nano-GO/M is at pH ≈ 5.5 (Liu et al., 2015). Thus the surface of Nano-GO/M was positively charged when pH < $pH_{pzc}$, and negatively charged when pH > $pH_{pzc}$. OFL is positively charged at pH values lower than the pKa1 (6.05), negatively charged at pH values above the pKa2 (8.11), and neutral at pH values between pKa1 and pKa2 (Peres, Maniero & Guimarães, 2015). Therefore, pH 4 and 10 are not suitable for OFL adsorption on the Nano-GO/M surface, since there is electronic repulsion between the charges of the compound and the catalyst with the same sign. At pH 6.5, both the Nano-GO/M molecule and the OFL are in their neutral forms, and no repulsion occurs between them. Photocatalysis degradation efficiencies at pH 4 and 10 were lower than those obtained for the same process at pH 6.5. This was probably due to the charge-repulsion phenomenon, which is not favorable to OFL adsorption on Nano-GO/M.

Peres, Maniero & Guimarães, (2015), were investigated the effect of pH on the photocatalytic degradation of OFL (initial conc. 500 µg/L) onto the $TiO_2$. They researched the degradation experiments with 8g/L of $TiO_2$ at different pH values between 3, 6 and 10 for 60 min irradiation time at room temperature. Results show that the degree of photodegradation efficiency was increased with increasing the solution pH up to 6 and then decreased.

Figure 6.82 summarizes the photocatalytic removal yields versus pH levels and OFL concentrations. Consequently, the maximum OFL (initial OFL concentration was 1 mg/L) photocatalytic removal yield was obtained at pH 6.5 (96%), but at alkaline pH lowest OFL photocatalytic removal yield (60%) was obtained whilst at acidic pH lower OFL adsorption yield was obtained (79%).

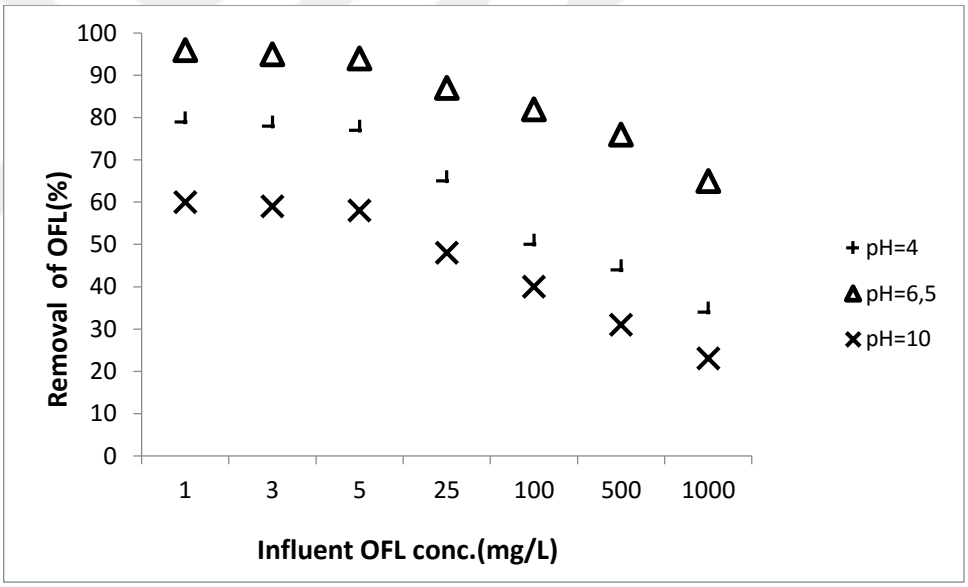


Figure 6.82 Effect of different pHs (4, 6.5 and 10) on the yield of OFL photooxidation efficiency at a Nano-GO/M concentration of 0.5 g/L, at 21°C and 60 min irradiation time and with a power of 300 W UV light (<α (0.05)).

Table 6.16 represents the effects of different pHs on the photocatalytic removal efficiency of OFL (for 1 mg/L initial OFL concentration) at 21°C. Photocatalytic removals of OFL on Nano-GO/M was relatively high at pH 6.5.

Table 6.16 Shows the maximum photocatalytic removal efficiencies of OFL (1mg/L) at acidic, neutral and alkaline pHs (4, 6.5 and 10) at 21°C and at 0.5 g/L constant Nano-GO/M concentration at 60 min irradiation time.

| pH | Removal efficiencies (%) |
|---|---|
| 4 | 79 |
| 6.5 | 96 |
| 10 | 60 |

A linear relationship between pH and maximum OFL photocatalytic removal efficiencies (for 1 mg/L initial OFL concentration) was not obtained (R=0.61) and this regression is not significant (ANOVA $p=0.39>\alpha$ (0.05) and F=0.58).

#### *6.3.2.5 Effect of Temperature on the Photocatalytic Removal of OFL with Nano-GO/M composite*

Temperature is another important parameter for the photocatalytic process. In order to investigate the effect of temperature, OFL removal was studied under different temperatures (21°C, 40°C, 60°C and 80°C). For maximum OFL removal optimum Nano-GO/M concentration (0.5 g/L) and optimum irradiation time (60 min) were determined in the preliminary studies as mentioned above. Therefore, all experiments were realized after 60 min irradiation time, at increasing OFL concentrations (1, 3, 5, 25, 100, 500 and 1000 mg/L) and at original pH (6.5) of OFL solution at 0.5 g/L Nano-GO/M. Figure 6.83 summarizes the photocatalytic removal efficiencies of OFL at 21°C, with 0.5 g/L constant Nano-GO/M, at increasing OFL concentrations (1, 3, 5, 25, 100, 500 and 1000 mg/L). OFL photocatalytic efficiencies were found as 96 %, 95%, 94%, 87%, 82%, 76% and 65 for 1, 3, 5, 25, 100, 500 and 1000 mg/L OFL concentrations, respectively. As a consequence, the OFL photocatalytic removal efficiencies were high (96-95%) at low OFL concentrations (1-3 mg/L).

A linear relationship between OFL photocatalytic treatment efficiencies and influent OFL concentration was obtained (R=0.93) and this regression is significant (ANOVA $p=0.0001<\alpha$ (0.05) and F=33.22).

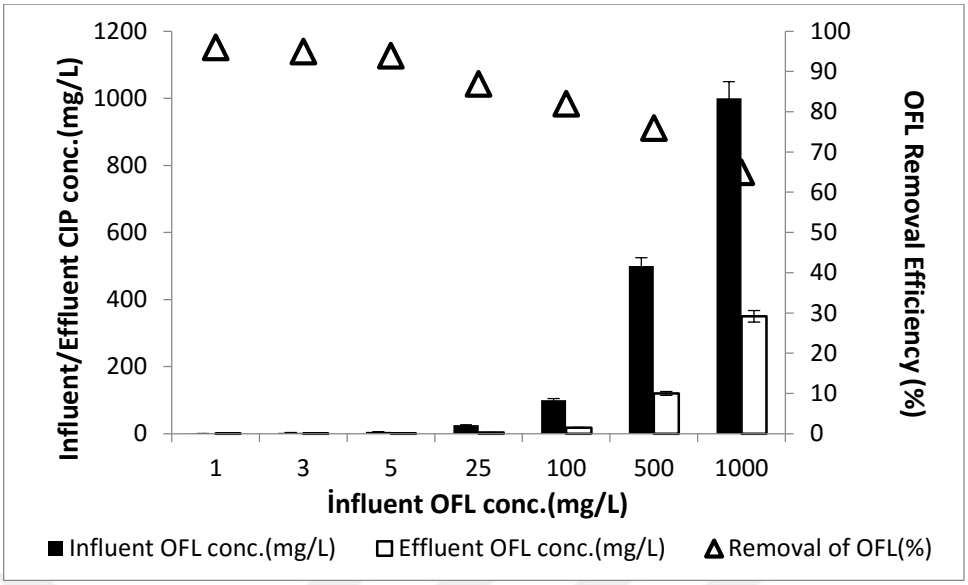


Figure 6.83 Effect of increasing OFL concentration on the yields of OFL photooxidation at a Nano-GO/M concentration of 0.5 g/L at pH=6.5, at 21°C and 60 min irradiation time and with a power of 300 W UV light (<α (0.05)).

Figure 6.84 shows the photocatalytic removal efficiencies of OFL at 40°C, with 0.5 g/L constant Nano-GO/M, at increasing OFL concentrations (1, 3, 5, 25, 100, 500 and 1000 mg/L). The photocatalytic removal efficiencies of OFL were found as 88%, 87%, 86%, 74%, 65%, 56% and 45%, respectively. As the OFL concentrations were increased, the removal efficiencies decreased. The maximum OFL removal efficiency is 88% at 40°C, with 0.5 g/L constant Nano-GO/M concentration for 1 mg/L influent OFL concentration. According to this results it can be concluded that the OFL adsorption removals were high (88-87%) at low OFL concentrations (1-3 mg/L) at 40°C.

A linear relationship between OFL photocatalytic removal efficiencies and influent OFL concentration was obtained (R=0.90) and this regression is significant (ANOVA p=0.006<α (0.05) and F=20.59).

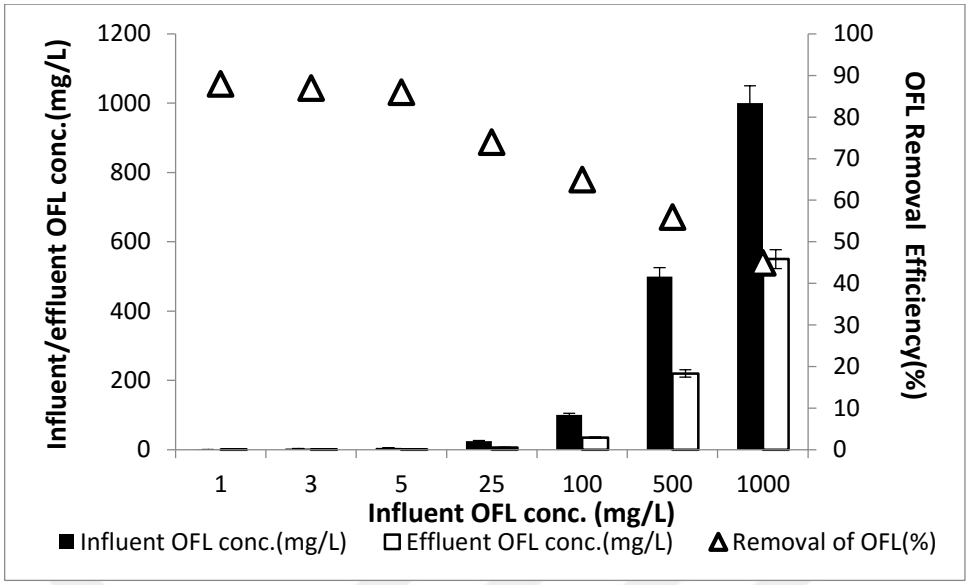


Figure 6.84 Effect of increasing OFL concentration on the yields of OFL removal at a Nano-GO/M concentration of 0.5 g/L at pH=6.5, at 40°C and 60 min irradiation time and at a power of 300 W UV light (<α (0.05)).

Figure 6.85 shows the photocatalytic removal efficiencies of OFL at increasing OFL concentrations (1, 3, 5, 25, 100, 500 and 1000 mg/L) for 60°C at 0.5 g/L constant Nano-GO/M and at pH of 6.5. According these OFL concentrations the photocatalytic removal yields were 72%, 71%, 70%, 54%, 48%, 39% and 30%, respectively. As the OFL concentrations were increased, the photocatalytic removal efficiencies decreased. The maximum OFL removal efficiency is 72% at 60°C for 1 mg/L influent OFL concentration. According to this results it can be concluded that the OFL adsorption removals were lower (72-71%) at low OFL concentrations (1-3 mg/L) at 60°C.

A linear relationship between OFL photocatalytic removal efficiencies and influent OFL concentration was obtained (R=0.86) and this regression is significant (ANOVA p=0.005<α (0.05) and F=14.51).

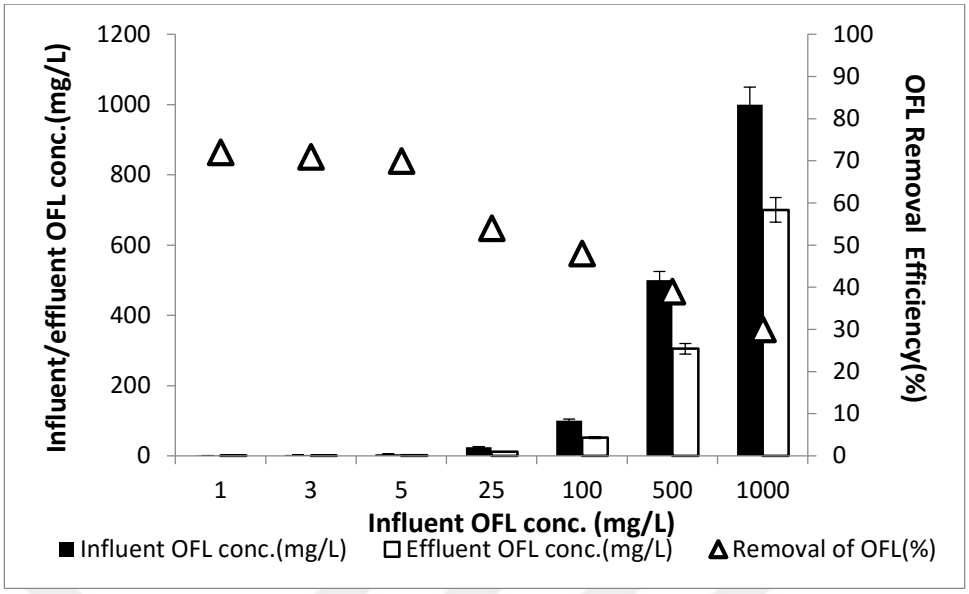


Figure 6.85 Effect of increasing OFL concentration on the yields of OFL photooxidation at a Nano-GO/M concentration of 0.5 g/L at pH=6.5, at 60°C and 60 min irradiation time and at a power of 300 W UV light (<α (0.05)).

Figure 6.86 shows the photocatalytic removal efficiencies of OFL at increasing OFL concentrations (1, 3, 5, 25, 100, 500 and 1000 mg/L) for 80°C at 0.5 g/L constant Nano-GO/M. According these OFL concentrations the photocatalytic removal yields were 64%, 63%, 62%, 53%, 45%, 36% and 27%, respectively. As the OFL concentrations were increased, the photocatalytic removal efficiencies decreased. The maximum OFL removal efficiency is 64% at 80°C for 1 mg/L influent OFL concentration. According to these results it can be concluded that the OFL adsorption removals were lowest (64-63%) at low OFL concentrations (1-3 mg/L) at 80°C.

A linear relationship between OFL photocatalytic removal efficiencies and influent OFL concentration was obtained (R=0.91) and this regression is significant (ANOVA p=0.004<α (0.05) and F=23.43).

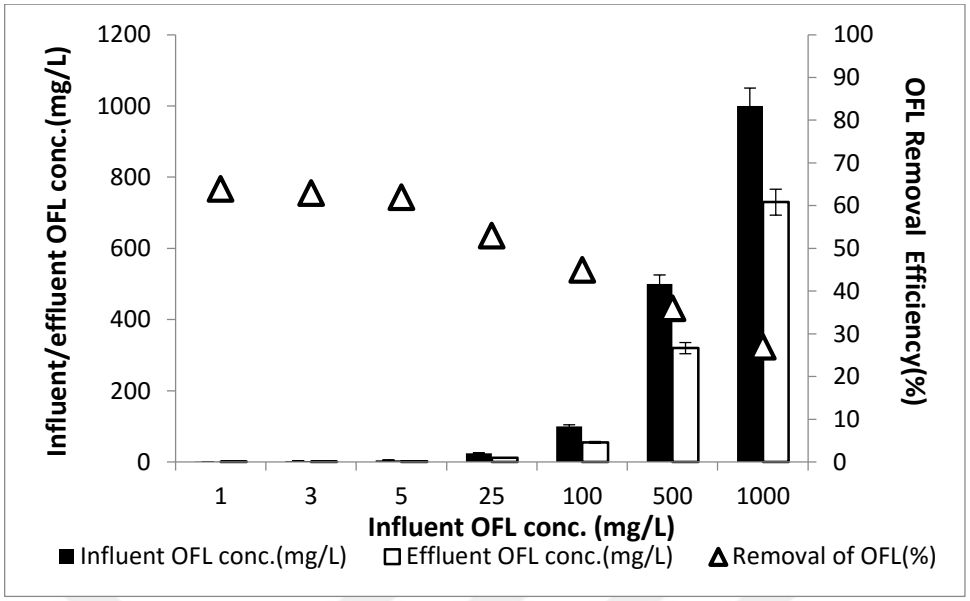


Figure 6.86 Effect of increasing OFL concentration on the yields of OFL removal at a Nano-GO/M concentration of 0.5 g/L at pH=6.5, at 80°C and 60 min irradiation time and at a power of 300 W UV light (<α (0.05)).

Figure 6.87 summarizes the effects of increasing temperatures (21°C, 40°C, 60°C and 80°C) on OFL photocatalytic removal yields at a OFL concentration of 5 mg/L after 60 min irradiation time at pH=6.5 and at constant Nano-GO/M concentration (0.5 g/L). Increasing the temperature from 21°C to 40-60-80°C yielded a decrease on the photocatalytic removal efficiencies of OFL.

Among these four different temperatures (21°C, 40°C, 60°C and 80°C), the maximum OFL photocatalytic removal yields was found as 94% for 5 mg/L initial OFL concentration at 21°C. This low temperature reduced the operational cost of photocatalytic process.

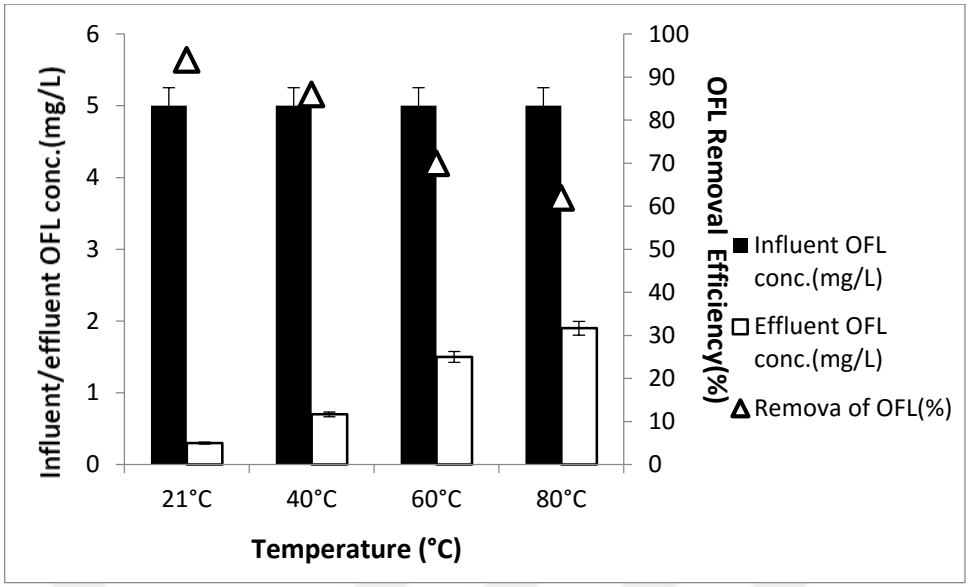


Figure 6.87 Effect of temperature time on the yields of constant OFL concentration (5 mg/L), at a constant Nano-GO/M (0,5 g/L), at a pH of 6.5 and at 21°C, 40°C, 60°C and 80°C and at a power of 300 W UV light, at 60 min irradiation time (<α (0.05)).

Table 6.17 represents the effects of different temperatures on the photocatalytic removal efficiency of OFL for 1 mg/L initial OFL concentration. Photocatalytic removal of OFL on Nano-GO/M was high at 21°C.

Table 6.17 Shows the maximum photocatalytic removal efficiencies of OFL (1mg/L) at 21°C, 40°C, 60°C and 80°C and at 0.5 g/L constant Nano-GO/M concentration and at a power of 300 W UV light.

| Temperature (°C) | Removal efficiencies (%) |
|---|---|
| 21 | 96 |
| 40 | 88 |
| 60 | 72 |
| 80 | 65 |

A linear relationship between temperature and maximum OFL photocatalytic removal efficiencies (for 1 mg/L initial OFL concentration) was obtained (R=0.99) and this regression is significant (ANOVA p=0.006 <α (0.05) and F=84.19).

#### *6.3.2.6 Effect of UV Power on the Photocatalytic Removal of OFL with Nano-GO/M composite*

UV power is another important parameter for the photocatalytic process. In order to investigate the effect of UV power, OFL removal was studied under different UV powers (100 W, 300 W, 400 W and 600 W). For maximum OFL removal the optimum Nano-GO/M concentration (0.5 g/L) and the optimum irradiation time (60 min) were determined in the preliminary studies as mentioned above. Therefore, all experiments were realized after 60 min irradiation time, at increasing OFL concentrations (1, 3, 5, 25, 100, 500 and 1000 mg/L) and at original pH (6.5) at 0.5 g/L Nano-GO/M. Figure 6.88 summarizes the photocatalytic removal efficiencies of OFL at 21°C, with 0.5 g/L constant Nano-GO/M, at increasing OFL concentrations (1, 3, 5, 25, 100, 500 and 1000 mg/L) and with a power of 100 W UV light. OFL photocatalytic efficiencies were found as 89%, 88%, 87%, 82%, 72%, 67% and 60% for 1, 3, 5, 25, 100, 500 and 1000 mg/L OFL concentrations, respectively. Consequently, the OFL photocatalytic removal efficiencies were high (89-88%) at low OFL concentrations (1-3 mg/L). The percentage of photodegradation decreased with increasing of initial concentration of OFL. When initial concentration increase, more substances are adsorbed on the surface of Nano-GO/M. Therefore, there are only a fewer active sites for adsorption of hydroxyl ions so the generation of hydroxyl radicals will be reduced. Further, as the concentration of OFL solution increase, the photons get intercepted before they can reach the catalyst surface, hence the adsorption of photons by the catalyst decreases, and consequently the degradation percent is reduced (Chakrabarti & Dutta, 2004; Shankar et al., 2004).

A linear relationship between OFL photocatalytic removal efficiencies and influent OFL concentration was obtained (R=0.89) and this regression is significant (ANOVA $p=0.006<\alpha$ (0.05) and F=19.79) and this regression is significant.

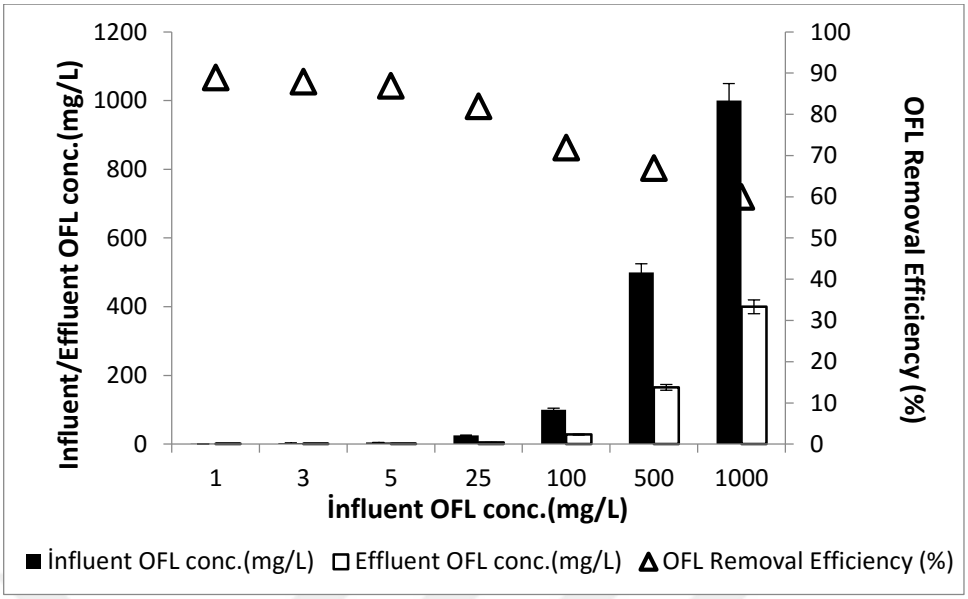


Figure 6.88 Effect of increasing OFL concentration on the yields of OFL removal at a Nano-GO/M concentration of 0.5 g/L at pH=6.5, with a power of 100 W UV light and 60 min irradiation time (<α (0.05)).

Figure 6.89 shows the photocatalytic removal efficiencies of OFL with 0.5 g/L constant Nano-GO/M, at increasing OFL concentrations (1, 3, 5, 25, 100, 500 and 1000 mg/L) and with a power of 300 W UV light. The photocatalytic removal efficiencies of OFL were found as 96%, 95%, 94%, 87%, 82%, 76% and 65% for 1, 3, 5, 25, 100, 500 and 1000 mg/L OFL concentrations, respectively. According to this results it can be concluded that the OFL photocatalytic treatment efficiencies removals were high (96-95%) at low OFL concentrations (1-3 mg/L). As the OFL concentrations were increased, the photocatalytic removal efficiencies decreased. The photodegradation efficiency was gradually decreased as a result of increasing OFL concentration. When the initial OFL concentration was decreased, the probability of the reaction between OFL and oxidizing species was increased, leading to an improvement of photodegradation efficiency. However, the excess OFL concentration reduced photodegradation efficiency. Therefore, there are only a fewer active sites for adsorption of hydroxyl ions so the generation of hydroxyl radicals will be reduced. Further, as the concentration of OFL solution increase, the photons get intercepted before they can reach the catalyst surface, hence the adsorption of photons by the catalyst decreases, and consequently the degradation percent is reduced (Chakrabarti & Dutta, 2004; Shankar et al., 2004).

A linear relationship between OFL photocatalytic treatment efficiencies and influent OFL concentration was obtained (R=0.93) and this regression is significant (ANOVA p=0.0001<α (0.05) and F=33.22).

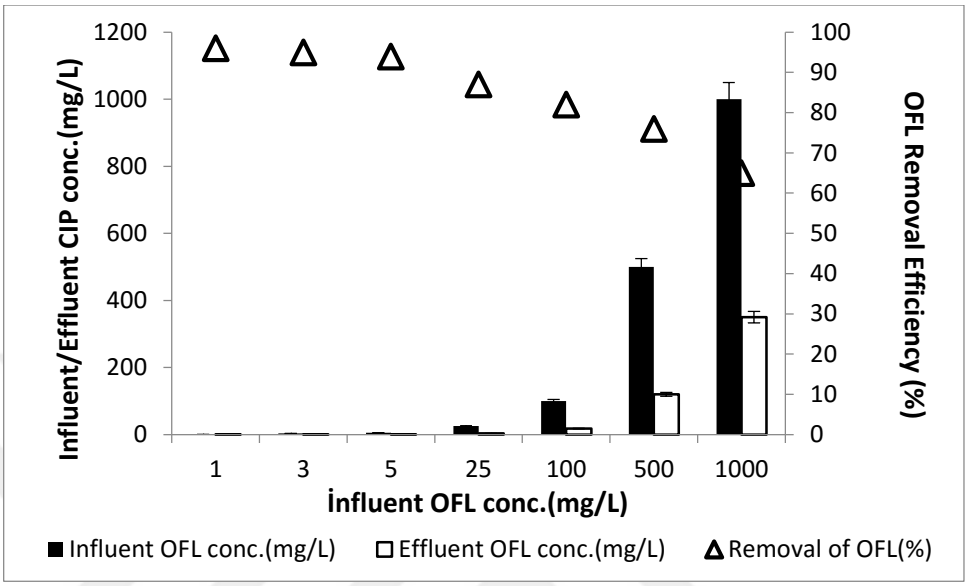


Figure 6.89 Effect of increasing OFL concentration on the yields of OFL photocatalytic treatment at a Nano-GO/M concentration of 0.5 g/L at pH=6.5, at 21°C and 60 min irradiation time and with a power of 300 W UV light (<α (0.05)).

Figure 6.90 shows the photocatalytic removal efficiencies of OFL with 0.5 g/L constant Nano-GO/M, at increasing OFL concentrations (1, 3, 5, 25, 100, 500 and 1000 mg/L) and with a power of 400 W UV light. The photocatalytic removal efficiencies of OFL were found as 97%, 96%, 95%, 89%, 83%, 74% and 67% for 1, 3, 5, 25, 100, 500 and 1000 mg/L OFL concentrations, respectively. According to this results it can be concluded that the OFL photocatalytic treatment efficiencies removals were high (97-96%) at low OFL concentrations (1-3 mg/L). The photodegradation efficiency was gradually decreased as a result of increasing OFL concentration. When the initial OFL concentration was decreased, the probability of the reaction between OFL and oxidizing species was increased, leading to an improvement of THE photodegradation efficiency. However, the excess OFL concentration reduced the photodegradation efficiency. Therefore, there are only a fewer active sites for adsorption of hydroxyl ions so the generation of hydroxyl radicals will be reduced. Further, as the concentration of OFL solution increase, the photons get intercepted before they can reach the catalyst surface, hence the adsorption of photons by the catalyst decreases,

and consequently the degradation percentage is reduced (Chakrabarti & Dutta, 2004; Shankar et al., 2004).

A linear relationship between OFL photocatalytic treatment efficiencies and influent OFL concentration was obtained (R=0.93) and this regression is significant (ANOVA p=0.002<α (0.05) and F=29.54).

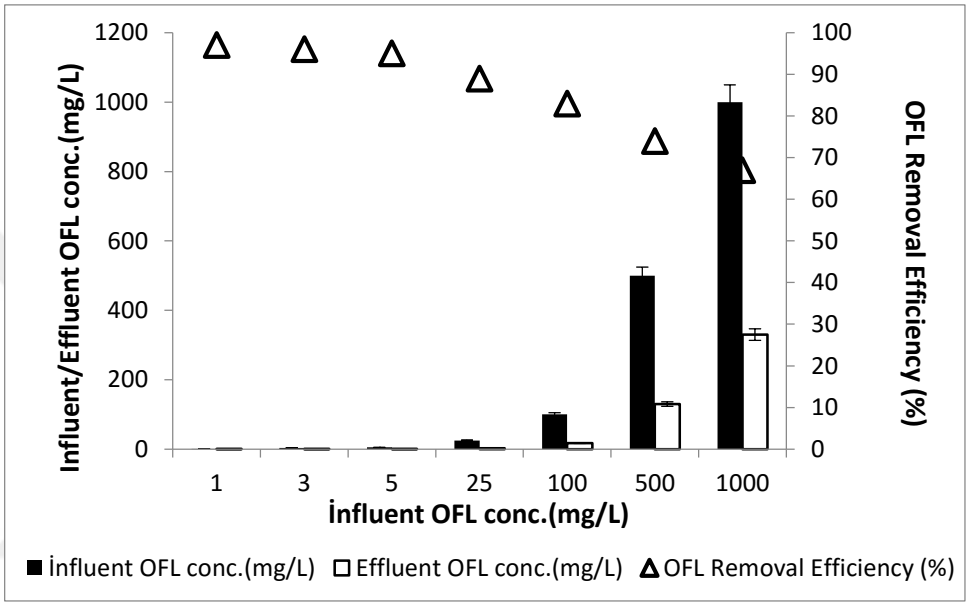


Figure 6.90 Effect of increasing OFL concentration on the yields of OFL photooxidation at a Nano-GO/M concentration of 0.5 g/L at pH=6.5, at 21°C and 60 min irradiation time and with a power of 400 W UV light (<α (0.05)).

Figure 6.91 shows the photocatalytic removal efficiencies of OFL with 0.5 g/L constant Nano-GO/M, at increasing OFL concentrations (1, 3, 5, 25, 100, 500 and 1000 mg/L) and with a power of 600 W UV light. The photocatalytic removal efficiencies of OFL were found as 99%, 98%, 97%, 90%, 84%, 77% and 69% for 1, 3, 5, 25, 100, 500 and 1000 mg/L OFL concentrations, respectively. According to this results it can be concluded that the OFL photocatalytic treatment efficiencies removals were high (99-98%) at low OFL concentrations (1-3 mg/L). Arapbour & Nezamzadeh-Ejhieh (2015), studied the photodegradation of cotrimaxazole antibiotic using iron oxide (IO) supported onto clinoptilolite nanoparticles and Hg-lamp as radiation source.

Their results showed that, at higher cotrimaxazole antibiotic concentration (initial concentrations of: original solution and 10, 50 and 100 times diluted solutions in the presence of 0.5 g $L^{-1}$ of the catalyst at pH 5.5) lower removal efficiencies were observed. Due to small lifetime of hydroxyl radicals, they should rapidly react where they formed. Thus, increasing in the concentration of cotrimaxazole brings more cotrimaxazole molecules near the catalyst surface which causes a faster reaction between cotrimaxazole molecules and hydroxyl radicals before they deactivate. Consequently, at high concentration of the pollutant a major part of photons can absorb by pollutant molecules in the solution and hence lesser photons absorbed by nanoparticle, cause to decrease in the generated hydroxyl and super oxide radicals (Nezamzadeh-Ejhieh & Moazzeni, 2013).

A linear relationship between OFL photocatalytic treatment efficiencies and influent OFL concentration was obtained (R=0.92) and this regression is significant (ANOVA p=0.003<α (0.05) and F=25.43).

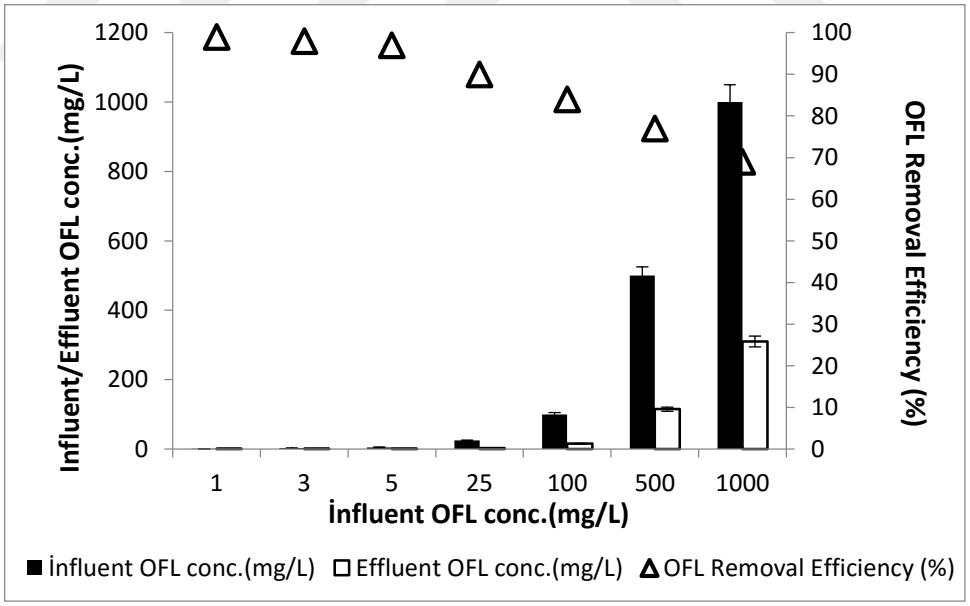


Figure 6.91 Effect of increasing OFL concentration on the yields of OFL photocatalytic treatment at a Nano-GO/M concentration of 0.5 g/L at pH=6.5, at 21°C and 60 min irradiation time and with a power of 600 W UV light (<α (0.05)).

Figure 6.92 represents the effect of UV powers on the photocatalytic removal of OFL with 0.5 g/L constant Nano-GO/M (at pH=6.5, at 21°C and 60 min irradiation

time). OFL concentration was chosen as 5 mg/L to compare the effects of each UV power. As the UV power increased, the OFL yields also increased. The maximum OFL (for 1 mg/L initial OFL concentration) yields obtained as 89%, 96%, 97% and 99% for 100 W, 300 W, 400 W and 600 W UV power, respectively.

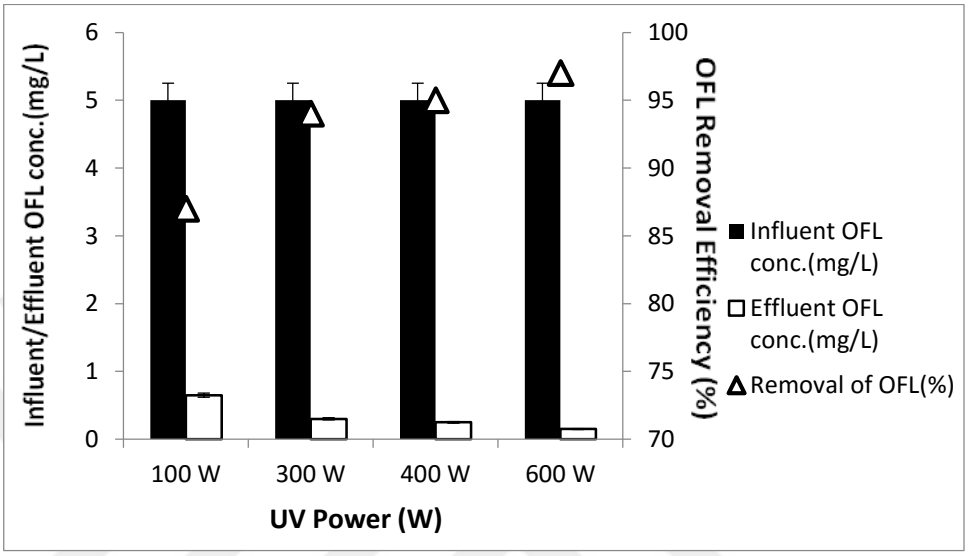


Figure 6.92 Effect of increasing UV light levels on the OFL photocatalytic treatment at a Nano-GO/M concentration of 0.5 g/L at pH=6.5, at 21°C and 60 min irradiation time and with increasing UV power (100, 300, 400 and 600 W).

Table 6.18 represents the effects of different UV light powers on the photocatalytic removal efficiency of OFL for 1 mg/L initial OFL concentration. Our results reveal that the photooxidation increases between 100 W and 600 W but the increase is not significant in the range of 300–400 W. In the present work, we have used 300 W UV light power as the optimum UV level for maximum photooxidation yield of OFL.

Table 6.18 Shows the maximum photocatalytic removal efficiencies of OFL (1mg/L) at 21°C and at 0.5 g/L constant Nano-GO/M concentration and at increasing power of (100 W, 300 W, 400 W and 600 W) UV light at 60 min irradiation time.

| UV Power (W) | Removal efficiencies (%) |
|---|---|
| 100 | 89 |
| 300 | 96 |
| 400 | 97 |
| 600 | 99 |

A linear relationship between temperature and maximum OFL photocatalytic removal efficiencies (for 1 mg/L initial OFL concentration) was obtained (R=0.94) and this regression is significant (ANOVA $p=0.006<\alpha$ (0.05) and F=14.86).

The UV power determines the amount of photons absorbed by the catalyst. In the photocatalytic treatment process with Nano-GO/M, at increased light power electron-hole pair separation competes with recombination, causing less effect on the reaction efficiency (Konstantinou & Albanis, 2004). With the increase of the UV power, the catalyst absorbs more photons, producing more electron-hole pairs in the catalyst surface, and this increases the concentration of hydroxyl radicals and consequently increases the removal percent. Earlier studies on the effect of UV light power on different pollutants such as dye, have shown almost the same results. Muruganandham & Swaminathan (2006), researched the influence of UV power on the decolourisation of reactive yellow 14 (RY14) at varying UV power from 16 W to 62 W. Results showed that an increase of UV power from 16 W to 62 W increases the decolourisation from 35.9% to 87.9% at 20 min for initial RY14 concentration of $5x10^{-4}$ M.

*6.3.2.7 OFL Metabolites*

In this study we also investigated two different metabolites (POF: 9-piperazino ofloxacin and MOF: des-methyl ofloxacin) of OFL which are released during photocatalytic processes. In order to measure the metabolites of OFL (initial OFL conc. 100 mg/L), all experiments were realized after 60 min irradiation time, at room temperature and at original pH (6.5) of OFL solution with 0.5 g/L Nano-GO/M. Results showed that, after photocatalytic treatment from 100 mg/L OFL 82 mg/L OFL was photodegraded (Table 6.19). The OFL was photodegraded with a yield of 82%. 18 mg/L OFL was remained in the effluent and cannot be photodegraded with UV and Nano-GO/M. OFL was photodegraded to two metabolites namely POF and MOF. From 82 mg/L OFL; 0.8211 mg/L POF and 2.2110 MOF were produced (Table 6.19). 0.8211 mg/L POF was degraded with a yield of 1.001% while 2.2110 mg/L MOF was degraded with a yield of 2.70%. As a result, from 82 mg/L OFL; totally 3.0321 mg/L metabolites were discharged. The rest of OFL (82 mg/L – 3.0321 mg/L= 78.97 mg/L)

was completely transformed to $CO_2$ and $H_2O$. Table 6.19 shows the percentage of removed or transformed products.

Table 6.19 Shows the influent/effluent and removed/transformed OFL, POF (9-piperazino ofloxacin) and MOF (des-methyl ofloxacin) (operational conditions: 60 min, pH 6.5, 0.5 g/L Nano-GO/M, 21°C and 300 W UV power).

| | Influent (mg/L) | Effluent (mg/L) | Removed concentration (mg/L) |
|---|---|---|---|
| OFL | 100 | 18 | 82 |
| POF (9-piperazino ofloxacin) | 0 | 0.8211 | 0.8211 |
| MOF (des-methyl ofloxacin) | 0 | 2.2110 | 2.2110 |
| Total metabolites | 0 | 3.032 | 3.032 |
| The rest of OFL | 100 | 78.79 | 78.79 |

Figure 6.93 shows the HPLC analysis of OFL and its metabolites. POF and MOF were obtained as 0.82 and 2.21 mg/L, respectively.

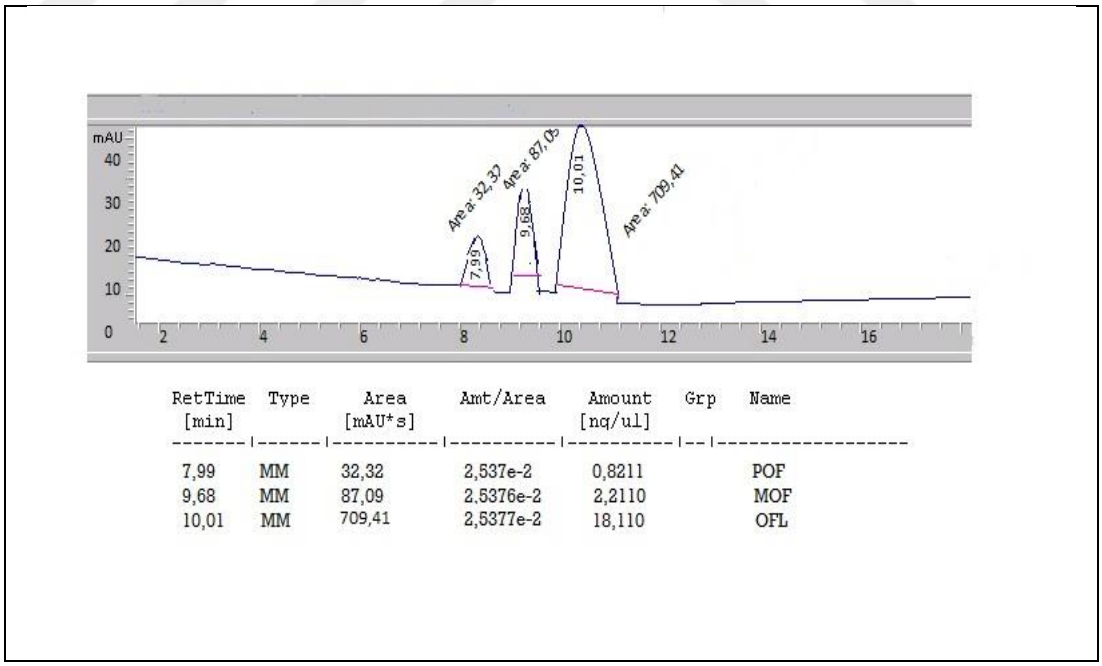


| RetTime [min] | Type | Area [mAU*s] | Amt/Area | Amount [ng/ul] | Grp | Name |
|---|---|---|---|---|---|---|
| 7,99 | MM | 32,32 | 2,537e-2 | 0,8211 | | POF |
| 9,68 | MM | 87,09 | 2,5376e-2 | 2,2110 | | MOF |
| 10,01 | MM | 709,41 | 2,5377e-2 | 18,110 | | OFL |

Figure 6.93 HLPC analysis of OFL (initial 100 mg/L) treatment with 300 W UV light at 60 min irradiation time and with 0.5 g/L Nano-GO/M.

### 6.3.2.8 *Investigation of Photocatalytic Degradation Kinetic of OFL Using Nano-GO/M Composite*

In this step of the study, zero-order kinetic, first-order kinetic and second-order kinetic models were discussed to indicate the removal kinetics of OFL on the surface of Nano-GO/M composite throughout photodegradation under UV.

*6.3.2.8.1. Zero-Order Kinetics.* The $R^2$ value for pseudo-zero-order reaction was found as 1 for OFL in the photocatalytic studies performed with Nano-GO/M (Figure 6.94). Pseudo-zero-order reaction's the zero order rate kinetic constant is $k_0$. The $k_0$ values evaluated from Pseudo-zero-order reaction plots were found as 0.078 $min^{-1}$ for OFL from the Eq. (5.11).

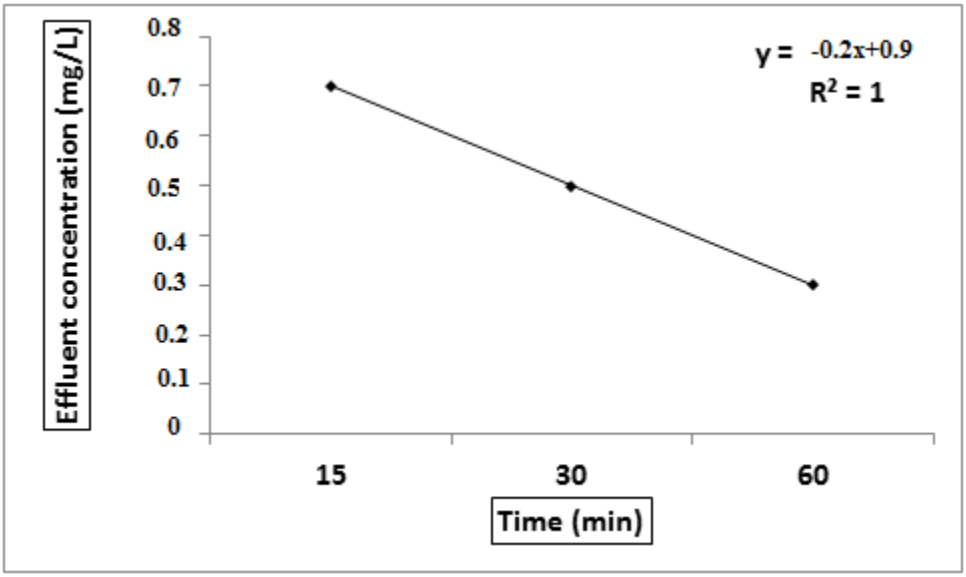


Figure 6.94 Pseudo-zero-order reaction of OFL (OFL: 5 mg/L, T: room temperature, irradiation time: 60 min., concentration of Nano-GO/M: 0.5 g/L, 300 watt UV light).

*6.3.2.8.2. First-Order Kinetics.* The $R^2$ value for first-order reaction was obtained as 0.986 for OFL in the photocatalytic studies performed with Nano-GO/M (Figure 6.95). First-order reaction's in the first order rate kinetic constant is $k_1$. The $k_1$ values evaluated from first-order reaction plots were found to be 0.423 $min^{-1}$ for OFL from the Eq. (5.13).

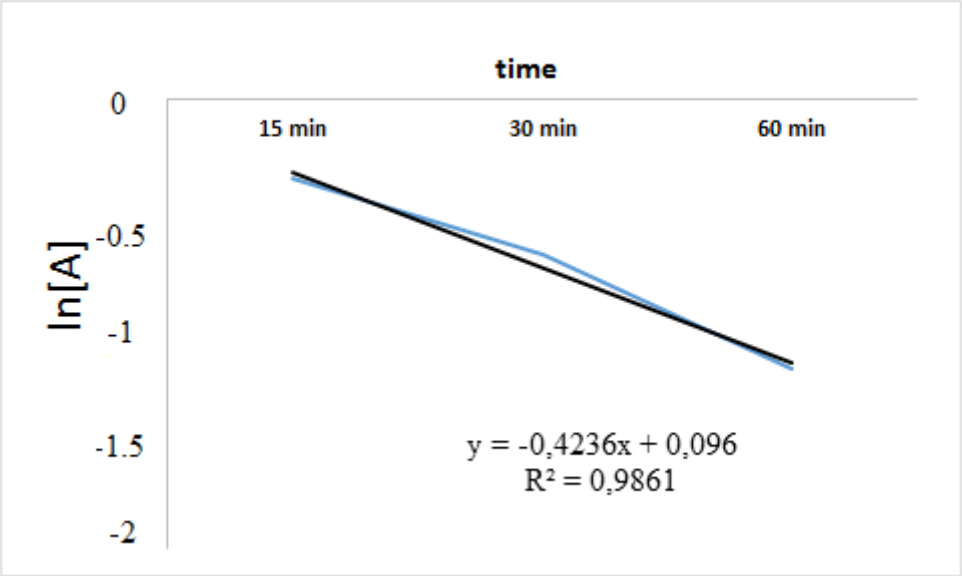


Figure 6.95 First-order reaction of OFL (OFL concentration: 5 mg/L, T: room temperature, irradiation time: 60 min, concentration of Nano-GO/M: 0.5 g/L, 300 watt UV light).

*6.3.2.8.3 Second-Order Kinetics*. The $R^2$ value for second-order reaction was found as 0.95 for OFL in the photocatalytic studies performed with Nano-GO/M (Figure 6.96). Second-order reaction's the second order rate kinetic constant is $k_2$. The $k_2$ values evaluated from second-order reaction plots were found as 0.986 $min^{-1}$ for OFL from the Eq. (5.14).

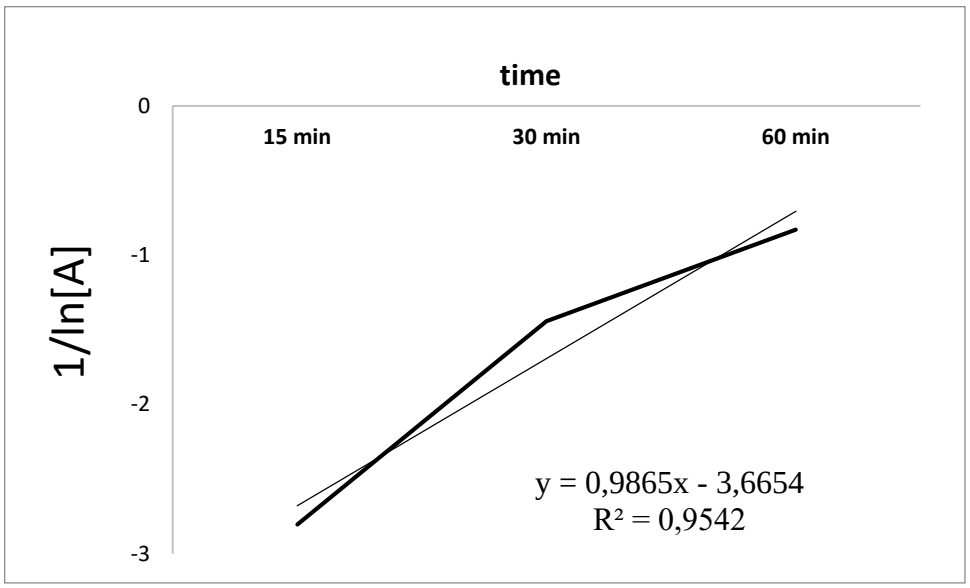


Figure 6.96 Second-order reaction of OFL (OFL concentration: 5 mg/L, T: room temperature, irradiation time: 60 min, concentration of Nano-GO/M: 0.5 g/L, 300 watt UV light).

As results of kinetic studies it was found that the OFL was photodegraded according to zero order reaction kinetic since the $k_0$ value calculated is meaningful than first order and second order reaction kinetics with highest $R^2$ value (1). From the zero order reaction plots $k_0$ value for OFL photodegradation was found to be 0.078 $min^{-1}$. In the other words, OFL was removed under 300 W UV irradiation according to zero order reaction kinetics.

### *6.3.2.9 UV Absorption Spectra of OFL*

The UV–visible spectra of the OFL were measured with a spectro-photometer in the wave lengths range varying from 190 nm to 1100 nm. UV absorption spectra of raw OFL and treated OFL under UV irradiation can be seen in Figure 6.97 and in Figure 6.98, respectively. The maximum absorbance peaks were seen at 265 nm as 9.999 A (absorbance) in raw OFL. After the OFL was treated under 300 W UV light with 0.5 g/L Nano-GO/M composite, the measured absorbance values were illustrated in Figure 6.98. The maximum absorbance peaks after UV irradiation were seen almost the same of before UV irradiation. This can be attributed to photodegradation of OFL to metabolites namely POF (9-piperazino ofloxacin) and MOF (des-methyl ofloxacin) and to end, ultimate products of $CO_2$ and $H_2O$ via mineralization process.

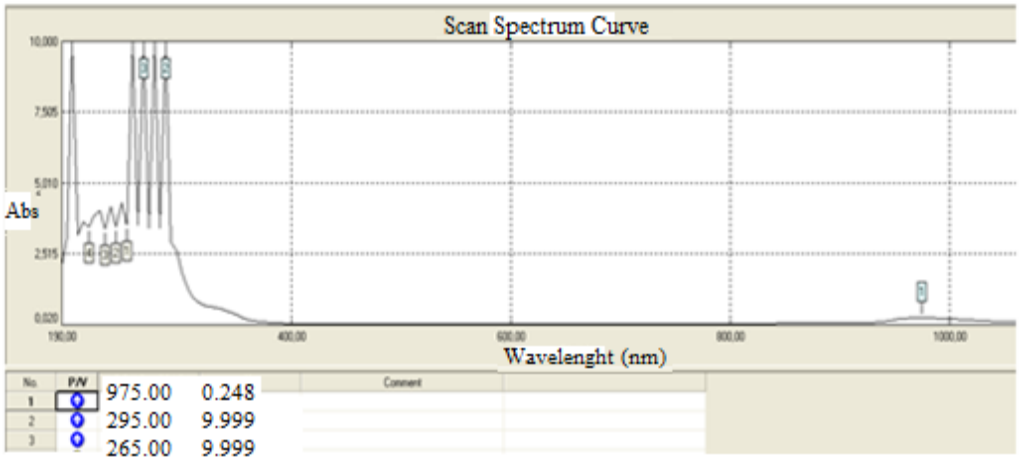


Figure 6.97 UV absorption spectra of raw OFL (100 mg/L).

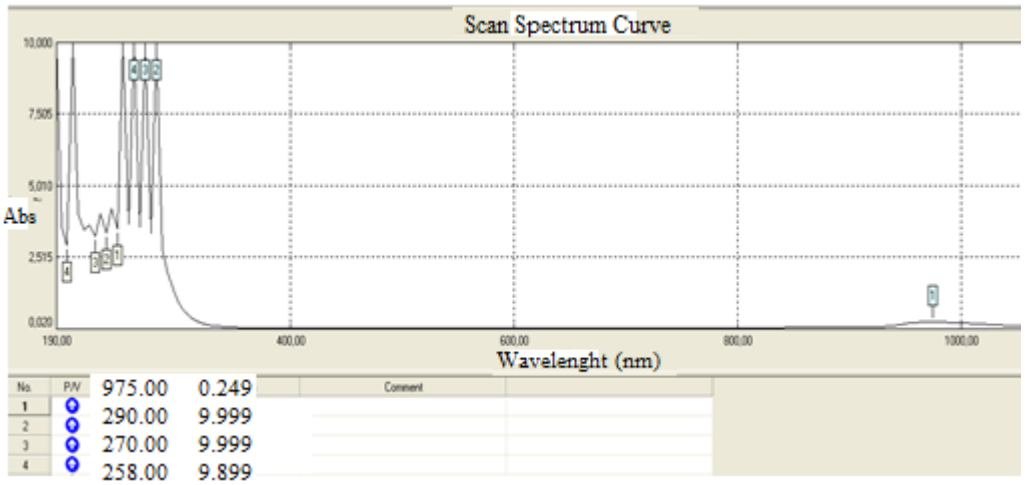


Figure 6.98 UV absorption spectra of the treated OFL under UV irradiation (T: room temperature, irradiation time: 30 min, concentration of Nano-GO/M: 0.5 g/L, 300 watt UV light).

## 6.4 Treatment of CIP and OFL under Sunlight

### *6.4.1 CIP Treatment under Sunlight*

#### *6.4.1.1 Effects of concentration of Nano-GO/M composite on the treatment of CIP under Sunlight*

Effects of 0.5 g/L, 2 g/L, 3.5 g/L, 5 g/L and 10 g/L Nano-GO/M composite concentrations on the removals of CIP were studied with constant sunlight time (250 min was chosen due to preliminary studies results) at original pH of CIP solution (pH=6.5) under sunlight irradiation with a power of 80 W at outdoor temperature (35°C ± 5°C). The results were given in Figure 6.99 for 0.5 g/L Nano-GO/M concentration at increasing CIP concentrations (1, 3, 5, 25, 100, 500 and 1000 mg/L). CIP removal efficiencies were obtained as 49%, 48%, 47%, 40%, 34 %, 28% and 19% for 1, 3, 5, 25, 100, 500 and 1000 mg/L CIP concentrations, respectively. According to this results it can be concluded that the CIP removal efficiencies were high (49-48%) at low CIP concentrations (1-3 mg/L). Increasing the CIP in the aqueous solution from 1 mg/L to 1000 mg/L resulting a decrease in removal efficiencies from 49% to 19 %. Increased concentration of the CIP could occupy more active sites of Nano-GO/M, which inhibits generation of the oxidants (Yan, Yu & Ray, 2008).

A linear relationship between CIP removal efficiencies and influent CIP concentration was obtained (R=0.92) and this regression is significant (ANOVA p=0.003<α (0.05) and F=27.13).

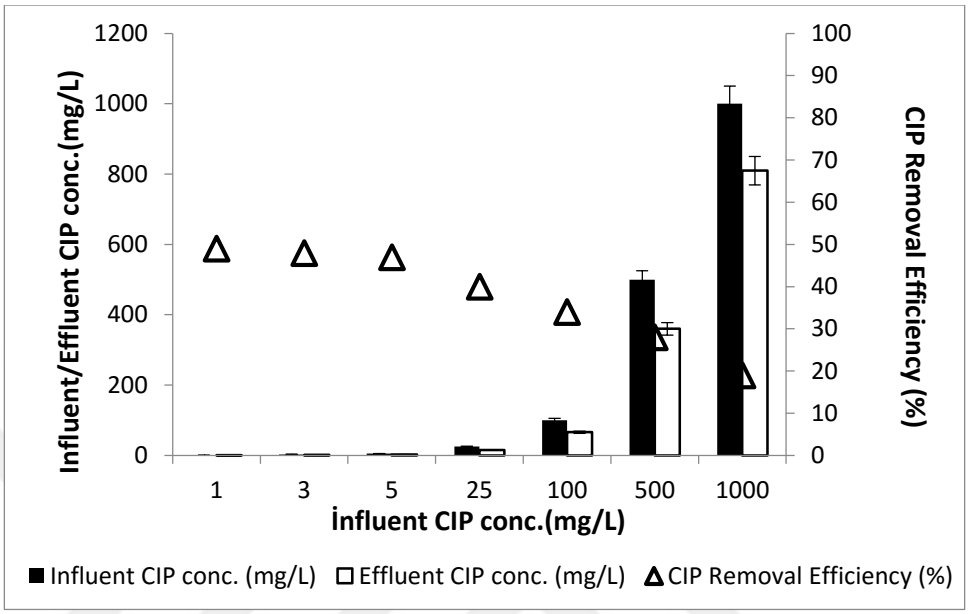


Figure 6.99 Effect of increasing CIP concentration on the yields of CIP removal efficiencies at a Nano-GO/M concentration of 0.5 g/L at pH=6.5, at 35°C ± 5°C and 250 min irradiation time and with a power of 80 W sunlight (<α (0.05)).

Figure 6.100 shows the removal efficiencies of CIP at increasing CIP concentrations (1, 3, 5, 25, 100, 500 and 1000 mg/L). The CIP yields were found as 80%, 79%, 78%, 70%, 64%, 53% and 47% at 2 g/L Nano-GO/M, respectively**.** As the CIP concentrations were increased from 1 mg/L to 1000 mg/L, the removal efficiencies decreased from 80% to 47%, respectively. The maximum CIP removal efficiency is 80% at 2 g/L Nano-GO/M concentration and at 1 mg/L influent CIP concentration. According to these results it can be concluded that the CIP photocatalytic treatment efficiency were high (80-79%) at low CIP concentrations (1-3 mg/L). At highest CIP concentration (1000 mg/L) the photocatalytic treatment efficiency was obtained as 47% at 2g/L Nano-GO/M concentration. The reason of this may be explained by the only parts of CIP could interact with limited active sites on the Nano-GO/M surface, thereby causing lower photocatalytic treatment efficiency of CIP at higher initial CIP concentration.

A linear relationship between CIP removal efficiencies and influent CIP concentration was obtained (R=0.90) and this regression is significant (ANOVA $p=0.005<\alpha$ (0.05) and F=21.58).

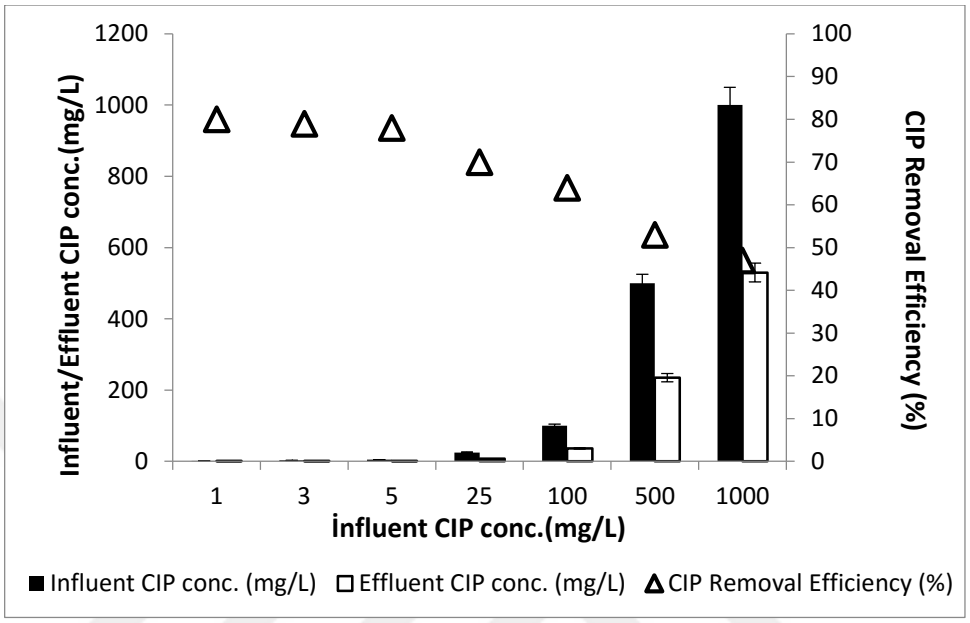


Figure 6.100 Effect of increasing CIP concentration on the yields of CIP removal efficiencies at a Nano-GO/M concentration of 2 g/L at pH=6.5, at 35°C ± 5°C and 250 min irradiation time and with a power of 80 W sunlight ($<\alpha$ (0.05)).

Figure 6.101 shows the removal efficiencies of CIP at increasing CIP concentrations (1, 3, 5, 25, 100, 500 and 1000 mg/L) for 3.5 g/L Nano-GO/M. According these CIP concentrations, the removal yields were 81%, 80%, 79%, 72%, 66%, 54% and 49%, respectively. The maximum CIP removal efficiency is 81% at 3.5 g/L Nano-GO/M concentration for 1 mg/L influent CIP concentration. According to these results it can be concluded that the CIP removals were high (81-80%) at low CIP concentrations (1-3 mg/L) while CIP removals were lower (54-49%) at high CIP concentrations (500-1000 mg/L). The removal efficiency is low at high CIP concentrations. In other words, the Nano-GO/M remove small amount of CIP at high CIP concentrations as reported by Hong et al. (2009). Highest removal efficiency (81%) obtained for lowest CIP concentration (1 mg/L) while lowest removal efficiency (49%) obtained for highest CIP concentration (1000 mg/L). The decrease in the photodegradation efficiencies of CIP in sunlight irradiation with 3.5 g/L Nano-GO/M

composite after 250 min irradiation time might be related to the limitation of incident photons and the light screening effect.

A linear relationship between CIP removal efficiencies and influent CIP concentration was obtained (R=0.90) and this regression is significant (ANOVA $p=0.006<\alpha$ (0.05) and F=20.80).

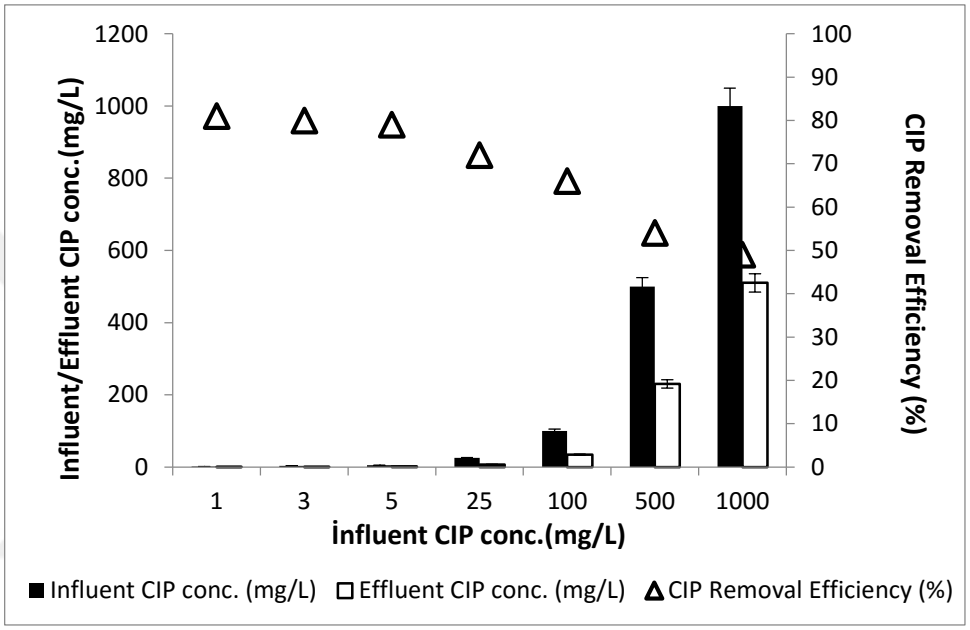


Figure 6.101 Effect of increasing CIP concentration on the yields of CIP removal efficiencies at a Nano-GO/M concentration of 3,5 g/L at pH=6.5, at 35°C ± 5°C and 250 min irradiation time and with a power of 80 W sunlight ($<\alpha$ (0.05)).

Figure 6.102 shows the removal efficiencies of CIP at increasing CIP concentrations (1, 3, 5, 25, 100, 500 and 1000 mg/L) for 5 g/L Nano-GO/M. According these CIP concentrations, the removal yields were 79%, 78%, 77%, 73%, 67%, 53% and 45%, respectively. The maximum CIP removal efficiency is 79% at 5 g/L Nano-GO/M concentration for 1 mg/L influent CIP concentration. According to this results it can be concluded that the CIP removals were high (79-78%) at low CIP concentrations (1-3 mg/L) while CIP removals were lower (53-45%) at high CIP concentrations (500-1000 mg/L). The removal efficiency is low at high CIP concentrations. Increased concentration of the CIP could occupy more active sites of Nano-GO/M, which inhibits generation of the oxidants (Yan, Yu & Ray, 2008).

A linear relationship between CIP removal efficiencies and influent CIP concentration was obtained (R=0.91) and this regression is significant (ANOVA p=0.004<α (0.05) and F=24.93).

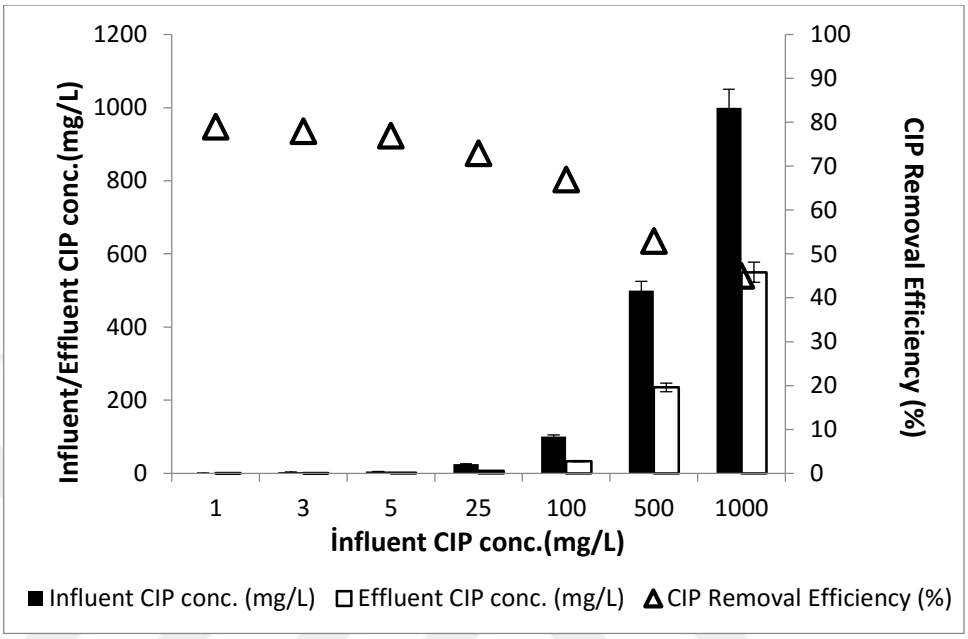


Figure 6.102 Effect of increasing CIP concentration on the yields of CIP removal efficiencies at a Nano-GO/M concentration of 5 g/L at pH=6.5, at 35°C ± 5°C and 250 min irradiation time and with a power of 80 W sunlight (<α (0.05)).

Figure 6.103 shows the removal efficiencies of CIP at increasing CIP concentrations (1, 3, 5, 25, 100, 500 and 1000 mg/L) for 10 g/L Nano-GO/M. According these CIP concentrations, the removal yields were 75%, 74%, 73%, 69%, 62%, 51% and 43%, respectively. The maximum CIP removal efficiency is 75% at 10 g/L Nano-GO/M concentration for 1 mg/L influent CIP concentration. According to this results it can be concluded that the CIP removals were high (75-74%) at low CIP concentrations (1-3 mg/L) while CIP removals were lower (51-43%) at high CIP concentrations (500-1000 mg/L). The removal efficiency is low at high CIP concentrations. Increased concentration of the CIP could occupy more active sites of Nano-GO/M, which inhibits generation of the oxidants (Yan, Yu & Ray, 2008).

A linear relationship between CIP removal efficiencies and influent CIP concentration was obtained (R=0.93) and this regression is significant (ANOVA p=0.002<α (0.05) and F=33.16).

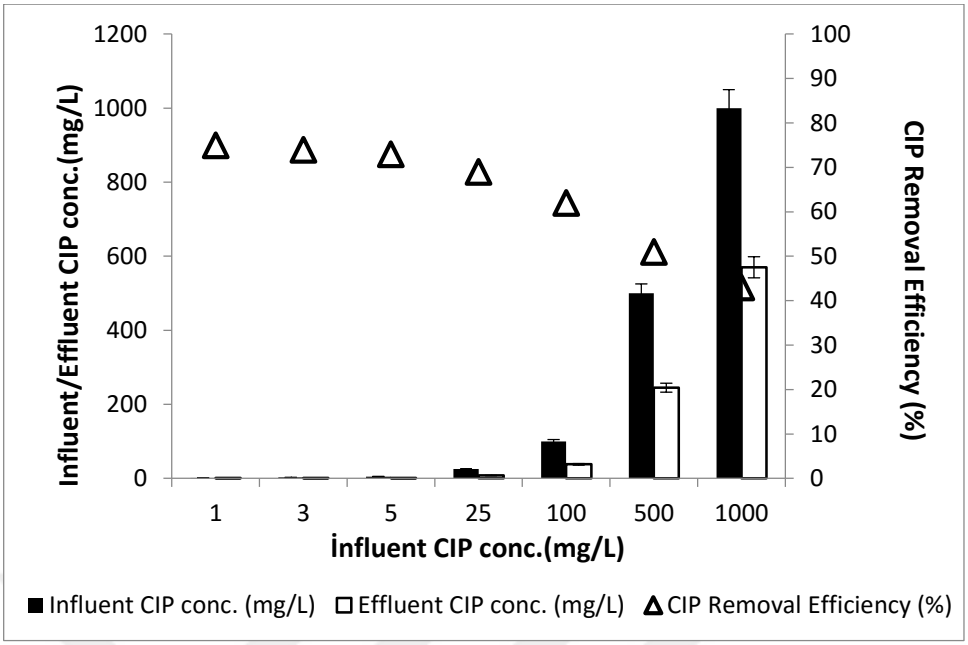


Figure 6.103 Effect of increasing CIP concentration on the yields of CIP removal efficiencies at a Nano-GO/M concentration of 10 g/L at pH=6.5, at 35°C ± 5°C and 250 min irradiation time and with a power of 80 W sunlight (<α (0.05)).

Figure 6.104 summarizes the effects of increasing Nano-GO/M concentrations (0,5, 2, 3.5, 5 and 10g/L) on CIP removal yields at a CIP concentration of 5 mg/L after 250 min irradiation time at pH=6.5 and at 35°C ± 5°C and with a power of 80 W sunlight.

As the concentration of Nano-GO/M was increased from 0.5 g/L to 2 g/L and to 3.5 g/L, the CIP removal efficiency increased from 47% to 78% and to 79% for initial CIP concentration of 5 mg/L (Figure 6.104). Further increase in concentration of Nano-GO/M from 3.5 g/L to 5 g/L and to 10 g/L decreased the CIP removal yield slightly from 79% to 77% and to 75%, respectively, at the same operational conditions. The optimum Nano-GO/M concentration was chosen as 2 g/L in order to reduce the operational cost of photocatalytic treatment process.

A linear relationship between maximum CIP removal efficiencies and Nano-GO/M composite was not obtained (R=0.62) and this regression is not significant (ANOVA p=0.07>α (0.05) and F=0.68).

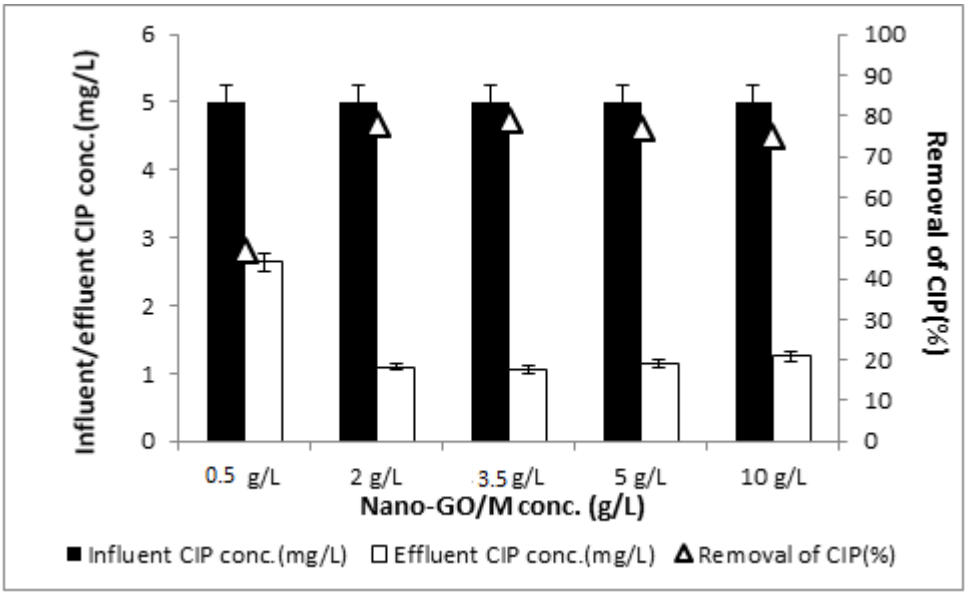


Figure 6.104 Effect of increasing concentration of Nano-GO/M (0.5, 2, 3.5, 5 and 10 g/L) on the yields of CIP removal for constant CIP concentration (5 mg/L) at pH=6.5, at 35°C ±5°C and 250 min irradiation time and with a power of 80 W sunlight (<α (0.05)).

The effect of Nano-GO/M concentration on the degradation efficiency of CIP was investigated over the concentration range from 0.5 to 10 g/L. A significant increase is observed in the efficiency of degradation of CIP within the range of Nano-GO/M concentration from 0.5 to 3.5 g/L. The number of available adsorption and Nano-GO/M sites on the Nano-GO/M surface increases with increasing in Nano-GO/M concentration, resulting in the observed enhancement in degradation efficiency (Zhe-Qi et al., 2015). However, a further increase in Nano-GO/M (from 3.5 to 10 g/L) concentration also reduces the specific activity of the catalyst because of agglomeration of catalyst particles and light scattering and screening effect, thus leading to the decreased photocatalytic degradation efficiency from 79% to 75% for 5 mg/L initial CIP concentration. Therefore, all experiments were carried out with 2 g/L Nano-GO/M to avoid the excessive usage of the catalyst.

There are only a few studies about the removal of CIP under sunlight. One of them reported by Gad-Allah, Mohamed & Badawy (2011). They researched CIP photocatalytic degradation using $TiO_2$ ($TiO_2$ concentrations were varying between 0 to 1500 mg/L) under simulated sunlight. Results showed that more catalyst concentration reduces the constant rate due to limitations of light transmittance. Another study

remarked the effect of $TiO_2$ catalyst concentration on the photocatalytic degradation efficiency of methylene blue (MB) ranging from 0.05 to 0.30 g/L. Degree of photodegradation of MB within the range of catalyst concentration from 0.05 to 0.25 g/L was increased. Further increase in catalyst concentration decreased the photodegradation efficiency (Zhe-Qi et al., 2015). Last literature surveys showed that our results are well fitted with the previous studies done by authors.

The application of graphene/metal oxide nanocomposites as photocatalysts and for water purification owing to its exceptional properties exhibited by the composites such as higher adsorptivity, conductivity, tunable optical behavior, stability and longevity (Upadhyay, Soin & Roy, 2013). Graphene derivatives provide plenty of reactive sites as well as efficiently accelerate the electrons transfer process that from the inside of photocatalyst particles to reactive sites to suppress the recombination of photo-induced electron–hole pairs (Jia, Wang, Huang, Xu & Yu, 2011; Zhang, Li, Cui & Lin, 2010). Also, the formation of π–π stacking between aromatic rings of graphene and organic pollutants also facilitates the adsorption of pollutants on the photocatalyst thereby enhancing the quenching of pollutants (Eunwoo, Jin-Yong, Haeyoung & Jyongsik, 2012). Under UV irradiation, the Nano-GO/M nanoparticles generate an excitation of electrons in valence band into the conduction band (electron–hole separation). The generated electron (hole) transfer to the adsorbed CIP on the Nano-GO/M surface has always been considered as the first step of the photocatalytic action of nanoparticles (Wang, Von, Volman &Neckers, 1995). The photodegradation of CIP probably involves (Sponza & Oztekin, 2014)**:**

• adsorption of efficient photons by Nano-GO/M composite
• oxygen adsorption followed by generation of superoxide radicals,
• generation of [H] atoms through photoelectrons,
• formation of hydroxyl radicals (OH●) from transient hydrogen peroxide ($H_2O_2$) and
• oxidation of organic molecule via successive attack of OH● radicals.

*6.4.1.2 Effects of Irradiation Time on the Treatment of CIP under Sunlight*

In order to determine the optimum irradiation time for maximum CIP removal yields, increasing irradiation (30 min, 120 min, 250 min, 350 min and 24h) times were used. As aforementioned in the upper section, the optimum Nano-GO/M composite concentration was found as 2 g/L. Therefore, the effects of irradiation times of sunlight on the removal of CIP studied under same conditions (for constant CIP concentration 5 mg/L) at five different sunlight irradiation times (30 min, 120 min, 250 min, 350 min and 24h), at a pH of 6.5 and at constant 2 g/L Nano-GO/M composite concentration with a power of 80 W sunlight).

As the irradiation time was increased from 30 min to 120 min, to 250 min and to 350 min the CIP removals increased from 53% to 73% to 78% and to 79% for initial CIP concentration of 5 mg/L (Figure 6.105). Further increase in irradiation time from 350 min to 24 h did not affect the CIP removal yield significantly. CIP removal efficiency was increased only 2% (from 79% to 81%). The optimum sunlight irradiation time can be considered as 250 min for the maximum removal efficiency of CIP (78%- for 5 mg/L CIP) to be cost-effective. Zhe-Qi et al. (2015), showed that methylene blue (MB) was degraded as a function of time at a $TiO_2$ concentration of 0.25 g/L. The efficiency of photo-degradation of MB (initial concentration 0.0535 mmol/L) reached 58% after 120 min and then decreased with time. They also reported that after 120 min irradiation time the degradation efficiency did not show a significant increase compared to our study.

A linear relationship between maximum CIP removal efficiencies and irradiation times was not obtained (R=0.50) and this regression is not significant (ANOVA $p=0.06>\alpha$ (0.05) and F=0.99).

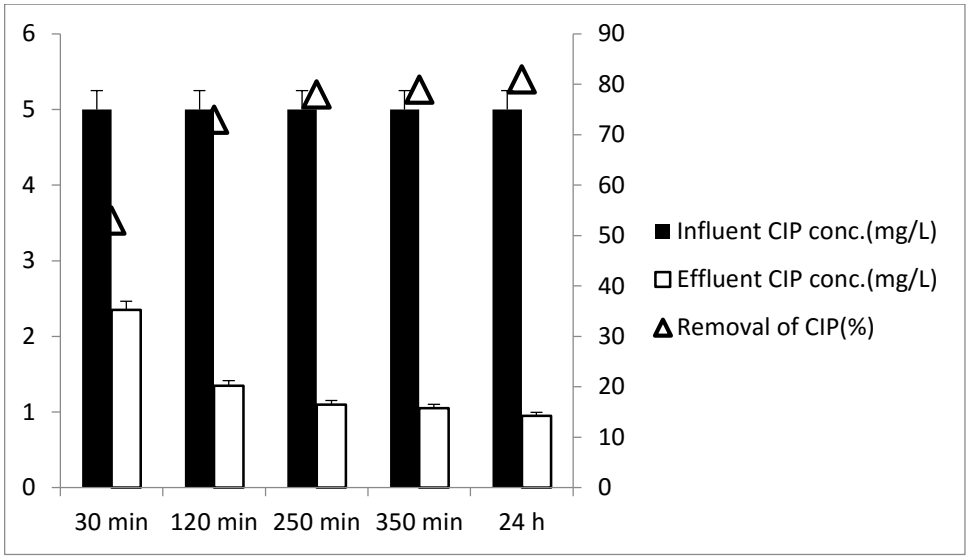


Figure 6.105 Effect of irradiation time on the yields of constant CIP concentration (5 mg/L), at a constant Nano-GO/M concentration (2g/L), at a pH of 6.5 and at 35°C ± 5°C and at increasing irradiation time and with a power of 80 W sunlight (<α (0.05)).

### *6.4.1.3 Effect of Increasing CIP Concentrations on the CIP Treatment Yields under Sunlight*

In this step, the effects of increasing CIP concentrations (1 mg/L, 3 mg/L, 5 mg/L, 25 mg/L, 100 mg/L, 500 mg/L, 1000 mg/L) on the CIP removals were studied at a Nano-GO/M concentration of 2 g/L, after 250 min irradiation time, at pH= 6.5 and at a temperature of 35°C ± 5°C with a power of 80 W sunlight (Figure 6.106). Results showed that increasing in the CIP concentration reduced the removal efficiency of CIP. For 1 mg/L initial CIP concentration the maximum CIP removal efficiency was found as 80% while the removal efficiency of 1000 mg/L CIP was found as 47%. This increase in the CIP concentrations after sunlight irradiation results in decrease in the removal efficiencies of CIP. This can be a result of blocking of the photocatalytically active sites on the Nano-GO/M and reducing the interaction of photons with these sites as reported by Lin & Wu (2014). Besides, the light absorbed by Nano-GO/M is more than that at higher concentration of CIP, which can reduce the photocatalytic degradation efficiency to a certain extent (Hassani, Khataee & Karaca, 2015).

As the influent CIP concentration increased the CIP removal yields decreased. A linear relationship between CIP removal efficiencies and influent CIP concentration

was obtained (R=0.90) and this regression is significant (ANOVA p=0.005<α (0.05) and F=21.58).

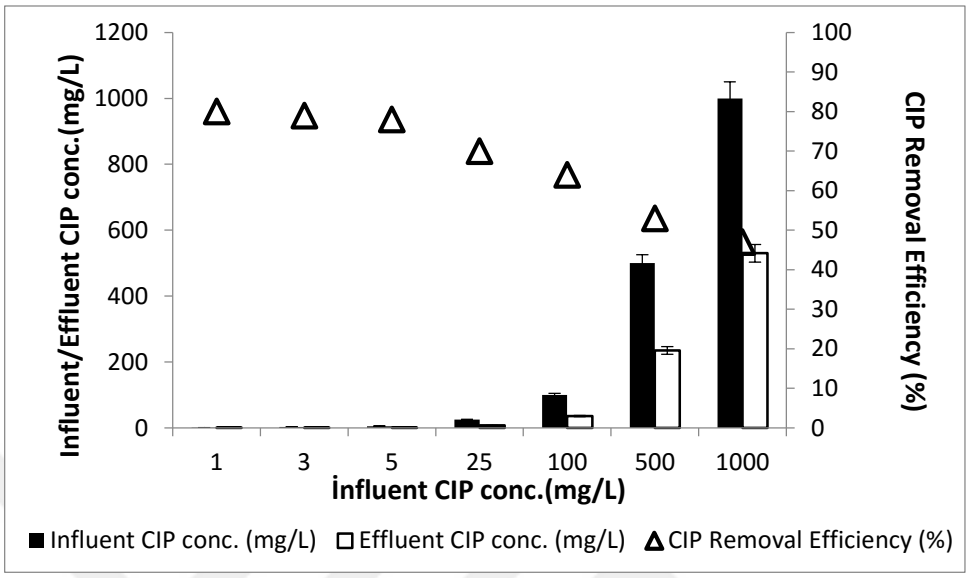


Figure 6.106 Effect of increasing CIP concentration on the yields of CIP removal efficiencies at a Nano-GO/M concentration of 2 g/L at pH=6.5, at 35°C ± 5°C and 250 min irradiation time and with a power of 80 W sunlight (<α (0.05)).

### *6.4.1.4 Effects of pH on the of Removal CIP throughout Photodegradation under Sunlight*

The effects of pH on the on the increasing CIP concentrations (1, 3, 5, 25, 100, 500 and 1000 mg/L) were studied under acidic, neutral and alkaline pHs (4, 6.5 and 10) at an irradiation time of 250 min, at a Nano-GO/M concentration of 2 g/L and at 35°C ± 5°C. Table 6.20 represents the effects of different pHs on the removal efficiency of CIP. Photocatalytic removal efficiency of CIP on nano-GO-M was relatively high at pH 6.5.

Table 6.20 Shows the photocatalytic removal efficiencies of increasing CIP at acidic, neutral and alkaline pHs (4, 6.5 and 10) at 35°C ± 5°C and at 2 g/L constant Nano-GO/M concentration at 250 min under 80W sunlight.

| **CIP concentrations (mg/L)** | **1** | **3** | **5** | **25** | **100** | **500** | **1000** |
|---|---|---|---|---|---|---|---|
| **Removal efficiency (%) at pH= 4** | 69 | 68 | 67 | 60 | 51 | 42 | 33 |
| **Removal efficiency (%) at pH= 6.5** | 80 | 79 | 78 | 70 | 64 | 53 | 47 |
| **Removal efficiency (%) at pH= 10** | 50 | 49 | 48 | 40 | 33 | 26 | 20 |

In this study, the maximum removal efficiency was found as 80% at pH=6.5 at 1 mg/L CIP concentration and at 2 g/L Nano-GO/M concentration. As the pH values decreased from 6.5 to 4 the CIP removal yields decreased to 69% for 1mg/L CIP concentration and constant Nano-GO/M concentration (2 g/L). Under alkaline conditions photodegradation yields decrease to 50%. As the CIP concentrations were increased from 1 to 1000 mg/L the removal yields decreased significantly to 33%, 47% and 20% at pH 4, 6.5 and 10, respectively.

The photooxidation of CIP does not depend only on Nano-GO/M concentration but also on pH value of CIP solution, since it determines the surface charge properties of the photocatalyst and therefore the adsorption behavior of the organic substrate. Therefore, the influence of pH on the degradation of CIP in aqueous suspensions of Nano-GO/M was studied at pH ranging from 4 to 10. The removal efficiency of CIP reached the maximum at pH 6.5, which is the natural pH of CIP solution. CIP has two proton-binding sites, carboxyl and piperazinyl group (Rakshit et al., 2013). CIP has positively charged (cationic; pH=3), negatively charged (anionic; pH=7.5), and/or zwitterionic (pH=10) species at pHs due to different pKas of 6.1 and 8.7, respectively (Gu & Karthikeyan, 2005). At pH < 6.1, CIP molecules mainly exist as cations ($CIP^+$) because of the protonation of the amine group in the piperazine moiety (Wang et al., 2010). At pH > 8.7, CIP molecules exist as anions ($CIP^-$) due to the loss of a proton from the carboxylic group (Jalil, Baschini & Sapag, 2015). In the pH range 6.1–8.7, the pH values are higher than p*K*a1 of the carboxylic group, thus deprotonating the carboxylic group to the negatively charged carboxylate (Jalil, Baschini & Sapag, 2015). However, the amine group stays protonated and positively charged as this pH range is still lower than p*K*a2 of the amine group (Drakopoulos & Ioannou, 1997).

Accordingly, in the above mentioned pH range, zwitterionic species of CIP molecules dominate in the aqueous solution. This behavior can be explained by the relationship between the surface charge of Nano-GO/M and the CIP total charge and by the presence of the cationic form (CIP) that favors a strong removal on the negative surface of the Nano-GO/M. On the other hand, both Nano-GO/M and CIP were negatively charged in basic conditions, leading to electrostatic repulsion between them and the lower photodegradation efficiency of CIP. In the case of pH 6.5 (the natural pH of CIP), photocatalytic removal efficiency was the highest and the surface of Nano-GO/M was still in the positive form and the CIP was in its neutral form (Jalil, Baschini & Sapag, 2015).

Gad-Allah, Mohamed & Badawy (2011), researched the effect of pH on CIP photocatalytic degradation using $TiO_2$ ($TiO_2$ concentration was 1000 mg/L) under simulated sunlight. They researched the degradation of 75 mg/L CIP at different pH values between 3.0 and 9. Results show that the photodegradation efficiency was giving the best results at neutral pH of CIP solution. These results are similar to our study.

Figure 6.107 summarizes the photocatalytic removal yields versus pH levels and CIP concentrations. Consequently, the maximum CIP (initial CIP concentration was 1 mg/L) photocatalytic removal yield (80%) was obtained at pH 6.5, but at alkaline and acidic pHs lowest CIP photocatalytic removal yields (69% and 50%, respectively) was obtained.

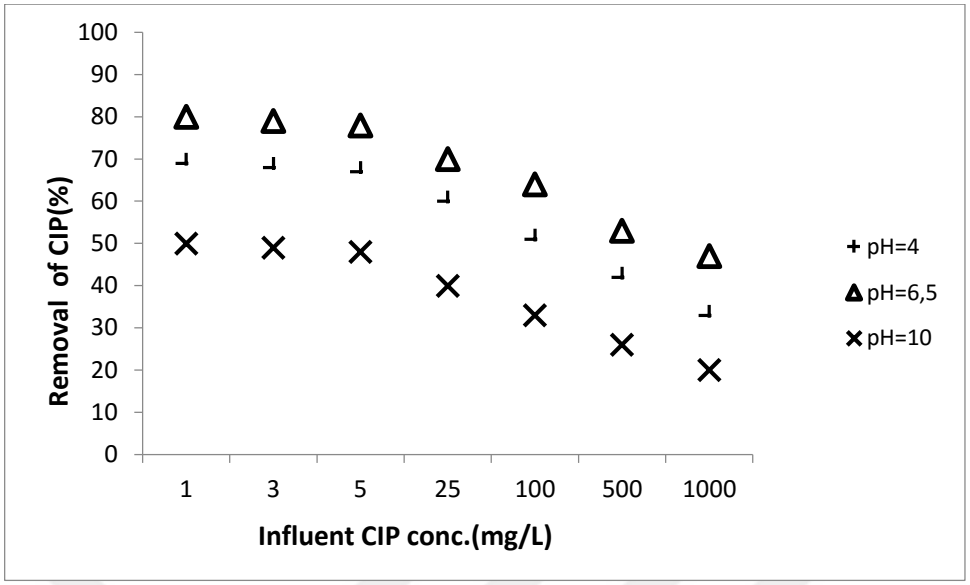


Figure 6.107 Effect of different pHs (4, 6.5 and 10) on the yield of CIP photocatalytic removal efficiency at a Nano-GO/M concentration of 2g/L, at 35°C ± 5°C and 250 min irradiation time and with a power of 80 W sunlight (<α (0.05)).

Table 6.21 summarizes shortly the effects of different pHs on the photocatalytic removal efficiency of CIP (for 1 mg/L initial CIP concentration) at 35°C ± 5°C. Photocatalytic removal of CIP on Nano-GO/M was relatively high at pH 6.5.

Table 6.21 Shows the maximum photocatalytic removal efficiencies of CIP (1mg/L) at acidic, neutral and alkaline pHs (4, 6.5 and 10) at 35°C ± 5°C and at 2 g/L constant Nano-GO/M concentration at 350 min under 80W sunlight.

| pH | Removal efficiencies (%) |
|---|---|
| 4 | 69 |
| 6.5 | 80 |
| 10 | 50 |

A linear relationship between pH and maximum CIP photocatalytic removal efficiencies (for 1 mg/L initial CIP concentration) was not obtained (R=0.66) and this regression is not significant (ANOVA p=0.3>α (0.05) and F=0.79).

As the pH increases from 4.0 to 6.5 the correlation between CIP and positively charged Nano-GO/M became more feasible. Above pH 6.5, both CIP and Nano-GO/M

became increasingly negatively charged with increasing pH, resulting in decreased photocatalytic removal efficiency (Rakshit et al., 2013).

### *6.4.2 OFL Treatment under Sunlight*

#### *6.4.2.1 Effects of Concentration of Nano-GO/M Composite on the Treatment of OFL under Sunlight*

Effects of 0.5 g/L, 2 g/L, 3.5 g/L, 5 g/L and 10 g/L Nano-GO/M composite concentrations on the removals of OFL studied with constant sunlight time (350 min was chosen due to preliminary studies results) at original pH of OFL solution (pH=6.5) under sunlight irradiation with a power of 80 W at outdoor temperature (35°C ± 5°C). The results were given in Figure 6.108 for 0.5 g/L Nano-GO/M concentration at increasing OFL concentrations (1, 3, 5, 25, 100, 500 and 1000 mg/L). OFL removal efficiencies were obtained as 53%, 52%, 51%, 44%, 37%, 31% and 22% for 1, 3, 5, 25, 100, 500 and 1000 mg/L OFL concentrations, respectively. According to these results it can be concluded that the OFL removal efficiencies were high (53-52%) at low OFL concentrations (1-3 mg/L). Increased concentration of the OFL could occupy more active sites of Nano-GO/M, which inhibits the generation of the oxidants (Yan, Yu & Ray, 2008).

A linear relationship between OFL removal efficiencies and influent OFL concentration was obtained (R=0.94) and this regression is significant (ANOVA $p=0.004<\alpha$ (0.05) and F=24.74).

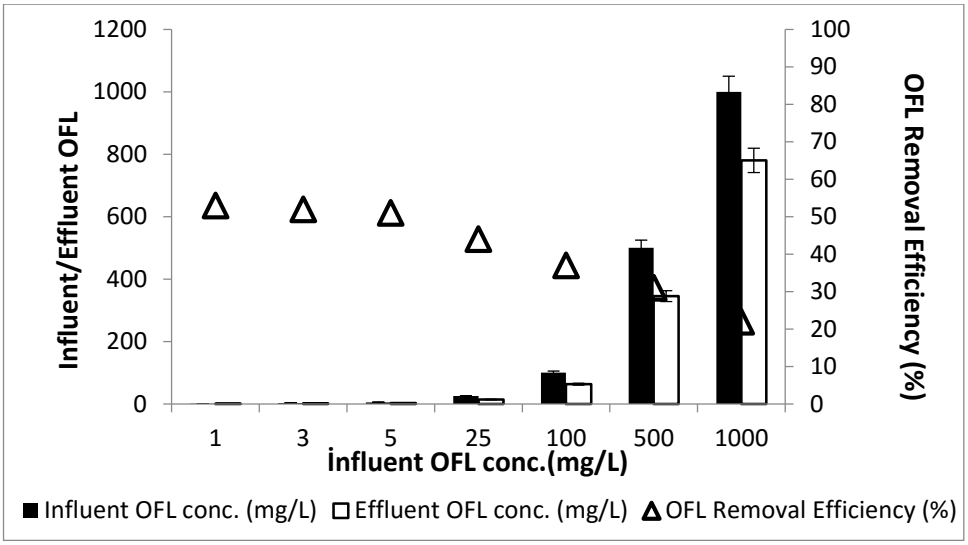


Figure 6.108 Effect of increasing OFL concentration on the yields of OFL removal efficiencies at a Nano-GO/M concentration of 0.5 g/L at pH=6.5, at 35°C ± 5°C and 350 min irradiation time and with a power of 80 W sunlight (<α (0.05)).

Figure 6.109 shows the removal efficiencies of OFL at increasing OFL concentrations (1, 3, 5, 25, 100, 500 and 1000 mg/L). The OFL yields were found as 82%, 81%, 80%, 74%, 67%, 57% and 51% at 2 g/L Nano-GO/M, respectively**.** As the OFL concentrations were increased from 1 mg/L to 1000 mg/L, the removal efficiencies decreased from 82% to 51%, respectively. The maximum OFL removal efficiency is 82% at 2 g/L Nano-GO/M concentration at 1 mg/L influent OFL concentration. According to this results it can be concluded that the OFL photocatalytic treatment efficiency were high (82-81%) at low OFL concentrations (1-3 mg/L). At highest OFL concentration (1000 mg/L) the photocatalytic treatment efficiency was obtained as 51% at 2g/L Nano-GO/M concentration. The reason of this may be explained by the interaction of only some parts of OFL with limited active sites on the Nano-GO/M surface, thereby causing lower photocatalytic treatment efficiency of OFL at higher initial OFL concentration.

A linear relationship between OFL removal efficiencies and influent OFL concentration was obtained (R=0.92) and this regression is significant (ANOVA p=0.004<α (0.05) and F=26.47).

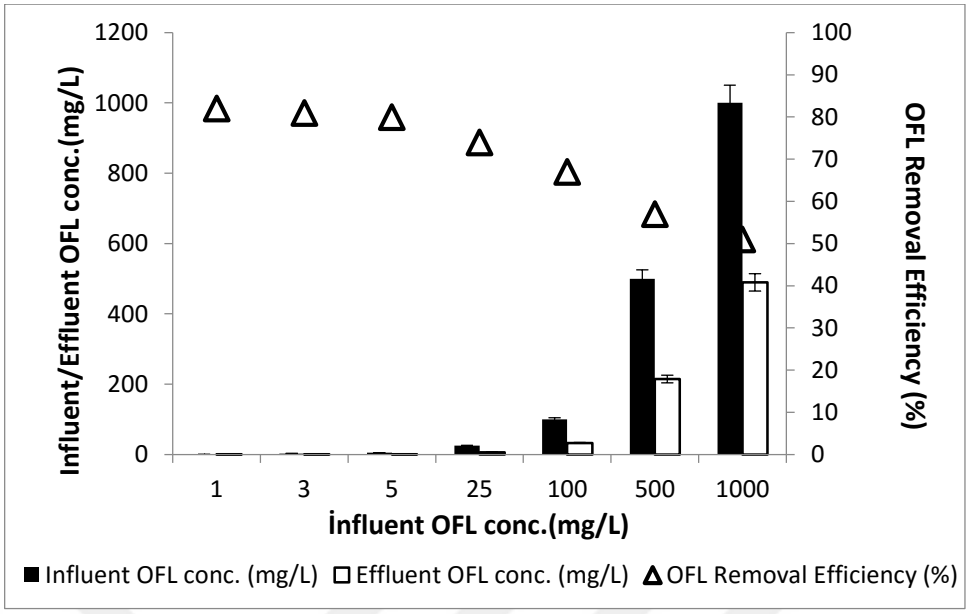


Figure 6.109 Effect of increasing OFL concentration on the yields of OFL removal efficiencies at a Nano-GO/M concentration of 2 g/L at pH=6.5, at 35°C ± 5°C and 350 min irradiation time and with a power of 80 W sunlight (<α (0.05)).

Figure 6.110 shows the removal efficiencies of OFL at increasing OFL concentrations (1, 3, 5, 25, 100, 500 and 1000 mg/L) for 3.5 g/L Nano-GO/M. According these OFL concentrations the removal yields were 83%, 82%, 81%, 76%, 68%, 58% and 53%, respectively. The maximum OFL removal efficiency is 83% at 3.5 g/L Nano-GO/M concentration for 1 mg/L influent OFL concentration. According to these results it can be concluded that the OFL removals were high (83-82%) at low OFL concentrations (1-3 mg/L) while OFL removals were lower (58-53%) at high OFL concentrations (500-1000 mg/L). The removal efficiency is low at high OFL concentrations. In other words, the Nano-GO/M remove small amount of OFL at high OFL concentrations as reported by Hong et al. (2009).

A linear relationship between OFL removal efficiencies and influent OFL concentration was obtained (R=0.91) and this regression is significant (ANOVA p=0.004<α (0.05) and F=24.78).

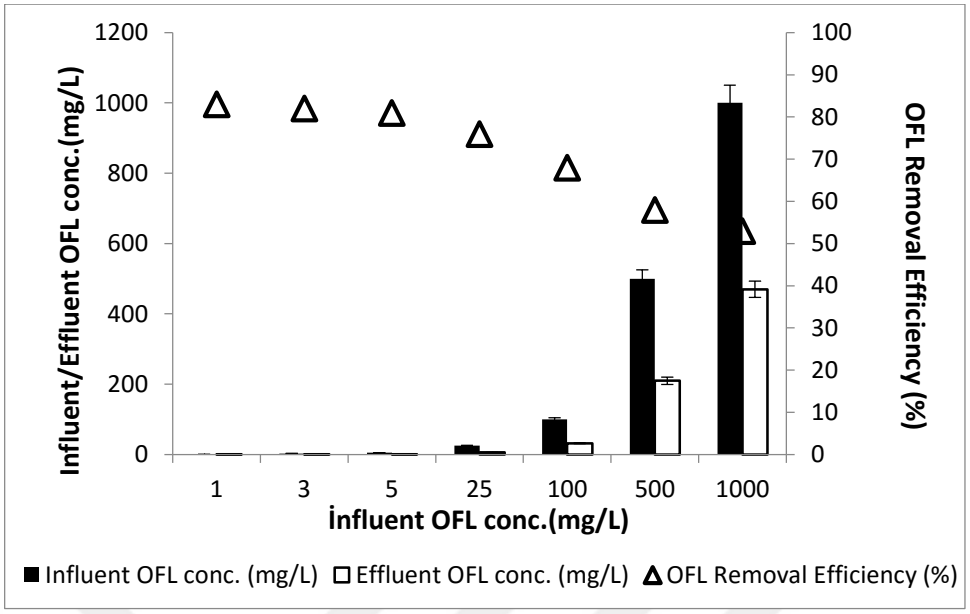


Figure 6.110 Effect of increasing OFL concentration on the yields of OFL removal efficiencies at a Nano-GO/M concentration of 3,5 g/L at pH=6.5, at 35°C ± 5°C and 350 min irradiation time and with a power of 80 W sunlight (<α (0.05)).

Figure 6.111 shows the removal efficiencies of OFL at increasing OFL concentrations (1, 3, 5, 25, 100, 500 and 1000 mg/L) for 5 g/L Nano-GO/M. According these OFL concentrations the removal yields were 78%, 77%, 76%, 72%, 66%, 54% and 48%, respectively. The maximum OFL removal efficiency is 78% at 5 g/L Nano-GO/M concentration for 1 mg/L influent OFL concentration. According to these results it can be concluded that the OFL removals were high (78-77%) at low OFL concentrations (1-3 mg/L) while OFL removals were lower (54-48%) at high OFL concentrations (500-1000 mg/L). The removal efficiency is low at high OFL concentrations. Increased concentration of the OFL could occupy more active sites of Nano-GO/M, which inhibits generation of the oxidants (Yan, Yu & Ray, 2008).

A linear relationship between OFL removal efficiencies and influent OFL concentration was obtained (R=0.94) and this regression is significant (ANOVA p=0.001<α (0.05) and F=39.16).

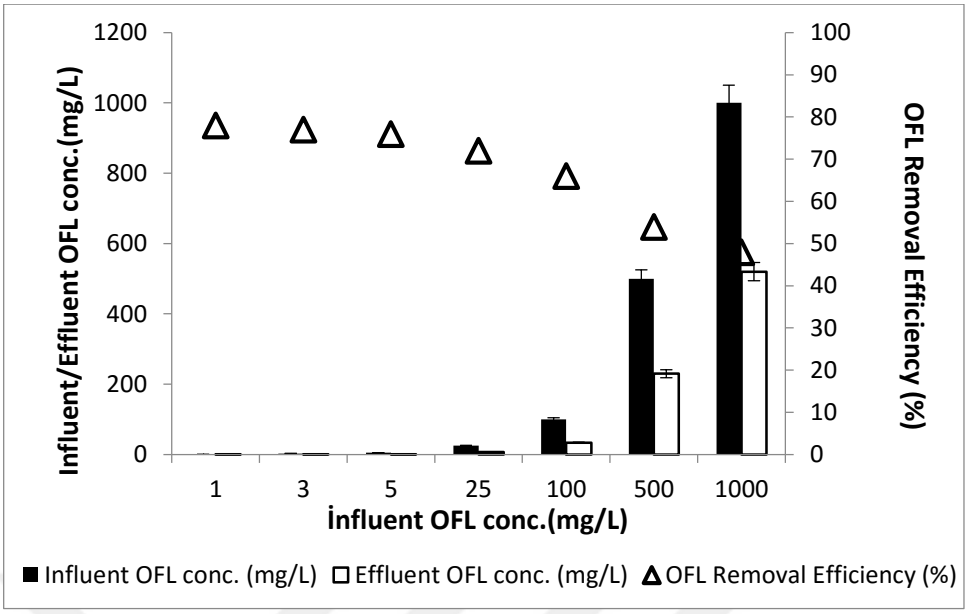


Figure 6.111 Effect of increasing OFL concentration on the yields of OFL removal efficiencies at a Nano-GO/M concentration of 5 g/L at pH=6.5, at 35°C ± 5°C and 350 min irradiation time and with a power of 80 W sunlight (<α (0.05)).

Figure 6.112 shows the removal efficiencies of OFL at increasing OFL concentrations (1, 3, 5, 25, 100, 500 and 1000 mg/L) for 10 g/L Nano-GO/M. According these OFL concentrations the removal yields were 73%, 72%, 71%, 66%, 59%, 50% and 40%, respectively. The maximum OFL removal efficiency is 73% at 10 g/L Nano-GO/M concentration for 1 mg/L influent OFL concentration. According to these results it can be concluded that the OFL removals were high (73-72%) at low OFL concentrations (1-3 mg/L) while OFL removals were lower (50-40%) at high OFL concentrations (500-1000 mg/L). The removal efficiency is low at high OFL concentrations. Increased concentration of the OFL could occupy more active sites of Nano-GO/M, which inhibits generation of the oxidants (Yan, Yu & Ray, 2008).

A linear relationship between OFL removal efficiencies and influent OFL concentration was obtained (R=0.95) and this regression is significant (ANOVA p=0.001<α (0.05) and F=43.17).

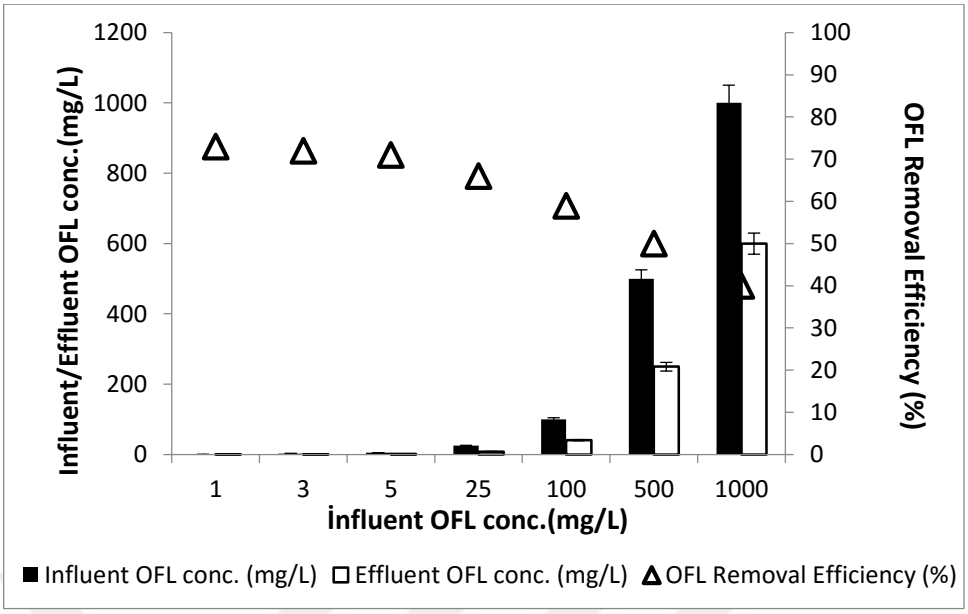


Figure 6.112 Effect of increasing OFL concentration on the yields of OFL removal efficiencies at a Nano-GO/M concentration of 10 g/L at pH=6.5, at 35°C ± 5°C and 350 min irradiation time and with a power of 80 W sunlight (<α (0.05)).

Figure 6.113 summarizes the effects of increasing Nano-GO/M concentrations (0,5, 2, 3.5, 5 and 10g/L) on OFL removal yields at a OFL concentration of 5 mg/L after 350 min irradiation time at pH=6.5 and at 35°C ± 5°C and with a power of 80 W sunlight.

As the concentration of Nano-GO/M was increased from 0.5 g/L to 2 g/L and to 3.5 g/L the OFL removal efficiency increased from 51% to 80% and to 81% for initial OFL concentration of 5 mg/L (Figure 6.113). Further increase in concentration of Nano-GO/M from 3.5 g/L to 5 g/L and to 10 g/L decreased the OFL removal yield slightly from 81% to 76% and to 71%, respectively, at the same operational conditions. The optimum Nano-GO/M concentration was chosen as 2 g/L in order to reduce the operational cost of photocatalytic treatment process.

A linear relationship between maximum OFL removal efficiencies and Nano-GO/M composite was not obtained (R=0.29) and this regression is not significant (ANOVA p=0.06>α (0.05) and F=0.268).

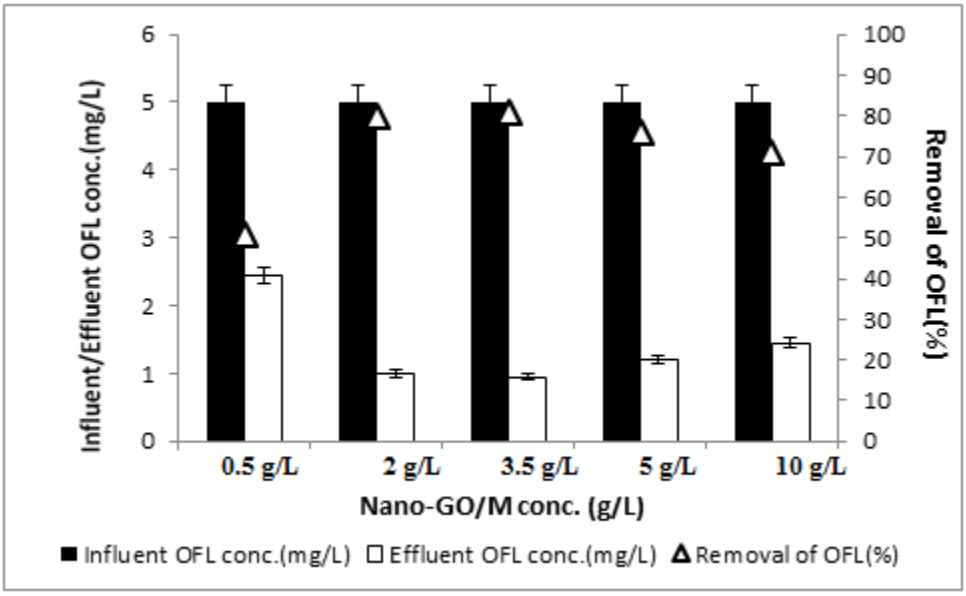


Figure 6.113Effect of increasing concentration of Nano-GO/M (0.5, 2, 3.5, 5 and 10 g/L) on the yields of OFL removal for constant OFL concentration (5 mg/L) at pH=6.5, at 35°C ± 5°C and 350 min irradiation time and with a power of 80 W sunlight (<α (0.05)).

The effect of Nano-GO/M concentration on the degradation efficiency of OFL was investigated over the concentration range from 0.5 to 10 g/L. A significant increase is observed in the efficiency of degradation of OFL within the range of Nano-GO/M concentration from 0.5 to 3.5 g/L. The number of available adsorption and Nano-GO/M sites on the Nano-GO/M surface increases with increasing in Nano-GO/M concentration, resulting in an enhancement in degradation efficiency (Zhe-Qi et al., 2015). However, a further increase in Nano-GO/M (from 3.5 to 10 g/L) concentration also reduces the specific activity of the catalyst because of agglomeration of catalyst particles and light scattering and screening effect, thus leading to the decreased photocatalytic degradation efficiency from 82% to 73% for 1 mg/L initial OFL concentration. Therefore, all experiments were carried out with 2 g/L Nano-GO/M to avoid the excessive usage of the catalyst.

### *6.4.2.2 Effects of Irradiation Time on the Treatment of OFL under Sunlight*

In order to determine the optimum irradiation time for maximum OFL removal yields, increasing irradiation (30 min, 120 min, 250 min, 350 min and 24h) times were used (Figure 6.114). As aforementioned in the upper section, the optimum Nano-

GO/M composite concentration was found as 2 g/L. Therefore, the effects of irradiation times of sunlight on the removal of OFL studied under the same operational conditions {at constant OFL concentration (5 mg/L), at five different sunlight irradiation times (30 min, 120 min, 250 min, 350 min and 24h), at a pH of 6.5 and at constant 2 g/L Nano-GO/M composite concentration with a power of 80 W sunlight)}.

As the irradiation time was increased from 30 min to 120 min to 250 min and to 350 min the OFL removals increased from 55% to 75% to 77% and to 80% for initial OFL concentration of 5 mg/L (Figure 6.114). Further increase in irradiation time from 350 min to 24 h did not affect the OFL removal yield significantly. OFL removal efficiency was increased only 3% (from 80% to 83%). The optimum sunlight irradiation time can be considered as 350 min for the maximum removal efficiency of OFL (80%- for 5 mg/L OFL).

A linear relationship between maximum OFL removal efficiencies and irradiation times was not obtained (R=0.42) and this regression is not significant (ANOVA p=0.08>α (0.05) and F=0.63).

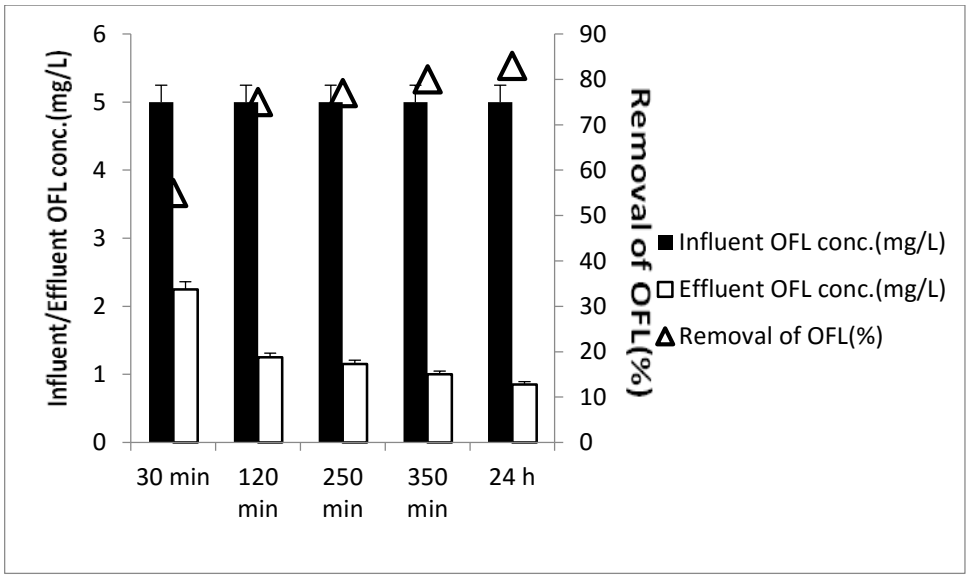


Figure 6.114 Effect of irradiation time on the yields of constant OFL concentration (5 mg/L), at a constant Nano-GO/M concentration (2g/L), at a pH of 6.5 and at 35°C ± 5°C and at increasing irradiation time and with a power of 80 W sunlight (<α (0.05)).

#### *6.4.2.3 Effect of Increasing OFL Concentrations on the OFL Treatment Yields under Sunlight*

In this step, the effects of increasing OFL concentrations (1 mg/L, 3 mg/L, 5 mg/L, 25 mg/L, 100 mg/L, 500 mg/L, 1000 mg/L) on the OFL removals were studied at a Nano-GO/M concentration of 2 g/L, after 350 min irradiation time, at pH= 6.5 and at a temperature of 35°C ± 5°C with a power of 80 W sunlight (Figure 6.115). Results showed that increasing the OFL concentration reduced the removal efficiency of OFL. For 1 mg/L initial OFL concentration the maximum OFL removal efficiency was found as 82% while the removal efficiency of 1000 mg/L OFL was found as 51%. At high OFL concentrations the OFL photodegradation yields decreased under sunlight irradiation. This can be a result of blocking of the photocatalytically active sites on the Nano-GO/M and reducing the interaction of photons with these sites as reported by Lin & Wu (2014). Besides, the light absorbed by Nano-GO/M at low concentration is more than that at higher concentration of OFL. This can reduce the photocatalytic degradation efficiency to a certain extent (Hassani, Khataee & Karaca, 2015).

A linear relationship between OFL removal efficiencies and influent OFL concentration was obtained (R=0.92) and this regression is significant (ANOVA p=0.004<α (0.05) and F=26.47).

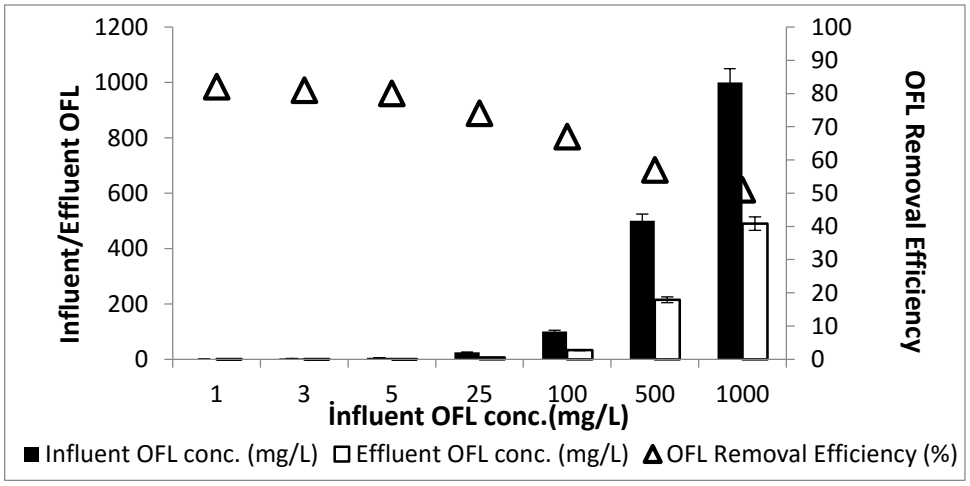


Figure 6.115 Effect of increasing OFL concentration on the yields of OFL removal efficiencies at a Nano-GO/M concentration of 2 g/L at pH=6.5, at 35°C ± 5°C and 350 min irradiation time and with a power of 80 W sunlight (<α (0.05)).

#### *6.4.2.4 Effects of pH on the of Removal OFL throughout Photodegradation under Sunlight*

The effects of pH on the on the increasing OFL concentrations (1, 3, 5, 25, 100, 500 and 1000 mg/L) were studied under acidic, neutral and alkaline pHs (4, 6.5 and 10) at an irradiation time of 350 min, at a Nano-GO/M concentration of 2 g/L and at 35°C ± 5°C. Table 6.22 represents the effects of different pHs on the removal efficiency of OFL. Photocatalytic removal efficiency of OFL on nano-GO-M was relatively high at pH 6.5.

Table 6.22 Shows the photocatalytic removal efficiencies of increasing OFL at acidic, neutral and alkaline pHs (4, 6.5 and 10) at 35°C ± 5°C and at 2 g/L constant Nano-GO/M concentration at 350 min under 80W sunlight.

| **OFL concentrations (mg/L)** | **1** | **3** | **5** | **25** | **100** | **500** | **1000** |
|---|---|---|---|---|---|---|---|
| **Removal efficiency (%) at pH= 4** | 71 | 70 | 69 | 60 | 52 | 44 | 35 |
| **Removal efficiency (%) at pH= 6.5** | 82 | 81 | 80 | 74 | 67 | 57 | 51 |
| **Removal efficiency (%) at pH= 10** | 53 | 52 | 51 | 42 | 34 | 27 | 20 |

In this study, the maximum removal efficiency was found as 82% at pH=6.5 at 1 mg/L OFL concentration and at 2 g/L Nano-GO/M concentration. As the pH values decreased from 6.5 to 4 the OFL removal yields decreased to 71% for 1mg/L OFL concentration and constant Nano-GO/M concentration (2 g/L). Under alkaline conditions photodegradation yields decrease to 53%. As the OFL concentrations were increased from 1 to 1000 mg/L the removal yields decreased significantly to 35%, 51% and 20% at pH 4, 6.5 and 10, respectively.

The photooxidation of OFL depends on pH value of OFL solution, since it determines the surface charge properties of the photocatalyst and therefore the adsorption behaviour of the organic substrate. Therefore, the influence of pH on the degradation of OFL in aqueous suspensions of Nano-GO/M was studied at pH ranging from 4 to 10. The zero charge point of ($pH_{pzc}$) Nano-GO/M is at pH ≈ 5.5 (Liu et al., 2015). Thus, the surface of Nano-GO/M was positively charged when pH < $pH_{pzc}$, and negatively charged when pH > $pH_{pzc}$. OFL is positively charged at pH values lower

than the pKa1 (6.05), negatively charged at pH values above the pKa2 (8.11), and neutral at pH values between pKa1 and pKa2 (Peres, Maniero & Guimarães, 2015). Therefore, pH 4 and 10 are not suitable for OFL adsorption on the Nano-GO/M surface, since there is electronic repulsion between the charges of the compound and the catalyst with the same sign. At pH 6.5, both the Nano-GO/M molecule and the OFL are in their neutral forms, and no repulsion occurs between them. Photocatalysis degradation efficiencies at pH 4 and 10 were lower than those obtained for the same process at pH 6.5. This was probably due to the charge-repulsion phenomenon, which is not favourable to OFL adsorption on Nano-GO/M.

The literature surveys showed that no data was found investigating the photo-removal of OFL under sunlight by Nano-GO/M, yet.

Figure 6.116 summarizes the photocatalytic removal yields versus pH levels and OFL concentrations. Consequently, the maximum OFL (initial OFL concentration was 1 mg/L) photocatalytic removal yield (82%) was obtained at pH 6.5, but at alkaline and acidic pHs lowest OFL photocatalytic removal yields (71% and 53%, respectively) was obtained.

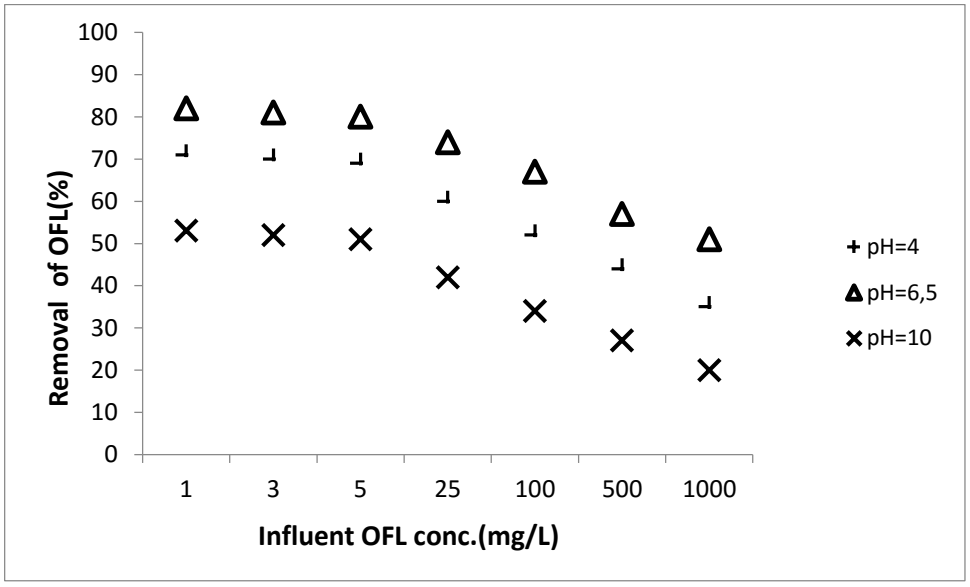


Figure 6.116 Effect of different pHs (4, 6.5 and 10) on the yield of OFL photocatalytic removal efficiency at a Nano-GO/M concentration of 2g/L, at 35°C ± 5°C and 350 min irradiation time and with a power of 80 W sunlight (<α (0.05)).

Table 6.23 summarizes shortly the effects of different pHs on the photocatalytic removal efficiency of OFL (for 1 mg/L initial OFL concentration) at 35°C ± 5°C. Photocatalytic removals of OFL on nano-GO-M was relatively high at pH 6.5.

Table 6.23 Shows the maximum photocatalytic removal efficiencies of OFL (1mg/L) at acidic, neutral and alkaline pHs (4, 6.5 and 10) at 35°C ± 5°C and at 2 g/L constant Nano-GO/M concentration at 350 min under 80W sunlight.

| pH | Removal efficiencies (%) |
|---|---|
| 4 | 71 |
| 6.5 | 82 |
| 10 | 53 |

A linear relationship between pH and maximum OFL photocatalytic removal efficiencies (for 1 mg/L initial OFL concentration) was not obtained (R=0.69) and this regression is not significant (ANOVA $p=0.3>\alpha$ (0.05) and F=0.90).

## 6.5 Recovery of Nano-GO/M

One of the most fascinating characteristics of magnetic nanoparticles, showing advantage over other nanoparticles, is their magnetism (Tang & Lo, 2013). Most water or wastewater treatment systems require a settling, filtration or centrifuge process to separate solids. However, magnetic nanoparticles can be separated and recovered with an external magnetic field due to the intrinsic magnetic characteristic of the nanoparticles, aiding in prominent nanoparticles recovery without a filtration process (Tang & Lo, 2013).

In photocatalytic processes catalyst cost is a very important issue. In this aspect, Nano-GO/M nanoparticles could be reused to solve this problem. A novel photocatalyst with ferromagnetic properties such as magnetite for recovery of Nano-GO/M and high effectiveness in the treatment of CIP and OFL was developed. Magnetic separation provides a very convenient approach for removing and recycling magnetic particles (such as magnetite) by applying external magnetic fields.

In this study, six sequential treatment steps were investigated for determination of reusability of Nano-GO/M composite. Same 0.5 g/L Nano-GO/M composite were used for sequential six treatments of CIP and OFL without change the composite under same operational conditions {(for CIP degradation-30 min, for OFL degradation-60 min) UV irradiation (300 Watt), for 1 mg/L CIP and OFL at original pH of solutions (6.5), at room temperature}. CIP and OFL removal efficiencies measured to determine the removal of CIP and OFL after six sequential with the same nano Nano-GO/M composite.

In order to reuse Nano-GO/M composite after first treatment step, Nano-GO/M composite separated magnetically and then regenerated using ethanol (adjusted to pH 2.0 with 0.1 mol/ L HCl) as eluent (Chowdhury & Balasubramanian, 2014). After using ethanol Nano-GO/M composite dried under vacuum then The Nano-GO/M reused for second treatment process to treat 1 mg/L CIP/OFL again. For every new treatment step same procedure was applied to Nano-GO/M composite. From Figure 6.117, it can be clearly seen that the utilization of Nano-GO/M composite after first, second, third, fourth, fifth and sixth times, the removal efficiency of CIP decreased from 93% to 91%, to 88%, to 84%, to 79% and to 75%. Likewise, the removal efficiencies of OFL decreased from 96% to 94%, to 91%, to 87%, to 82 and to 78%, respectively.

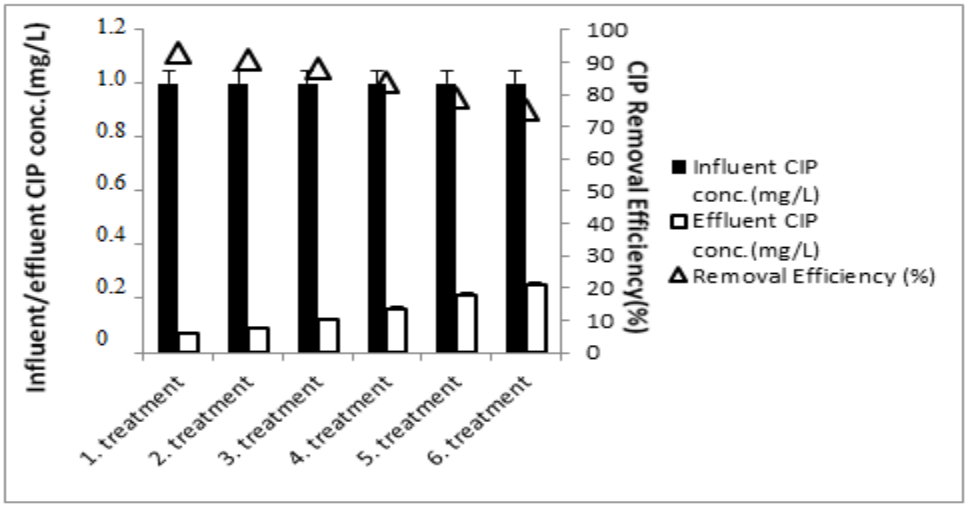


Figure 6.117 CIP measurement by recovery of Nano-GO/M composite (T: room temperature, Nano-GO/M composite concentration: 0.5 g/L, UV irradiation time: 30 min, UV power: 300 Watt, pH: 6.5 (original pH of CIP), initial concentration of CIP: 1 mg/L).

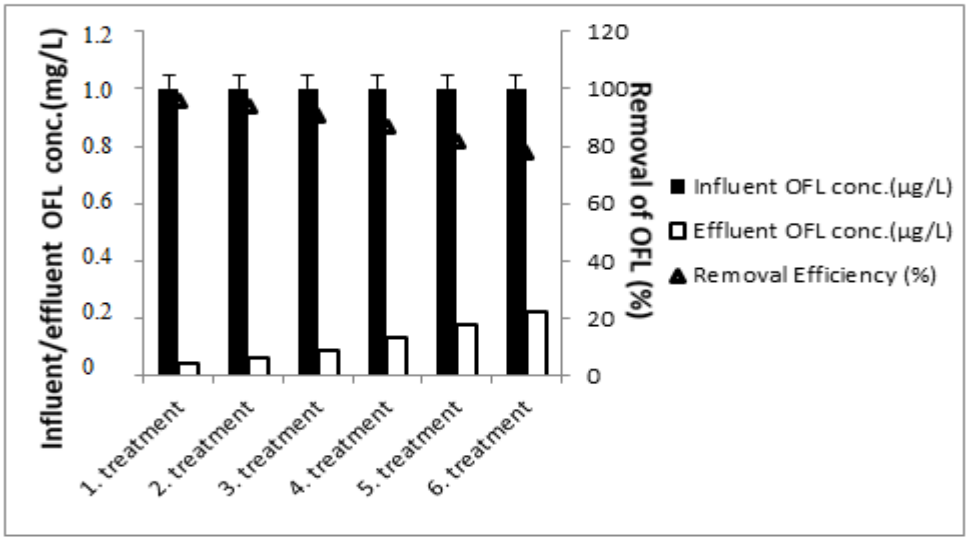


Figure 6.118 OFL measurement by recovery of Nano-GO/M composite (T: room temperature, Nano-GO/M composite concentration: 0.5 g/L, UV irradiation time: 60 min, UV power: 300 Watt, pH: 6.5 (original pH of OFL), initial concentration of OFL: 1 mg/L).

## 6.6 Cost Analysis

Cost analysis was investigated for liter treatment of CIP and OFL with Nano-GO/M composite under UV light. Considering the removal efficiencies for CIP and OFL, the optimum Nano-GO/M composite concentration was found as 0.5 g/L for the maximum removals of CIP and OFL via photocatalysis. Electricity, UV lamp (10 UV lamps) and Nano-GO/M composite was used for treatment. All the consumptions were calculated and are given in Table 6.24 and Table 6.25. Total cost of treatment for CIP and OFL were 253.683 TL (77.04 €) and 253.706 TL (77.06 €), respectively. 250 TL (75.88 €) was spent for 10 UV lamps, while the chemical cost, electricity consumption and nanocomposite cost were only 3.683 TL (1.12 €) and 3.706 TL (1.13 €) for the treatment of 1 liter of CIP and OFL, respectively.

Table 6.24 Cost analysis for photocatalytic treatment of CIP under UV light

| **Cost Analysis** | **Treatment of CIP under UV light** |
|---|---|
| **UV** | **1 UV lamp:** 25 TL<br>**10 UV lamp:** 10 * 25 = 250 TL |
| **Electricity consumption** | **30 min UV irradiation:** 0.023 TL |
| **Chemicals** | **Magnetite ($Fe_3O_4$) (1 kg):** 12.99 €<br>**Graphene (1000 g):** 151.95 € |
| **Cost analysis for treatment of 1 liter CIP:**<br>0.5 g Nano-GO/M was used for treatment of 1 liter CIP under UV light. 25 mg magnetite, 5 g graphene was used for prepare 0.5 g Nano-GO/M. | **For 0.5 g Nano-GO/M:**<br>**25 g magnetite**: 0.35 € (1.16TL)<br>**5 g:** 0.76 € (2.50 TL) |
| **Total cost for treatment of 1 liter CIP** | 250 TL + 0.023 TL + 1.16 TL + 2.50 TL =<br>**253.683 TL** (77.04 €) |
| The cost of chemicals is calculated according to market prices. Electricity costs are calculated according to the consumer price industrial units. Recent euro exchange rate was used to convert the Euro currency Turkey (1€ = 3.28 TL). | |

Table 6. 25 Cost analysis for photocatalytic treatment of OFL under UV light

| **Cost Analysis** | **Treatment of OFL under UV light** |
|---|---|
| **UV** | **1 UV lamp:** 25 TL<br>**10 UV lamp:** 10 * 25 = 250 TL |
| **Electricity consumption** | **60 min UV irradiation:** 0.046 TL |
| **Chemicals** | **Magnetite ($Fe_3O_4$) (1 kg):** 12.99 €<br>**Graphene (1000 g):** 151.95 € |
| **Cost analysis for treatment of 1 liter CIP:**<br>0.5 g Nano-GO/M was used for treatment of 1 liter OFL under UV light. 25 mg magnetite, 5 g graphene was used for prepare 0.5 g Nano-GO/M. | **For 0.5 g Nano-GO/M:**<br>**25 g magnetite**: 0.35 € (1.16TL)<br>**5 g:** 0.76 € (2.50 TL) |
| **Total cost for treatment of 1 liter OFL** | 250 TL + 0.023 TL + 1.16 TL + 2.50 TL =<br>**253.706 TL** (77.06 €) |
| The cost of chemicals is calculated according to market prices. Electricity costs are calculated according to the consumer price industrial units. Recent euro exchange rate was used to convert the Euro currency Turkey (1€ = 3.28 TL). | |

## 6.7 A Summary for Statistical ANOVA Test Results

Analysis of variance (ANOVA) is a collection of statistical models used to analyze the differences among group means and their associated procedures. In this section the relationships between CIP and OFL removals and operating parameters of three treatment methods (adsorption, UV treatment and sunlight treatment) were investigated according to regressions based on linearity and non-linearity purposes, and alpha (α) values to detect the significance of the linear regressions.

**For adsorption processes;**

Significant linear regressions between CIP removals and increasing Nano-GO/M composite concentrations, increasing contacting times, increasing CIP concentrations and increasing temperatures were observed (Table 6.26). On the other hand, linear regression between CIP removals and increasing pH levels were not observed. Regressions of increasing Nano-GO/M composite concentrations, increasing CIP concentrations are significant but increasing contacting times, increasing temperatures and increasing pH levels are not significant.

Significant linear regressions between OFL removals and increasing Nano-GO/M composite concentrations, increasing contacting times, increasing OFL concentrations and increasing temperatures were observed (Table 6.27). On the other hand, linear regression between OFL removals and increasing pH levels were not observed. Regressions of increasing CIP concentrations and increasing temperatures are significant but increasing Nano-GO/M composite concentrations, increasing contacting times, and increasing pH levels are not significant.

**For photooxidation with UV process;**

Significant linear regressions between CIP removals and increasing Nano-GO/M composite concentrations, increasing irradiation times, increasing CIP concentrations, increasing temperatures and increasing UV powers (Watt) were observed (Table 6.26.) and these regressions are significant. On the other hand, linear regression between CIP removals and increasing pH levels were not observed and this regression is not significant.

Significant linear regressions between OFL removals and increasing Nano-GO/M composite concentrations, increasing irradiation times, increasing OFL concentrations, increasing temperatures and increasing UV powers (Watt) were observed (Table 6.27) and these regressions are significant. On the other hand, linear regression between OFL removals and increasing pH levels were not observed and this regression is not significant.

**For photooxidation with sunlight treatment process;**

Significant linear regressions between CIP removals and increasing CIP concentrations were observed (Table 6.26) and this regression is significant. On the other hand, linear regression between CIP removals and increasing Nano-GO/M composite concentrations, increasing irradiation times and increasing pH levels were not observed and these regressions are not significant except irradiation times.

Significant linear regressions between OFL removals and increasing OFL concentrations were observed (Table 6.27) and this regression is significant. On the other hand, linear regression between OFL removals and increasing Nano-GO/M composite concentrations, increasing irradiation times and increasing pH levels were not observed and these regressions are significant except pH levels.

Table 6.26 Anova summary of treatment process of CIP.

| | **Adsorption Process** | | **UV process** | | **Sunlight Process** | |
|---|---|---|---|---|---|---|
| **Linear/α values** | ***Linear*** | ***α values (Significant)*** | ***Linear*** | ***α values (Significant)*** | ***Linear*** | ***α values (Significant)*** |
| **Concentration of Nano-GO/M composite** | ✓ | **X** | ✓ | ✓ | **X** | **X** |
| **Adsorption/ Irradiation Time** | ✓ | **X** | ✓ | ✓ | **X** | **X** |
| **Initial CIP concentration** | ✓ | ✓ | ✓ | ✓ | ✓ | ✓ |
| **pH** | **X** | **X** | **X** | **X** | **X** | **X** |
| **Temperature** | ✓ | **X** | ✓ | ✓ | | |
| **Watt** | | | ✓ | ✓ | | |

**✓: means significant X: means not significant**

Table 6.27 Anova summary of treatment process of OFL.

| | **Adsorption Process** | | **UV process** | | **Sunlight Process** | |
|---|---|---|---|---|---|---|
| **Linear/α values** | ***Linear*** | ***α values (Significant)*** | ***Linear*** | ***α values (Significant)*** | ***Linear*** | ***α values (Significant)*** |
| **Concentration of Nano-GO/M composite** | ✓ | **X** | ✓ | ✓ | **X** | **X** |
| **Adsorption/ Irradiation Time** | ✓ | **X** | ✓ | ✓ | **X** | **X** |
| **Initial OFL concentration** | ✓ | ✓ | ✓ | ✓ | ✓ | ✓ |
| **pH** | **X** | **X** | **X** | **X** | **X** | **X** |
| **Temperature** | ✓ | ✓ | ✓ | ✓ | | |
| **Watt** | | | ✓ | ✓ | | |

**✓: means significant X: means not significant**

# CHAPTER SEVEN
# CONCLUSION

This work aimed to study CIP and OFL treatment process based on adsorption and photocatalytic oxidation using Nano-GO/M. Treatment of CIP and OFL were studied under different operational conditions to obtain the optimum operational conditions. The maximum adsorption and photodegradation yields. Effect of concentration of Nano-GO/M composite, adsorption/irradiation time, pH of CIP and OFL, temperature affects and UV power affects were investigated and two energy sources (UV light and sunlight) were used for photooxidation to compare the removal efficiencies. Table 7.1 shows the removal efficiencies of adsorption, UV oxidation and sunlight oxidation.

Table 7.1 The comparison of removal efficiencies.

| **Treatment Processes/Micropollutant** | **Maximum Removal Efficiencies (%)** | |
|---|---|---|
| | **CIP (1mg/L)** | **OFL (1mg/L)** |
| **Adsorption** (0.5 g/L Nano-GO/M and 30 min adsorption time, pH:6.5, T:21ºC) | 30% | 35% |
| **Photocatalytic treatment under UV light** (0.5 g/L Nano-GO/M pH:6.5, T:21ºC and 300W UV power) | 93% -30 min irradiation time | 96% -60 min irradiation time |
| **Photocatalytic treatment under sun light** (2 g/L Nano-GO/M pH:6.5, T:35±5ºC and 80W sunlight power) | 80%- 250 min irradiation time | 82%- 350 min irradiation time |

According to results in Table 7.1;

Adsorption with Nano-GO/M composite is not suitable when compared with photooxidation with UV or sunlight. Removal efficiencies of CIP (30%- for initial 1 mg/L) are too low. Yields of CIP are high at original pH of CIP solutions (6.5), at room temperature for adsorption. As the initial concentrations of CIP increased from 1 mg/L to 1000 mg/L, removal efficiencies decreased gradually. Freundlich isotherm was well fitted with meaningful kinetic constants indicating the low adsorption capacity of Nano-GO/M ($K_F$ and n were calculated as 1.31 (unitless) and 1.38 (unitless), respectively. The removal efficiencies of CIP (93%-80%) and from the photocatalytic studies under UV using Nano-GO/M are higher from the sunlight studies. For maximum 93% CIP (initial 1 mg/L) removal efficiencies under photooxidation the optimum operational conditions were 0.5 g/L Nano-GO/M, 300 W UV power, at original pH of CIP solutions (6.5), at room temperature and after 30 min irradiation time. CIP was photodegraded according to first order reaction kinetic since the $k_1$ value calculated is meaningful than that calculated in the first order and second order reaction kinetics with highest $R^2$ value (1). For maximum removal efficiencies (1 mg/L initial CIP concentration) 250 min irradiation time were obtained as optimum time for photooxidation via sunlight (80W). Best results were obtained at 1 mg/L initial concentration of CIP, at original pH of CIP solutions (6.5). This decrease the cost of the chemical utilized in both photocatalytic studies (under UV light and sunlight).

For OFL adsorption process, adsorption efficiencies were also low (35%- for initial 1 mg/L). Best results obtained at original pH of OFL solutions (6.5), at room temperature. As the initial concentrations of OFL increased from 1 mg/L to 1000 mg/L, removal efficiencies decreased gradually. Among the five adsorption isotherms used in this study (Langmuir, Freundlich, Temkin, D-R and Flory-Huggins) the higher $R^2$ (0.986) value vas obtained in the D-R isotherm with meaningful kinetic constants ($K'$ and $X'_m$ were calculated as 8.84E-07($mol^2\ kJ^{-2}$), and 0.7 mg/g respectively). The removal efficiencies of OFL (96%-82%) from the photocatalytic studies under UV using Nano-GO/M are higher from the sunlight studies. For maximum 96% OFL (initial 1 mg/L) removal efficiencies under photooxidation the optimum operational conditions were 0.5 g/L Nano-GO/M, 300 W UV power, at original pH of CIP

solutions (6.5), at room temperature and after 60 min irradiation time. As results of kinetic studies it was found that the OFL was photodegraded according to zero order reaction kinetic since the $k_0$ value calculated is meaningful than first order and second order reaction kinetics with highest $R^2$ value (1). In sunlight studies, for maximum removal efficiencies (1 mg/L initial OFL concentration) 350 min irradiation time were obtained as optimum time for photooxidation via sunlight (80W). Also OFL photodegrades more slowly than OFL, undergoing defluorination (Fasani, Rampi & Albini, 1999). Best results were obtained at 1 mg/L initial concentration of OFL, at original pH of OFL solutions (6.5). This decrease the cost of the chemical utilized in both photocatalytic studies (under UV light and sunlight).

CIP metabolites namely M1 (desethyleneciprofloxacin) and M3 (oxociprofloxacin) were obtained in the photocatalytic process via UV light. Results showed that, after photocatalytic treatment from 100 mg/L CIP 83 mg/L CIP was photodegraded (Table 6.14). The CIP was photodegraded with a yield of 83%. 17 mg/L CIP was remained in the effluent and cannot be photodegraded with UV and Nano-GO/M. CIP was photodegraded to two metabolites namely M1 and M3. From 83 mg/L CIP; 20.22 mg/L M1 and 3.4 mg/L M2 were produced (Table 6.14). 20.22 mg/L M1 was degraded with a yield of 24.36% while 3.4 mg/L M3 was degraded with a yield of 4.096%. As a result, from 83 mg/L CIP; totally 23.26 mg/L metabolites were discharged. The rest of CIP (83 mg/L – 23.26 mg/L= 59.74 mg/L) was completely transformed to $CO_2$ and $H_2O$.

The OFL was photodegraded with a yield of 82%. 18.11 mg/L OFL was remained in the effluent and cannot be photodegraded with UV and Nano-GO/M. OFL was photodegraded to two metabolites namely POF and MOF. From 82 mg/L OFL; 0.8211 mg/L POF and 2.2110 MOF were produced (Table 6.19). 0.8211 mg/L POF was degraded with a yield of 1.001% while 2.2110 mg/L MOF was degraded with a yield of 2.70%. As a result, from 82 mg/L OFL; totally 3.0321 mg/L metabolites were discharged. The rest of OFL (82 mg/L – 3.0321 mg/L= 78.97 mg/L) was completely transformed to $CO_2$ and $H_2O$. Table 6.19 shows the percentage of removed or transformed products.

In this study, the recovery of Nano-GO/M after six sequential treatment steps was investigated. Although the removal efficiencies of CIP and OFL decreased from 93% to 75%, from 96% to 78%, respectively, after sixth sequential treatment 1 mg/L CIP or OFL, Nano-GO/M can be recovered and can be reused again as photocatalyst. This decrease and minimize the operating costs of the treatment process.

Cost analysis were performed throughout removal of CIP and OFL under UV irradiation. Total cost of treatment CIP and OFL was obtained as 253.683 TL (77.04 €) and 253.706 TL (77.06 €), respectively, while 250 TL (75.88 €) was spent for 10 UV lamps. Only 3.683 TL (1.12 €) and 3.706 TL (1.13 €) were spent for the treatment of 1 liter CIP and OFL, respectively. Sunlight is natural source and can be used for treatment with high Nano-GO/M composite concentrations and irradiation times.

**Recommendations for future studies**

Some of the recommendations for future studies are listed below:

- Nano-GO/M composite have been recommended to be efficient composite for the photodegradation of CIP and OFL because their removal yields for both micropollutants were high.
- The investigations also suggest that the coexistence of photocatalyst and lights exposure is necessary for photocatalytic degradation of CIP and OFL.
- Different operating parameters such as irradiation time of UV light and sunlight, pH of CIP and OFL solutions, temperature, UV power and concentration of catalyst and type of catalysts have considerable effect on degradation efficiency of CIP and OFL. These important operational parameters should be taken into consideration during photocatalytic treatment of other antibiotics.
- Optimization of the photodegradation parameters is essential from the viewpoint of efficient design and the application of photocatalytic oxidation processes to sustainable CIP and OFL treatment process.
- Reusability of nanocomposite decreases the cost of treatment; Nano-GO/M composite can be used for removal different types of pollutants and micropollutants.

## REFERENCES


Afkhami, A., Saber-Tehrani, M. & Bagheri, H. (2010). Modified maghemite nanoparticles as an efficient adsorbent for removing some cationic dyes from aqueous solution. *Desalination, 263,* 240–24.

Ai, L., Zhang, C., & Chen, Z. (2011). Removal of methylene blue from aqueous solution by a solvothermal-synthesized graphene/magnetite composite. *Journal of Hazardous Materials, 192,* 1515– 1524.

Al-Heetimi, D., Kadhum, M. & Alkhazrajy, O. (2014). Adsorption of ciprofloxacin hydrochloride from aqueous solution by ıraqi porcelinaite adsorbent. *Journal of Al-Nahrain University, 17 (1),* 41-49.

An, T., Yang, H., Song, W., Li, G., Luo, H., & Cooper, W.J. (2010). Mechanistic considerations for the advanced oxidation treatment of fluoroquinolone pharmaceutical compounds using $TiO_2$ heterogeneous catalysis. *Journal of Physical Chemistry A, 114,* 2569-2575.

Aniekeme-Abasi, I., Okon, O., Saviour, U. & Ubong, E. (2013). Kinetic and equilibrium studies of adsorption of lead (ıi) ıons from aqueous solution using coir dust (cocos nucifera l.) and ıt's modified extract resins. *The Holistic Approach to Environment, 34,* 209-222.

Appelbaum, P. C. & Hunter, P.A. (2000). The fluoroquinolone antibacterials: past, present and future perspectives. *International Journal of Antimicrobial Agents, 16,* 5–15.

Arapbour, N. & Nezamzadeh-Ejhieh, A. (2015). Modification of clinoptilolite nano-particles with iron oxide: Increased composite catalytic activity for photodegradation of cotrimaxazole in aqueous suspension. *Materials Science in Semiconductor Processing, 31,* 684-692.

Balcioglu, I. A. & Ötker, M. (2004). Pre-treatment of antibiotic formulation wastewater by $O_3$, $O_3/H_2O_2$, and $O_3$/UV processes. *Journal of Environmental Engineering Science, 28,* 325-331.

Batt, A. L., Kim, S. & Aga, D. S. (2007). Comparison of the occurrence of antibiotics in four full-scale wastewater treatment plants with varying designs and operations. *Chemosphere, 68,* 428–435.

Barjasteh-Moghaddam, M. & Habibi-Yangjeh, A. (2010). Effect of operational parameters on photodegradation of methylene Blue on ZnS nanoparticles prepared in presence of an ionic liquid as a highly efficient photocatalyst. *Journal of Iran Chemical Society, 8,* 169-175.

Belden, J. B., Maul, J. D. & Lydy, M. J. (2007). Partitioning and photodegradation of ciprofloxacin in aqueous systems in the presence of organic matter. *Chemosphere, 66(8),* 1390–1395.

Bhandari, A., Close, L. I., Kim, W., Hunter, R. P., Koch, D. E. & Surampalli, R. Y. (2008). Occurrence of ciprofloxacin, sulfamethoxazole, and azithromycin in municipal wastewater treatment plants. *Practice Periodical of Hazardous, Toxic, and Radioactive Waste Management, 12(4),* 275–281.

Bila, D. M. & Dezotti, M. (2003). Fármacos no meio ambiente. *Quimica Nova, 24,* 523-530.

Carabineiro, S., Amornsri, T., Pereira, M. & Figueiredo, J. (2011). Adsorption of ciprofloxacin on surface-modified carbon materials. *Water Research, 45,* 4583-4591.

Carmosini, N. & Lee, L. S. (2009). Ciprofloxacin sorption by dissolved organic carbon from reference and bio-waste materials. *Chemosphere, 77(6),* 813–820.

Chakrabarti, S. & Dutta, B. (2004). Photocatalytic degradation of model textile dyes in wastewater using zno as semiconductor catalyst. *Journal of Hazardous Material B, 112,* 269–278.

Chan, H. B. S., Ellis, B. L., Sharma, H.L., Frost, W., Caps, V., Shields, R.A., & et al. (2004). Carbon-encapsulated radioactive 99mTc nanoparticles. *Advanced Materials*, *16*, 144-149.

Chan, S.H.S., Wu, T.Y, Juan, J.C., & Teh, C.Y. (2011). Recent developments of metal oxide semiconductors as photocatalysts in advanced oxidation processes (AOPs) for treatment of dye waste-water. *Journal of Chemical Technology and Biotechnology*, *86*, 1130-1158.

Chatterjee, D. & Dasgupta, S. (2005). Visible light induced photocatalytic degradation of organic pollutants. *Journal of Photochemistry and Photobiology C: Photochemistry Reviews, 6,* 186–205.

Chen, H., Gao, B., & Li, H. (2015). Removal of sulfamethoxazole and ciprofloxacin from aqueous solutions by graphene oxide. *Journal of Hazardous Materials, 282,* 201-207.

Chowdhury, S. & Balasubramanian, R. (2014). Recent advances in the use of graphene-family nanoadsorbents for removal of toxic pollutants from wastewater. *Advances İn Colloid And Interface Science, 204,* 35–56.

Cornel, R.M. & Schwertmann, U. (1996). The iron oxides: structure, properties, reactions, occurrences and uses weinheim. *2. Edition New York: Wiley-VCH.*

Cong, H., He, J., Lu, Y., Yu, S. (2009). Water-Soluble Magnetic-Functionalized Reduced Graphene Oxide Sheets: In situ Synthesis and Magnetic Resonance Imaging Applications. *Small, 6,* 169-173.

Crespo-Alonso, M., Nurchi, V., Biesuz, R., Alberti, G., Spano, N., Pilo, M. & et al. (2013). Biomass against emerging pollution in wastewater: ability of cork for the removal of ofloxacin from aqueous solutions at different pH. *Journal of Environmental Chemical Engineering*, *1,* 1199–1204.

Daneshvar, N., Aber, S., Dorraji, M.S., Khataeea, R. & Rasoulifardm, H. (2007). Photocatalytic degradation of the insecticide diazinon in the presence of prepared nanocrystalline zno powders under irradiation of UV-C light. *Separation and Purification Technology, 58,* 91–98.

De Witte, B., Van, Langenhove, H., Demeestere, K., Saerens, K., De, Wispelaere, P. & Dewulf, J. (2010). Ciprofloxacin ozonation in hospital wastewater treatment plant effluent: effect of pH and $H_2O_2$. *Chemosphere, 78(9),* 1142–1147.

Dias, A.M.G.C., Hussain, A., Marcos, A.S. & Roque, A.C.A. (2011). A biotechnological perspective on the application of iron oxide magnetic colloids modified with polysaccharides. *Biotechnology Advances*, *29,* 142–155.

Drakopoulos, A. & Ioannou, P.C. (1997). Spectrofluorimetric study of the acid–base equilibria and complexation behavior of the fluoroquinolone antibiotics ofloxacin, norfloxacin, ciprofloxacin and pefloxacin in aqueous solution. *Analytica Chimica Acta, 354,* 197-204.

Dong, L., Zhu, Z., Qiu, Y., & Zhao, J. (2010). Removal of lead from aqueous solution by hydroxyapatite/magnetite composite adsorbent. *Chemical Engineering Journal, 165,* 827–834.

Dong, S., Sun, Y., Wu, J., Wu, B., Creamer, A. N. & Gao, B. (2015). Graphene oxide as filter media to remove levofloxacin and lead from aqueous solution. *Chemospehere, 150,* 759-764.

Dubinin, M.M. & Radushkevich, L.V. (1947). The equation of the characteristic curve of activated charcoal. *Proceedings of the USSR Academiy of Sciences*, *55,* 331.

Duong, H. A., Pham, N. H., Nguyen, H. T., Hoang, T. T., Pham, H. V., Pham, V.C. & et al. (2008). Occurrence, fate and antibiotic resistance of fluoroquinolone antibacterials in hospital wastewaters in Hanoi, Vietnam. *Chemosphere, 72,* 968–973.

Eba, F., Gueu, S., Mvongbote, A., Ondo, J., Yao, B., Nlo, J. & et al. (2010). Evaluation of the absorption capacity of the natural clay from bikougou (gabon) to remove MN (ii) from aqueous solution. *International Journal of Engineering Science and Technology, 2(10),* 5001-5016.

Eunwoo, L., Jin-Yong, H., Haeyoung, K., & Jyongsik, J. (2012). Synthesis of $TiO_2$ nanorod-decorated graphene sheets and their highly efficient photocatalytic activities under visible-light irradiation. *Journal of Hazardous Materials*, *219–220*, 13–18.

Fakhri, H., Mahjoub, A. R., & Khavar, A. H. C. (2016). Improvement of visible light photocatalytic activity over graphene oxide/$CuInS_2$/ZnO nanocomposite synthesized by hydrothermal method. *Materials Science in Semiconductor Processing, 41*, 38–44.

Farzadkia, M., Esrafili, A., Ali, M., Baghapour, Shahamat, Y. & Okhovat, N. (2014). Degradation of metronidazole in aqueous solution by nano-ZnO/UV photocatalytic process. *Desalination and Water Treatment, 52*, 25-27.

Fasani, E., Rampi, M., & Albini, A. (1999). Photochemistry of some fluoroquinolones: effect of pH and chloride ion. *Journal of Chemical Society Perkin Transaction, 29,* 1901–1907.

Fink, L., Dror, I. & Berkowitz, B. (2012). Enrofloxacin oxidative degradation facilities by metal oxide nanoparticles. *Chemosphere, 86,* 144-149.

Frade, V. M. F., Dias, M., Teixeira, A. C. S. C., & Palma, M. S. A. (2014). Environmental contamination by fluoroquinolones. *Brazilian Journal of Pharmaceutical Sciences, 50*, 41-54.

Freundlich & H.M.F U. (1906). Ber die adsorption in lo¨sungen. *Zeitschrift für Physikalische Chemie, 57*, 385-470.

Fu, D., Han, H., Chang, Y., & Dong, J. (2012). The synthesis and properties of ZnO–graphene nano hybrid for photodegradation of organic pollutant in water. *Materials Chemistry and Physics,* 132, 673–681.

Gad-Allah, Ali, M. & Badawy, M. (2011). Photocatalytic oxidation of ciprofloxacin under simulated sunlight. *Journal of Hazardous Materials, 186,* 751–755.

Gao, Y., Zhang, L., Huang, H., Hu, J., Shah, S. & Su, X. (2012). Adsorption and removal of tetracycline antibiotics from aqueous solution by graphene oxide. *Journal of Colloid Interface Science, 1,* 540–546.

Ge, L., Chen, J., Wei, X., Zhang, S., Qiao, X., Cai, X. & et al. (2010). Aquatic photochemistry of fluoroquinolone antibiotics: kinetics, pathways, and multivariate effects of main water constituents. *Environmental Science Technology, 44,* 2400-2405.

Golet, E. M., Alder, A. C. & Giger, W. (2002). Environmental exposure and risk assessment of fluoroquinolones antibacterial agents in wastewater and river water of the Glatt Valley Watershed, Switzerland. *Environmental Science Technology, 36,* 3645-3651.

Goyne, K. W., Chorover, J., Kubicki, J. D., Zimmerman, A. R. & Brantley, S. (2005). Sorption of the antibiotic ofloxacin to mesoporous and nonporous alumina and silica. *Journal of Colloid and Interface Science, 283,* 160–170.

Gu, C., & Karthikeyan, K. (2005). Sorption of the antimicrobial ciprofloxacin to aluminum and iron hydrous oxides. *Environmental Science Technology, 39 (23),* 9166–9173.

Guinea, E., Brillas, E., Centellas, F., Cañizares, P., Rodrigo, M. A. & Sáez, C. (2009). Oxidation of enrofloxacin with condutive-diamond electrochemical oxidation, ozonation and fenton oxidation. *A comparison. Water Research, 43,* 2131-2138.

Guney, G. & Sponza, D.T. (2016). Comparison of biological and advanced treatment processes for ciprofloxacin removal in a raw hospital wastewater. *Environmental Technology,* DOI: 10.1080/09593330.2016.1179348.

Han, X., Wang, W. & Ma, X. (2011). Adsorption characteristics of methylene blue onto low cost biomass material lotus leaf. *Chemical Engineering Journal, 171,* 1–8.

Hapeshi, E., Achilleos, A., Vasquez, M. I., Michael, C., Xekoukoulotakis, N. P., Mantzavinos, D. & et al. (2010). Drugs degrading photocatalytically: kinetics and mechanisms of ofloxacin and atenolol removal on titania suspensions. *Water Research, 44,* 1737–1746.

Hapeshi, E., Fotiou, I., & Fatta-Kassinos, D. (2013). Sonophotocatalytic treatment of ofloxacin in secondary treated effluent and elucidation of its transformation products. *Chemical Engineering Journal, 2,* 96–105.

Hashimoto, K., Irıe, H., & Fujıshıma, A. (2005). $TiO_2$ Photocatalysis: A historical overview and future prospects. *Japanese Journal of Applied Physics, 44,* 8269–8285.

Hassani, A., Khataee, A. & Karaca, S. (2015). Photocatalytic degradation of ciprofloxacin by synthesized $tio_2$ nanoparticles on montmorillonite: effect of operation parameters and artificial neural network modeling. *Journal of Molecular Catalysis A: Chemical, 409,* 149–161.

Hong, Z., Donghong, L., Yan, Z., Shuping, L. & Zhe, L. (2009). Sorption isotherm and kinetic modeling of aniline on Cr-bentonite. *Journal of Hazardous Materials, 167,* 141–147.

Huamin, Q., Chuannan, L., Min, S., Fuguang, L., Lulu, F. & Xiangjun, L. (2012). A chemiluminescence sensor for determination of epinephrine using graphene oxide–magnetite-molecularly imprinted polymers. *Carbon, 50,* 4052–4060.

Hummers, W., & Offeman, R. (1958). Preparation of graphitic oxide. *Journal of American Chemical Society, 80 (6),* 1339–1339.

Ikehata, K., Naghashkar, N. J. & El-Din, M. G. (2006). Degradation of aqueous pharmaceuticals by ozonation and advanced oxidation process: a review. *Ozone-Science Engineering, 28,* 353-414.

Jalil, M., Baschini, M. & Sapag, K. (2015). Influence of pH and antibiotic solubility on the removal of ciprofloxacin from aqueous media using montmorillonite. *Applied Clay Science, 114,* 69-76.

Ji, L.L., Chen, W., Duan, L. & Zhu, D.Q. (2009). Mechanisms for strong adsorption of tetracycline to carbon nanotubes: a comparative study using activated carbon and graphite as adsorbents. *Environmental Science Technology, 7,* 2322–2327.

Jia, L., Wang, D., Huang, Y., Xu, A. & Yu, H. (2011). Highly durable n-doped graphene/cds nanocomposites with enhanced photocatalytic hydrogen evolution from water under visible light irradiation. *Journal of Physical Chemical C, 115,* 11466–11473.

Jiang, W., Chang, P-H., Wang, Y-S., Tsai, Y., Jean, J-S., Li, Z. & Krukowski, K. ( 2013). Removal of ciprofloxacin from water by birnessite. *Journal of Hazardous Materials, 250–251,* 362–369.

Kagle, J., Porter, A.W., Murdoch, R.W., Rivera-Cancel, G. & Hay, A.G. (2009). Biodegradation of pharmaceutical and personal care products. *Advance Applied Microbiology, 67,* 65–108.

Khataee, A., Karimi, A., Arefi-Oskoui, S., Darvishi, R., Hanifehpour, Y., Soltani, B. & et al. (2015). Sonochemical synthesis of pr-doped ZnO nanoparticles for sonocatalytic degradation of acid red 17 ultrason. *Sonochemical, 22,* 371–381.

Kim, M. J. & Chea, G-H. (2012). Study on the pv driven dehumidifying system with oyster shell and thermoelectric device. *Journal of the Korean Society of Marine Environment & Safety, 18,* 287-293.

Konstantinou, K. & Albanis, T. (2004). $TiO_2$-assisted photocatalytic degradation of azo dyes in aqueous solution: kinetic and mechanistic investigations: a review. *Applied Catalyst. B, 49,* 1–14.

Kümmerer, K. (2009). Antibiotics in the aquatic environment – a review – part II *Chemosphere, 75 (4),* 435–441.

Kümmerer, K., Al-Ahmad, A. & Mersch-Sundermann, V. (2000). Biodegradability of some antibiotics, elimination of the genotoxicity and affection of wastewater bacteria in a simple test. *Chemosphere, 40,* 701–710.

Kyzas, G., Fu, J., Lazaridis, N., Bikiaris, D., & Matis, K. (2015). New approaches on the removal of pharmaceuticals from wastewaters with adsorbent materials. *Journal of Molecular Liquids, 209,* 87–93.

Langmuir, I. (1918). The adsorption of gases on plane surfaces of glass, mica and platinum. *Journal of American Chemical Society, 40,* 1361-1403.

Larsson, D.G., Pedro, C. & Paxeus, N. (2007). Effluent from drug manufactures contains extremely high levels of pharmaceuticals. *Jornal of Hazardous Materials, 148,* 751–755.

Le-Minh, N., Khan, S. J., Drewes, J. E. & Stuetz, R.M.(2010). Fate of antibiotics during municipal water recycling treatment processes. *Water Reseacrh, 44,* 4295–4323.

Lerf, A., He, H., Forster, M., Klinowski, J. (1998). Structure of graphite oxide revisited. *Journal of Physical and Chemical Society B, 102,* 4477-4482.

Li, H., Zhang, D., Han, X. & Xing, B. (2014). Adsorption of antibiotic ciprofloxacin on carbon nanotubes: ph dependence and thermodynamics. *Chemosphere, 95,* 150–155.

Li, Y., Dua, Q., Liua, T., Pengb, X., Wang, J., Suna, J., & et al. (2013). Comparative study of methylene blue dye adsorption onto activated carbon, graphene oxide, and carbon nanotubes. *Chemical Engineering Research and Design, 91,* 361–368.

Li, Y., Niu, J. & Wang, W. (2011). Photolysis of enrofloxacin in aqueous systems under simulated sunlight irradiation: kinetics, mechanism and toxicity of photolysis products. *Chemosphere, 85,* 892-897.

Li, Y., Sheng, G. & Sheng, J. (2014). Magnetite decorated graphene oxide for the highly efficient immobilization of Eu(III) from aqueous solution. *Journal of Molecular Liquids, 199,* 474–480.

Li, Y., Du, Q., Wang, J., Liu, T., Sun, J, Wang, Y., & et al. (2013). Defluoridation from aqueous solution by manganese oxide coated graphene oxide. *Journal of Fluorine Chemistry, 148,* 67–73.

Lin, A.Y.-C., Yu, T.-H. & Lateef, S.K. (2009). Removal of pharmaceuticals in secondary wastewater treatment processes in Taiwan. *Journal of Hazardous Materials, 167,* 1163–1169.

C-C., Lin H-Y. & Hsu L-J. (2016). Degradation of ofloxacin using UV/$H_2O_2$ process in a large photoreactor. *Separation and Purification Technologhy*, *168*, 57-61.

Lin, C. & Wu, M. (2014). Degradation of ciprofloxacin by UV/$S_2O_8^{2-}$ process in a large photoreactor. *Journal of Photochemistry And Photobiology A: Chemistry, 285*, 1–6.

Liu, G., Wang, N., Zhou, J., Wang, A., Wang, J., Jin, R. & et al.. (2015). Microbial preparation of magnetite/reduced graphene oxide nanocomposites for the removal of organic dyes from aqueous solutions. *RSC Advances, 5*, 95857-95865.

Liu, T., Li, Y., Dua, Q., Suna, J., Jiao, Y., Yanga, Z., & et al. (2012). Adsorption of methylene blue from aqueous solution by graphene. *Colloids and Surfaces B: Biointerfaces, 90*, 197–203.

Ma, Q., Song, T.Y., Yuan, P.F., Wang, C. & Su, X.G. (2008). Qds-Labeled microspheres for the adsorption of rabbit immunoglobulin g and fluoroimmunoassay. *Colloids Surface,B, 2*, 248–254.

Ma, S., Xue, J., Zhou, Y., & Zhang, Z. (2014). Photochemical synthesis of ZnO/$Ag_2O$ heterostructures with enhanced ultraviolet and visible photocatalytic activity. *Journal of Materials Chemistry A., 2,* 7272–7280.

Mchenry, M. E., & Laughlin, D. E. (2000). Nano-scale materials development for future magnetıc applıcatıons. *Acta materials, 48*, 223-238.

Mostofizadeh, A., Li, Y., Song, B., & Huang, Y. (2011). Synthesis, properties, and applications of low dimensional carbon-related nanomaterials. *Journal of Nanomaterial, 68*, 50-81.

Muruganandham, M. & Swaminathan, M. (2006). $TiO_2$–UV photocatalytic oxidation of reactive yellow 14: effect of operational parameters. *Journal of Hazardous Materials*, *135*, 78–86.

Nengsheng, Y., Yali, X., Pengzhi, S., Ting, G. & Jichao, M. (2014). Synthesis of magnetite/graphene oxide/chitosan composite and its application for protein adsorption. *Materials Science and Engineering C, 45,* 8–14.

Nezamzadeh-Ejhieh, A. & Moazzeni, N. (2013). Sunlight photodecolorization of a mixture of methyl orange and bromocresol green by CuS incorporated in a clinoptilolite zeolite as a heterogeneous catalyst. *Journal of Industrial Engineering Chemistry, 19.* 1433–1442.

Nurchi, V., Crespo-Alonso, M., Pilo, M., Spano, N., Sanna, G., Toniolo, R. (2015). Sorption of ofloxacin and chrysoidine by grape stalk. a representative case of biomass removal of emerging pollutants from wastewater. *Arabian Journal of Chemistry (In Press).*

Olakitan, I.C., Mi-Hwa, B & Dong-Su, K. (2009). Montmorillonite surface properties and sorption characteristics for heavy metalremoval from aqueous solutions. *Journal of Hazardous Materials, 166,* 538-546.

Panahi, H. & Alaei, H. (2014). β-Cyclodextrin/thermosensitive containing polymer brushes grafted onto magnetite nano-particles for extraction and determination of venlafaxine in biological and pharmaceutical samples. *International Journal of Pharmaceutics, 476,* 178–184.

Park, H-R., Kim, T. H. & Bark, K-M. (2002). Physicochemical properties of quinolone antibiotics in various environments. *European Journal of Medicinal Chemistry, 37,* 443–460.

Pavan, P., Crepaldi, E., Gomes, A. & Valim, J. (1999). Adsorption of sodium dodecylsulfate on a hydrotalcite-like compound, effect of temperature, pH and ionic strength. *Colloids and Surfaces A: Physicochemical and Engineering Aspects,* 399-410.

Peik-See, T., Pandikumar, A., Ngee, L., Ming, H., & Huad, C. (2014). Magnetically separable reduced graphene oxide/iron oxide nanocomposite materials for environmental remediation. *Catalyst Science Technology, 4*, 43-96.

Pelaez, M., Nolan, N., Pillai, S., Seery, M., Falaras, P., Kontos, A. & et al. (2012). A review on the visible light active titanium dioxide photocatalysts for environmental applications. *Applied catalysis b: Environmental, 25*, 331–349.

Peng, H., Pan, B., Wu, M., Liu, R., Zhang, D., Wu, D. & et al. (2012). Adsorption of ofloxacin on carbon nanotubes: Solubility, pH and cosolvent effects. *Journal of Hazardous Materials, 211–212*, 342–348.

Peres, M. S., Maniero, M. G. & Guimarães, J. R. (2015). Photocatalytic degradation of ofloxacin and evaluation of the residual antimicrobial activity. *Photochemical Photobiology Science, 3*, 556-62.

Punyapalakul, P. & Sitthisorn, T. (2010). Removal of ciprofloxazin and carbamazepine by adsorption on functionalized mesoporous silicates. *World Academy of Science Engineering and Technology, 69*, 546–550.

Rakshit, S., Sarkara, D., Elzingab, E., Punamiyaa, P. & Dattac, R. (2013). Mechanisms of ciprofloxacin removal by nano-sized magnetite. *Journal Of Hazardous Materials, 246– 247*, 221– 226.

Rodríguez, E., Márquez, G., Tena, M., Álvarez, P. & Beltrán, F. (2015). Determination of main species involved in the first steps of $TiO_2$ photocatalytic degradation of organics with the use of scavengers: the case of ofloxacin. *Applied Catalysis B: Environmental Photocatalysis: Science and Applications , 178*, 44–53.

Rouquerol, F., Rouquerol, J., Sing, K. S. W., Llewellyn, P. & Maurin, G. (2014). Adsorption by powders and porous solids principles, methodology and applications. *2. Editions, France: Elsevier*.

Serpone, N., & Emiline, A. V. (2002). Suggested terms and definitions in photocatalysis and radiocatalysis. *International Journal of Photoenergy , 4,* 91-131.

Shahriary, L. & Athawale, A. (2014). Graphene oxide synthesized by using modified hummers approach. *International Journal of Renewable Energy and Environmental Engineering, 2,* 2348-0157.

Shankar, M., Anandan, S., Venkatachalam, N., Arabindoo, B., & Muruge-San, V. (2004). Novel thin-film reactor for photocatalytic degradation of pesticides inaqueous solutions. *Journal of Chemical Technology Biotechnology, 79,* 1258–1279.

Shaoling, W., Xindong, Z. , Yanhui, L., Chunting, Z., Qiuju, D., Jiankun, S. & et al. (2013). Adsorption of ciprofloxacin onto biocomposite fibers of graphene oxide/calcium alginate. *Chemical Engineering Journal, 230,* 389–39.

Sheng, G., Li, Y., Yang, X., Ren, X., Yang, S., Hu, J., & et al. (2012). Efficient removal of arsenate by versatile magnetic graphene oxide composites. *RSC Advances, 2,* 12400-12407.

Shi, M., Shen, J., Ma, H., Li, Z., Lu, X., Li, N. & et al (2012). Preparation of graphene–$TiO_2$ composite by hydrothermal method from peroxotitanium acid and its photocatalytic properties. *Colloids and Surfaces A: Physicochemical and Engineering Aspects, 405,* 30–37.

Sponza, D. & Oztekin, R. (2014). Ciproxin removal from a raw wastewater by nano bentonite-zno: comparison of adsorption and photooxidation processes. *Advances In Environmental And Biological Engineering ISBN: 978-1-61804-259-0.*

Stankovich, S., Pinet, R., Nguven, S. & Ruoff, R. (2006). Synthesis and exfoliation of isocyanate-treated graphene oxide nanoplatelets. *Carbon, 44,* 3342–3347.

Sturini, M., Speltini, A., Maraschi, F., Profumo, A., Pretali, L., Fasani, E. & et al. (2012). Sunlight-induced degradation of soil-adsorbed veterinary antimicrobials marbofloxacin and enrofloxacin. *Chemosphere, 86*, 130- 137.

Sukul, P. & Spiteller, M. (2007). Fluoroquinolone antibiotics in the environment. *Rev. Environmental Contamination Toxicology, 191*, 131–162.

Sun, S. P., Guo, H. Q., Ke, Q., Sun, J. H., Shi, S. H., Zhang, M. L. (2009). Degradation of antibiotic ciprofloxacin hydrochloride by photo-fenton oxidation process. *Environmental Engineering Science, 26(4)* 753–759.

Tang S. & Lo I. (2013). Magnetic nanoparticles: essential factors for sustainable environmental applications. *Water Research, 47,* 2613 -2632.

Tang, Y., Guo, H., Xiao, L., Yu, S., Gao, N. & Wang, Y. (2013). Synthesis of reduced graphene oxide/magnetite composites and ınvestigation of their adsorption performance of fluoroquinolone antibiotics. *Colloids and Surfaces A: Physicochemical and Engineering Aspects, 424*, 74-80.

Tayyebi, A., Outokesh, M., Moradi, S. & Doram, A. (2015). Synthesis and characterization of ultrasound assisted "graphene oxide–magnetite" hybrid, and investigation of its adsorption properties for Sr(II) and Co(II) ions. *Applied Surface Science, 353*, 350–362.

Temkin, M., & Pyzhev, V. (1940). Kinetics of ammonia synthesison promotedıron catalysts. *Acta Physiochemical, 12*, 327–356.

UIPAC, (2002). Chemisorption and physisorption. Retrieved May, 09, 2002 from http://old.iupac.org/reports/2001/colloid_2001/manual_of_s_and_t/node16.html.

Umukoro, H. E., Peleyeju, M. G., Ngila, J. C. & Arotiba, O. A. (2016). Photocatalytic degradation of acid blue 74 in water using Ag–$Ag_2O$–Zno nanostuctures anchored on graphene oxide. *Solid State Sciences, 51,* 66–73.

Upadhyay, R., Soin, N. & Roy, S. (2013). Role of graphene/metal oxide composites as photocatalysts,adsorbents and disinfectants in water treatment: a review. *RSC Advances, 114,* 69–76.

Vasconcelos, T. G., Henriques, D. M., König, A., Martins, A. F. & Kümmerer, K. (2009). Photo-degradation of the antimicrobial ciprofloxacin at high pH: Identification and biodegradability assessment of the primary by-products. *Chemosphere, 76,* 487–493.

Wang, C. J., Li, Z. H., & Jiang, W. T. (2011). Adsorption of ciprofloxacin on 2:1 dioctahedral clay minerals. *Applied Clay Science, 53(4)* 723–728.

Wang, C. J., Li, Z. H., Jiang, W. T., Jean, J. S. & Chuan, C. C. (2010). Cation exchange interaction between antibiotic ciprofloxacin and montmorillonite. *Journal of Hazardous Materials B, 183(1- 3)* 309–314.

Wang, M., Huang, J., Tong, Z., Li, W. & Chen, J. (2013). Reduced graphene oxide–cuprous oxide composite via facial deposition for photocatalytic dye-degradation. *Journal of Alloys and Compounds, 568,* 26–35.

Wang, P., He, Y-L. & Haung, C-H. (2010). Oxidation of fluoroquinolones antibiotics and structurally related amines by chlorine dioxide: reaction kinetics, product and pathway evaluation. *Water Research, 44,* 5989-5598.

Wang, Y., Von, G., Volman, D.H. & Neckers, D.C. (1995). In advances in photochemistry, *in: Bünau (Eds.), New York: Wiley,* 179–234.

Wankasi, D. & Tarawou, T. (2008). studies on the effect ph on the sorption of Pb(ii) and Cu(ii) ions from aqueous media by nipa palm (nypa fruticans wurmb). *Journal of Applied Science Environmental Manage, 12(4)* 87–94.

Wikipedia, (2016a). *Rate equation*. Retrieved June, 22, 2016 from https://en.wikipedia.org/wiki/Rate_equation

Wikipedia, (2016b). *Regression analysis*. Retrieved June, 22, 2016 from https://en.wikipedia.org/wiki/Regression_analysis.

Wood, G.O. (2002). Review and comparisons of d/r models of equilibrium adsorption of binary mixtures of organic vapors on activated carbons. *Carbon, 40,* 231–239.

Xinlin, L., Peng, L., Guanxin, Y., Changchang, M., Yangfeng, T., Yuting, W. & et al. (2014). Selective degradation of ciprofloxacin with modified NaCl/$TiO_2$ photocatalyst by surface molecular ımprinted technology. *Colloids and Surfaces A: Physicochemical and Engineering Aspects, 441*, 420–426.

Xu, P., Zeng, G. Z., Huang, D. L., Feng, C. L., Hu, S., Zhao, M. H. & et al. (2012). Use of iron oxide nanomaterials in wastewater treatment: A review. *Science of the Total Environment , 424,* 1–10.

Yahya, M. S., Oturan, N., Kacemi, K. E., Karbane, M. E., Aravindakumar, C. T., & Oturan, M. A. (2014). Oxidative degradation study on antimicrobial agent ciprofloxacin by electro-fenton process: Kinetics and oxidation products. *Chemosphere*, *117*, 447–454.

Yan, Y., Shaofang, S., Yang, S., Xu, Y., Weisheng, G., Xinlin, L. & et al. (2013). Microwave-assisted ın situ synthesis of reduced graphene oxide-$Bivo_4$ composite photocatalysts and their enhanced photocatalytic performance for the degradation of ciprofloxacin. *Journal of Hazardous Materials, 250–251*, 106–114.

Yan, L., Yu, L. & Ray, M. (2008). Degradation of paracetamol in aqueous solutions by $TiO_2$ photocatalysis. *Water Research, 42,* 3480–3488.

Yang, X., Chen, C., Li, J., Zhao, G., Ren, X. & Wang, X. (2012). Graphene oxide-iron oxide and reduced graphene oxide-iron oxide hybrid materials for the removal of organic and inorganic pollutants. *RSC Advances, 2,* 8821–8826.

Yuanyuan, S., Qinyan, Y., Baoyu, G., Yuan, G., Xing, X., Qian, L. & et al. (2014). Adsorption and cosorption of ciprofloxacin and Ni(II) on activated carbon-mechanism study. *Journal of the Taiwan Institute of Chemical Engineers, 45,* 681–688.

Zhanel, G., Ennis, K., Vercaigne, L., Walkty, A., Gin, A.S., Embil, J. & et al. (2002). A critical review of the fluoroquinolones: focus on respiratory tract infections. *Drugs, 62,* 13–59.

Zhang, C., Qiao, G., Zhao, F. & Wang, Y. (2011). Thermodynamic and kinetic parameters of ciprofloxacin adsorption onto modified coal fly ash from aqueous solution. *Journal of Molecular Liquids, 163,* 53–56.

Zhang, H. & Huang, C-H. (2007). Adsorption and oxidation of fluoroquinolone antibacterial agents and structurally related amines with goethite. *Chemosphere, 66,* 1502-1512.

Zhang, W., Zhou, C., Zhou, W., Lei, A., Zhang, Q., Wan, Q. & et al. (2011). Fast and considerable adsorption of methylene blue dye onto graphene oxide. *Bulletin of Environmental Contamination and Toxicology , 87,* 86-90.

Zhang, X., Li, R., Jia, M., Wang, S., Huang, Y. & Chen, C. (2015). Degradation of ciprofloxacin in aqueous bismuth oxybromide (BiOBr) suspensions under visible light irradiation: A direct hole oxidation pathway. *Chemical Engineering Journal, 274,* 290–297.

Zhang, X., Lin, H., Cui, X. & Lin, Y. (2010). Graphene/$TiO_2$ Nanocomposites: synthesis, characterization and application in hydrogen evolution from water photocatalytic splitting. *Journal of Material Chemical, 20,* 2801–2806.

Zhang, F., Song, Y., Song, S., Zhang, R., Hou W. (2015).Synthesis of Magnetite-Graphene Oxide-Layered Double Hydroxide Composites and Applications for the removal of Pb(II) and 2,4-Dichlorophenoxyacetic Acid from Aqueous Solutions. *ACS Applied Material Interfaces, 7,* 7251-7263.

Zhao, G., Li, J., Ren, X., Chen, C., & Wang, X. (2011). Few-layered graphene oxide nanosheets as superior sorbents for heavy metal ion pollution management. *Environmental Science and Technology, 45,* 10454-10462.

Zhen, Y., Han, Y., Hu, Y., Haibo, L., Aimin, L. & Rongshi, C. (2013). Flocculation performance and mechanism of graphene oxide for removal of various contaminants from water. *Water Research, 47,* 3037–3046.

Zhe-Qi, L., Hui-Long, W., Long-Yun, Z., Jian-Jun, Z., & Yao-Shan, Z. (2015). Preparation and photocatalytic performance of magnetic $TiO_2$–$Fe_3O_4$/Graphene (RGO) composites under vıs-light ırradiation. *Ceramics International, 41,* 10634–10643.

Zivanovic, L., Zigic, G., & Zecevic, M. (2006). Investigation of chromatographic conditions for the separation of ofloxacin and its degradation products. *Journal of Chromatography A, 1119,* 224–230.

Zorita, S., Mårtensson, L. & Mathiasson, L. (2009). Occurrence and removal of pharmaceuticals in a municipal sewage treatment system in the south of Sweden. *Science Total Environmental, 407,* 2760–2770.